Positive Geometry of the S-Matrix

Yuntao Bai

A Dissertation

Presented to the Faculty

of Princeton University

in Candidacy for the Degree

of Doctor of Philosophy

Recommended for Acceptance

by the Department of

Physics

Adviser: Nima Arkani-Hamed

September 2018

Abstract

The search for a theory of the S-Matrix has revealed unprecedented structures underlying amplitudes. In this text, we present a new framework for understanding a class of amplitudes that includes Yang-Mills, Non-linear Sigma Model, the bi-adjoint cubic scalar, planar $\mathcal{N} = 4$ super Yang-Mills, and more. We introduce *positive geometries*, which are generalizations of convex polytopes to geometries with higher order (i.e. non-linear) boundaries. Our construction provides a unique differential form called the *canonical form* of the positive geometry, whose pole structure is completely controlled by the geometric boundaries. The central claim of this text is that positive geometries play a fundamental role in our class of scattering amplitudes, whereby the corresponding canonical form determines a physical quantity. Our primary examples are (1) the bi-adjoint cubic scalar for which the positive geometry is the famous associahedron polytope whose canonical form gives the color-ordered tree amplitude, and (2) planar $\mathcal{N} = 4$ super Yang-Mills for which the positive geometry is the amplituhedron whose canonical form gives the scattering integrand. One recurrent theme in our text is that physical properties of amplitudes like local poles and factorization are direct consequences of the boundary structure. We are therefore led to the point of view that locality and unitarity are emergent properties of the positive geometry. Furthermore, we discuss unexpected connections between positive geometry and on-shell diagrams, BCFW recursion, scattering equations, color-kinematics duality and the open string.

Acknowledgements

First and foremost, I am deeply indebted to Nima Arkani-Hamed for being my adviser and an amazing collaborator. It is very hard to overstate his intellectual prowess not just in particle physics but more generally in science. His work will undoubtedly continue to shape particle physics for decades to come. It was therefore an absolute privilege to have worked along his side. Nima also taught me the importance of persistence, and I am thankful to him for encouragement during moments of self-doubt. Furthermore, Nima is not just a great physicist, but also an amazingly fun person to talk to. It is rare to find such a fantastic combination of wit, charm and intellect in one person.

I am deeply thankful to Thomas Lam for many insightful discussions, for being an outstanding collaborator, and for kindly inviting me to Ann Arbor for two very productive visits. Thomas played the key role in translating our work on the S-Matrix to a more rigorous mathematical framework, which established the bedrock foundations for the subject of positive geometry.

I also owe great a debt of gratitude to Song He for many fruitful discussions over the years, and for collaboration on my first paper and subsequent papers. His expertise on the CHY formalism was central to connecting our work on positive geometries to the scattering equations. In real life, he is also a great friend to have.

Furthermore, I am grateful to Freddy Cachazo and Jaroslav Trnka for stimulating discussions, and for their hospitality during my travels. I would also like to thank Steven Karp, Hugh Thomas, Lauren Williams, and Gongwang Yan.

Moreover, I am grateful to Herman Verlinde and Dan Marlow for serving on my FPO committee, and especially to Dan for letting me help him on an undergraduate lab project. I am grateful to Steven Gubser for kindly providing me with work during the summer. I also want to thank the Department of Physics at Princeton, the Institute for Advanced Study, and NSERC for supporting my academic career.

I would also like to thank my friends back home for our continued friendship despite the long distances.

Finally and most importantly, I would like to thank my parents for supporting me throughout the years.

The material presented in this thesis is based on publications [1, 2, 3, 4] by the author and collaborators Nima Arkani-Hamed, Thomas Lam, Song He, and Gongwang Yan. Parts of the material were presented at various physics seminars, conferences and meetings at Harvard University, QMAP UC Davis, Perimeter Institute, Princeton University, Bhaumik Institute, Higgs Centre for Theoretical Physics, and National Taiwan University.

For my family

Contents

Chapter 1

Introduction

In recent years, we have witnessed tremendous progress in the theory of scattering amplitudes, including Witten's twistor string [5], on-shell recursion relations [6, 7], hidden symmetries such as dual conformal symmetry [8], unprecedented simplifications (e.g. see [9] for a loop level example), scattering equations of Cachazo, He and Yuan [10, 11, 12, 13], BCJ duality [14, 15], Grassmannian geometry [16] and the amplituhedron [17].

In this text, we present a new point of view for studying a class of scattering amplitudes that includes Yang-Mills, Non-linear Sigma Model, a colored cubic scalar theory called the bi-adjoint scalar [13], planar $\mathcal{N} = 4$ super Yang-Mills, and more. We begin by introducing the concept of a *positive geometry* [2], which is a generalization of convex polytopes to geometries with higher order (i.e. non-linear) boundaries. Our construction requires the existence and uniqueness of a top form called the *canonical form* of the geometry, whose singularities are controlled by the boundary structure of the underlying geometry. Specifically, the form has logarithmic singularities on the boundaries of the geometry in a precise sense as described in Section 2.1. The crucial observation is that positive geometries appear in physics. For physically relevant positive geometries, the canonical form is a physical quantity, which we summarize

schematically as follows.

$$\text{positive geometry} \quad \rightarrow \quad \text{canonical form} \quad \rightarrow \quad \text{physical quantity}$$

Positive geometries have two important properties. Firstly, they can be triangulated; that is, provided a subdivision of a positive geometry into many non-overlapping pieces, the canonical form of the geometry is the sum of the canonical form of every piece. An extension to the case of over-lapping pieces also exists, provided the the orientation of the pieces is taken into account. In practice this simplifies the computation of canonical forms, since a complicated geometry can be subdivided into simpler ones whose canonical forms are already known. Secondly, canonical forms are related via diffeomorphisms. That is, given a diffeomorphic map from one positive geometry to another, pushing the canonical form of the former gives the canonical form of the latter. This is a rather subtle observation which very non-trivial consequences. We also discuss an interesting connection between positivity of the form and convexity of the geometry, which may be related to positivity of amplitudes as described in [18].

The simplest non-trivial example is the *associahedron*, a famous polytope discovered by mathematicians in the 1960's [19, 20, 21] from a combinatorial point of view, which we find to be intimately related to the scattering of color-ordered particles—a connection that is most clearly illuminated from the point of view of positive geometries. More specifically, for each cyclic ordering of n external particles, there exists an infinite family of $(n-3)$-dimensional associahedra foliating the interior of on-shell kinematic space—the space spanned by all Mandelstam invariants. The boundaries of every associahedron correspond in a one-to-one fashion to all the physical poles of the relevant ordering; that is, going to a boundary of an associahedron corresponds to taking a virtual particle on shell. We find a striking fact: the canonical form of every associahedron is the tree level scattering amplitude for the bi-adjoint cubic scalar

theory.

kinematic associahedron $\rightarrow$ canonical form $\rightarrow$ tree amplitude of bi-adjoint scalar

Furthermore, we find that universal properties of amplitudes like locality and unitarity (and hence factorization of the amplitude) follow directly from the geometric construction. In brief, this is due to the observation that every boundary of the associahedron is a direct product of two lower-dimensional associahedron, in completely parallel to the fact that the amplitude factors into a product of two lower point amplitudes on each cut. We take the point of view that the positive geometry is the most basic element of our construction. From this point of view, locality and unitarity are *emergent* properties of the positive geometry—a theme to which we return many times throughout this text. In particular, we find that *positivity* plays a crucial role, since the boundary structure of the geometry is controlled by positivity conditions. Another novel aspect of our story is the construction of scattering amplitudes as differential forms of kinematic space, in a sense described in Section 6.2. While these forms appear naturally as canonical forms of the underlying positive geometry, they also have many other purposes in life—they encode information about color/flavor (see Section 6) and in some cases even helicities (see Section 10 of [22]). Finally, we compute these scattering amplitudes in multiple ways by exploiting different ways of triangulating the assocahedron. In particular, we find the striking fact that the Feynman diagram expansion is just one of many triangulations of the associahedron. Moreover, by following our geometric intuition, we identify triangulations that give even simpler expressions for the amplitude.

Our second example of positive geometry is the moduli space of the open string worldsheet. It is well-known that the Deligne-Mumford-Knutson compactification of the moduli space [23, 24] is an associahedron. We find that the *worldsheet associa-*

hedron can be naturally understood as a positive geometry whose canonical form is precisely the famous Parke-Taylor form, whose Koba-Nielsen-regulated integral gives the open string tree amplitude. Furthermore, we discover that the scattering equations can also be interpreted from the geometric point of view—in fact, they provide a diffeomorphic map from the worldsheet associahedron to the kinematic associahedron. It follows therefore that the scattering equations must "push" the Parke-Taylor form to the canonical form of the kinematic associahedron, thus leading to the CHY formula for the bi-adjoint scalar tree amplitude.

$$\text{worldsheet associahedron} \quad \to \quad \text{canonical form} \quad \to \quad \text{Parke-Taylor form}$$

In our attempt to generalize the associahedron to a broader class of theories, we find a unexpected connection between color/flavor and kinematics, which involves a number of observations. First we find a direct connection between color-ordered amplitudes and differential forms on kinematic space called *scattering forms*, which serve as generalizations of the canonical form for the associahedron. This relies on a peculiar observation: the differential forms satisfy "Jacobi relations" analogous to the Jacobi relations satisfied by the structure constants. Furthermore, we find that many aspects off the well-known BCJ duality such as kinematic Jacobi relations and BCJ relations are consequences of a simple property of the scattering form—local GL(1) invariance, i.e. projectivity. This suggests a close connection between positive geometries and color-kinematics duality. Finally, we establish the scattering forms for Yang-Mills and Non-linear Sigma Model and discuss their properties, such as uniqueness (see [25] for an independent discussion on uniqueness of the amplitudes) and relation to the worldsheet.

Our third example of positive geometry is the *amplituhedron*, first proposed in [17] as an independent, geometric formulation of planar $\mathcal{N} = 4$ super Yang-Mills. A follow-

up was given in [26] which provided detailed computations, and a more intrinsic "winding number" description was givne later in [22]. We make this construction more precise from the viewpoint of positive geometries. We argue that the n-particle N^{k}MHV planar L-loop integrand (for $L = 0$ the "integrand" is the amplitude) is determined by the canonical form of the amplituhedron $\mathcal{A}(k, n; L)$ which is indexed by the same quantum numbers. While the canonical form is a purely "bosonic" quantity, the required super-amplitude is obtained by a straightforward prescription that involves integrating out auxiliary Grassmann variables as described in [17] and Section 8.2.

$$\text{amplituhedron} \quad \rightarrow \quad \text{canonical form} \quad \rightarrow \quad \text{planar integrand of } \mathcal{N} = 4 \text{ sYM}$$

In parallel with our discussion for the associahedron, locality and unitarity emerge as properties of the underlying geometry, with positivity playing the central role. We find that every codimension-1 boundary corresponds to a physical pole of the amplitude, and is given by a product of two lower dimensional amplituhedra, thus providing a geometric origin for the factorization property of the planar integrand. Furthermore, we computations of the canonical form by triangulations of the amplituhedron; and we present the striking fact that the famous BCFW expansion [6, 27, 28] provides just one class of infinitely many possible triangulations for the amplituhedron. The geometric point of view is very satisfying, because it provides a geometric understanding for the highly non-trivial algebraic identities that equate all possible BCFW representations of the same integrand; that is every BCFW representation provides a different triangulation of the same underlying positive geometry.

Moving ahead, we present a novel recursive diagrammatic procedure for computing any BCFW term, called *momentum twistor diagrams*. We find that for each BCFW term, there is a "cell" of the amplituhedron called a "BCFW cell". We discover the

satisfying fact that the canonical form of the BCFW cell determines the corresponding BCFW term. Furthermore, given a BCFW expansion for a particular integrand, we find that the corresponding BCFW cells form a triangulation of the amplituhedron. It follows therefore that the sum of the BCFW terms gives the canonical form of the amplituhedron, exactly as anticipated. This geometric understanding explains the cancellation of spurious poles, which correspond to spurious boundaries appearing in the triangulation. Since the canonical form for the amplituhedron is independent of triangulation, these spurious poles must cancel. The cancellation of spurious poles was an important insight first described in [29].

$$\text{BCFW cell} \quad \rightarrow \quad \text{canonical form} \quad \rightarrow \quad \text{BCFW term}$$

These diagrams make manifest a connection between BCFW recursion and the positive Grassmannian [30], as discussed in [16] and explored further in [4]. Finally, we demonstrate techniques for computing these diagrams, and provide detailed examples up to two loops. We also devote an entire section to a detailed exploration of the one-loop amplituhedron and its associated diagrams.

We provide a precise definition of positive geometries and canonical forms in Section 2.1. Subsequently, we discuss triangulations and maps between positive geometries. Furthermore, we separate positive geometries into two classes: generalized simplices and generalized polytopes, for which we provide many examples. In Section 3 we discuss systematic methods for computing canonical forms, including direct construction from poles and zeros, triangulations, pushforwards and integrals over dual or related geometries. The associahedron is introduced in Section 4, which includes a detailed construction of the polytope in kinematic space, and its canonical form as a scattering amplitude. We emphasize the emergence of locality and unitarity in Section 4.3. The worldsheet and its relation to the kinematic associahedron and

scattering equations are discussed in Section 5, and the geometric properties of color and kinematics are discussed in Section 6. Finally, the amplituhedron is constructed in Section 7, and the connection to planar $\mathcal{N} = 4$ super Yang-Mills is delineated in Section 8. Momentum twistor diagrams are described in Section 9. We also provide a detailed analysis of the one-loop amplituhedron in Section 10.

Chapter 2

Positive geometries

We introduce positive geometries, which form the mathematical foundations on which the remainder of our discussion is built. Naively, a positive geometry is simply a geometry with boundaries of all codimensions. Positive geometries with linear boundaries are polytopes, while more generally higher order boundaries are also permitted. For every positive geometry, there exists a unique meromorphic top form called its canonical form, whose residues reflect the boundary structure. In particular, it is uniquely constrained by the property of having logarithmic singularities on the boundaries of the geometry and unit leading singularities, and a few other assumptions. The canonical form provides the connection between positive geometries and physics. We find that for physically relevant positive geometries such as the amplituhedron (Section 7), the associahedron (Section 4) and many others discussed throughout this text, the canonical form determines scattering amplitudes and other related physical quantities. In particular, the canonical form of the amplituhedron determines scattering amplitudes in planar $\mathcal{N} = 4$ super Yang-Mills to all loops, while the canonical form of the associahedron determines scattering amplitudes in a cubic scalar theory called the bi-adjoint ϕ^3 theory at tree level.

We begin in Section 2.1 by discussing general properties of positive geometries and define their canonical forms. In Section 2.2, we discuss triangulation of positive geometries, which can be thought of as a generalization of polytopal subdivision to more general geometries. We then discuss, in Section 2.3, how canonical forms of different geometries are related through diffeomorphisms by a powerful tool called the pushforward. Finally, in Sections 2.4 and Section 2.5, we provide an extensive list of examples.

2.1 Positive geometries and their canonical forms

We begin with a precise definition of positive geometries and their canonical forms. Let $\mathbb{P}^N$ denote the N-dimensional complex projective space with the standard projection $\mathbb{C}^{N+1} \setminus \{0\} \to \mathbb{P}^N$. We also let $\mathbb{P}^N(\mathbb{R})$ denote the image of the real part. We define a D-dimensional *positive geometry* to be a pair $(X, X_{\geq 0})$ with the following properties.

1. The space $X \subset \mathbb{P}^N$ has complex dimension D, and is cut out by finitely many homogeneous polynomials with real coefficients. We denote by $X(\mathbb{R})$ the *real part* of X, which is the solution set in $\mathbb{P}^N(\mathbb{R})$ of the same set of equations.

2. The space $X_{\geq 0}$ is nonempty with real dimension D, and is a union of closed subsets of $X(\mathbb{R})$, each of which is cut out by finitely many real polynomial inequalities. To make sense of inequalities in projective space, we first find solutions in $\mathbb{R}^{N+1} \setminus \{0\}$, and then take its image in $\mathbb{P}^N(\mathbb{R})$.

We assume that the complex dimension of X matches the real dimension of $X(\mathbb{R})$, which we henceforth refer to as the dimension of the positive geometry. Additional technical assumptions are explained in Appendix A of [2], where the important notion of *boundary components* is explained. Furthermore, we assume that for every pos-

itive geometry $(X, X_{\geq 0})$, there exists a unique nonzero rational D-form $\Omega(X, X_{\geq 0})$ satisfying the following properties.

- For $D = 0$: X is a single point and we must have $X_{\geq 0} = X$. We define the 0-form $\Omega(X, X_{\geq 0})$ on X to be ± 1 depending on the orientation of $X_{\geq 0}$.
- For $D > 0$: we have

  (P1) Every boundary component $(C, C_{\geq 0})$ of $(X, X_{\geq 0})$ is a positive geometry of dimension $D-1$.

  (P2) The form satisfies $\mathrm{Res}_C \Omega(X, X_{\geq 0}) = \Omega(C, C_{\geq 0})$ along every boundary component C, with no singularities elsewhere.

In particular, all *leading residues* of $\Omega(X, X_{\geq 0})$ must be unity ± 1. We refer to X as the *embedding space*. The form $\Omega(X, X_{\geq 0})$ is called the *canonical form* of the positive geometry. For convenience, we usually write $X_{\geq 0}$ to denote a positive geometry $(X, X_{\geq 0})$, and write $\Omega(X_{\geq 0})$ for the associated canonical form. We point out however that the space X usually contains infinitely many positive geometries, hence the notation $X_{\geq 0}$ can be misleading. Nevertheless, the correct interpretation should always be clear based on context. In some instances, we wish to focus on the interior $X_{>0}$ of $X_{\geq 0}$, in which case $X_{\geq 0}$ is called the nonnegative part and $X_{>0}$ the positive part. We also refer to the *codimension d boundary components* of a positive geometry $(X, X_{\geq 0})$, which are obtained by taking successive boundary components d times. We stress that the existence of the canonical form is very non-trivial, and the most general conditions under which they exist are still unclear. Nonetheless, in the sections that follow, we give many non-trivial examples of positive geometries and develop methods for computing their canonical forms.

For technical purposes, we often also work with a generalization of positive geometries. We define a D-dimensional *pseudo-positive geometry* to be a pair $(X, X_{\geq 0})$ of

the same kind as a positive geometry, but the non-negative part $X_{\geq 0}$ may be empty. Furthermore, we modify the axioms as follows:

- For $D = 0$: X is a point. If $X_{\geq 0} = X$, then we define the 0-form $\Omega(X, X_{\geq 0})$ on X to be ± 1 depending on the orientation of $X_{\geq 0}$. However, if $X_{\geq 0} = \emptyset$, then we set $\Omega(X, X_{\geq 0}) = 0$.

- For $D > 0$: if $X_{\geq 0}$ is empty, we set $\Omega(X, X_{\geq 0}) = 0$. Otherwise, we require:

(P1*) Every boundary component $(C, C_{\geq 0})$ of $(X, X_{\geq 0})$ is a pseudo-positive geometry of dimension $D-1$.

(P2*) There exists a unique rational D-form $\Omega(X, X_{\geq 0})$ on X satisfying the residue relation $\mathrm{Res}_C \Omega(X, X_{\geq 0}) = \Omega(C, C_{\geq 0})$ along every boundary component C with no singularities elsewhere.

While we use the same notation for $X, X_{\geq 0}, \Omega$ as in the case of positive geometries, the important differences are that we allow the geometry $X_{\geq 0}$ to be empty, and we allow the form to vanish identically. Note, however, that there are pseudo-positive geometries with $\Omega(X, X_{\geq 0}) \neq 0$ that are not positive geometries; for instance, the disjoint union of a positive geometry and a pseudo-positive geometry. It is also possible for a non-empty geometry to have an identically vanishing form, such as a disk.

We describe some simple ways to obtain new positive geometries from old ones. Our discussion in this section applies equally well to pseudo-positive geometries. First, if $(X, X_{\geq 0})$ is a positive geometry, then so is $(X, X^-_{\geq 0})$, where $X^-_{\geq 0}$ denotes the same space $X_{\geq 0}$ with reversed orientation. Moreover, its boundary components C_i^- also acquire the reversed orientation, and the canonical form acquires a sign $\Omega(X, X_{\geq 0}) = -\Omega(X, X^-_{\geq 0})$. Second, suppose $(X, X^1_{\geq 0})$ and $(X, X^2_{\geq 0})$ are positive geometries, and suppose that they are disjoint: $X^1_{\geq 0} \cap X^2_{\geq 0} = \emptyset$. Then the disjoint union $(X, X^1_{\geq 0} \cup X^2_{\geq 0})$ is itself a positive geometry, and the canonical form is obtained by addition

$\Omega(X^1_{\geq 0} \cup X^2_{\geq 0}) = \Omega(X^1_{\geq 0}) + \Omega(X^2_{\geq 0})$. Third, suppose $(X, X_{\geq 0})$ and $(Y, Y_{\geq 0})$ are positive geometries. Then the direct product $(Z, Z_{\geq 0}) := (X \times Y, X_{\geq 0} \times Y_{\geq 0})$ is again a positive geometry. The boundary components of $(Z, Z_{\geq 0})$ are of the form $(C \times Y, C_{\geq 0} \times Y_{\geq 0})$ or $(X \times D, X_{\geq 0} \times D_{\geq 0})$, where $(C, C_{\geq 0})$ and $(D, D_{\geq 0})$ are boundary components of $(X, X_{\geq 0})$ and $(Y, Y_{\geq 0})$, respectively. The canonical form for the direct product is given by the wedge product of the canonical forms.

$$\Omega(Z, Z_{\geq 0}) = \Omega(X, X_{\geq 0}) \wedge \Omega(Y, Y_{\geq 0}) \tag{2.1}$$

The simplest non-trivial examples of pseudo-positive geometries $(X, X_{\geq_0})$ are of dimension 1, for which the embedding space X is isomorphic to the Riemann sphere $\mathbb{P}^1$ while the real part $X_{\geq 0}$ is a closed subset of $\mathbb{P}^1(\mathbb{R})$. In the special cases where $X_{\geq 0} = \mathbb{P}^1(\mathbb{R})$ or $X = \emptyset$, we have $\Omega(X_{\geq 0}) = 0$ and so $X_{\geq 0}$ is only a pseudo-positive geometry. Otherwise, $X_{\geq 0}$ is a union of disjoint closed intervals, which is a positive geometry. See Section 2.4 [2] for a more rigorous discussion. A generic closed interval is given by the following:

Example 2.1.1. The closed interval $[a, b] \subset \mathbb{P}^1(\mathbb{R})$ is the set of points $\{(1, x) \mid a \leq x \leq b\} \subset \mathbb{P}^1(\mathbb{R})$, where $a < b$. The canonical form is given by

$$\Omega([a, b]) = \frac{dx}{x - a} - \frac{dx}{x - b} = \frac{(b - a)}{(b - x)(x - a)} dx. \tag{2.2}$$

where $(1, x) \in \mathbb{P}^1$. We assumed that the segment is oriented in the positive direction; otherwise, the sign of the form would be reversed. Furthermore, the canonical form of a disjoint union of line segments is the sum of the canonical forms of those line segments.

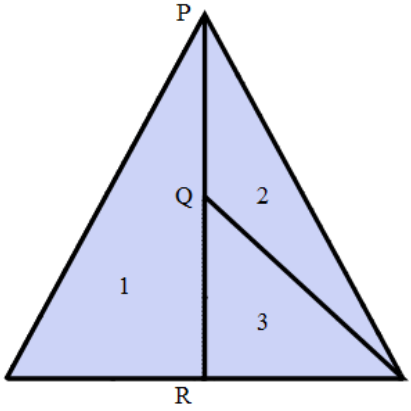

Figure 2.1: A triangle $X_{\geq 0}$ triangulated by three smaller triangles $X_{i,\geq 0}$ for $i = 1, 2, 3$. Three of the vertices are labeled P, Q and R.

2.2 Triangulations

Triangulations play an important role in the theory of positive geometries. The main result of this section is the fact that canonical forms are triangulation independent. This means that the canonical form of any positive geometry can be obtained by triangulating the geometry and summing over the canonical form for each piece. In practice, this vastly simplifies the computation of canonical forms.

2.2.1 Triangulations of pseudo-positive geometries

Let $X_{\geq 0}$ denote a pseudo-positive geometry, and let $X_{i,\geq 0}$ for $i = 1, \ldots, t$ denote a finite collection of pseudo-positive geometries. We assume they all live in the same embedding space X. We say that the collection $\{X_{i,\geq 0}\}$ *triangulates* $X_{\geq 0}$ if the following properties are satisfied:

- Each $X_{i,>0}$ is contained in $X_{>0}$ and the orientations agree.
- The interiors $X_{i,>0}$ of $X_{i,\geq 0}$ are mutually disjoint.
- The union of all $X_{i,\geq 0}$ gives $X_{\geq 0}$.

A triangulation of $X_{\geq 0}$ can be thought of as a collection of pseudo-positive geometries that tiles $X_{\geq 0}$. In Section 3.2 of [2] we also establish the notion of *signed triangulations* whereby overlapping pieces (possibly with opposite orientations) are permitted.

Triangulations are very closely connected to the properties of the canonical form in the following way.

$$\text{If } \{X_{i,\geq 0}\} \text{ triangulates } X_{\geq 0} \text{ then } \Omega(X_{\geq 0}) = \sum_{i=1}^{t} \Omega(X_{i,\geq 0}). \tag{2.3}$$

We provide a sketch of the argument here, and we encourage the reader to read Section 3.1 of [2] for a more rigorous discussion. It is sufficient to show that the right hand side satisfies the defining properties of the canonical form of $X_{\geq 0}$, in which case the desired result follows from uniqueness. Most importantly, we need to show that it has the required poles and residues. We argue by induction on dimension, starting with the zero-dimensional case, which is trivial. For dimension $D \geq 1$, consider for instance a boundary component $(C, C_{\geq 0})$ of $(X, X_{\geq 0})$. We let $(C, C_{i,\geq 0})$ denote the boundary components along C of the triangulating pieces $(X, X_{i,\geq 0})$. For simplicity we assume that all the triangulating pieces $X_{i,\geq 0}$ lie on the same side of $C_{\geq 0}$. Then clearly $\{C_{i,\geq 0}\}$ forms a triangulation of $C_{\geq 0}$. It follows that

$$\text{Res}_C \Omega(X, X_{\geq 0}) = \Omega(C, C_{\geq 0}) = \sum_i \Omega(C, C_{i,\geq 0}) = \sum_i \text{Res}_C \Omega(X, X_{i,\geq 0}) \tag{2.4}$$

where the induction hypothesis is applied on the second equality, since C is one dimension lower. This shows that the right hand side of (2.3) has the required residue along C. However, we are not done, since there are other types of boundaries that need to be checked. For instance, the triangulation may introduce boundaries that do not appear in $X_{\geq 0}$. Consequently, poles would appear in the individual terms on the right hand side of (2.3) that cancel in the sum. For instance, consider a collection of boundary components $(B, B_{i,\geq 0})$ of $(X, X_{i,\geq 0})$, respectively, all along the

same hypersurface B. For simplicity, assume that $X_{\geq 0}$ has no boundary component along B. Moreover, we divide the boundary components $B_{i,\geq 0}$ into two subcollections $\{B^+_{a,\geq 0}\}$ and $\{B^-_{b,\geq 0}\}$ depending on which side of $B(\mathbb{R})$ they live on. The union of each collection is the same, which we denote as $(B, B_{\geq 0})$. It follows that

$$\sum_i \text{Res}_B \Omega(X, X_{i,\geq 0}) = \sum_a \Omega(B, B^+_{a,\geq 0}) - \sum_b \Omega(B, B^-_{b,\geq 0}) \tag{2.5}$$

$$= \Omega(B, B_{\geq 0}) - \Omega(B, B_{\geq 0}) = 0 \tag{2.6}$$

where again we applied the induction hypothesis on the second equality. This completes the argument, since $\Omega(X, X_{\geq 0})$ has no pole along B. While we lost some generality in our simplifying assumptions, a complete proof is given in Appendix B of[2].

We caution that even if all the $\{X_{i,\geq 0}\}$ are positive geometries, the $X_{\geq 0}$ may only be a pseudo-positive geometry. A straightforward example is a unit disk thought of as the union of two half disks. Moreover, if all the positive geometries involved are polytopes, our notion of triangulation reduces to the usual notion of polytopal subdivision. If furthermore $\{X_{i,\geq 0}\}$ are all simplices, then we recover the usual notion of a triangulation of a polytope. Finally, note that the word "triangulation" does not necessarily imply that the geometries $X_{i,\geq 0}$ are "triangular" or "simplicial".

2.2.2 Physical vs. spurious boundaries

We now make an important distinction between *physical* and *spurious boundaries*, which correspond to *physical* and *spurious* poles, respectively. This is an important distinction which has important physical consequences for BCFW recursion and the amplituhedron, as discussed in Section 8.3.

Consider a triangulation $\{X_{i,\geq 0}\}$ of a positive geometry $X_{\geq 0}$. The boundary components of $X_{i,\geq 0}$ that are also a subset of boundary components of $X_{\geq 0}$ are called

physical boundaries; otherwise they are called *spurious boundaries*. Furthermore, poles of $\Omega(X_{i,\geq 0})$ at physical boundaries are called *physical poles*, while poles at spurious boundaries are called *spurious poles*. We find that the triangulation independence of the canonical form (2.3) can be interpreted as cancellation of spurious poles, since spurious poles do not appear in the sum.

We now give an example which illustrates a subtle point regarding spurious pole cancellation. While it may be tempting to think that spurious poles cancel *in pairs* along spurious boundaries, this does not occur in general. In fact multiple pieces may be needed to cancel the same pole. For instance, consider a triangle $X_{\geq 0}$ triangulated by three smaller pieces $X_{i,\geq 0}$ as shown in Figure 2.1, but instead of adding all three terms in (2.3), we only add the $i = 1, 2$ terms. Since the triangles 1 and 2 have adjacent boundaries along the line PQ, it may be tempting to think that $\Omega(X, X_{1,\geq 0}) + \Omega(X, X_{2,\geq 0})$ has no pole there. But this is false since the boundary components of 1 and 2 along line PR forms a (signed) triangulation of the line segment QR, whose canonical form is non-vanishing. Pairwise pole cancellation therefore does not occur in this case. Nonetheless, the pole would cancel as a triplet had all three terms been included.

2.3 Maps between positive geometries

We argue that the canonical forms of different positive geometries can be related by considering maps between the geometries. Let $(X, X_{\geq 0})$ and $(Y, Y_{\geq 0})$ be positive geometries of the same dimension D. Furthermore, consider a mermorphic map $\Phi : X \to Y$ with the property that the restriction $\Phi|_{X_{>0}} : X_{>0} \to Y_{>0}$ is a diffeomorphism that preserves orientation. We refer to such maps as *morphisms* between positive geometries, which we denote as $\Phi : (X, X_{\geq 0}) \to (Y, Y_{\geq 0})$. In particular, if

$\Phi : (X, X_{\geq 0}) \to (Y, Y_{\geq 0})$ and $\Psi : (Y, Y_{\geq 0}) \to (Z, Z_{\geq 0})$ are morphisms, then so is $\Pi = \Psi \circ \Phi$.

Morphisms are closely related to pushforwards, which we now explain. Given a map $\Phi : X \to Y$ (not necessarily a morphism) and a differential form ω on X, we obtain a differential form η on Y in the following way. Consider a point $y \in Y$, and all the roots $x \in X$ for which $\Phi(x) = y$. We assume that there are only finitely many such roots. Then for each root x, we locally invert Φ near x and apply the pullback $(\Phi^{-1})^*(\omega(x))$. Finally, we sum the result over all roots:

$$\eta(y) = \sum_{x \,:\, \Phi(x)=y} (\Phi^{-1})^*(\omega(x)) \tag{2.7}$$

This is called the pushforward, which we denote as $\Phi_*(\omega) := \eta$.

We now present an important heuristic.

Heuristic 2.3.1. *Given a morphism $\Phi : (X, X_{\geq 0}) \to (Y, Y_{\geq 0})$ of positive geometries, the pushforward of the canonical form of $(X, X_{\geq 0})$ is the canonical form of $(Y, Y_{\geq 0})$.*

$$\Phi_*(\Omega(X, X_{\geq 0})) = \Omega(Y, Y_{\geq 0}) \tag{2.8}$$

We therefore say that the pushforward preserves the canonical form. The intuition behind the heuristic is the fact that "pushforward commutes with taking residues", formulated precisely in Proposition H1 of [2]. Also in [2], the authors prove the heuristic for a number of non-trivial examples, and more specfically in Section 4 discuss a strategy for proving the most general case.

2.4 Generalized simplices

We now move on to discuss more substantial examples. In each dimension, the simplex is the simplest non-trivial example of a positive geometry. In this section, we

establish a simple generalization of the simplex which encompasses a substantial class of positive geometries. We say that the positive geometry $(X, X_{\geq 0})$ is a *generalized simplex* or that it is *simplex-like* if its canonical form does not vanish anywhere. In particular, the boundary components of a generalized simplex is again a generalized simplex, since the residues of a meromorphic top form with no zeros is again a meromorphic top form with no zeroes. While simplex-like positive geometries do not include all possible positive geometries, they already provide a broad class of interesting examples. We begin by studying the standard simplex before moving on to more examples in later sections.

2.4.1 The standard simplex

The prototypical example of a generalized simplex is the positive geometry $(\mathbb{P}^m, \Delta^m)$, where we denote $\Delta^m := \mathbb{P}^m_{\geq 0}$ as the set of points in $\mathbb{P}^m(\mathbb{R})$ representable by nonnegative coordinates, which can be thought of as a projective simplex (see Section 2.4.2) whose vertices are the standard basis vectors. We refer to Δ^m as the *standard simplex*. The canonical form is given by

$$\Omega(\Delta^m) = \prod_{i=1}^{m} \frac{d\alpha_i}{\alpha_i} = \prod_{i=1}^{m} d\log \alpha_i \tag{2.9}$$

for points $(\alpha_0, \alpha_1, \ldots, \alpha_m) \in \mathbb{P}^m$ where we "gauge-fixed" the zeroth coordinate $\alpha_0 = 1$. Here we can identify the interior of Δ^m with $\mathbb{R}^m_{>0}$. Note that the pole corresponding to the facet at $\alpha_0 \to 0$ does not appear explicitly in the expression, but this is simply due to the "gauge choice" (i.e. choice of chart) $\alpha_0 = 1$. As we will see in many examples, boundary components do not necessarily appear manifestly as poles in every chart, and different choices of chart can make manifest different collections of boundary

components. A gauge-invariant way of writing the same form is the following,

$$\Omega(\Delta^m) = \frac{1}{m!}\frac{\langle \alpha\, d^m\alpha\rangle}{\alpha_0\cdots\alpha_m} \tag{2.10}$$

where the brackets denote the determinant (see Appendix C of [2]). This makes manifest the $(m+1)$ boundary components corresponding to the poles $\alpha_i \to 0$ for $i = 0, \ldots, m$.

We say that a positive geometry $(X, X_{\geq 0})$ of dimension m is Δ-*like* if there exists a *degree one* morphism $\Phi : (\mathbb{P}^m, \Delta^m) \to (X, X_{\geq 0})$. The projective coordinates on Δ^m are called $\Delta-$*like coordinates* of $X_{\geq 0}$. We point out that Δ-like positive geometries are not necessarily simplex-like. Important examples include BCFW cells discussed in Section 8.3. For now, we content ourselves by giving an example of how new zeros can develop under pushforwards.

Example 2.4.1. Consider the rational top-form on $\mathbb{P}^2$, given by

$$\omega = \frac{1}{(x+1)(y+1)}dxdy \tag{2.11}$$

in the chart $\{(1, x, y)\} \subset \mathbb{P}^2$. The form ω has three poles (one of which is the line at infinity), and no zeros. Consider the rational map $\Phi : \mathbb{P}^2 \to \mathbb{P}^2$ given by $(1, x, y) \mapsto (1, u, v) := (1, x, y/x)$. The map Φ has degree one, and using $dy = udv + vdu$ we compute that

$$\Phi_*(\omega) = \frac{u}{(u+1)(uv+1)}dudv \tag{2.12}$$

So a new zero along $u = 0$ has appeared.

2.4.2 Projective simplices

A *projective m-simplex* $(\mathbb{P}^m, \Delta)$ is a positive geometry in $\mathbb{P}^m$ cut out by exactly $m{+}1$ linear inequalities. We use $Y \in \mathbb{P}^m$ to denote a point in projective space with homogeneous components Y^I indexed by $I = 0, 1, \ldots, m$. A linear inequality is of the form $Y \cdot W := Y^I W_I \geq 0$ for some *dual vector* $W \in \mathbb{R}^{m+1}$ with components W_I, and the repeated index I is implicitly summed as usual. A projective simplex can be described as follows:

$$\Delta = \{Y \in \mathbb{P}^m(\mathbb{R}) \mid Y \cdot W_i \geq 0 \text{ for } i = 1, \ldots, m{+}1\} \tag{2.13}$$

where the inequality is evaluated for Y in Euclidean space before mapping to projective space. Here the W_i's are dual vectors corresponding to the *facets* of the simplex. Every boundary of a projective simplex is again a projective simplex, so it is easy to see that projective simplices satisfy the requirements of a positive geometry. For notational purposes, we may sometimes write $Y^I = (1, x, y, \ldots)$ or $Y^I = (x_0, x_1, \ldots, x_m)$ or something similar.

We now give formulae for the canonical form $\Omega(\Delta)$ in terms of both the vertices and the facets of Δ. Let $Z_i \in \mathbb{R}^{m+1}$ denote the vertices for $i = 1, \ldots, m{+}1$, which carry upper indices like Z_i^I. We allow the indices i to be represented mod $m{+}1$. We have

$$\Omega(\Delta) = \frac{s_m \langle Z_1 Z_2 \cdots Z_{m+1} \rangle^m \, \langle Y d^m Y \rangle}{m! \, \langle Y Z_1 \cdots Z_m \rangle \, \langle Y Z_2 \cdots Z_{m+1} \rangle \cdots \langle Y Z_{m+1} \cdots Z_{m-1} \rangle} \tag{2.14}$$

where the angle brackets $\langle \cdots \rangle$ denote the determinant of vectors $\cdots$, which is $SL(m{+}1)$-invariant, and $s_m = -1$ for $m = 1, 5, 9, \ldots$, and $s_m = +1$ otherwise. We also define the following quantity which we call the canonical rational function.

$$\underline{\Omega}(\mathcal{A}) := \Omega(\mathcal{A}) / \langle Y d^m Y \rangle \tag{2.15}$$

Now suppose the vertices are indexed so that the facet W_i is adjacent to $Z_{i+1}, \ldots, Z_{i+m}$, then $W_i \cdot Z_j = 0$ for $j = i{+}1, \ldots, i{+}m$. It follows that

$$W_{iI} = (-1)^{(i-1)(m-i)} \epsilon_{II_1 \cdots I_m} Z_{i+1}^{I_1} \cdots Z_{i+m}^{I_m} \tag{2.16}$$

where the sign is chosen so that $Y \cdot W_i > 0$ for $Y \in \mathrm{Int}(\mathcal{A})$. We can therefore rewrite the canonical form in W space as follows.

$$\Omega(\Delta) = \frac{\langle W_1 W_2 \cdots W_{m+1} \rangle \, \langle Y d^m Y \rangle}{m!(Y \cdot W_1)(Y \cdot W_2) \cdots (Y \cdot W_{m+1})} \tag{2.17}$$

Now we provide a few comments on notation. We often write i for Z_i inside an angle bracket, so for example we may write $\langle i_0 i_1 \cdots i_m \rangle := \langle Z_{i_0} Z_{i_1} \cdots Z_{i_m} \rangle$ and $\langle Y i_1 \cdots i_m \rangle := \langle Y Z_{i_1} \cdots Z_{i_m} \rangle$. Furthermore, the square bracket $[1, 2, \ldots, m{+}1]$ is defined to be the coefficient of $\langle Y d^m Y \rangle$ in (2.14). Thus,

$$[1, 2, \ldots, m{+}1] = \underline{\Omega}(\Delta) \tag{2.18}$$

Note that the square bracket is antisymmetric in exchange of any pair of indices. These conventions are used only in Z space.

Finally, the simplest simplices are the one-dimensional line segments. In comparison with Example 2.1.1, we can think of a line segment $[a, b]$ as a simplex with vertices

$$Z_1^I = (1, a), \quad Z_2^I = (1, b) \tag{2.19}$$

where $a < b$. Applying the Z-space formula (2.14) gives us the canonical form

$$\Omega([a, b]) = -\frac{\langle Z_1 Z_2 \rangle \, \langle Y dY \rangle}{\langle Y Z_1 \rangle \, \langle Y Z_2 \rangle} = \frac{(b-a)dx}{(x-a)(b-x)} \tag{2.20}$$

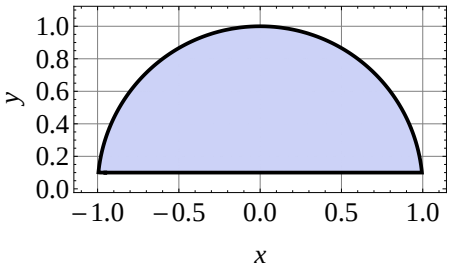

Figure 2.2: A segment of the disk

in agreement with Example 2.1.1.

In Section 2.5.1, we provide an extensive discussion on convex projective polytopes as positive geometries, which can be triangulated by projective simplices.

2.4.3 Generalized simplices on the projective plane

We now give a brief overview of simplex-like positive geometries on the projective plane, and provide some interesting examples. A general argument given in Section 5.3 of [2] shows that every boundary component is either linear or quadratic, under certain technical assumptions such as "normality". This provides a useful constraint on the kinds of examples that are permitted.

Example 2.4.2. Consider a region $\mathcal{S}(a) \subset \mathbb{P}^2(\mathbb{R})$ bounded by one linear function $q(x, y)$ and one quadratic function $f(x, y)$, where $q = y - a \geq 0$ for some constant in the range $-1 < a < 1$, and $f = 1 - x^2 - y^2 \geq 0$. This is a "segment" of the unit disk. A picture for $a = 1/10$ is given in Figure 2.2. We claim that $\mathcal{S}(a)$ is a positive geometry with the following canonical form

$$\Omega(\mathcal{S}(a)) = \frac{2\sqrt{1-a^2}dxdy}{(1-x^2-y^2)(y-a)} \tag{2.21}$$

Note that for the special case of $a = 0$, we get the canonical form for the "northern half disk".

$$\Omega(\mathcal{S}(0)) = \frac{2dxdy}{(1-x^2-y^2)y} \tag{2.22}$$

We prove our result by showing that the form for general a has the correct residues on both boundaries. On the flat boundary we have

$$\text{Res}_{y=a}\Omega(\mathcal{S}(a)) = \frac{2\sqrt{1-a^2}dx}{1-a^2-x^2} = \frac{2\sqrt{1-a^2}dx}{(\sqrt{1-a^2}-x)(x+\sqrt{1-a^2})} \tag{2.23}$$

Recall that this is simply the canonical form on the line segment $|x| \leq \sqrt{1-a^2}$, with positive orientation since the boundary component inherits the counter-clockwise orientation from the interior. The residue on the arc is more subtle. We first rewrite our form as

$$\Omega(\mathcal{S}(a)) = \left(\frac{\sqrt{1-a^2}dy}{x(y-a)}\right)\frac{df}{f} \tag{2.24}$$

which is shown by applying $df = -2(xdx+ydy)$. The residue along the arc is therefore

$$\text{Res}_{f=0}\Omega(\mathcal{S}(a)) = \frac{\sqrt{1-a^2}dy}{x(y-a)} \tag{2.25}$$

Substituting $x = \sqrt{1-y^2}$ for the right-half of the arc gives residue $+1$ at the boundary $y = a$, and substituting $x = -\sqrt{1-y^2}$ for the left-half of the arc gives residue -1.

We can also compute these residues in a different way. Let us parametrize (x, y) by a parameter t as follows.

$$(x, y) = \left(\frac{(t+t^{-1})}{2}, \frac{(t-t^{-1})}{2i}\right) \tag{2.26}$$

which of course satisfies the arc constraint $f(x, y) = 0$ for all t. Rewriting the form on the arc in terms of t gives us

$$\text{Res}_{f=0}\Omega(\mathcal{S}(a)) = \frac{2\sqrt{1-a^2}dt}{t^2 - 2iat - 1} = \frac{(t_+ - t_-)dt}{(t - t_+)(t - t_-)} \tag{2.27}$$

where $t_\pm = ia \pm \sqrt{1-a^2}$ are the two roots of the quadratic expression in the denominator satisfying

$$t_+ + t_- = 2ia, \quad t_+ t_- = -1 \tag{2.28}$$

The corresponding roots $(x_\pm, y_\pm)$ are

$$(x_\pm, y_\pm) = (\pm\sqrt{1-a^2}, a) \tag{2.29}$$

which of course correspond to the boundary points of the arc. The residues at $t_\pm$ and hence $(x_\pm, y_\pm)$ are ± 1, as expected.

By substituting $a = -1$ in the preceding Example 2.4.2 we discover that the unit disk $\mathcal{D}^2 := \mathcal{S}(-1)$ has vanishing canonical form, and is therefore a null geometry. Alternatively, one can derive this by triangulating (see Section 2.2) the unit disk into the northern half disk and the southern half disk, whose canonical forms must add up to $\Omega(\mathcal{D}^2)$. Indeed, a quick computation shows that the canonical forms of the two half disks are negatives of each other. A third argument goes as follows. The only pole of $\Omega(\mathcal{D}^2)$, if any, appears along the unit circle, which has a vanishing canonical form since it has no boundary components. So in fact $\Omega(\mathcal{D}^2)$ has no poles, and must therefore vanish by uniqueness of the form. More generally, a pseudo-positive geometry is a null geometry if and only if all its boundary components are null geometries.

One may be tempted to think that all conic sections are null, but this is not true. Hyperbolas are notable exceptions. From our point of view, the distinction between

hyperbolas and circles is that the former intersects a line at infinity. So a hyperbola has two boundary components, while a circle only has one. We demonstrate this as a special case of the next example.

Example 2.4.3. Let us consider a generic region in $\mathbb{P}^2(\mathbb{R})$ bounded by one quadratic and one linear polynomial. Let us denote the linear polynomial by $q = Y \cdot W \geq 0$ with $Y^I = (1, x, y) \in \mathbb{P}^2(\mathbb{R})$ and the quadratic polynomial by $f = YY \cdot Q := Y^I Y^J Q_{IJ}$ for some real symmetric bilinear form Q_{IJ}. We denote our region as $\mathcal{U}(Q, W)$. The canonical form is given by

$$\Omega(\mathcal{U}(Q, W)) = \frac{\sqrt{QQWW}\langle Y dY dY\rangle}{(YY \cdot Q)(Y \cdot W)} \tag{2.30}$$

where $QQWW := -\frac{1}{2}\epsilon^{IJK}\epsilon^{I'J'K'}Q_{II'}Q_{JJ'}W_K W_{K'}$ and ϵ^{IJK} is the Levi-Civita symbol with $\epsilon^{012} = 1$, and $\langle \cdots \rangle$ denotes the determinant. The appearance of $\sqrt{QQWW}$ ensures that the result is invariant under rescaling Q_{IJ} and W_I independently, which is necessary. It also ensures the correct overall normalization as we show in examples.

It will prove useful to look at this example by putting the line W at infinity $W_I = (1, 0, 0)$ and setting $Y^I = (1, x, y)$, with $YY \cdot Q = y^2 - (x - a)(x - b)$ for $a \neq b$, which describes a hyperbola. The canonical form becomes

$$\Omega(\mathcal{U}(Q, W)) = \frac{2dxdy}{y^2 - (x - a)(x - b)} \tag{2.31}$$

Note that taking the residue on the quadric pole gives us the 1-form on the quadric.

$$\mathrm{Res}_Q \Omega(\mathcal{U}(Q, W)) = dx/y = 2dy/((x - a) + (x - b)) \tag{2.32}$$

Since $a \neq b$, this form is smooth as $y \to 0$ where $x \to a$ or $x \to b$, which is evident in the second expression above. The only singularities of this 1-form are on the line W, which can be seen by reparametrizing the projective space as $(z, w, 1) \sim (1, x, y)$ so

that $z = 1/y, w = x/y$, which gives the 1-form on $1 - (w - az)(w - bz) = 0$:

$$\begin{aligned} \text{Res}_Q \Omega(\mathcal{U}(Q, W)) &= dw - \frac{dz}{z} \\ &= \frac{[(w - az)(-1 + bz) + (w - bz)(-1 + az)]dz}{z((w - az) + (w - bz))} \end{aligned} \tag{2.33}$$

Evidently, there are only two poles $(z, w) = (0, \pm 1)$, which of course are the intersection points of the quadric Q with the line W. The other "pole" in (2.33) is not a real singularity since the residue vanishes.

Note however that as the two roots collide $a \to b$, the quadric degenerates to the product of two lines $(y + x - a)(y - x + a)$ and we get a third singularity at the intersection of the two lines $(x, y) = (a, 0)$.

Note also another degenerate limit here, where the line W is taken to be tangent to the quadric Q. We can take the form in this case to be $(dxdy)/(y^2 - x)$. Taking the residue on the parabola gives us the 1-form dy, that has a double-pole at infinity, which violates our assumptions. This corresponds to the two intersection points of the line W with Q colliding to make W tangent to Q. In fact, we can get rid of the line W all together and find that the parabolic boundary is completely smooth and hence only a null geometry.

Moreover, we can consider the form $(dxdy)/(x^2 + y^2 - 1)$ associated with the interior of a circle. But for the same reason as for the parabola, the circle is actually a null geometry. Despite this, it is of course possible by analytic continuation of the coefficients of a general quadric to go from a circle to a hyperbola which *is* a positive geometry.

Now let us return to the simpler example of the segment $\mathcal{U}(Q,W) := \mathcal{S}(a)$, where

$$Q_{IJ} = \begin{pmatrix} 1 & 0 & 0 \\ 0 & -1 & 0 \\ 0 & 0 & -1 \end{pmatrix}, \quad W_I = (-a, 0, 1) \tag{2.34}$$

Substituting these into the canonical form we find

$$QQWW = (1-a^2) > 0, \quad YY \cdot Q = 1 - x^2 - y^2, \quad Y \cdot W = a - y, \tag{2.35}$$

and therefore

$$\Omega(\mathcal{U}(Q,W)) = \Omega(\mathcal{S}(a)) \tag{2.36}$$

as expected.

2.4.4 An example of a geometry with self-intersections

In this text, we generally exclude geometries with self-intersections for the sake of technical convenience, but there are many such examples that deserve to be studied under a more general context. We now give an example on the projective plane. In Section 5.3.1 of [2], this is referred to as a "non-normal" positive geometry.

Consider the geometry $\mathcal{U}(C) \subset \mathbb{P}^2(\mathbb{R})$ defined by a cubic polynomial $YYY \cdot C \geq 0$, where $YYY \cdot C := C_{IJK} Y^I Y^J Y^K$ for some real symmetric tensor C_{IJK}. The canonical form must have the following form,

$$\Omega(\mathcal{U}(C)) = \frac{C_0 \langle Y dY dY \rangle}{YYY \cdot C} \tag{2.37}$$

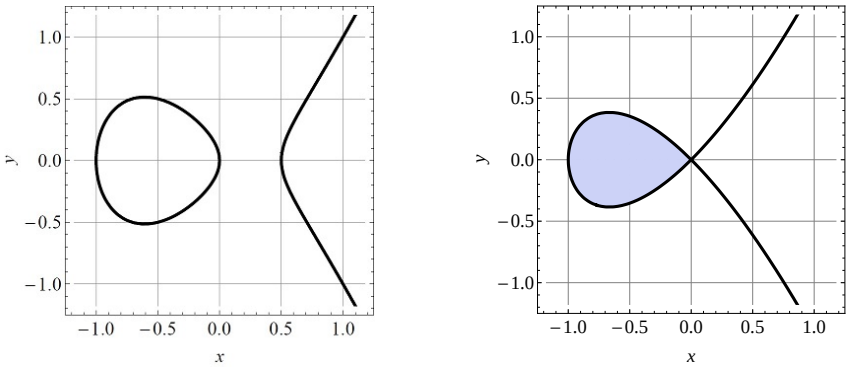

Figure 2.3: (a) A non-degenerate vs. (b) a degenerate elliptic curve. The former does not provide a valid embedding space for a positive geometry, while the shaded "tear-drop" is a valid (non-normal) positive geometry.

where C_0 is a constant needed to ensure that all leading residues are ± 1. Of course, C_0 must scale linearly as C_{IJK} and must depend on the Aronhold invariants. For our purposes we will work out C_0 only in specific examples.

Let us consider a completely generic cubic, which by an appropriate change of variables can always be written as $YYY \cdot C = y^2 - (x-a)(x-b)(x-c)$ for constants a, b, c. If the three constants are distinct, then there is no positive geometry associated with this case because the 1-form obtained by taking a residue on the cubic is dx/y which is the standard holomorphic one-form associated with a *non-degenerate* elliptic curve; we can see directly that dx/y has no singularities as $x \to a, b, c$; and as we go to infinity, we can set $y \to 1/t^3, x \to 1/t^2$ with $t \to 0$ giving $dx/y \to -2dt$ which is smooth. The existence of such a form makes the canonical form non-unique, and hence ill-defined. By extension, no positive geometry can have the non-degenerate cubic as a boundary component either.

However, if the cubic degenerates by having two of the roots of the cubic polynomial in x collide, then we *do* get a beautiful (non-normal) positive geometry, one which has only one zero-dimensional boundary. Without loss of generality let us put the double-root at the origin and consider the cubic $y^2 - x^2(x+a^2)$. Taking the residue on the cubic, we can parametrize $y^2 - x^2(x+a^2) = 0$ as $y = t(t^2-a^2), x = (t^2-a^2)$,

then $dx/y = dt/(t^2 - a^2)$ has logarithmic singularities at $t = \pm a$. Note that these two points correspond to the same point $y = x = 0$ on the cubic! But the boundary is oriented, so we encounter the same logarithmic singularity point from one side and then the other as we go around. We can cover the whole interior of the "teardrop" shape for this singular cubic by taking

$$x = u(t^2 - a^2), \quad y = ut(t^2 - a^2) \tag{2.38}$$

which, for $u \in (0, 1)$ and $t \in (-a, a)$ maps 1-1 to the teardrop interior, dutifully reflected in the form

$$\frac{dxdy}{y^2 - x^2(x + a^2)} = \frac{dt}{(a - t)(t + a)} \frac{du}{u(1 - u)} \tag{2.39}$$

Note that if we *further* take $a \to 0$, we lose the positive geometry as we get a form with a double-pole, much as our example with the parabola in Example 2.4.3.

2.4.5 Generalized simplices in higher-dimensional projective spaces

Let us now consider generalized simplices $(\mathbb{P}^m, \mathcal{A})$ for higher-dimensional projective spaces. Let $(C, C_{\geq 0})$ be a boundary component of $\mathcal{A}$, which is an irreducible *normal* hypersurface in $\mathbb{P}^m$. For $(C, C_{\geq 0})$ to be a positive geometry, C must have no nonzero holomorphic forms. Equivalently, the *geometric genus* of C must be 0. This is the case if and only if C has degree less than or equal to m. Thus in $\mathbb{P}^3$, the boundaries of a positive geometry are linear, quadratic, or cubic hypersurfaces.

It is easy to generalize Example 2.4.2 to simplex-like positive geometries in $\mathbb{P}^m(\mathbb{R})$. Take a positive geometry bounded by $(m-1)$ hyperplanes W_i and a quadric Q, which

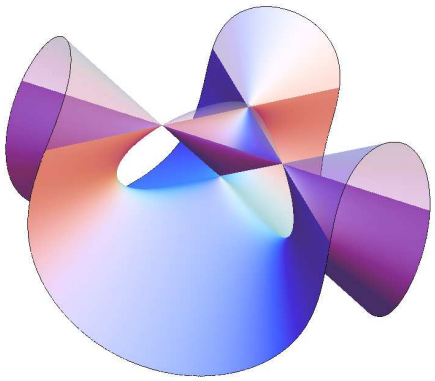

Figure 2.4: The Cayley cubic curve. The plane separating the translucent and solid parts of the surface is given by $x_0 = 0$.

has canonical form

$$\Omega(\mathcal{A}) = \frac{C_0\langle Y d^m Y\rangle}{(Y\cdot W_1)\cdots(Y\cdot W_{m-1})(YY\cdot Q)}. \tag{2.40}$$

for some constant C_0. Note that the $(m-1)$ planes intersect generically on a line, that in turn intersects the quadric at two points, so as in our two-dimensional example this positive geometry has two zero-dimensional boundaries.

Let us consider another generalized simplex, this time in $\mathbb{P}^3(\mathbb{R})$. We take a three-dimensional region $\mathcal{A} \subset \mathbb{P}^3(\mathbb{R})$ bounded by a cubic surface and a plane. If we take a generic cubic surface C and generic plane W whose intersection is a cubic in W, then it cannot contain a positive geometry, as discussed in Section 2.4.3. On the other hand, we can make a special choice of cubic surface C that does give a positive geometry. A pretty example is provided by the "Cayley cubic" (see Figure 2.4). If $Y^I = (x_0, x_1, x_2, x_3)$ are coordinates on $\mathbb{P}^3$, let the cubic C be defined by

$$C\cdot YYY := x_0x_1x_2 + x_1x_2x_3 + x_2x_3x_0 + x_3x_0x_1 = 0 \tag{2.41}$$

which has four singular points at $X_0 = (1,0,0,0), \ldots, X_3 = (0,0,0,1)$. Note that C gives a singular surface, but it still satisfies the normality criterion of a positive geometry. Let us choose three of the singular points, say X_1, X_2, X_3, and let W be the hyperplane passing through these three points; we consider the form

$$\Omega(\mathcal{A}) = C_0 \frac{\langle Y d^3 Y\rangle}{(YYY \cdot C)\langle Y X_1 X_2 X_3\rangle} \tag{2.42}$$

where C_0 is a constant. A natural choice of variables turns this into a "dlog" form. Consider

$$x_i = s y_i, \text{ for } i = 1,2,3; \qquad x_0 = -\frac{y_1 y_2 y_3}{y_1 y_2 + y_2 y_3 + y_3 y_1} \tag{2.43}$$

Then if we group the three y's as coordinates of $\mathbb{P}^2 = \{y = (y_1, y_2, y_3)\}$, we have

$$\Omega(\mathcal{A}) = \frac{\langle y d^2 y\rangle}{2 y_1 y_2 y_3} \frac{ds}{(s-1)} \tag{2.44}$$

This is the canonical form of the positive geometry given by the bounded component of the region cut out by $YYY \cdot C \geq 0$ and $\langle X_1 X_2 X_3 Y\rangle \geq 0$.

We can generalize this construction to $\mathbb{P}^m(\mathbb{R})$, with $Y = (x_0, \cdots, x_m)$ and a degree m hypersurface

$$Q_m \cdot Y^m = \sum_{i=0}^{m} x_0 \cdots \hat{x}_i \cdots x_m,$$

where $Q_m \cdot Y^m := Q_{m I_1 \ldots I_m} Y^{I_1} \cdots Y^{I_m}$ and the singular points are $X_0 = (1, 0, \cdots, 0), \ldots,$ $X_m = (0, \cdots, 0, 1)$. Then if we choose m of these points and a linear factor corresponding to the hyperplane going through them,

$$\Omega(\mathcal{A}) = C_0 \frac{\langle Y d^m Y\rangle}{(Y^m \cdot Q_m)\langle Y X_1 \cdots X_m\rangle} \tag{2.45}$$

is the canonical form associated with the bounded component of the positive geometry cut out by $Y^m \cdot Q_m \geq 0, \langle X_1 \cdots X_m Y\rangle \geq 0$, for some constant C_0.

2.4.6 Grassmannians and positivity

We begin by reviewing the *positroid stratifiction* of the positive Grassmannian. Much like how a polytope is made up of boundaries of all codimensions, the positive Grassmannian is made up of boundaries called *positroid cells*. In this section, we show that every positroid cell is a simplex-like positive geometry whose complex embedding space is a *positroid variety*.

Let $G(k,n)$ denote the Grassmannian of k-dimensional linear subspaces of $\mathbb{C}^n$. We can represent every point in $G(k,n)$ as a $k \times n$ complex matrix

$$C = (C_1, C_2, \ldots, C_n) \tag{2.46}$$

of maximal rank, where $C_i \in \mathbb{C}^k$ denote column vectors; moreover the corresponding subspace is obtained by taking the span of the rows, hence two such matrices are equivalent if and only if they are related by a $\mathrm{GL}(k)$ action from the left. Given $C \in G(k,n)$ we define a function f by the condition that

$$C_i \in \mathrm{span}\left\{C_{i+1}, C_{i+2}, \ldots, C_{f(i)}\right\} \tag{2.47}$$

and $f(i)$ is the minimal index satisfying this property. In particular, if $C_i = 0$, then $f(i) = i$. Here, the indices are taken mod n. The function f is called an *affine permutation*, or *decorated permutation*, or sometimes just *permutation* [30, 31, 16]. Classifying points of $G(k,n)$ according to the affine permutation f gives the positroid stratification

$$G(k,n) = \bigsqcup_f \mathring{\Pi}_f. \tag{2.48}$$

where, for every affine permutation f, the set $\mathring{\Pi}_f$ consists of those C matrices satisfying (2.47) for every integer i. We let the *positroid variety* $\Pi_f \subset G(k,n)$ be the

closure of $\mathring{\Pi}_f$. If $k = 1$ then $G(k, n) \cong \mathbb{P}^{n-1}$ and the stratification (2.48) decomposes $\mathbb{P}^{n-1}$ into coordinate hyperspaces.

Now let $G(k, n)(\mathbb{R})$ denote the real Grassmannian. The *(totally) nonnegative Grassmannian* $G_{\geq 0}(k, n)$ (resp. *(totally) positive Grassmannian* $G_{>0}(k, n)$) consists of those points $C \in G(k, n)(\mathbb{R})$ all of whose $k \times k$ minors, called Plücker coordinates, are nonnegative (resp. positive) [30]. The intersections

$$\Pi_{f,>0} := G_{\geq 0} \cap \mathring{\Pi}_f, \qquad \Pi_{f,\geq 0} := G_{\geq 0} \cap \Pi_f \tag{2.49}$$

are loosely called (open and closed) *positroid cells*.

For any permutation f, we have

$$(\Pi_f, \Pi_{f,\geq 0}) \text{ is a positive geometry.} \tag{2.50}$$

The boundary components of $(\Pi_f, \Pi_{f,\geq 0})$ are certain other positroid cells $(\Pi_g, \Pi_{g,\geq 0})$ of one lower dimension. The canonical form $\Omega(f) := \Omega(\Pi_f, \Pi_{f,\geq 0})$ was studied in [31, 16]. We remark that $\Omega(f)$ has no zeros, so $(\Pi_f, \Pi_{f,\geq 0})$ is simplex-like.

The canonical form $\Omega(G_{\geq 0}(k, n))$ of the positive Grassmannian was worked out and discussed in [16],

$$\Omega(G_{\geq 0}(k, n)) := \frac{\prod_{s=1}^{k} \langle C' d^{n-k} C'_s \rangle}{((n-k)!)^k \prod_{i=1}^{n} (i, i+1, \ldots, i+k-1)} \tag{2.51}$$

where $C := (C'_1, \ldots, C'_k)^T$ is a $k \times n$ matrix representing a point in $G(k, n)$, and the bracket $(i_1, i_2, \ldots, i_k)$ denotes the $k \times k$ minor of C corresponding to columns $i_1, i_2, \ldots, i_k$ in that order. Note that the C'_s denote row vectors of C. The canonical forms $\Omega(f)$ on Π_f are obtained by iteratively taking residues of $\Omega(G_{\geq 0}(k, n))$.

The Grassmannian $G(k, n)$ has the structure of a cluster variety [32]. The cluster coordinates of $G(k, n)$ can be constructed using plabic graphs or on-shell diagrams.

Given a sequence of *cluster coordinates* $(c_0, c_1, \ldots, c_{k(n-k)}) \in \mathbb{P}^{k(n-k)}$ for the Grassmannian $G(k,n)$, the positive Grassmannian is precisely the subset of points representable by positive coordinates. It follows that $G_{\geq}(k,n)$ is Δ-like with the degree-one cluster coordinate morphism $\Phi : (\mathbb{P}^{k(n-k)}, \Delta^{k(n-k)}) \to (G(k,n), G_{\geq 0}(k,n))$. Note of course that a different degree-one morphism exists for each choice of cluster.

According to Heuristic 2.3.1, we expect that the canonical form on the positive Grassmannian is simply the pushforward of $\Omega(\Delta^{k(n-k)})$. That is,

$$\Omega(G_{\geq 0}(k,n)) = \pm \Phi_* \left(\frac{\langle c\, d^{k(n-k)} c \rangle}{(k(n-k))! \prod_{I=0}^{k(n-k)} c_I} \right) \tag{2.52}$$

where the overall sign depends on the ordering of the cluster coordinates. Equation (2.52) is worked out in [33]. It follows in particular that the right hand side of (2.52) is independent of the choice of cluster.

2.5 Generalized polytopes

In this section we investigate the much richer class of *generalized polytopes*, or *polytope-like* geometries, which are positive geometries whose canonical form may have zeros.

2.5.1 Projective polytopes

The fundamental example is a convex polytope embedded in projective space. Most of our notation was already established back in Section 2.4.2. Let $Z_1, Z_2, \ldots, Z_n \in \mathbb{R}^{m+1}$, and denote by Z the $n \times (m+1)$ matrix whose rows are given by the Z_i. Define $\mathcal{A} := \mathcal{A}(Z) := \mathcal{A}(Z_1, Z_2, \ldots, Z_n) \subset \mathbb{P}^m(\mathbb{R})$ to be the convex hull

$$\mathcal{A} = \mathrm{Conv}(Z) = \mathrm{Conv}(Z_1, \ldots, Z_n) := \left\{ \sum_{i=1}^{n} C_i Z_i \in \mathbb{P}^m(\mathbb{R}) \mid C_i \geq 0, i = 1, \ldots, n \right\} \tag{2.53}$$

We make the assumption that $Z_1, \ldots, Z_n$ are all vertices of $\mathcal{A}$. In (2.53), the vector $\sum_{i=1}^n C_i Z_i \in \mathbb{R}^{m+1}$ is thought of as a point in the projective space $\mathbb{P}^m(\mathbb{R})$. The polytope $\mathcal{A}$ is well-defined if and only if $\sum_{i=1}^n C_i Z_i$ is never equal to 0 unless $C_i = 0$ for all i. A basic result, known as "Gordan's theorem" [34], states that this is equivalent to the following condition.

$$\text{There exists a (dual) vector } X \in \mathbb{R}^{m+1} \text{ such that } Z_i \cdot X > 0 \text{ for } i = 1, 2, \ldots, n \tag{2.54}$$

The polytope $\mathcal{A}$ is called a convex *projective polytope*.

Every projective polytope $(\mathbb{P}^m, \mathcal{A})$ is a positive geometry. This follows from the fact that every polytope $\mathcal{A}$ can be triangulated (see Section 2.2) by projective simplices. By Section 2.4.2, we know that every simplex is a positive geometry, so by the arguments in Section 2.2 we conclude that $(\mathbb{P}^m, \mathcal{A})$ is a positive geometry. The canonical form $\Omega(\mathcal{A})$ of a projective polytope will be discussed in further detail from multiple points of view in Section 3.

It is clear that the polytope $\mathcal{A}$ is unchanged if each Z_i is replaced by a positive multiple of itself. This gives an action of the little group $\mathbb{R}^n_{>0}$ on Z that fixes $\mathcal{A}$. To visualize a polytope, it is often convenient to work with *Euclidean polytopes* instead of projective polytopes. To do so, we use the little group to "gauge fix" the first component of Z to be equal to 1 (if possible), so that $Z = (1, Z')$ where $Z' \in \mathbb{R}^m$. The polytope $\mathcal{A} \subset \mathbb{P}^m$ can then be identified with the set

$$\left\{ \sum_{i=1}^n C_i Z_i' \subset \mathbb{R}^m \mid C_i \geq 0, i = 1, \ldots, n \text{ and } C_1 + C_2 + \cdots + C_n = 1 \right\} \tag{2.55}$$

inside Euclidean space $\mathbb{R}^m$. The C_i variables in this instance can be thought of as center-of-mass weights. Points in projective space for which the first component is zero lie on the $(m-1)$-plane at infinity.

The points $Z_1, \ldots, Z_n$ can be collected into a $n \times (m+1)$ matrix Z, which can be thought of as a linear map $Z : \mathbb{R}^n \to \mathbb{R}^{m+1}$ or a rational map $Z : \mathbb{P}^{n-1} \to \mathbb{P}^m$. The polytope $\mathcal{A}$ is then the image $Z(\Delta^{n-1})$ of the standard $(n-1)$-dimensional simplex in $\mathbb{P}^{n-1}(\mathbb{R})$.

2.5.2 Cyclic polytopes

We call the point configuration $Z_1, Z_2, \ldots, Z_n$ *positive* if $n \geq m+1$, and all the $(m+1) \times (m+1)$ *ordered* minors of the matrix Z are strictly positive. Positive Z always satisfy condition (2.54). In this case, the polytope $\mathcal{A}$ is known as a *cyclic polytope*. For notational convenience, we identify $Z_{i+n} := Z_i$, so the vertex index is represented mod n.

For even m, the facets of the cyclic polytope are

$$\mathrm{Conv}(Z_{i_1-1}, Z_{i_1}, \ldots, Z_{i_{m/2}-1}, Z_{i_{m/2}}) \tag{2.56}$$

for $1 \leq i_1-1 < i_1 < i_2-1 < i_2 < \cdots < i_{m/2}-1 < i_{m/2} \leq n+1$. For odd m, the facets are

$$\mathrm{Conv}(Z_1, Z_{i_1-1}, Z_{i_1}, \ldots, Z_{i_{(m-1)/2}-1}, Z_{i_{(m-1)/2}}) \tag{2.57}$$

for $2 \leq i_1-1 < i_1 < i_2-1 < i_2 < \cdots < i_{(m-1)/2}-1 < i_{(m-1)/2} \leq n$ and

$$\mathrm{Conv}(Z_{i_1-1}, Z_{i_1}, \ldots, Z_{i_{(m-1)/2}-1}, Z_{i_{(m-1)/2}}, Z_n) \tag{2.58}$$

for $1 \leq i_1-1 < i_1 < i_2-1 < i_2 < \cdots < i_{(m-1)/2}-1 < i_{(m-1)/2} \leq n-1$. This description of the facets is commonly known as *Gale's evenness criterion* [34].

An important example for the physics of scattering amplitudes in planar $\mathcal{N} = 4$ super Yang-Mills theory is the $m = 4$ cyclic polytope which has boundaries:

$$\text{Conv}(Z_{i-1}, Z_i, Z_{j-1}, Z_j) \tag{2.59}$$

for $1 \leq i{-}1 < i < j{-}1 < j \leq n{+}1$. The physical applications are explained in Section 7.1.

2.5.3 Dual polytopes

Let $(\mathbb{P}^m, \mathcal{A})$ be a convex polytope and let $Y \in \mathbb{P}^m(\mathbb{R})$ be a point away from any boundary component. We now define the *dual of* $\mathcal{A}$ *at* Y, denoted $\mathcal{A}_Y^*$, which is a convex polytope in the linear dual of $\mathbb{P}^m$ (also denoted $\mathbb{P}^m$). For the moment let us "de-projectivize" Y so that $Y \in \mathbb{R}^{m+1}$.

Recall that each facet of $\mathcal{A}$ is given by the zero-set (along $\partial\mathcal{A}$) of some dual vector $W \in \mathbb{R}^{m+1}$. Before going to projective space, we pick the overall sign of W so that $W \cdot Y > 0$ for our Y. We say that the facets are *oriented relative to* Y. Now assume that the facets of $\mathcal{A}$ are given by $W_1, \ldots, W_r$. Then we define the dual.

$$\mathcal{A}_Y^* := \text{Conv}(W_1, \ldots, W_r) := \left\{ \sum_{j=1}^{r} C_j W_j \in \mathbb{P}^m \mid C_j \geq 0, j = 1, \ldots, r \right\} \tag{2.60}$$

Not that the (relative) signs of the W_j's are crucial, hence so is the position of Y relative to the facets. It should be obvious that $(\mathbb{P}^m, \mathcal{A}_Y^*)$ is a positive geometry for each Y.

In the special case where $Y \in \text{Int}(\mathcal{A})$, we let $\mathcal{A}^* := \mathcal{A}_Y^*$ and refer to this simply as the *dual of* $\mathcal{A}$. An equivalent definition of the dual of $\mathcal{A}$ is:

$$\mathcal{A}^* = \{W \in \mathbb{P}^m \mid W \cdot Y \geq 0 \text{ for all } Y \in \mathcal{A}\}. \tag{2.61}$$

A priori, the inequality $W \cdot Y \geq 0$ may not make sense when W and Y are projective. As in (2.60), we give it precise meaning by working first in $\mathbb{R}^{m+1}$, and then taking the images in $\mathbb{P}^m$ (see also Appendix C of [2] on cones). For generic Y, we also wish to assign an orientation to $\mathcal{A}_Y^*$ as follows. Suppose we orient the facets $W_1, \ldots, W_r$ relative to the *interior* of $\mathcal{A}$. Let s denote the number of terms $W_j \cdot Y$ that are negative. Then we orient $\mathcal{A}_Y^*$ based on the parity of s. In particular, the dual for $Y \in \mathrm{Int}(\mathcal{A})$ is positively oriented.

An important observation about the dual polytope $\mathcal{A}_Y^*$ is that it has "opposite" combinatorics to $\mathcal{A}$. In other words, vertices of $\mathcal{A}$ correspond to the facets of $\mathcal{A}_Y^*$ and vice versa. Since we assumed that $\mathcal{A}$ has n vertices $Z_1, Z_2, \ldots, Z_n$, the dual polytope $\mathcal{A}_Y^*$ has n facets corresponding to $\{W \mid W \cdot Z_i = 0\}$ for $i = 1, 2, \ldots, n$. Suppose a facet of $\mathcal{A}$ is adjacent to vertices $Z_{i_1}, \ldots, Z_{i_m}$, then the dual vertex W satisfies $W \cdot Z_{i_1} = \ldots = W \cdot Z_{i_m} = 0$ so that

$$W_I = \epsilon_{II_1 \ldots I_m} Z_{i_1}^{I_1} \ldots Z_{i_m}^{I_m} \tag{2.62}$$

where we have ordered the vertices so that $Y \cdot W > 0$. This is a straightforward generalization of (2.16). Sometimes we also write

$$W = (i_1 \ldots i_m) \tag{2.63}$$

to denote the same quantity. Applying this to Section 2.5.2 gives us all the vertices of the polytope dual to a cyclic polytope.

Finally we make a comment on triangulations. Given a *signed* triangulation $\mathcal{A} = \sum_i \mathcal{A}_i$ of a convex polytope $\mathcal{A}$ by other convex polytopes $\mathcal{A}_i$ (see Sections 2.2), and a point Y not along any boundary component, we have

$$\mathcal{A} = \sum_i \mathcal{A}_i \quad \Rightarrow \quad \mathcal{A}_Y^* = \sum_i \mathcal{A}_{iY}^* \tag{2.64}$$

In words, we say that

$$\text{Dualization of polytopes “commutes” with triangulation.} \tag{2.65}$$

This is a crucial geometric phenomenon to which we will return. While we do not provide a direct geometric proof, we will argue its equivalence to the triangulation independence of the canonical form and the existence of a volume interpretion for the form in Section 3.4.1.

2.5.4 Generalized polytopes on the projective plane

Let us now discuss a class of positive geometries in $\mathbb{P}^2$ which includes Examples 2.4.2 and 2.4.3. Let $C \subset \mathbb{R}^2$ be a closed curve that is piecewise linear or quadratic. Thus C is the union of curves $C_1, C_2, \ldots, C_r$ where each C_i is either a line segment, or a closed piece of a conic. We assume that C has no self-intersections, and let $\mathcal{U} \subset \mathbb{R}^2$ be the closed region enclosed by C. We will further assume that $\mathcal{U}$ is a convex set. Define the degree $d(\mathcal{U})$ of $\mathcal{U}$ to be the sum of the degrees of the C_i.

We now argue that if $d \geq 3$,

$$(\mathbb{P}^2, \mathcal{U}) \text{ is a positive geometry.} \tag{2.66}$$

We will proceed by induction on $d = d(\mathcal{U})$. For the base case $d = 3$, there are two possibilities: (a) $\mathcal{U}$ is a triangle, or (b) $\mathcal{U}$ is a convex region enclosed by a line and a conic. For case (a), $\Omega(\mathcal{U})$ was discussed in Section 2.4.2. For case (b), $\Omega(\mathcal{U})$ was studied in Example 2.4.3. In both cases, $(\mathbb{P}^2, \mathcal{U})$ is a positive geometry. Now suppose that $d(\mathcal{U}) = d \geq 4$ and that one of the C_i is a conic. Let L be the line segment joining the endpoints of C_i. By convexity, L lies completely within $\mathcal{U}$, and thus decomposes $\mathcal{U}$ into the union $\mathcal{U} = \mathcal{U}_1 \cup \mathcal{U}_2$ of two regions where $\mathcal{U}_1$ has C_i and L as its “sides”, while $\mathcal{U}_2$ satisfies the same conditions as $\mathcal{U}$, but has more linear sides. In other words,

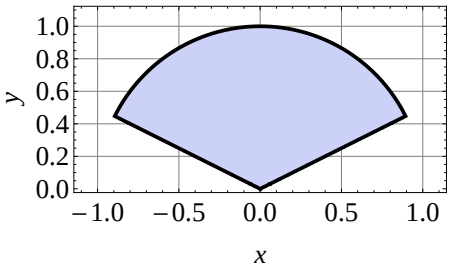

Figure 2.5: A pizza slice

$\mathcal{U}$ is triangulated by $\mathcal{U}_{1,2}$, and by the discussion in Section 2.2, $\mathcal{U}$ is a pseudo-positive geometry with $\Omega(\mathcal{U}) = \Omega(\mathcal{U}_1)+\Omega(\mathcal{U}_2)$. In addition, we argue that $\mathcal{U}$ must be a positive geometry, since all its boundary components (line segments on the projective line) are positive geometries. If none of the C_i is a conic, then $\mathcal{U}$ is a convex polygon in $\mathbb{R}^2$. We can slice off a triangle and repeat the same argument.

Let us explicitly work out a simple example defined by two linear boundaries and one quadratic: a "pizza" slice.

Example 2.5.1. Consider a "pizza" shaped geometry; that is, a sector $\mathcal{T}(\theta_1, \theta_2)$ of the unit circle between polar angles θ_1, θ_2, which is bounded by two linear equations $q_1 = -x\sin\theta_1 + y\cos\theta_1 \geq 0$ and $q_2 = x\sin\theta_2 - y\cos\theta_2 \geq 0$, and an arc $f = 1-x^2-y^2 \geq 0$. Let us assume for simplicity of visualization that $0 \leq \theta_1 < \theta_2 \leq \pi$. See Figure 2.5 for a picture for the case $(\theta_1, \theta_2) = (\pi/6, 5\pi/6)$.

The canonical form is given by

$$\Omega(\mathcal{T}(\theta_1, \theta_2)) = \frac{[\sin(\theta_2 - \theta_1) + (-x\sin\theta_1 + y\cos\theta_1) + (x\sin\theta_2 - y\cos\theta_2)]}{(1 - x^2 - y^2)(-x\sin\theta_1 + y\cos\theta_1)(x\sin\theta_2 - y\cos\theta_2)} dxdy \tag{2.67}$$

Let us take the residue along the linear boundary $q_1 = 0$ via the limit $x \to y\cot\theta_1$, and confirm that the result is the canonical form on the corresponding boundary component. We get

$$\mathrm{Res}_{q_1=0}\Omega(\mathcal{T}(\theta_1, \theta_2)) = \frac{(\sin\theta_1)}{(\sin\theta_1 - y)y} dy \tag{2.68}$$

which is the canonical form on the line segment $y \in [0, \sin\theta_1]$ with positive orientation. The upper bound $y < \sin\theta_1$ is simply the vertical height of the boundary $q_1 = 0$. Similarly, the residue at $q_2 = 0$ is given by

$$\mathrm{Res}_{q_2=0}\Omega(\mathcal{T}(\theta_1, \theta_2)) = -\frac{(\sin\theta_2)}{(\sin\theta_2 - y)y}dy \tag{2.69}$$

which is the canonical form on the line segment $y \in [0, \sin\theta_2]$, again with negative orientation. The residue along the arc can be computed in a similar manner as for the segment of the disk in Example 2.4.2, so we leave this as an exercise for the reader.

For $\theta_1 = 0, \theta_2 = \pi$, we are reduced to the northern half disk from Example 2.4.2, so $\mathcal{T}(0, \pi) = \mathcal{S}(0)$. A quick substitution shows that the canonical forms match as well.

2.5.5 Loop Grassmannians

We now define the *L-loop Grassmannian* $G(k, n; \underline{k})$, where $\underline{k} := (k_1, \ldots, k_L)$ is a sequence of positive integers. A point V in the L-loop Grassmannian $G(k, n; \underline{k})$ is a collection of linear subspaces $V_S \subset \mathbb{C}^n$ indexed by S, where $S := \{s_1, \ldots, s_l\}$ is any subset of $\{1, 2, \ldots, L\}$ for which $k_S := k_{s_1} + \ldots + k_{s_L} \leq n - k$. Moreover, we require that $\dim V_S = k + k_S$, and $V_S \subset V_{S'}$ whenever $S \subset S'$. For simplicity we sometimes write $V_i = V_{\{i\}}, V_{ij} = V_{\{i,j\}}$, and so on and so forth. In particular, $V_\emptyset \subset V_s$ for any one-element set $S = \{s\}$.

We say that a point $V \in G(k, n; \underline{k})$ is "generic" if $V_i \cap V_j = V_\emptyset$ for any $i \neq j$. For such points, we have $V_S = \mathrm{span}(V_{s_1}, V_{s_2}, \ldots, V_{s_\ell})$ for any $S = \{s_1, s_2, \ldots, s_\ell\}$, so that V is determined completely by $V_1, V_2, \ldots, V_L$. The space $G(k, n; \underline{k})$ is naturally a subvariety of a product of Grassmannians, and in particular it is a projective variety.

If $L = 0$, then the 0-loop Grassmannian reduces to the usual Grassmannian $G(k, n)$. If $L = 1$, the 1-loop Grassmannian reduces to the partial flag variety

$\mathrm{Fl}(n; k, k+k_1)$ (see Section 5.8 of [2]). We may refer to the 0-loop Grassmannian as the *tree Grassmannian*. The distinction between "trees" and "loops" comes from the terminology of scattering amplitudes. We caution that "loop Grassmannian" commonly refers to another infinite dimensional space in the mathematical literature, which is also called the affine Grassmannian.

We now define the positive part $G_{>0}(k, n; \underline{k})$ of $G(k, n; \underline{k})$. Consider the set of $(k+K) \times n$ matrices $M(k+K, n)$, where $K := k_1 + \ldots + k_L$. We will denote each matrix as follows:

$$P := \begin{pmatrix} C \\ D_1 \\ \cdots \\ D_L \end{pmatrix} \tag{2.70}$$

where C has k rows, and D_i has k_i rows for $i = 1, \ldots, L$. We say that P is *positive* if for each $S = \{s_1, s_2, \ldots, s_\ell\}$ the matrix formed by taking the rows of $C, D_{s_1}, D_{s_2}, \ldots, D_{s_\ell}$ is positive, that is, has positive $(k + k_S) \times (k + k_S)$ minors. Each positive matrix P gives a point $V \in G(k, n; \underline{k})$, where V_S is the span of the rows of $C, D_{s_1}, D_{s_2}, \ldots, D_{s_\ell}$. Two points $P_{1,2}$ are equivalent if they map to the same point V. Each equivalence class defines a point on the (strictly) positive part $G_{>0}(k, n; \underline{k})$. The nonnegative part $G_{\geq 0}(k, n; \underline{k})$ is the closure of $G_{>0}(k, n; \underline{k})$ in $G(k, n; \underline{k})(\mathbb{R})$.

There exists a subgroup $\mathcal{G}(k; \underline{k})$ of $\mathrm{GL}(k+K)$ acting on the left whose orbits in $M(k+K, n)$ are equivalence classes of matrices P defining the same point V. Elements of $\mathcal{G}(k; \underline{k})$ allow row operations within each of C, or the D_i, and also allows adding rows of C to each D_i.

We caution that not every point $V \in G(k, n; \underline{k})$ is representable by a matrix P. For example, for $G(0, 3; 1, 1)$, the P matrix is a 2×3 matrix. Consider a point on the boundary where the two rows of P are scalar multiples of each other, then $V_1 = V_2$

and additional information is required to specify the 2-plane $V_{1,2}$. So there are even points in the boundary of $G_{\geq 0}(k,n;\underline{k})$ that cannot be represented by P.

Let us focus our attention on the L-loop Grassmannian $G(k,n;\ell^L)$ where $l^L := (l,\ldots,l)$ with l appearing L times. The case $l=2$ is the case of primary physical interest. The L-loop Grassmannian $G(k,n;l^L)$ has an action of the symmetric group S_L on the set $\{1,2,\ldots,L\}$ with L elements. For a permutation $\sigma \in S_L$, we have $\sigma(V)_S = V_{\sigma(S)}$. In addition, when l is even, the action of S_L on $G(k,n;l^L)$ preserves the positive part: permuting the blocks D_i of the matrix P preserves the positivity conditions.

The L-loop Grassmannian $G(k,n;\underline{k})$ is still very poorly understood in full generality. For instance, a complete stratification extending the positroid stratification of the positive Grassmannian is still unknown. The existence of the canonical form is also unknown. Nonetheless, we have identified the canonical form for some $L=1$ cases, which we discuss in Section 10.1, and some $L=2$ cases.

The proven existence of some $L=1$ canonical forms is highly non-trivial. We therefore speculate that

$$(G(k,n;\underline{k}), G_{\geq 0}(k,n;\underline{k})) \text{ is a positive geometry.} \tag{2.71}$$

Note that for even ℓ, the speculative positive geometry $G(k,n;\ell^L)$ should have an action of S_L: the symmetric group acts on the boundary components, and furthermore the canonical form will be invariant under S_L.

We may also denote a generic point in the loop Grassmannian as

$$\mathcal{Y} = (Y, Y_1, \ldots, Y_L) \tag{2.72}$$

where $V_S = \text{span}\{Y, Y_{s_1}, \ldots, Y_{s_l}\}$ for any S. Or, for $\underline{k} = 2^L$ we may use various kinds of notation like $(Y, (AB)_1, \ldots, (AB)_L)$ or $(Y, AB, CD, EF, \ldots)$, which are common in the physics literature.

Example 2.5.2. Consider the space $G(0, 4; 2^2)$ which is isomorphic to the "double Grassmannian" $(G(2, 4) \times G(2, 4))$, and has an action of the symmetric group S_2. Let $(C_1, C_2) \in G(2, 4)^2$ denote a point in the space, with both C_1 and C_2 thought of as 2×4 matrices modded out by GL(2) from the left. The interior of the positive geometry is given by the following points in matrix form.

$$(G(2,4)^2)_{>0} := \{(C_1, C_2) \ : \ C_1, C_2 \in G_{>0}(2,4) \text{ and } \det \begin{pmatrix} C_1 \\ C_2 \end{pmatrix} > 0\} \tag{2.73}$$

In other words, both C_1, C_2 are in the positive Grassmannian, and their combined 4×4 matrix (i.e. the two rows of C_1 stacked on top of the two rows of C_2) has positive determinant.

We can parametrize the interior with eight variables as follows:

$$\begin{pmatrix} C_1 \\ C_2 \end{pmatrix} = \begin{pmatrix} 1 & x_1 & 0 & -w_1 \\ 0 & y_1 & 1 & z_1 \\ 1 & x_2 & 0 & -w_2 \\ 0 & y_2 & 1 & z_2 \end{pmatrix} \tag{2.74}$$

The conditions $C_1, C_2 \in G_{>0}(2, 4)$ impose that all eight variables be positive, while the final condition requires

$$\det \begin{pmatrix} C_1 \\ C_2 \end{pmatrix} = -(x_1 - x_2)(z_1 - z_2) - (y_1 - y_2)(w_1 - w_2) > 0 \tag{2.75}$$

The canonical form can be computed by a triangulation argument given in [26].

$$\Omega((G(2,4)^2)_{\geq 0}) = \frac{dx_1 dy_1 dz_1 dw_1 dx_2 dy_2 dz_2 dw_2 (x_1 z_2 + x_2 z_1 + y_1 w_2 + y_2 w_1)}{x_1 x_2 y_1 y_2 z_1 z_2 w_1 w_2 [(x_1 - x_2)(z_1 - z_2) + (y_1 - y_2)(w_1 - w_2)]} \quad (2.76)$$

The 9 poles appearing in the denominator account for the boundaries defined by the 9 inequalities. Note that the form is symmetric under exchanging $1 \leftrightarrow 2$, as expected from the action of S_2.

Let us illustrate the simple method by which this result is obtained by looking at a smaller example: a 4-dimensional boundary where $y_{1,2} = w_{1,2} = 0$. The geometry is then simply given by

$$x_{1,2} > 0, z_{1,2} > 0, \ (x_1 - x_2)(z_1 - z_2) < 0 \quad (2.77)$$

But this can clearly be triangulated (see Section 2.2) in two pieces. We either have $z_1 > z_2 > 0$ and $x_1 < x_2$, or vice-versa. For instance we can trivially parametrize the region $z_1 > z_2 > 0$ by writing $z_2 = a, z_1 = a + b$ with $a > 0, b > 0$ and so the form is $da\ db/ab = dz_2 dz_1 / z_2(z_1 - z_2)$. Thus the full form is

$$dx_1 dx_2 dz_2 dz_2 \ \times \ \left(\frac{1}{z_2(z_1 - z_2)} \frac{1}{x_1(x_2 - x_1)} + \frac{1}{z_1(z_2 - z_1)} \frac{1}{x_2(x_1 - x_2)} \right) \quad (2.78)$$

$$= \ \frac{dx_1 dx_2 dz_1 dz_2 (x_2 z_1 + x_1 z_2)}{x_1 x_2 z_1 z_2 (x_2 - x_1)(z_1 - z_2)}. \quad (2.79)$$

which of course can be obtained from (2.76) by taking residues at the corresponding boundaries.

Chapter 3

Canonical forms

The main purpose of this section is to establish a list of methods and strategies for computing the canonical form of positive geometries. A summary of the main methods is given below.

- **Direct construction from poles and zeros**: We propose an ansatz for the canonical form as a rational function and impose appropriate constraints from poles and zeros.
- **Triangulations**: We triangulate a generalized polytope by generalized simplices and sum the canonical form of each piece.
- **Pushforwards**: We find morphisms from simpler positive geometries to more complicated ones, and apply the pushforward via Heuristic 2.3.1.
- **Integral representations**: We find expressions for the canonical form as a volume integral over a "dual" geometry, or as a contour integral over a related geometry.

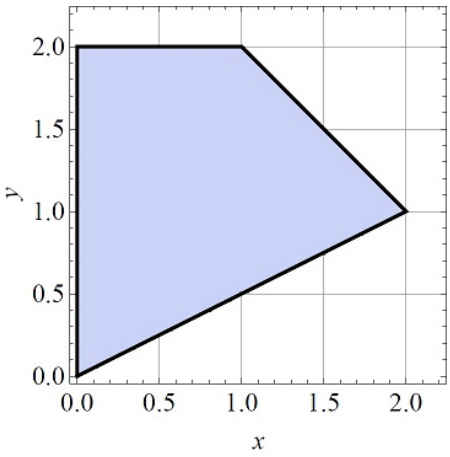

Figure 3.1: A quadrilateral

3.1 Direct construction from poles and zeros

Suppose $\mathcal{A}$ is defined by homogeneous polynomial inequalities $q_i(Y) \geq 0$ indexed by i for $Y \in \mathbb{P}^m$. Then an ansatz for the canonical form is the following:

$$\Omega(\mathcal{A}) = \frac{q(Y)\,\langle Y d^m Y\rangle}{\prod_i q_i(Y)} \tag{3.1}$$

for some homogeneous polynomial $q(Y)$ in the numerator which must satisfy:

$$\deg q = \sum_i \deg q_i - m - 1 \tag{3.2}$$

so that the form is invariant under *local* GL(1) action $Y \to \alpha(Y)Y$. The method of *undetermined numerator* is the idea that the numerator can be solved by imposing residue constraints. Note that this method operates under the *assumption* that a solution to the numerator exists, which in most cases is a non-trivial fact. We illustrate the idea with a few simple examples below.

Example 3.1.1. Consider the quadrilateral $\mathcal{A} := \mathcal{A}(Z_1, Z_2, Z_3, Z_4)$ in $\mathbb{P}^2(\mathbb{R})$ with facets given by the four inequalities $q_1 = x \geq 0,\ q_2 = 2y - x \geq 0,\ q_3 = 3 - x - y \geq 0,\ q_4 =$

$2 - y \geq 0$. The picture is given in Figure 3.1, and the vertices are

$$Z_1^I = (1,0,0), \quad Z_2^I = (1,2,1), \quad Z_3^I = (1,1,2), \quad Z_4^I = (1,0,2) \tag{3.3}$$

with $(1, x, y) \in \mathbb{P}^2(\mathbb{R})$ as usual.

We will derive the canonical form with the following ansatz.

$$\Omega(\mathcal{A}) = \frac{(A + Bx + Cy)dxdy}{x(2y - x)(3 - x - y)(2 - y)} \tag{3.4}$$

for undetermined coefficients A, B, C. Note that the numerator must be linear by (3.2).

There are six (4 choose 2) double residues. Those corresponding to vertices of the quadrilateral must have residue ± 1 (the sign is chosen based on orientation), while those corresponding to two opposite edges must have residue zero. We list these requirements as follows, where we denote $\mathrm{Res}_{ji} := \mathrm{Res}_{q_j=0}\mathrm{Res}_{q_i=0}\Omega(\mathcal{A})$.

$$\begin{aligned}
\mathrm{Res}_{12} &= \frac{A}{12} = +1 && (3.5)\\
\mathrm{Res}_{23} &= \frac{A + 2B + C}{6} = +1 && (3.6)\\
\mathrm{Res}_{34} &= \frac{A + B + 2C}{3} = +1 && (3.7)\\
\mathrm{Res}_{41} &= \frac{A + 2C}{4} = +1 && (3.8)\\
\mathrm{Res}_{13} &= \frac{A + 3C}{6} = 0 && (3.9)\\
\mathrm{Res}_{24} &= -\frac{A + 4B + 2C}{12} = 0 && (3.10)
\end{aligned}$$

By inspection, the only solution is $(A, B, C) = (12, -1, -4)$. It follows that

$$\Omega(\mathcal{A}) = \frac{(12 - x - 4y)dxdy}{x(2y - x)(3 - x - y)(2 - y)} \tag{3.11}$$

We observe that since there are many more equations than undetermined coefficients, the existence of a solution is non-obvious.

This method becomes complicated and intractable pretty fast. However, in the case of cyclic polytopes, a general solution was identified in [18] which we review below.

3.1.1 Cyclic polytopes

We now apply the numerator method to the cyclic polytope geometry, described in [18]. Let us illustrate how it works for the case of a quadrilateral $\mathcal{A} := \mathcal{A}(Z_1, Z_2, Z_3, Z_4)$. We know that the form must have poles when $\langle Y12\rangle, \langle Y23\rangle, \langle Y34\rangle, \langle Y41\rangle \to 0$; together with weights this tells us that

$$\underline{\Omega}(\mathcal{A}) = \frac{L_I Y^I}{2!\langle Y12\rangle\langle Y23\rangle\langle Y34\rangle\langle Y41\rangle} \tag{3.12}$$

for some L_I. We must also require that the codimension 2 singularities of this form only occur at the corners of the quadrilateral. But for generic L, this will not be the case; writing (ij) for the line $\langle Yij\rangle = 0$, we will also have singularities at the intersection of the lines (12) and (34), and also at the intersection of $(23), (14)$. The numerator must put a zero on these configurations, and thus we have that L must be the line that passes through $(12) \cap (34)$ as well as $(23) \cap (41)$:

$$L_I = \epsilon_{IJK}((12) \cap (34))^J((23) \cap (14))^K \tag{3.13}$$

If we expand out $(ab) \cap (cd) := Z_a\langle bcd\rangle - Z_b\langle acd\rangle = -Z_c\langle abd\rangle + Z_d\langle abc\rangle$, we can reproduce the expressions for this area in terms of triangulations.

Note that we can interpret the form as the area of the dual quadrilateral bounded by the edges Z_1, Z_2, Z_3, Z_4 and hence the vertices $W_1 = (12), W_2 = (23), W_3 =$

$(34), W_4 = (41)$. See (2.63) for the notation. By going to the affine space with Y at infinity as $Y = (1, 0, 0)$, $W_i = (1, W_i')$, we find the familiar expression for the area of a quadrilateral with the vertices W_1', W_2', W_3', W_4',

$$(W_3' - W_1') \times (W_4' - W_2') \tag{3.14}$$

where the $\times$ denotes the Euclidean cross product.

We can continue in this way to determine the form for any polygon. For instance for a pentagon $\mathcal{A}$, we have the general form

$$\underline{\Omega}(\mathcal{A}) = \frac{L_{IJ} Y^I Y^J}{2! \langle Y12\rangle \langle Y23\rangle \langle Y34\rangle \langle Y45\rangle \langle Y51\rangle} \tag{3.15}$$

but now the numerator must put a zero on all the 5 bad singularities where $(12), (34)$ intersect, $(23), (45)$ intersect and so on. Thus L_{IJ} must be the unique conic that passes through all these five points. If we let $B_i^I = [(i, i{+}1) \cap (i{+}2, i{+}3)]^I$ be the bad points, then

$$L_{IJ} = \epsilon_{(I_1 J_1)\cdots(I_5 J_5)(IJ)} (B_1 B_1)^{(I_1 J_1)} \cdots (B_5 B_5)^{(I_5 J_5)} \tag{3.16}$$

where $\epsilon_{(I_1 J_1)(I_2 J_2)\cdots(I_6 J_6)}$ is the unique tensor that is symmetric in each of the (IJ)'s but antisymmetric when swapping $(I_i J_i) \leftrightarrow (I_j J_j)$.

This construction for the numerator generalizes for all n-gons. Just from the poles $\Omega(\mathcal{A})$ takes the form

$$\Omega(\mathcal{A}) = \frac{L_{I_1 \cdots I_{n-3}} Y^{I_1} \cdots Y^{I_{n-3}}}{\langle Y12\rangle \cdots \langle Yn1\rangle} \tag{3.17}$$

Now there are $N = n(n-1)/2 - n = (n^2 - 3n)/2$ "bad" intersections $B_{a,b}$ of non-adjacent lines, $B_{a,b}^I = [(a, a+1) \cap (b, b+1)]^I$. But there is a unique (up to scale) numerator that puts a zero on these bad intersections:

$$L_{I_1 \cdots I_{n-3}} = \epsilon_{(I_1^{(1)} \cdots I_{n-3}^{(1)})(I_1^{(2)} \cdots I_{n-3}^{(2)}) \cdots (I_1^{(N)} \cdots I_{n-3}^{(N)})(I_1 \cdots I_{n-3})} \prod_{S=1}^{N} B_S^{I_1^{(S)}} \cdots B_S^{I_{n-3}^{(S)}} \tag{3.18}$$

where we have re-labeled the intersections as B_S for $S = 1, \ldots, N$. Note that in order for the ϵ tensor to exist, it is crucial that $N+1$ is the dimension of rank $n-3$ symmetrc tensors on $\mathbb{R}^3$. It is interesting that the polygon lies entirely inside the zero-set defined by the numerator: the "bad" singularities are "outside" the good ones.

For higher-dimensional polytopes the story is much more interesting as described in [18]. Here we content ourselves with presenting one of the examples which illustrates the novelties that arise. Consider the $m = 3$ cyclic polytope for $n = 5$, with vertices $Z_1, \ldots, Z_5$. The boundaries of the cyclic polytope in $m = 3$ dimensional projective space are of the form $(1, i, i + 1)$ and $(n, j, j + 1)$, which here are simply $(123), (134), (145), (125), (235), (345)$.

$$\frac{L_{IJ}Y^I Y^J}{\langle Y123\rangle\langle Y134\rangle\langle Y145\rangle\langle Y125\rangle\langle Y235\rangle\langle Y345\rangle} \tag{3.19}$$

The numerator corresponds to a quadric in $\mathbb{P}^3$ which has $4 \times 5/2 = 10$ degrees of freedom, and so can be specified in principle by vanishing on 9 points.

Naively, however, much more is required of the numerator than vanishing on points. The only edges of this polytope correspond to the lines (i, j), but there are six pairs of the above faces that do not intersect on lines (i, j); we find spurious residues at $L_1 = (123) \cap (145), L_2 = (123) \cap (345), L_3 = (134) \cap (125), L_4 = (134) \cap (235), L_5 = (145) \cap (235), L_6 = (125) \cap (345)$. So the numerator must vanish on these lines; the quadric must contain the six lines L_i. Also the zero-dimensional boundaries must simply correspond to the Z_i, while there are six possible intersections of the denominator planes that are not of this form, so the numerator must clearly vanish on these six points $X_{1,\ldots,6}$ as well. Of course these 6 "bad points" all lie on the "bad lines", so if the numerator kills the bad lines the bad points are also killed.

But there is a further constraint that was absent for the case of the polygon. In the polygon story, the form Ω was guaranteed to have sensible logarithmic singularities

and we only had to kill the ones in the wrong spots, but even this is not guaranteed for cyclic polytopes. Upon taking two residues, for generic numerators we can encounter double (and higher) poles. Suppose we approach the point $Y \to Z_1$, by first moving Y to the line (13) which is the intersection of the planes $(123), (134)$. If we put $Y = Z_1 + yZ_3$, then two of the remaining poles are $\langle Y145\rangle = -y\langle 1345\rangle$ and $\langle Y125\rangle = y\langle 1235\rangle$, and so we get a double-pole y^2. In order to avoid this and have sensible logarithmic singularities, the numerator must vanish linearly as $Y \to Z_1$; the same is needed as $Y \to Z_3$ and $Y \to Z_5$. Thus in addition to vanishing on the six lines L_i, the numerator must also vanish at $Y \to Z_1, Z_3, Z_5$. It is not a-priori obvious that this can be done; however quite beautifully the geometry is such that the 6 lines L_i break up into two sets, which mutually intersect on the 9 points X_i and $Z_{1,3,5}$, with three intersection points lying on each line. The numerator can thus be specified by vanishing on these points, which guarantees that it vanishes as needed on the lines.

More intricate versions of the same phenomenon happens for more general cyclic polytopes: unlike for polygons, apart from simply killing "bad points" the zero-set of the numerator must "kiss" the positive geometry at codimension 2 and lower surfaces, to guarantee getting logarithmic singularities. The form for $m = 4$ cyclic polytopes were constructed in this way. We have thus seen what this most brute-force, direct approach to determining the canonical form by understanding zeros and poles entails. The method can be powerful in cases where the geometry is completely understood, though as we have seen this can be somewhat involved even for polytopes.

3.1.2 Generalized polytopes on the projective plane

Let us return to the study of positive geometries $\mathcal{A}$ in $\mathbb{P}^2$, in view of the current discussion of canonical forms. In Sections 2.4.3 and 2.5.4 we explained that under the assumptions of Appendix A of [2], the boundary components are smooth curves and are thus either linear or quadratic.

Let us suppose that we allow the boundary components to be singular curves $p(Y) = 0$, as in Section 2.4.4, and furthermore we now allow $p(Y)$ to be of arbitrary degree d, and have r double-points. For a degree d curve with r double-points, the genus is given by $(d-1)(d-2)/2 - r$. Now recall that curves of non-zero genus admit non-trivial holomorphic top forms, which leads to non-unique canonical forms, thus violating our assumptions. We therefore require the curve to have $(d-1)(d-2)/2$ double-points and hence genus zero. This means that $p(Y) = 0$ can be rationally parametrized as $Y^I = Y^I(t)$, or equivalently, that the normalization of the curve $P(Y) = 0$ is isomorphic to $\mathbb{P}^1$. In practice, it is easy to reverse-engineer the polynomial defining the curve of interest from a rational parametrization. Working with co-ordinate $Y = (1, x, y)$, a rational parametrization is of the form $x(t) = P_x(t)/Q(t), y(t) = P_y(t)/Q(t)$. Then, the resultant $p(x, y) = R(P_x(t) - xQ(t); P_y(t) - yQ(t))$ gives us the polynomial defining the parametrized curve. For instance taking $x(t) = (t(t^2+1))/(1+t^4), y(t) = (t(t^2-1))/(1+t^4)$ yields the quartic "lemniscate" curve $p(x, y) = 4((x^2+y^2)^2 - (x^2-y^2))$, which has three double-points; one at $x = y = 0$ and two at infinity.

As for the canonical form, the numerator (see Section 3.1) must be chosen to kill all the undesired residues. Recall that for a d-gon, the numerator has to put zeros on $d(d-1)/2 - d = (d^2-3d)/2$ points, and that there is a unique degree $(d-3)$ polynomial that passes through those points, which determines the numerator uniquely up to overall scale. It is interesting to consider an example which is the opposite extreme of a polygon. Consider an irreducible degree d polynomial, with $(d-1)(d-2)/2 = (d^2-3d)/2 + 1$ singular points. To get a positive geometry, we can kill the residues on all but one of these singular points, leaving just a single zero-dimensional boundary just as in our teardrop cubic example of Section 2.4.4. These are the same number $(d^2-3d)/2$ of points we want to kill as in the polygon example, and once again there is a unique degree $(d-3)$ curve that passes through those points.

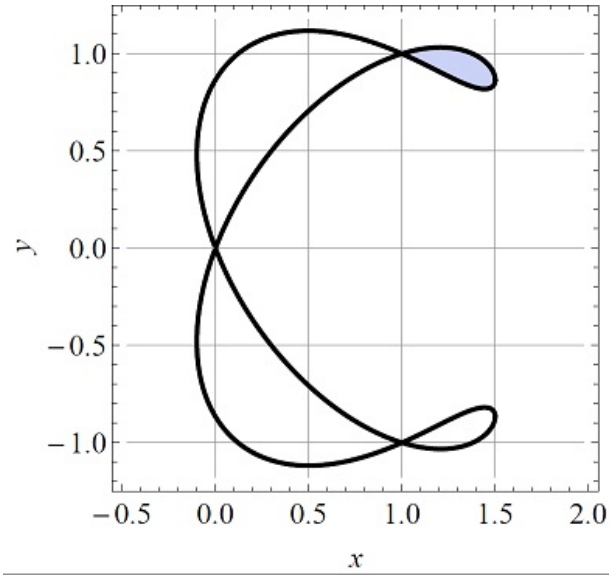

Figure 3.2: An "ampersand" curve with boundary given by a quartic polynomial. The shaded "teardrop" is a positive geometry.

An example is provided by the "ampersand" geometry (see Figure 3.2) associated with the quartic curve $P(x,y) = (y^2 - x^2)(x-1)(2x-3) - 4(x^2+y^2-2x)^2$, which has three singular points at $(0,0), (1,1), (1,-1)$. If we choose the numerator to be the line that kills e.g. the points $(0,0)$ and $(1,-1)$, then we get a positive geometry corresponding to the "teardrop" in the upper quadrant.

Two more examples: consider a region bounded by two quadrics Q_1 and Q_2. The numerator of the form is $Y \cdot L$ for some line L. Now two generic quadrics intersect at four points P_1, P_2, P_3, P_4. Mirroring the determination of the form for the case of the quadrilateral, we can choose the line L appearing in the numerator to kill two of P_i's, and this will give us the canonical form associated with the geometry $(Q_{1,2} \cdot YY) \geq 0$. Similarly, consider a positive geometry defined by a singular cubic C and a line W. Again we have a numerator of the form $Y \cdot L$. The line W intersects the cubic in three points P_1, P_2, P_3. If we pick the the line L to pass through one of the P_i as well as the singular point of the cubic, we get the canonical form associated with the geometry. These constructions can be extended to higher dimensions, where (as with the cyclic

polytope example) we will generically encounter numerators whose zeros touch the positive geometry on co-dimension two (and lower dimensional) boundaries.

3.2 Triangulations

Recall from Section 2.2 that if a positive geometry is triangulated by a collection of other positive geometries, its canonical form is given by the sum of the canonical forms of the collection. We now apply this method to compute the canonical form of various generalized polytopes.

3.2.1 Projective polytopes

Let $\mathcal{A} := \mathcal{A}(Z_1, \ldots, Z_n)$ be a convex projective polytope. The canonical form $\Omega(\mathcal{A})$ can be obtained from a triangulation of $\mathcal{A}$ (see Section 2.2). Let $\Delta_1, \Delta_2, \ldots, \Delta_r$ be a triangulation of $\mathcal{A}$ into simplices. For simplicity let us assume that the simplex interiors are mutually non-overlapping. The canonical form $\Omega(\mathcal{A})$ is given by

$$\Omega(\mathcal{A}) = \sum_i \Omega(\Delta_i) \tag{3.20}$$

The fact that the simplicial canonical forms *add* is dependent on the assumption that the orientation of the interior of Δ_i agrees with that of $\mathcal{A}$ for each i. More generally, for any polytopal subdivision of $\mathcal{A}$ into polytopes $\mathcal{A}_i$ (i.e. a "triangulation" by polytopes), we have

$$\Omega(\mathcal{A}) = \sum_i \Omega(\mathcal{A}_i). \tag{3.21}$$

We begin with the simplest case: line segments in $\mathbb{P}^1(\mathbb{R})$.

Example 3.2.1. Consider a triangulation of the segment $[a, b]$ from Example 2.2 by a sequence of successively connected segments:

$$[a, b] = \bigcup_{i=1}^{r} [c_{i-1}, c_i] \tag{3.22}$$

where $a = c_0 < c_1 < \ldots < c_r = b$. It is straightforward to check that

$$\Omega([a, b]) = \frac{(b-a)dx}{(b-x)(x-a)} = \sum_{i=1}^{r} \frac{(c_i - c_{i-1})dx}{(c_i - x)(x - c_{i-1})} = \sum_{i=1}^{r} \Omega([c_{i-1}, c_i]) \tag{3.23}$$

More generally, for the positive geometry $\mathcal{A} = \bigcup_i [a_i, b_i] \subset \mathbb{P}^1$ which is triangulated by finitely many line segments with mutually disjoint interiors, the canonical form is:

$$\Omega\left(\bigcup_i [a_i, b_i]\right) = \sum_i \Omega([a_i, b_i]) \tag{3.24}$$

Example 3.2.2. Suppose $\mathcal{A}$ is a convex projective polytope, and Z_* is a point in its interior, then $\mathcal{A}$ is triangulated by

$$\mathcal{A} = \bigcup_{\text{facets}} \text{Conv}(Z_*, Z_{i_1}, Z_{i_2}, \ldots, Z_{i_m}) \tag{3.25}$$

where we take the union over all choice of indices $i_1, \ldots, i_m$ for which $\text{Conv}(Z_{i_1}, Z_{i_2} \ldots, Z_{i_m})$ is a facet of the polytope, and we avoid repeated permutations of the same set of indices. For each facet, we order the indices so that $Z_*, Z_{i_1}, \ldots, Z_{i_m}$ is positively oriented. It follows that

$$\Omega(\mathcal{A}) = \sum_{\text{facets}} [*, i_1, \ldots, i_m] \tag{3.26}$$

Recalling the facets of cyclic polytopes from Section 2.5.2, we have the following corollaries.

Example 3.2.3. The canonical rational function of a cyclic polytope $\mathcal{A}$ for even m can be obtained as follows.

$$\underline{\Omega}(\mathcal{A}) = \sum_{1\leq i_1-1<i_1<\cdots<i_{m/2}-1<i_{m/2}\leq n+1} [*, i_1-1, i_1, \ldots, i_{m/2}-1, i_{m/2}] \tag{3.27}$$

For arbitrary Z_*, this is called a *CSW triangulation*. For $Z_* = Z_i$ for some i, this is called a *BCFW triangulation*.

Example 3.2.4. The canonical rational function of a cyclic polytope $\mathcal{A}$ for odd m can be obtained as follows.

$$\underline{\Omega}(\mathcal{A}) = \sum_{2\leq i_1-1<i_1<\cdots<i_{(m-1)/2}-1<i_{(m-1)/2}\leq n} -[*, 1, i_1-1, i_1, \ldots, i_{(m-1)/2}-1, i_{(m-1)/2}] \tag{3.28}$$

$$+ \sum_{1\leq i_1-1<i_1<\cdots<i_{(m-1)/2}-1<i_{(m-1)/2}\leq n-1} [*, i_1-1, i_1, \ldots, i_{(m-1)/2}-1, i_{(m-1)/2}, n] \tag{3.29}$$

for any Z_*. If we set $Z_* = Z_1$ or Z_n, then we get

$$\underline{\Omega}(\mathcal{A}) = \sum_{2\leq i_1-1<i_1<\cdots<i_{(m-1)/2}-1<i_{(m-1)/2}\leq n-1} [1, i_1-1, i_1, \ldots, i_{(m-1)/2}-1, i_{(m-1)/2}, n] \tag{3.30}$$

3.2.2 Generalized polytopes on the projective plane

In this section we verify that the canonical form for the "pizza slice" geometry from Example 2.5.1 can be obtained by triangulation.

Example 3.2.5. Recall the "pizza slice" geometry $\mathcal{T}(\theta_1, \theta_2)$ from Example 2.5.1. For simplicity, we will assume reflection symmetry about the y-axis and let $\mathcal{T}(\theta) := \mathcal{T}(\theta, \pi-\theta)$ for some $0 \leq \theta < \pi/2$. Denote the vertices of the geometry by $Z_i^I \in \mathbb{P}^1(\mathbb{R})$ for $i = 1, 2, 3$, where

$$Z_1^I = (1, 0, 0), \quad Z_2^I = (1, \cos\theta, \sin\theta), \quad Z_3^I = (1, -\cos\theta, \sin\theta) \tag{3.31}$$

The geometry is clearly the union of a segment of the disk (see Example 2.4.2) and a triangle (see Section 2.4.2).

$$\mathcal{T}(\theta) = \mathcal{S}(\sin\theta) \cup \mathcal{A}(Z_1, Z_2, Z_3) \tag{3.32}$$

It follows that

$$\begin{aligned}
\Omega(\mathcal{T}(\theta)) &= \Omega(\mathcal{S}(\sin\theta)) + \Omega(\mathcal{A}(Z_1, Z_2, Z_3)) \\
&= \frac{(2\cos\theta)dxdy}{(1-x^2-y^2)(y-\sin\theta)} + \frac{(2\sin^2\theta\cos\theta)dxdy}{(\sin\theta-y)(-x\sin\theta+y\cos\theta)(x\sin\theta+y\cos\theta)} \\
&= \frac{2\cos\theta(y+\sin\theta)dxdy}{(1-x^2-y^2)(-x\sin\theta+y\cos\theta)(x\sin\theta+y\cos\theta)}
\end{aligned} \tag{3.33}$$

which is equivalent to (2.67) for $\theta_1 = \theta$ and $\theta_2 = \pi - \theta$, with $y - \sin\theta = 0$ as a spurious pole.

3.3 Pushforwards

Recall from Heuristic 2.3.1 that for any morphism $\Phi : (X, X_{\geq 0}) \to (Y, Y_{\geq 0})$, we expect the pushforward to preserve the canonical form:

$$\Phi_*(\Omega(X, X_{\geq 0})) = \Omega(Y, Y_{\geq 0}) \tag{3.34}$$

This procedure is useful for computing the canonical form of the image when the canonical form of the domain is already known. However, very often morphisms of degree > 1 are required, which are challenging to construct. We demonstrate a few non-trivial examples in this section.

3.3.1 Projective simplices

We consider morphisms $\Phi : (\mathbb{P}^m, \Delta) \to (X, X_{\geq 0})$ from projective simplices to positive geometries $X_{\geq 0}$. In most cases we will assume that $\Delta = \Delta^m$ is the standard simplex.

We begin with morphisms $\Phi : (\mathbb{P}^m, \Delta^m) \to (X, X_{\geq 0})$ of degree one, in which case $X_{\geq 0}$ is $\Delta-$like (as defined in Section 2.4.1), and its canonical form is given by,

$$\Omega(X, X_{\geq 0}) = \Phi_* \left(\prod_{i=1}^{m} \frac{d\alpha_i}{\alpha_i} \right) \tag{3.35}$$

where $(1, \alpha_1, \ldots, \alpha_m) \in \mathbb{P}^m$. The simplest Δ-like positive geometry is a projective simplex.

Example 3.3.1. A projective simplex $\Delta \subset \mathbb{P}^m(\mathbb{R})$ is isomorphic to the standard simplex Δ^m by the following map $\Phi : (\mathbb{P}^m, \Delta^m) \to (\mathbb{P}^m, \Delta)$,

$$\Phi(\alpha) = \sum_{i=0}^{m} \alpha_i Z_{i+1} \tag{3.36}$$

where $Z_i \in \mathbb{P}^m(\mathbb{R})$ are the vertices of Δ for $i = 1, \ldots, m+1$. As a matter of convention, the projective variables and the vertices are indexed slightly differently. Note that the positive part Δ^m (i.e. $\alpha_i > 0$ for each i) is mapped diffeomorphically onto the interior of Δ.

The canonical form on Δ is therefore

$$\Omega(\Delta) = \Phi_* \left(\prod_{i=1}^{m} \frac{d\alpha_i}{\alpha_i} \right) \tag{3.37}$$

where we have made the "gauge choice" $\alpha_0 = 1$ as usual. Alternatively, pulling back the form (2.14) onto Δ^m gives the form on α-space.

The image of the hyperplane $\{\alpha_i = 0\} \subset \mathbb{P}^m$ intersects Δ along the facet opposite the vertex Z_{i+1}. Taking the residue of $\Omega(\Delta^m)$ along $\alpha_i = 0$ before pushing forward

gives the canonical form of that facet. We note that the pole for localizing on the facet opposite Z_1 is hidden, as explained in Section 2.4.1.

We now consider *higher degree* morphisms $\Phi : (\mathbb{P}^m, \Delta^m) \to (X, X_{\geq 0})$. Let us assume for the moment that $X = \mathbb{P}^m$. We now provide a general analytic argument for why the pushforward should have no poles on $X_{>0}$. The behavior of the pushforward near the boundary of $X_{\geq 0}$ is more subtle and will be discussed subsequently on a case-by-case basis.

Suppose the map is given by $\alpha \mapsto \Phi(\alpha)$ and let β_0 be a point in $X_{>0}$. Furthermore, assume if possible that the pushforward has a singularity at β_0. It follows that the Jacobian $J(\alpha)$ of $\Phi(\alpha)$ must vanish at some point α_0 for which $\Phi(\alpha_0) = \beta_0$. Let $\beta = \Phi(\alpha)$ which we expand near the critical point,

$$\beta = \Phi(\alpha_0) + \lambda \sum_i \epsilon_i \frac{\partial \Phi(\alpha_0)}{\partial \alpha_i} + \frac{1}{2}\lambda^2 \sum_{i,j} \epsilon_i \epsilon_j \frac{\partial^2 \Phi(\alpha_0)}{\partial \alpha_i \partial \alpha_j} + O(\lambda^3) \tag{3.38}$$

where we have set $\alpha = \alpha_0 + \lambda\epsilon$ with λ a small parameter and ϵ a constant vector. Since the Jacobian vanishes at α_0, a generic point β in a small neighborhood of β_0 cannot be approximated by the linear term. However, unless the quadratic term degenerates, β can be approximated quadratically by choosing ϵ so that the first variation vanishes. Namely,

$$\sum_a \epsilon_i \frac{\partial \Phi(\alpha_0)}{\partial \alpha_i} = 0 \tag{3.39}$$

It follows that the variation is even in λ, so there are two roots $\lambda_\pm$ (corresponding to points $\alpha_\pm$, respectively) that approximate β, with $\lambda_+ = -\lambda_-$. Since the Jacobian is clearly linear in λ for small variations near α_0, therefore $J(\alpha_+) = -J(\alpha_-) + O(\lambda_-^2)$. Since the pushforward is a sum of $1/J(\alpha) \sim 1/\lambda$ over all the roots, the roots corresponding to $\alpha_\pm$ therefore cancel in the limit $\beta \to \beta_0$, and there is no pole.

We now show a few examples of higher degree pushforwards, beginning with self-morphisms of the standard simplex.

Example 3.3.2. Let $\Phi : (\mathbb{P}^m, \Delta^m) \to (\mathbb{P}^m, \Delta^m)$ be a morphism of the standard simplex with itself, defined by

$$\Phi(1, \alpha_1, \ldots, \alpha_m) = (1, \beta_1, ..., \beta_m) \tag{3.40}$$

$$\beta_j = \prod_{i=1}^{m} \alpha_i^{a_{ij}} \tag{3.41}$$

where a_{ij} is an invertible integer matrix. We assume the determinant is positive so that the map is orientation preserving. While this map is a self-diffeomorphism of $\mathrm{Int}(\Delta^m)$, it is not necessarily one-to-one on $\mathbb{P}^m$. The pushforward gives

$$\Phi_* \left(\prod_{i=1}^{m} \frac{d\alpha_i}{\alpha_i} \right) = \sum_{\text{roots}} \frac{d^m \beta}{\frac{\partial(\beta_1 \ldots \beta_m)}{\partial(\alpha_1 \ldots \alpha_m)} \prod_{i=1}^{m} \alpha_i} = \frac{\deg(\Phi)}{\det(a_{ij})} \prod_{j=1}^{m} \frac{d\beta_j}{\beta_j} \tag{3.42}$$

where $\deg(\Phi)$ is the number of roots, and we have substituted the Jacobian:

$$\frac{\partial(\beta_1 \ldots \beta_m)}{\partial(\alpha_1 \ldots \alpha_m)} = \det(a_{ij}) \frac{\prod_{j=1}^{m} \beta_j}{\prod_{i=1}^{m} \alpha_i} \tag{3.43}$$

It is easy to see that the degree of Φ must be $|\det(a_{ij})|$: after an integral change of basis, the matrix (a_{ij}) can be put into Smith normal form, that is, made diagonal. For a diagonal matrix (a_{ij}) it is clear that the degree of Φ is simply the product of diagonal entries. Thus (3.42) verifies Heuristic 2.3.1 in this case. By contrast, we note that the pull-back along Φ gives $\Phi^*(\Omega(\Delta^m)) = \det(a_{ij})\Omega(\Delta^m)$, which does not preserve leading residues.

The next few examples explore the pushforward in one dimension. They are all applications of Cauchy's theorem in disguise.

Example 3.3.3. A simple non-trivial example is a quadratic pushforward $\Phi : \Delta^1 \to \Delta^1$ given by $\Phi(1, \alpha) = (1, a\alpha^2 + 2b\alpha)$ for some real constants $a > 0; b \geq 0$. The

assumptions suffice to make Φ a self-morphism of Δ^1. Setting $(1, \beta) = \Phi(1, \alpha)$ we get two roots $\alpha_\pm$ from solving a quadratic equation. The pushforward is therefore

$$\Phi_*(d\log\alpha) = \sum_\pm d\log(\alpha_\pm) = \sum_\pm d\log\left(\frac{-b \pm \sqrt{b^2 + a\beta}}{a}\right) \tag{3.44}$$

Since we are summing over roots, a standard Galois theory argument implies that the result should be rational. Indeed, the square-root disappears, and direct computation gives $\Phi_*(d\log\alpha) = d\log\beta$.

We can also do the sum without directly solving the quadratic equation. The result should only depend on the sum and product of the roots $x_\pm$, since the result must be a rational function.

$$\Phi_*(d\log\alpha) = \sum_\pm \frac{d\beta}{\alpha_\pm \left(\frac{d\beta}{d\alpha}\right)_\pm} = \sum_\pm \frac{1}{2\alpha_\pm(a\alpha_\pm + b)} \tag{3.45}$$

Substituting $\alpha_\pm(a\alpha_\pm + b) = \beta - b\alpha_\pm$, which comes from the original equation, we get

$$f_*(d\log\alpha) = \sum_\pm \frac{1}{2(\beta - b\alpha_\pm)} = \frac{2\beta - b(\alpha_+ + \alpha_-)}{2(\beta^2 - b\beta(\alpha_+ + \alpha_-) + b^2\alpha_+\alpha_-)} \tag{3.46}$$

We now use the identities $\alpha_+ + \alpha_- = -2b/a$ and $\alpha_+\alpha_- = -\beta/a$, which give the desired result $\Phi_*(d\log\alpha) = d\log\beta$.

Example 3.3.4. We now go ahead and tackle the same example for a polynomial of arbitrary degree. Suppose Φ is a self-morphism of Δ^1 given by $\beta = f(\alpha) = \alpha^n + a_{n-1}\alpha^{n-1} + \ldots + a_1\alpha$. We first define the holomorphic function

$$g(\alpha) = \frac{1}{\alpha(f(\alpha) - \beta)} \tag{3.47}$$

which has no pole at infinity since $f(\alpha)$ is at least of degree one. The sum over all the residues of the function is therefore zero by Cauchy's theorem. It follows that

$$-\frac{1}{\beta}+\sum_i \frac{1}{\alpha_i f'(\alpha_i)}=0 \tag{3.48}$$

where we sum over all the roots α_i of $f(\alpha)=\beta$. Therefore,

$$\Phi_*(d\log\alpha)=\sum_i \frac{d\beta}{\alpha_i f'(\alpha_i)}=d\log\beta \tag{3.49}$$

Finally, we consider a simple but instructive pushforward of *infinite* degree.

Example 3.3.5. Consider the map $\Phi:(\mathbb{P}^1,[-\pi/2,\pi/2])\to(\mathbb{P}^1,[-1,1])$ between two closed line segments given by:

$$\Phi(1,\theta)=(1,\sin\theta) \tag{3.50}$$

While this map is not rational, we can nevertheless verify Heuristic 2.3.1 for Φ by explicit computation. For any point $(1,\sin\theta)$ in the image, there are infinitely many roots of (3.50) given by $\theta_n:=\theta+2\pi n$ and $\theta'_n:=-\theta+\pi(2n+1)$ for $n\in\mathbb{Z}$. It is easy to show that both sets of roots contribute the same amount to the pushforward, so we will just sum over θ_n twice,

$$\begin{aligned}\Phi_*\left(\frac{\pi d\theta}{(\pi/2-\theta)(\theta+\pi/2)}\right) &= 2\sum_{n\in\mathbb{Z}}\frac{\pi dx}{(\pi/2-\theta_n)(\theta_n+\pi/2)\cos\theta_n}=2\frac{dx}{\cos^2\theta}\\ &= \frac{2dx}{(1-x)(x+1)}\end{aligned} \tag{3.51}$$

which of course is the canonical form of $[-1,1]$. The infinite sum can be computed by an application of Cauchy's theorem.

We note here that our definition of the pushforward only allows finite degree maps while Φ is of infinite degree. Nonetheless, it appears that Heuristic 2.3.1 still

holds when the pushforward is an *absolutely convergent* series like (3.51). We stress that some pushforwards give conditionally convergent series, such as the morphism $(\mathbb{P}^1, \Delta^1) \to (\mathbb{P}^1, [0,1])$ given by $(1,x) \to (1, e^{-x})$, in which case the pushforward is ill-defined since there is no canonical order in which to sum the roots.

3.3.2 Projective polytopes from Newton polytopes

In this section we discuss morphisms from $(\mathbb{P}^m, \Delta^m)$ to convex polytopes $(\mathbb{P}^m, \mathcal{A})$ and their pushforwards. Our main results here overlap with a discussion on toric varieties in Section 5.6 of [2]. However, our intention here is to provide a self-contained discussion. Our focus here is also more geometric in nature, emphasizing the fact that any such morphism restricts to a diffeomorphism $\mathrm{Int}(\Delta^m) \to \mathrm{Int}(\mathcal{A})$.

Now let $\mathcal{A} \subset \mathbb{P}^m$ be a convex polytope in projective space with vertices Z_i for $i = 1, \ldots, n$. Let $z_1, z_2, \ldots, z_n \in \mathcal{Z}^{m+1}$ be an *integer* matrix with the same oriented matroid as $Z_1, \ldots, Z_n$. That is,

$$\langle Z_{i_0} \cdots Z_{i_m} \rangle \text{ and } \langle z_{i_0} \cdots z_{i_m} \rangle \text{ have the same sign} \tag{3.52}$$

for all $1 \leq i_0 < \cdots < i_m \leq n$. Here two real quantities have the same sign if they are both positive, both negative, or both zero. For simplicity we now assume that $z_i = (1, z_i') = (1, z_{1i}', z_{2i}', \ldots, z_{mi}')$. Furthermore, let us define a rational map $\Phi : (\mathbb{P}^m, \Delta^m) \to (\mathbb{P}^m, \mathcal{A})$ given by

$$\Phi(X) \;=\; \sum_i C_i(X) Z_i \tag{3.53}$$

$$C_i(X) \;:=\; X^{z_i} := X_1^{z_{1i}'} X_2^{z_{2i}'} \cdots X_m^{z_{m,i}'} \tag{3.54}$$

where $(1, X) \in \mathbb{P}^m$. This is called the *Newton polytope map* and the polytope with integer vertices z_i is called the *Newton polytope*.

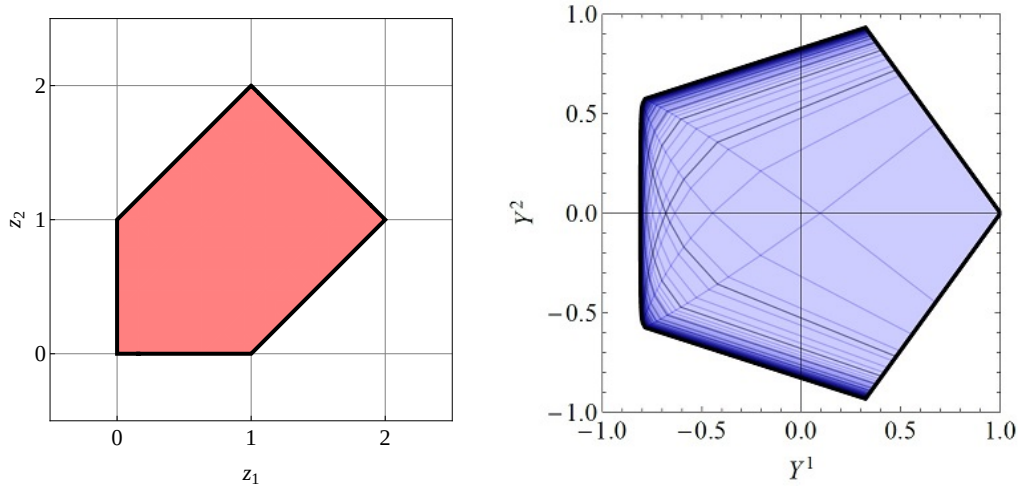

Figure 3.3: A Newton pentagon (left) with vertices $z' = ((0,0),(1,0),(2,1),(1,2),(0,1))$ and the image of the corresponding diffeomorphism $\Phi(X)$ (right). The dark lines in the interior of the pentagon (right) denote lines of constant X_1 or X_2. While the two pentagons are not identical as sets, they do have the same oriented matroid.

We make two claims in this section, beginning with:

Claim 1: The map Φ is a *morphism* provided that (3.52) holds. (3.55)

That is, it restricts to a *diffeomorphism* on $\text{Int}(\Delta^m) \to \text{Int}(\mathcal{A})$. This is a non-trivial fact for which two proofs are provided in Appendix E of [2]. At the heart of Claim (3.55) is that the Jacobian of Φ is uniformly positive on $\text{Int}(\Delta^m)$:

$$J(\Phi) = \sum_{1 \le i_0 < \cdots < i_m \le n} C_{i_0} \cdots C_{i_m} \langle z_{i_0} \cdots z_{i_m} \rangle \langle Z_{i_0} \cdots Z_{i_m} \rangle \tag{3.56}$$

where $J(\Phi)$ denotes the Jacobian of Φ with respect to $u_i := \log(X_i)$, which is clearly positive provided that z_i and Z_i have the same oriented matroid (see (3.52)). While this is only a *necessary* condition for Claim (3.55), it is nevertheless the key to proving it. We provide a graphical example of the diffeomorphism for the pentagon in Figure 3.3.

This establishes the way to our second claim, which is an instance of Heuristic 2.3.1.

Claim 2: The canonical form of the polytope is given by the pushforward:

$$\Omega(\mathcal{A}) = \Phi_* \left(\frac{d^m X}{\prod_{a=1}^m X_a} \right) \tag{3.57}$$

For computational purposes, a more convenient way to express the (canonical rational function of the) pushforward is the following integral formula:

$$\underline{\Omega}(\mathcal{A})(Y) = \int \frac{d^m X}{\prod_{a=1}^m X_a} \delta^m(Y; \Phi(X)) \tag{3.58}$$

where for any two points Y, Y' in projective space $\mathbb{P}^m$, the integral

$$\delta^m(Y, Y') = \frac{1}{m!} \int \frac{d\rho}{\rho} \delta^{m+1}(Y - \rho Y') \tag{3.59}$$

is the delta function with weights $(-m-1, 0)$. Here the sum over pre-images appearing in the pushforward is equivalent to the sum over solutions to the constraints imposed by the delta functions. The relevant Jacobian factors are taken care of by the delta functions as well. We treat the delta functions formally as an "analytic" object without taking absolute values in the Jacobian factor, and we sum over all *complex* roots. In most cases numerical methods are needed to compute the pushforward, which we have done extensively as verification of Claim (3.57). However, here we show a simple case where the pushforward can be done by hand.

Example 3.3.6. Let us consider a quadrilateral $\mathcal{A}$ on the projective plane. By a convenient gauge-fixing, we will take the external data and Y to be of the form

$$Z = \begin{pmatrix} 1 & 0 & 0 \\ 0 & 1 & 0 \\ 0 & 0 & 1 \\ a & -1 & b \end{pmatrix}, \quad Y = (y, 1, x) \tag{3.60}$$

We can trivially compute the canonical rational function by e.g. triangulation as $[123] + [134]$, and finding

$$\Omega(\mathcal{A}) = \frac{(ab + ax + by)}{xy(a + y)(b + x)} dxdy \tag{3.61}$$

and we will now reproduce this result from the Newton polytope map (3.53), with the Newton polytope being the square with vertices $(1, 0), (1, 1), (0, 1), (0, 0)$, respectively. Thus our map is

$$Y = \Phi(X) = X_1 Z_1 + X_1 X_2 Z_2 + X_2 Z_3 + Z_4 = \left(\frac{X_1 + a}{X_1 X_2 - 1}, 1, \frac{X_2 + b}{X_1 X_2 - 1} \right) \tag{3.62}$$

which are projective equalities. We must solve the equations

$$(X_1 X_2 - 1)y = X_1 + a, \quad (X_1 X_2 - 1)x = X_2 + b \tag{3.63}$$

We then have

$$\frac{d^2 X}{X_1 X_2} = dxdy \times \frac{(X_1 X_2 - 1)^2}{X_1 X_2 (x X_1 + y X_2 - 1)} \tag{3.64}$$

It therefore suffices to show that

$$\sum_{\text{roots}} \frac{(X_1 X_2 - 1)^2}{X_1 X_2 (x X_1 + y X_2 - 1)} = \frac{(ab + ax + by)}{xy(a + y)(b + x)} \tag{3.65}$$

If we define $\rho = (X_1X_2 - 1)$, then we have $X_1 = \rho y - a, X_2 = \rho x - b$ and so $(\rho + 1) = (\rho y - a)(\rho x - b)$. So ρ satisfies the quadratic equation

$$\rho^2 - \frac{(1 + ax + by)}{xy}\rho + \frac{ab - 1}{xy} = 0 \tag{3.66}$$

which has two roots $\rho_\pm$. Note that

$$xX_1 + yX_2 - 1 = x(\rho y - a) + y(\rho x - b) - 1 = 2xy\left(\rho - \frac{1}{2}\frac{(1 + ax + by)}{xy}\right) \tag{3.67}$$

Comparing with the quadratic equation for ρ, we can identify the term corresponding to the sum of the roots $(\rho_+ + \rho_-)$, giving:

$$(xX_1 + yX_2 - 1)_\pm = \pm xy(\rho_+ - \rho_-) \tag{3.68}$$

Thus, the sum over roots becomes

$$\begin{aligned} &\frac{1}{xy(\rho_+ - \rho_-)} \times \left(\frac{\rho_+^2}{(\rho_+ y - a)(\rho_+ x - b)} - \frac{\rho_-^2}{(\rho_- y - a)(\rho_- x - b)}\right) \\ &= \frac{1}{xy}\frac{ab(\rho_+ + \rho_-) - \rho_+\rho_-(by + ax)}{(\rho_+\rho_- y^2 - a(\rho_+ + \rho_-)y + a^2)(\rho_+\rho_- x^2 - b(\rho_+ + \rho_-)x + b^2)} \end{aligned} \tag{3.69}$$

And reading off

$$\rho_+\rho_- = \frac{ab - 1}{xy}, \qquad \rho_+ + \rho_- = \frac{1 + ax + by}{xy} \tag{3.70}$$

from the quadratic equation we finally find that (3.69) equals

$$\frac{ab + ax + by}{xy(a + y)(b + x)} \tag{3.71}$$

as expected.

3.3.3 Recursive properties of the Newton polytope map

We now derive the pushforward identity (3.57) for the Newton polytope by explicitly manipulating the pushforward computation and applying induction on dimension. In fact, we will derive a more general version for lower dimensional polytopes in $\mathbb{P}^m(\mathbb{R})$. The statement is the following.

Consider the variety $H \subset \mathbb{P}^m$ defined by linear equations $Y \cdot H_1, \ldots, Y \cdot H_s = 0$ for some dual vectors $H_1, \ldots, H_s \in \mathbb{P}^m(\mathbb{R})$ with $Y \in \mathbb{P}^m$. Let $\mathcal{A}$ denote a convex polytope in $H(\mathbb{R})$ of dimension $D = m-s$ with vertices $Z_1, \ldots, Z_n$. Let $\Phi : (\mathbb{P}^D, \Delta^D) \to (H, \mathcal{A})$ be a morphism defined by a Newton polytope with vertices $z_i = (1, z_i') \in \mathbb{R}^{D+1}$. Furthermore, we assume that $\mathcal{A}$ and the Newton polytope have the same oriented matroid. Namely, there exist constant vectors $K_1, \ldots, K_s \in \mathbb{P}^m(\mathbb{R})$ such that

$$\langle K_1 \cdots K_s Z_{i_0} \cdots Z_{i_D} \rangle \text{ and } \langle z_{i_0} \cdots z_{i_D} \rangle \text{ have the same sign} \tag{3.72}$$

for any set of indices $1 \leq i_0, \ldots, i_D \leq n$.

The $D = 0$ case is trivial. Now assume $D > 0$. Let $\mathcal{B}$ denote a facet of $\mathcal{A}$ with vertices $Z_{j_1}, \ldots, Z_{j_p}$, and let B denote the corresponding facet of the Newton polytope. We now argue that there exists a change of variables $(X_1, \ldots, X_D) \to (U_1, \ldots, U_D)$ given by $X_b = \prod_{a=1}^{D} {U_a}^{\alpha_{ab}}$ for some invertible integer matrix α_{ab} that has the following properties: (Note that we define $\Phi'(U) := \Phi(\psi(U))$ with $X := \psi(U)$)

- The map $U \to X$ is a self-morphism of Δ^D which may be of degree > 1. In particular, it is a self-diffeomorphism of $\mathrm{Int}(\Delta^D)$.
- The restriction of Φ' to $U_D = 0$ is a Newton polytope map $\Delta^{D-1} \to \mathcal{B}$ whose Newton polytope has the same shape as B.

We construct the change of variables as follows. Let us begin by considering the matrix formed by column vectors $(z_{j_1}, \ldots, z_{j_D}, z_j)$ where the first D columns are

vertices of B, while z_j is any vertex of the Newton polytope away from the facet. Let $\alpha := (\alpha_{ab})$ be the inverse of the matrix, which has only rational components. Finally, let us rescale the rows of α_{ab} (indexed by a) by positive integers so that all its components are integral. This provides the change of variables $X \to U$.

Let us redefine z_i for every i to be the vertex of the Newton polytope with respect to U, which again has the same oriented matroid as $\mathcal{A}$. In particular, the matrix of column vectors $(z_{j_1}, \ldots, z_{j_D}, z_j)$ is identity. Since every vertex of B is a linear combination of $z_{j_1}, \ldots, z_{j_D}$, it must therefore have zero as its last component. Furthermore, since every other vertex of the Newton polytope is a linear combination of $z_{j_1}, \ldots, z_{j_D}, z_j$ with positive coefficient in z_j, its last component must be positive. Geometrically, this means that the $U_D = 0$ limit is mapped to the facet $\mathcal{B}$ by Φ'.

Now, let $\Psi : \Delta^{D-1} \to \mathcal{B}$ denote the map Φ' restricted to $U_D = 0$, and let $w_{j_1}, \ldots, w_{j_p} \in \mathbb{R}^D$ denote the vertices of the Newton polytope of Ψ, which are equivalently the vectors $z_{j_1}, \ldots, z_{j_p}$, respectively, with the last component removed. It is straightforward to check that the Newton polytope of Ψ has the same oriented matroid as $\mathcal{B}$, so our induction hypothesis can be applied to Ψ.

We now argue that the pushforward by Φ' has a pole at the boundary $\mathcal{B}$ with the expected residue $\Omega(\mathcal{B})$. Let $Y = \Phi'(U)$. The main strategy is to observe that the roots $(U_1, \ldots, U_{D-1})$ are independent of U_D near $\mathcal{B}$.

Indeed, at $Y \in \mathcal{B}$ (i.e. $U_D = 0$), the map becomes

$$Y = C_{j_1} Z_{j_1} + \cdots + C_{j_p} Z_{j_p} \tag{3.73}$$

which gives us a collection of roots $(U_1, \ldots, U_{D-1})$ independent of U_D. It follows therefore from the induction hypothesis that

$$\sum_{\text{roots } (U_1, \ldots, U_{D-1})} \frac{d^{D-1}U}{U_1 \cdots U_{D-1}} = \Psi_* \left(\frac{d^{D-1}U}{U_1 \cdots U_{D-1}} \right) = \Omega(\mathcal{B}) \tag{3.74}$$

Moreover, the roots U_D are given by the equation

$$\langle K_1 \dots K_s Y j_1 \dots j_D \rangle \sim U_D^q F(U_1, \dots, U_{D-1}) \tag{3.75}$$

for some function F independent of U_D and some exponent q. Hence,

$$\sum_{\text{roots } U_D} \frac{dU_D}{U_D} = d \log \langle K_1 \dots K_s Y j_1 \dots j_D \rangle + \cdots \tag{3.76}$$

where the $\cdots$ denotes term proportional to $dU_1, \dots, dU_{D-1}$.

It follows that in the limit $Y \to \mathcal{B}$, we have

$$\begin{aligned} \sum_{\text{roots}} \frac{d^D U}{U_1 \cdots U_D} &= \left(\sum_{\text{roots } (U_1, \dots, U_{D-1})} \frac{d^{D-1} U}{U_1 \cdots U_{D-1}} \right) \left(\sum_{\text{roots } U_D} \frac{dU_D}{U_D} \right) + \cdots & (3.77) \\ &= \Psi_* \left(\frac{d^{D-1} U}{U_1 \cdots U_{D-1}} \right) d \log \langle K_1 \dots K_s Y j_1 \dots j_D \rangle + \cdots & (3.78) \\ &= \Omega(\mathcal{B})\, d \log \langle K_1 \dots K_s Y j_1 \dots j_D \rangle + \cdots & (3.79) \end{aligned}$$

where $\cdots$ denotes terms smooth in the limit, and we have applied (3.76) and (3.74). This of course is the expected pole and residue.

Furthermore, by the discussion in Section 3.3.1, we find that there are no poles on the interior of $\mathcal{A}$.

Finally, we can re-express our result as a pushforward from X-space by the following:

$$\Phi_* \left(\frac{d^D X}{X_1 \cdots X_D} \right) = \Phi'_* \left(\frac{d^D U}{U_1 \cdots U_D} \right) \tag{3.80}$$

since $\Phi'_* = \Phi_* \circ \psi_*$, and ψ_* pushes the standard simplex form on U to the same form on X (see (3.3.2)).

3.3.4 Newton polytopes from constraints

We now provide an alternative way of thinking about equation (3.58) as *constraints* on C space. Most of the notation in this section is borrowed from Section 3.4.3.

The map $X \to C_i(X)$ parametrizes a subset of the projective space $C \in \mathbb{P}^{n-1}$. This subset can be equivalently "cut out" using constraints on the C_i variables.

$$\prod_{i=1}^{n} C_i^{w_{pi}} = 1 \tag{3.81}$$

with one constraint for each value of $p = 1, ..., n-m-1$, where w_{pi} is a constant *integer* matrix to be determined. For the constraint to be well-defined projectively, we must have $\sum_i w_{pi} = 0$ for each p.

Substituting the parametrization $C_i(X) = \prod_{a=0}^{m} X_a^{z_{ai}}$, we find that

$$\sum_{i=1}^{n} z_{ai} w_{pi} = 0 \tag{3.82}$$

for each a, p.

We can now replace the pushforward formula (3.58) by an integral over all C_i with imposed constraints.

$$\underline{\Omega}(\mathcal{A}) = \frac{1}{m!} \int \frac{d^n C}{\prod_{j=1}^{n} C_j} \left[\prod_{p=1}^{n-m-1} \delta\left(1 - \prod_{i=1}^{n} C_i^{w_{pi}}\right) \right] \delta^{m+1}\left(Y - \sum_{i=1}^{n} C_i Z_i\right) \tag{3.83}$$

Note that each delta function in the square brackets imposes one constraint, and in the absence of constraints we arrive at the familiar cyclic measure on C space.

It is evident that explicitly summing over the roots of these polynomial equations will become prohibitively more difficult for large n. But of course there is a standard approach to summing rational functions of roots of polynomial equations, making use of the *global residue theorem* [35]. This method has been applied ubiquitously in the literature on scattering amplitudes, from the earliest understanding of the

relations between leading singularities and the connection between the twistor-string and Grassmannian formalisms [36, 37, 38], to the recent application to scattering equations [10, 11, 12, 13]. Appropriately taking care of some minor subtleties, the global residue theorem also works for our problem, naturally connecting the Newton polytope formula to triangulations of the polytope.

We now provide explicit computations for the quadrilateral and the pentagon with constraints.

Example 3.3.7. For $m = 2$, $n = 4$, there is only one constraint given by

$$w_p := w_{1p} = (Q_1, -Q_2, Q_3, -Q_4) \tag{3.84}$$

for some integers $Q_i > 0$, $i = 1, 2, 3, 4$. The positivity of the Q_i variables is imposed by the positivity of the Newton polytope.

Now recall that delta functions can be identified with residues in the following manner:

$$\int dz\ \delta(z) f(z) = \mathrm{Res}_{z\to 0}\left(\frac{1}{z} f(z)\right) = f(0) \tag{3.85}$$

We will therefore think of the delta function constraints appearing in the square brackets (3.83) as residues, and apply the global residue theorem [35].

We have

$$\underline{\Omega}(\mathcal{A}) = \frac{1}{2}\int \frac{d^4C}{C_1C_2C_3C_4}\left[\frac{C_2^{Q_2}C_4^{Q_4}}{\underline{C_2^{Q_2}C_4^{Q_4} - C_1^{Q_1}C_3^{Q_3}}}\right]\delta^3\left(Y - \sum_{i=1}^{4} C_i Z_i\right) \tag{3.86}$$

Here we have underlined the pole corresponding to the constraint. The reader should imagine that the three remaining constraints (i.e. $Y = C\cdot Z$) also appear as poles, but for notational convenience we will simply write them as delta functions. For higher n, we will have additional constraints, and hence additional underlined polynomials.

Now (3.86) instructs us to sum over all global residues where the four constraints vanish, which in general is very hard to compute by explicit summation. However, the global residue theorem vastly simplifies the problem. Note that there are eight poles in our integral (i.e. four constraints plus the four cyclic factors C_i). In order to apply the theorem, we will need to group the poles into four groups. Let us group the cyclic factors with the underlined constraint, and each of the delta function constraints forms its own group. It follows therefore that

$$\underline{\Omega}(\mathcal{A}) = -\frac{1}{2}\sum_{i=1}^{4}\int \frac{d^4C}{C_1\ldots\underline{C_i}\ldots C_4}\left[\frac{C_2^{Q_2}C_4^{Q_4}}{C_2^{Q_2}C_4^{Q_4}-C_1^{Q_1}C_3^{Q_3}}\right]\delta^3\left(Y-\sum_{i=1}^{4}C_iZ_i\right) \quad (3.87)$$

This gives us four residues corresponding to $C_i \to 0$ for each i. Now the positivitiy of $Q_i > 0$ comes into play. Clearly, the $C_2, C_4 \to 0$ residues vanish due to the appearance of $C_2^{Q_2}C_4^{Q_4}$ in the numerator. However, for the $C_1, C_3 \to 0$ residues, the square bracket becomes unity, and the result is equivalent to Res(1), Res(3), respectively, as defined in 3.154. It follows that

$$\underline{\Omega}(\mathcal{A}) = \text{Res}(1) + \text{Res}(3) = [234] + [124] \quad (3.88)$$

Alternatively, we could have assumed $Q_i < 0$ for each i. This would have given us another triangulation:

$$\underline{\Omega}(\mathcal{A}) = \text{Res}(2) + \text{Res}(4) = [134] + [123] \quad (3.89)$$

We note that our technique can be applied to convex cyclic Newton polytopes for any m, provided that $n = m+2$. The constraint matrix is given by a sequence with alternating signs.

$$w_p = (Q_1, -Q_2, Q_3, -Q_4, ..., (-1)^{m+1}Q_{m+2}) \quad (3.90)$$

where the constants Q_i are either all positive or all negative. If $Q_i > 0$, then the canonical rational function becomes

$$\underline{\Omega}(\mathcal{A}) = \sum_{i \text{ odd}} \text{Res}(i) \tag{3.91}$$

And for $Q_i < 0$, we get

$$\underline{\Omega}(\mathcal{A}) = \sum_{i \text{ even}} \text{Res}(i) \tag{3.92}$$

Example 3.3.8. Let us move on to the $n = 5, m = 2$ pentagon $\mathcal{A}$ with the Newton polytope having vertices $(0,0), (1,0), (2,1), (1,2), (0,1)$. Then the Newton polytope formula becomes

$$\underline{\Omega}(\mathcal{A}) = \int dC_1 dC_2 dC_3 dC_4 dC_5 \frac{1}{C_1 C_2 C_5} \underline{\frac{C_1^2}{C_1^2 C_3 - C_2^2 C_5}} \underline{\frac{C_1^2}{C_1^2 C_4 - C_2 C_5^2}} \delta^3(Y - C \cdot Z) \tag{3.93}$$

Now on the support of the delta function we have a two-dimensional integral, and the underline tells us to sum over all the roots of the two polynomials with $C_1 \neq 0$.

In order to use the global residue theorem for our pentagon problem, we group the denominator factors into five groups, given by the three delta function constraints and f_1, f_2:

$$f_1 = C_2 C_5 (C_1^2 C_3 - C_2^2 C_5), \quad f_2 = (C_1^2 C_4 - C_2 C_5^2), \quad g = C_1^3 \tag{3.94}$$

where g is the numerator.

The roots of $f_1 = 0, f_2 = 0$ certainly include the "complicated" solutions of the Newton polytope problem, where $C_1 \neq 0$, and at these the residues are well-defined. The only subtlety is that we have other roots, where $(C_2, C_1) = (0,0)$, and where

$(C_5, C_1) = (0, 0)$. These zeros are quite degenerate; the Jacobian factor vanishes and the residue is not directly well-defined.

We can deal with this by slightly deforming the functions; we will take instead

$$f_1 = C_2 C_5((C_1^2 - \epsilon_3^2)C_3 - C_2^2 C_5), \quad f_2 = ((C_1^2 - \epsilon_4^2)C_4 - C_2 C_5^2), \quad g = C_1^3 \tag{3.95}$$

where we will imagine that both ϵ_3, ϵ_4 are eventually sent to zero. The singular zeros we previously found, with $(C_2, C_1) = (0, 0)$ and with $(C_5, C_1) = (0, 0)$ will now be split into a number of non-degenerate solutions, and we will be able to use the global residue theorem.

Let us see where these deformed zeros are located. For $f_1 = 0$, we can set either $C_2 = 0, C_5 = 0$ or $(C_1^2 - \epsilon_3^2)C_3 - C_2^2 C_5 = 0$. The first two cases are of course trivial; the roots and corresponding residues, as we take $\epsilon_3, \epsilon_4 \to 0$, are

$$C_2 = 0, \quad C_4 = 0, \quad \text{Res} = [135] \tag{3.96}$$

$$C_5 = 0, \quad C_4 = 0, \quad \text{Res} = [123] \tag{3.97}$$

$$C_2 = 0, \quad C_1 = \pm\epsilon_4, \quad \sum_{\pm} \text{Res} = \frac{\epsilon_4^2}{\epsilon_4^2 - \epsilon_3^2}[345] \tag{3.98}$$

$$C_5 = 0, \quad C_1 = \pm\epsilon_4, \quad \sum_{\pm} \text{Res} = \frac{\epsilon_4^2}{\epsilon_4^2 - \epsilon_3^2}[234] \tag{3.99}$$

Note interestingly that the residues for the last two cases depend on the ratio ϵ_3/ϵ_4 even as $\epsilon_{3,4} \to 0$. We next have to look at the solutions to

$$(C_1^2 - \epsilon_3^2)C_3 - C_2^2 C_5 = 0, \, (C_1^2 - \epsilon_4^2)C_4 - C_2 C_5^2 = 0 \tag{3.100}$$

We are interested in the solutions where C_1 is close to zero; which here means that either C_1 is close to ϵ_3 or C_1 is close to ϵ_4. More formally, we can set $\epsilon_{3,4} = \epsilon E_{3,4}$ and ask what the solutions look like as $\epsilon \to 0$ with $E_{3,4}$ fixed. It is then easy to see

that if $C_1^2 \to \epsilon_3^2$, we must have that C_5 is non-zero and $C_2 \to (\epsilon_3^2 - \epsilon_4^2)C_4/C_5^2$, while if $C_1^2 \to \epsilon_4^2$, we must have that C_2 is non-zero and $C_5 \to (\epsilon_4^2 - \epsilon_3^2)C_3/C_2^2$. It is trivial to compute the residues in these cases, and we find

$$C_1 \to \pm\epsilon_3, \quad C_2 \to (\epsilon_3^2 - \epsilon_4^2)C_4/C_5^2, \quad \sum_{\pm} \text{Res} = \frac{\epsilon_3^2}{\epsilon_4^2 - \epsilon_3^2}[345] \tag{3.101}$$

$$C_1 \to \pm\epsilon_4, \quad C_5 \to (\epsilon_4^2 - \epsilon_3^2)C_3/C_2^2, \quad \sum_{\pm} \text{Res} = \frac{\epsilon_4^2}{\epsilon_3^2 - \epsilon_4^2}[234] \tag{3.102}$$

By the global residue theorem, the sum over all these residues gives us $\underline{\Omega}_(\mathcal{A})$, so we find

$$\begin{aligned} \underline{\Omega}(\mathcal{A}) &= [123] + [135] + [345]\left(\frac{\epsilon_4^2}{\epsilon_4^2 - \epsilon_3^2} - \frac{\epsilon_3^2}{\epsilon_4^2 - \epsilon_3^2}\right) + [234]\left(\frac{\epsilon_4^2}{\epsilon_4^2 - \epsilon_3^2} - \frac{\epsilon_4^2}{\epsilon_4^2 - \epsilon_3^2}\right) \\ &= [123] + [135] + [345] \end{aligned} \tag{3.103}$$

which is a standard triangulation of the pentagon.

It would be interesting to carry out the analog of this analysis for the general Newton polytope expression associated with the canonical form of any polytope. The same resolution of the the singular roots will clearly be needed, and it will be interesting to see how and which natural class of triangulations of the polytope emerges in this way.

3.3.5 Generalized polytopes on the projective plane

We now consider pushforwards onto generalized polytopes on the projective plane, particularly the pizza slice.

Example 3.3.9. We construct the canonical form of the pizza slice $\mathcal{T}(\theta_1, \theta_2)$ from Example 2.5.1 via pushforward. Let $z_1 = \tan(\theta_1/2)$ and $z_2 = \tan(\theta_2/2)$. Consider the

morphism $\Phi : (\mathbb{P}^1 \times \mathbb{P}^1, [z_1, z_2] \times [0, \infty]) \to \mathcal{T}(\theta_1, \theta_2)$ given by:

$$(1, x, y) = \Phi(z, t) := \left(1, \frac{1 - z^2}{(1 + z^2)}, \frac{2z}{(1 + z^2)}\right) + tZ_* \tag{3.104}$$

$$= \left(1, \frac{1 - z^2}{(1 + z^2)(1 + t)}, \frac{2z}{(1 + z^2)(1 + t)}\right) \tag{3.105}$$

where z, t are coordinates on the two $\mathbb{P}^1$'s, and $Z_*^I := (1, 0, 0)$ is the "tip" of the pizza. Note that the equations are projective. As z varies in $[z_1, z_2]$, the point $(\frac{1-z^2}{(1+z^2)}, \frac{2z}{(1+z^2)})$ sweeps out the circular arc $(\cos(\theta), \sin(\theta))$ where θ varies from θ_1 to θ_2. The variable t acts like a radial coordinate that goes from 0 (the unit arc) to ∞ (the tip).

For a generic point (x, y) there are two roots in $\Phi^{-1}(1, x, y)$, say (z, t) and $(-1/z, -t - 2)$. We compute

$$\Phi_* \left(\frac{(z_2 - z_1)}{(z_2 - z)(z - z_1)} dz \frac{1}{t} dt\right) \tag{3.106}$$

$$= \frac{(1 + t)^3}{2} \left(\frac{(1 + z^2)(z_2 - z_1)}{(z_2 - z)(z - z_1)} \frac{1}{t} - \frac{(1 + z^2)(z_2 - z_1)}{(zz_2 + 1)(1 + zz_1)} \frac{1}{(t + 2)}\right) dxdy \tag{3.107}$$

We have the two identities

$$\frac{1}{2} \frac{(1 + z^2)(z_2 - z_1)}{(z_2 - z)(z - z_1)} = \frac{\sin(\theta_2 - \theta_1) + \sin(\theta - \theta_1) + \sin(\theta_2 - \theta)}{2 \sin(\theta - \theta_1) \sin(\theta_2 - \theta)} \tag{3.108}$$

$$-\frac{1}{2} \frac{(1 + z^2)(z_2 - z_1)}{(zz_2 + 1)(1 + zz_1)} = \frac{\sin(\theta_2 - \theta_1) - \sin(\theta - \theta_1) - \sin(\theta_2 - \theta)}{2 \sin(\theta - \theta_1) \sin(\theta_2 - \theta)} \tag{3.109}$$

which are related by a shift $\theta \to \theta + \pi$. Substituting into (3.107) and using $1 - x^2 - y^2 = t(2 + t)/(1 + t)^2$ gives

$$\frac{[\sin(\theta_2 - \theta_1) + (-x \sin \theta_1 + y \cos \theta_1) + (x \sin \theta_2 - y \cos \theta_2)]}{(1 - x^2 - y^2)(-x \sin \theta_1 + y \cos \theta_1)(x \sin \theta_2 - y \cos \theta_2)} dxdy \tag{3.110}$$

which of course is the canonical form $\Omega(\mathcal{T}(\theta_1, \theta_2))$. Note that sine summation formulas were used to get the denominator factors.

The pushforward calculation can also be done with more intuitive angular coordinates, using an infinite degree map similar to Example 3.3.5. We take the map $\Psi : (\mathbb{P}^1 \times \mathbb{P}^1, [\theta_1, \theta_2] \times [0, \infty]) \to \mathcal{T}(\theta_1, \theta_2)$ given by:

$$(1, x, y) = \Psi(1, \theta, t) := (1, \cos\theta, \sin\theta) + tZ_* = \left(1, \frac{\cos\theta}{1+t}, \frac{\sin\theta}{1+t}\right) \tag{3.111}$$

The variable θ acts as an angular coordinate between θ_1 and θ_2. For any point on the plane $(x, y) = (\cos\theta, \sin\theta)/(1+t)$, there are two sets of roots given by:

$$\begin{aligned} (\theta_n, t_n) &= (\theta + 2\pi n, t) && (3.112)\\ (\theta'_n, t'_n) &= (\theta + \pi(2n+1), -t-2) && (3.113) \end{aligned}$$

where $n \in \mathbb{Z}$. Summing over all roots in the pushforward gives

$$\begin{aligned} \Psi_*\left(\frac{(\theta_2-\theta_1)d\theta}{(\theta_2-\theta)(\theta-\theta_1)}\frac{dt}{t}\right) &= \frac{(1+t)^3}{t}\sum_{n\in\mathbb{Z}}\frac{(\theta_2-\theta_1)}{(\theta_2-\theta_n)(\theta_n-\theta_1)}dxdy && (3.114)\\ &\quad + \frac{(1+t)^3}{t+2}\sum_{n\in\mathbb{Z}}\frac{(\theta_2-\theta_1)}{(\theta_2-\theta'_n)(\theta'_n-\theta_1)}dxdy && (3.115) \end{aligned}$$

Ignoring the rational t factors, the summations give:

$$\begin{aligned} \sum_{n\in\mathbb{Z}}\frac{(\theta_2-\theta_1)}{(\theta_2-\theta_n)(\theta_n-\theta_1)} &= \frac{\sin(\theta_2-\theta_1)+\sin(\theta-\theta_1)+\sin(\theta_2-\theta)}{2\sin(\theta-\theta_1)\sin(\theta_2-\theta)} && (3.116)\\ \sum_{n\in\mathbb{Z}}\frac{(\theta_2-\theta_1)}{(\theta_2-\theta'_n)(\theta'_n-\theta_1)} &= \frac{\sin(\theta_2-\theta_1)-\sin(\theta-\theta_1)-\sin(\theta_2-\theta)}{2\sin(\theta-\theta_1)\sin(\theta_2-\theta)} && (3.117) \end{aligned}$$

which are exactly (3.108) and (3.109). Thus we again obtain (3.110) as the canonical form of the pizza slice. The summation identities (3.116) and (3.117) can also be interpreted as the pushforward summation for the infinite degree map $\phi : \theta \mapsto z = \tan(\theta/2)$, and we have $\Psi = \Phi \circ (\phi \times \mathrm{id})$, where $\mathrm{id} : t \mapsto t$ is the identity map on the t coordinate.

3.4 Integral representations

We now present integral representations (e.g. volume integrals, contour integrals) of various canonical forms.

3.4.1 Dual polytopes

Consider a convex polytope $(\mathbb{P}^m, \mathcal{A})$ and a point Y not along any boundary component. We argue that the canonical rational function $\underline{\Omega}(\mathcal{A})$ at Y is given by the volume of the dual polytope $\mathcal{A}_Y^*$ (defined in Section 2.5.3) under a Y-dependent measure. More precisely,

$$\underline{\Omega}(\mathcal{A})(Y) = \text{Vol}\,(\mathcal{A}_Y^*) := \frac{1}{m!}\int_{W\in\mathcal{A}_Y^*} \frac{\langle W d^m W\rangle}{(Y\cdot W)^{m+1}} \tag{3.118}$$

In order for this integral to be well-defined on projective space, the integrand must be invariant under *local* GL(1) transformations $W \to W' = \alpha(W)W$, which is proven in (C5) of [2]. Moreover, observe that by construction of $\mathcal{A}_Y^*$, we have $Y\cdot W > 0$ for every point $W \in \text{Int}(\mathcal{A}_Y^*)$, which is important for the integral to converge. However, the overall sign of the integral is dependent on the orientation of the dual. We say therefore that the volume is *signed*.

Now let us prove this claim for simplices by explicit computation:

Example 3.4.1. Let $Y \in \text{Int}(\Delta)$ for some simplex. The volume of the dual simplex Δ_Y^* with vertices $W_1, \ldots, W_{m+1}$ (so that $Y\cdot W_i > 0$ for each i) can be computed using a Feynman parameter technique. Since the form is locally GL(1) invariant, we can gauge fix the integration to $W = W_1 + \alpha_1 W_2 + \cdots + \alpha_m W_{m+1}$ and integrate over

$\alpha_i > 0$. This gives

$$\begin{aligned} \text{Vol}\,(\Delta_Y^*) &= \int \frac{d^m\alpha\,\langle W_1\cdots W_{m+1}\rangle}{((Y\cdot W_1)+\alpha_1(Y\cdot W_2)+\cdots+\alpha_m(Y\cdot W_{m+1}))^{m+1}} \quad (3.119)\\ &= \frac{\langle W_1\cdots W_{m+1}\rangle}{m!(Y\cdot W_1)\cdots(Y\cdot W_{m+1})} \quad (3.120)\end{aligned}$$

agreeing with (2.17).

Note that the result is independent of the sign of the vertices W_i. If, for instance, we move Y outside Δ so that $Y\cdot W_1 < 0$ but $Y\cdot W_i > 0$ for every $i \neq 1$, then we would have needed to use $-W_1$ in the integration, but the result would still have the same form.

We now argue that the formula holds for an arbitrary convex polytope based on three observations:

- "Dualization of polytopes commutes with triangulation" (2.65). This means that

$$\mathcal{A} = \sum_i \mathcal{A}_i \quad \Rightarrow \quad \mathcal{A}_Y^* = \sum_i \mathcal{A}_{iY}^* \tag{3.121}$$

  For triangulation by simplices, this formula is known as *Filliman duality* [39].

- The signed nature of the volume is crucial, because it implies *triangulation independence*. This means that

$$\mathcal{A}_Y^* = \sum_i \mathcal{A}_{iY}^* \quad \Rightarrow \quad \text{Vol}\,(\mathcal{A}_Y^*) = \sum_i \text{Vol}\,(\mathcal{A}_{iY}^*) \tag{3.122}$$

- The canonical rational function is triangulation independent (Section 2.2):

$$\mathcal{A} = \sum_i \mathcal{A}_i \quad \Rightarrow \quad \underline{\Omega}(\mathcal{A}) = \sum_i \underline{\Omega}(\mathcal{A}_i) \tag{3.123}$$

Combining these three statements for a *signed* triangulation by simplices $\mathcal{A}_i = \Delta_i$, it follows that

$$\text{Vol}\,(\mathcal{A}_Y^*) = \sum_i \text{Vol}\,(\Delta_{iY}^*) = \sum_i \underline{\Omega}(\Delta_i) = \underline{\Omega}(\mathcal{A}) \tag{3.124}$$

which is the desired claim.

We have not given a proof of the first observation (3.121). In Section 3.4.2 we will give an independent proof of the volume formula (3.118). Then by the second and third assumptions, we find that $\text{Vol}\,(\mathcal{A}_Y^*) = \sum_i \text{Vol}\,(\mathcal{A}_{iY}^*)$ for every Y, which implies that $\mathcal{A}_Y^* = \sum_i \mathcal{A}_i^*$, thus deriving (3.121). Alternatively, we can also say that the the volume formula combined with the first two assumptions implies the triangulation independence of the canonical rational function.

The dual volume formula is particularly useful for computing the canonical form of simple polytopes. Recall that a polytope of dimension m is called simple if every vertex is adjacent to exactly m facets.

Example 3.4.2. Consider a convex simple polytope $\mathcal{A}$ of dimension m. Recall that the dual polytope of a simple polytope is simplicial, meaning that each facet is a simplex. The dual polytope can therefore be triangulated very easily. The idea is to take a reference point W_0 on the interior of the dual, then for every facet Z form a simplex by the convex hull of that facet and the reference point. These simplices then give the desired triangulation.

$$\text{Vol}(\mathcal{A}^*) = \sum_Z \text{sign}(Z) \frac{\langle W_0 W_1 \dots W_m \rangle}{m!(Y \cdot W_0) \prod_{a=1}^m (Y \cdot W_a)} \tag{3.125}$$

where for every facet Z the dual vectors W_a correspond to the m adjacent facets. Furthermore, the $\text{sign}(Z) \in \{\pm 1\}$ denotes the orientation of the ordered facets $W_1, \dots, W_{n-3}$, which of course is antisymmetric. Note that the sum can be thought of either as a sum over the facets of $\mathcal{A}^*$ or as a sum over the vertices of $\mathcal{A}$.

If we choose the reference point so that $(Y \cdot W_0) = 1$, then the canonical form can also be expressed in the following way

$$\Omega(\mathcal{A}) = \sum_{Z} \text{sign}(Z) \bigwedge_{a=1}^{m} d\log\left(Y \cdot W_a\right) \tag{3.126}$$

This formula can also be proven independently of the dual construction, by showing that it satisfies the recursive pole and residue properties required of the canonical form. See Appendix A.5 of [1] for more details.

We now wish to comment on the distinction between "physical" poles and "spurious" poles (see Section 2.2.2) in the context of the volume formula, first pointed out by Andrew Hodges as an interpretation of spurious poles appearing in BCFW recursion of NMHV tree amplitudes [29].

Given a triangulation of $\mathcal{A}$ by polytopes $\mathcal{A}_i$ with mutually non-overlapping interiors, spurious poles appear along boundary components of the triangulating pieces that do not belong to the boundary components of $\mathcal{A}$. From the dual point of view, the duals $\mathcal{A}_{iY}^*$ form an *overlapping* triangulation of $\mathcal{A}_Y^*$, and a spurious pole corresponds to a subset of volume terms $\text{Vol}\,(\mathcal{A}_{iY}^*)$ going to infinity individually, but whose sum remains finite. Geometrically, the signed volumes overlap and cancel. However, suppose instead that $Y \in \text{Int}(\mathcal{A})$ and the duals $\mathcal{A}_{iY}^*$ have non-overlapping interiors, then $\text{Vol}\,(\mathcal{A}_{iY}^*) \leq \text{Vol}\,(\mathcal{A}_Y^*)$. It follows that all the volume terms are finite on $\text{Int}(\mathcal{A})$, and there are no spurious poles. Of course, the sum is independent of X since the integral is surface-independent. This is called a *local triangulation*. An example of a local triangulation of cyclic polytopes in $\mathbb{P}^4(\mathbb{R})$ is given in [40].

On a final note, we argue that these simplicial volumes are identical to Feynman parameters [41] appearing in the computation of loop scattering amplitudes. A

general Feynman parameter formula takes the following form,

$$\frac{1}{\prod_{i=0}^{m} A_i} = m! \int_{x \in I^{m+1}} d^{m+1}x \frac{\delta(1 - \sum_{i=0}^{m} x_i)}{\left(\sum_{i=0}^{m} x_i A_i\right)^{m+1}} \tag{3.127}$$

where I^{m+1} is the unit cube given by $0 < x_i < 1$ for all i. Integrating over $0 < x_0 < 1$ yields

$$\frac{1}{\prod_{i=0}^{m} A_i} = m! \int_{\substack{x \in I^m \\ 0 < \sum_{i=1}^{m} x_i < 1}} d^m x \frac{1}{\left(A_0 + \sum_{i=1}^{m} x_i (A_i - A_0)\right)^{m+1}} \tag{3.128}$$

Now change variables $x_i \to \alpha_i$ so that

$$x_i = \frac{\alpha_i}{1 + \sum_{j=1}^{m} \alpha_i} \tag{3.129}$$

and $\alpha_i > 0$ for all i is the equivalent region of integration. The Jacobian for the change of measure is

$$d^m x = \frac{d^m \alpha}{(1 + \sum_{i=1}^{m} \alpha_i)^{m+1}} \tag{3.130}$$

Putting everything together, we get

$$\frac{1}{m!} \frac{1}{\prod_{i=0}^{m} A_i} = \int_{\alpha_i > 0} d^m \alpha \frac{1}{(A_0 + \sum_{i=1}^{m} \alpha_i A_i)^{m+1}} \tag{3.131}$$

We see that the right hand side is very reminiscent of the volume formula (3.118) for a (dual) simplex. The lesson here is that loop integrals can be reinterpreted as polytope volumes, and Feynman parameters are coordinates on the interior of the polytope over which we integrate.

3.4.2 Laplace transforms

For a convex projective polytope $\mathcal{A} \subset \mathbb{P}^m(\mathbb{R})$, we let $\bar{\mathcal{A}} \subset \mathbb{R}^{m+1}$ be the cone over $\mathcal{A}$, so that $\bar{\mathcal{A}} := \{Y \in \mathbb{R}^{m+1} \mid Y \in \mathcal{A}\}$. Similarly, one has the cone of the dual $\bar{\mathcal{A}}^*_Y \subset \mathbb{R}^{m+1}$ in the dual vector space. For simplicity, we will only consider the dual for which $Y \in \mathrm{Int}(\mathcal{A})$, in which case $\mathcal{A}^* := \mathcal{A}^*_Y$.

We argue that the canonical rational function at any point $Y \in \mathrm{Int}(\mathcal{A})$ is given by a Laplace transform over the cone of the dual:

$$\underline{\Omega}(\bar{\mathcal{A}})(Y) = \frac{1}{m!}\left(\int_{W \in \bar{\mathcal{A}}^*_Y} e^{-W\cdot Y} d^{m+1}W\right). \tag{3.132}$$

Such integral formulae have been considered in [42]. Extensions to the Grassmannian are discussed in [43].

We now show the equivalence of (3.132) with the dual volume (3.118). We begin with the Laplace transform, and change variables by writing $W = \rho\widehat{W}$ so that $\widehat{W}$ is a unit vector and $\rho > 0$ is the Euclidean norm of W. It follows that

$$d^{m+1}W = \frac{1}{m!}\rho^m d\rho \left\langle \widehat{W} d^m \widehat{W} \right\rangle \tag{3.133}$$

The Laplace transform rational function becomes

$$\underline{\Omega}(\mathcal{A}) = \frac{1}{m!}\int_{\rho>0, \widehat{W}\in\mathcal{A}^*} e^{-\rho\widehat{W}\cdot Y}\frac{\rho^m d\rho}{m!}\left\langle \widehat{W} d^m \widehat{W}\right\rangle = \frac{1}{m!}\int_{\widehat{W}\in\mathcal{A}^*}\frac{\left\langle \widehat{W} d^m \widehat{W}\right\rangle}{(\widehat{W}\cdot Y)^{m+1}}. \tag{3.134}$$

This result is identical to (3.118) but "gauge-fixed" so that $W = \widehat{W}$ has unit norm. Removing the gauge choice and rewriting $\widehat{W}$ as W recovers (3.118).

Let us confirm our result for a simplex.

Example 3.4.3. Suppose Δ is a simplex, so Δ^* is also a simplex, generated by facets $W_1, \ldots, W_{m+1} \in \mathbb{R}^{m+1}$. Then setting $W = \alpha_0 W_1 + \cdots \alpha_m W_{m+1}$, we compute

$$\underline{\Omega}(\bar{\Delta})(Y) = \frac{1}{m!}\left(\int_{W \in \bar{\mathcal{A}}^*} e^{-W \cdot Y} d^{m+1} W\right) \tag{3.135}$$

$$= \frac{1}{m!}\langle W_1 W_2 \cdots W_{m+1}\rangle \left(\int_{\mathbb{R}^{m+1}_{>0}} e^{-(\alpha_0 (W_1 \cdot Y) + \alpha_1 (W_2 \cdot Y) + \cdots + \alpha_m (W_{m+1} \cdot Y))} d^{m+1}\alpha\right) \tag{3.136}$$

$$= \frac{\langle W_1 W_2 \cdots W_{m+1}\rangle}{m!(Y \cdot W_1)(Y \cdot W_2)\cdots(Y \cdot W_{m+1})}, \tag{3.137}$$

in agreement with (2.17).

We recognize the result simply as the volume Vol (Δ^*) (note the implicit dependence on Y). For a general convex polytope $\mathcal{A}$, we may triangulate its dual $\mathcal{A}^* = \sum_i \Delta_i^*$ by (dual) simplices. Then the cone of the dual is also triangulated by the cones $\overline{\Delta_i}^*$ of the dual simplices. For simplicity let us assume that these dual cones are non-overlapping except possibly at mutual boundaries. We can therefore triangulate the Laplace transform integration and obtain:

$$\underline{\Omega}(\mathcal{A})(Y) = \sum_i \text{Vol}\,(\Delta_i^*) \tag{3.138}$$

which of course is equivalent to Vol $(\mathcal{A}^*)$ as expected.

Let us now try a sample computation for a quadrilateral.

Example 3.4.4. Let $\mathcal{A} \subset \mathbb{P}^2$ be the polytope with vertices:

$$\{(1,0,0),(0,1,0),(0,0,1),(1,1,-1)\}$$

Then the dual cone is

$$\bar{\mathcal{A}}^* = \{W = (W_0, W_1, W_2) \in \mathbb{R}^3_{\geq 0} \mid W_0 + W_1 \geq W_2\}. \tag{3.139}$$

We compute

$$\underline{\Omega}(\mathcal{A}) = \frac{1}{2!}\int_{W\in\bar{\mathcal{A}}^*} e^{-W\cdot Y} d^{m+1}W \tag{3.140}$$

$$= \frac{1}{2!}\int_0^\infty e^{-W_0 Y^0}\int_0^\infty e^{-W_1 Y^1}\int_0^{W_0+W_1} e^{-W_2 Y^2} dW_2 dW_1 dW_0 \tag{3.141}$$

$$= \frac{1}{2!}\frac{Y^0+Y^1+Y^2}{(Y^0+Y^2)(Y^1+Y^2)Y^0Y^1}. \tag{3.142}$$

To verify our calculation, we observe that

$$\frac{1}{2!}\frac{Y^0+Y^1+Y^2}{(Y^0+Y^2)(Y^1+Y^2)Y^0Y^1} = \frac{1}{2!}\left(\frac{1}{Y^0Y^1Y^2} - \frac{1}{(Y^0+Y^2)(Y^1+Y^2)Y^2}\right) \tag{3.143}$$

corresponding to the triangulation $\mathcal{A} = \Delta_1 \cup \Delta_2$ where Δ_1 has three vertices which are given by $\{(1,0,0),(0,1,0),(0,0,1)\}$ and Δ_2 has vertices $\{(1,0,0),(1,1,-1),(0,1,0)\}$.

Let us now argue that the Laplace transform makes manifest all the poles and residues of the canonical form, and thus satisfies the recursive properties of the form. Suppose $\{Y \in \partial\mathcal{A} \mid W_0 \cdot Y = 0\}$ defines one of the facets of the polytope $\mathcal{A}$, which we denote by $\mathcal{B}$, and hence W_0 is one of the vertices of $\mathcal{A}^*$. We now show that (3.132) has a first order pole along the hyperplane $W_0 \cdot Y = 0$ and identify its residue. Consider the expansion

$$W = \alpha W_0 + \bar{W} \tag{3.144}$$

where α is a scalar and $\bar{W} \in \gamma(W_0)$, where $\gamma(W_0)$ denotes the union of all the facets of the cone $\bar{\mathcal{A}}^*$ *not* adjacent to W_0. It is straightforward to prove that every point W in the interior of the integration region $\bar{\mathcal{A}}^*$ has a unique expression in the form (3.144) with $(\alpha, \bar{W}) \in \mathbb{R}_{>0} \times \gamma(W_0)$. Furthermore, some simple algebra shows that

$d^{m+1}W = d\alpha \left\langle W_0 d^m \bar{W} \right\rangle / m!$. It follows that

$$\underline{\Omega}(\mathcal{A}) = \frac{1}{m!} \int_0^\infty d\alpha \; e^{-\alpha(W_0 \cdot Y)} \int_{\bar{W} \in \gamma(W_0)} e^{-\bar{W} \cdot Y} \frac{\left\langle W_0 d^m \bar{W} \right\rangle}{m!} \tag{3.145}$$

The $\alpha > 0$ integral can be trivially computed to reveal the first order pole.

$$\underline{\Omega}(\mathcal{A}) = \frac{1}{m!} \frac{1}{(W_0 \cdot Y)} \int_{\bar{W} \in \gamma(W_0)} e^{-\bar{W} \cdot Y} \frac{\left\langle W_0 d^m \bar{W} \right\rangle}{m!} \tag{3.146}$$

If we now take a residue at $(W_0 \cdot Y) \to 0$, we see that the remaining integral is invariant under *local* shifts $\bar{W} \to \bar{W} + \beta(\bar{W}) W_0$ along the direction of W_0, where $\beta(\bar{W})$ is a scalar dependent on $\bar{W}$. So the integral is performed within the quotient space $\mathbb{P}^m / W_0$, which of course is just the dual of the co-dimension one variety $\{Y \mid Y \cdot W_0 = 0\}$ containing $\mathcal{B}$. We say that the integral has been *projected* through W_0.

We can change the region of integration to $\bar{\mathcal{B}}^*$ which we define to be the cone over the union of all the facets of $\mathcal{A}^*$ adjacent to W_0. The change is possible because the surface $\gamma(W_0) \cup \bar{\mathcal{B}}^*$ is closed under the projection. The choice of notation $\bar{\mathcal{B}}^*$ suggests that the region can be interpreted as the cone of the dual of $\mathcal{B}$. Indeed, the facets of $\mathcal{A}^*$ adjacent to W_0 correspond to the vertices of $\mathcal{B}$.

It follows that

$$\lim_{(W_0 \cdot Y) \to 0} \underline{\Omega}(\mathcal{A})(W_0 \cdot Y) = \frac{1}{m!} \left(\int_{\bar{W} \in \mathcal{B}^*} e^{\bar{W} \cdot Y} d^m \bar{W} \right) \tag{3.147}$$

where $d^m \bar{W}$ is defined to be the measure $\left\langle W_0 d^m \bar{W} \right\rangle / m!$ on $\mathbb{P}^m / W_0$. We can interpret the residue as a Laplace transform for $\mathcal{B}$, as expected from the recursive nature of the residue.

3.4.3 Projective space contours

We now turn to a new topic. We show that the canonical rational function of convex projective polytopes (and possibly more general positive geometries) can be represented as a contour integral over a related projective space.

Recall for convex projective polytopes $\mathcal{A}$ that the $n \times (m+1)$-matrix Z can be considered a linear map $\mathbb{P}^{n-1} \to \mathbb{P}^m$, sending the standard simplex Δ^{n-1} to the polytope $\mathcal{A}$. Letting $(C_j)_{j=1}^n$ denote the coordinates on $\mathbb{P}^{n-1}$, we have the equation $Y = Z(C) = \sum_{j=1}^n C_j Z_j$ describing the image $Y \in \mathbb{P}^m$ of a point $C \in \mathbb{P}^{n-1}$ under the map.

We begin with the simplex canonical form on $(C_j)_{j=1}^n \in \mathbb{C}^n$ constrained on the support of the expression $Y = \sum_{j=1}^n C_j Z_j$:

$$\int \frac{d^n C}{\prod_{j=1}^n C_j} \delta^{m+1}\left(Y - \sum_{j=1}^n C_j Z_j\right). \tag{3.148}$$

Typically, the delta function on projective space $\delta^m(Y, Z(C))$ is reduced from rank $m+1$ to m by integrating over a GL(1) factor like ρ in (3.59). Instead, we have absorbed the $d\rho/\rho$ measure into the canonical form on C-space, thus giving a rank-n measure on $\mathbb{C}^n$.

We now describe a contour in the C-space such that the above integral gives the canonical rational function $\underline{\Omega}(\mathcal{A})$. A naive integral over all $C \in \mathbb{R}^n$ is obviously ill-defined due to the $1/C_j$ singularities. However, with some inspiration from Feynman, we can integrate slightly away from the real line $C_j \to c_j = C_j + i\epsilon_j$ for some small constants $\epsilon_j > 0$, with $c_j \in \mathbb{R}$ being the contour. We will assume that $\sum_{j=1}^n \epsilon_j Z_j = \epsilon Y$ for some $\epsilon > 0$, and let $\bar{Y} := (1 + i\epsilon)Y$. After completing the contour integral, we can take the limit $\epsilon \to 0$ to recover $\bar{Y} \to Y$. This is reminiscent of the epsilons appearing in the loop integration of amplitudes. Finally, we assume that the Z_j vertices form a

real convex polytope and $\bar{Y}$ is a positive linear combination of the Z_j's. Note that $\bar{Y}$ is real and Y is now slightly imaginary due to the $i\epsilon$ shift.

We claim, in the $\epsilon_j \to 0$ limit,

$$\underline{\Omega}(\mathcal{A})(Y) = \frac{1}{(2\pi i)^{n-m-1} m!} \int \frac{d^n c}{\prod_{j=1}^n (c_j - i\epsilon_j)} \delta^{m+1}\left(\bar{Y} - \sum_{j=1}^n c_j Z_j\right) \tag{3.149}$$

with integration over $c_j \in \mathbb{R}$ for each j. The overall constants have been inserted to achieve the correct normalization.

Before proving this identity in full generality, we give a few examples.

Example 3.4.5. The simplest example occurs for $n = m+1$ where $\mathcal{A}$ is just a simplex in m dimensions. In that case, there is no contour, and we can immediately set $\epsilon_j \to 0$ for each j and thus $\epsilon \to 0$. We get

$$\underline{\Omega}(\mathcal{A})(Y) = \frac{1}{m!} \int \frac{d^{m+1} c}{\prod_{j=1}^{m+1} c_j} \delta^{m+1}\left(Y - \sum_{j=1}^{m+1} c_j Z_j\right) \tag{3.150}$$

We can uniquely solve for each c_j on the support of the delta function, which gives

$$c_j = (-1)^{j-1} \frac{\left\langle Y 12 \cdots \hat{j} \cdots (m+1) \right\rangle}{\langle 12 \cdots (m+1) \rangle} \tag{3.151}$$

where the "hat" denotes omission, and the Jacobian of the delta function is $\langle 12 \cdots (m+1) \rangle$. It follows that (see (2.18))

$$\underline{\Omega}(\mathcal{A})(Y) = [1, 2, \ldots, m+1] \tag{3.152}$$

which is the familiar canonical rational function for a simplex.

More generally, suppose we integrate over a contour in the original C space that picks up a set of poles at $C_j \to 0$ for all j except $j = j_0, \ldots, j_m$, which we assume to

be arranged in ascending order. Then the residue is given by

$$\frac{1}{m!}\int\left(\prod_{j\in J}\mathrm{Res}_{C_j=0}\right)\frac{d^nC}{\prod_{j=1}^n C_j}\delta\left(Y-\sum_{j=1}^n C_jZ_j\right)=[j_0,j_1,j_2,\ldots,j_m] \quad (3.153)$$

where $J=\{1,2,\ldots,n\}-\{j_0,j_1,j_2,\ldots,j_m\}$. Suppose the indices contained in J are $k_1,\ldots,k_{n-m-1}$ in increasing order, then we will denote the residue collectively as $\mathrm{Res}(J)$ or $\mathrm{Res}(k_1,k_2,\ldots,k_{n-m-1})$. So

$$\mathrm{Res}(J):=\mathrm{Res}(k_1,\ldots,k_{n-m-1}):=[j_1,j_2,\ldots,j_m] \quad (3.154)$$

We note that the result may come with a negative sign if the contour is negatively oriented. The Res operator, however, assumes a positive orientation. This formula will be very convenient for the subsequent examples.

We now move on to higher n examples for the polygon (i.e. $m=2$).

Example 3.4.6. We now perform the contour integral explicitly at $n=4$ points for the $m=2$ quadrilateral. There are four integrals over c_i constrained by three delta functions. We will integrate out $c_{1,2,3}$ to get rid of the delta functions with a Jacobian factor $\langle 123\rangle^3$, which gives us

$$\frac{1}{2!(2\pi i)}\int_{c_4\in\mathbb{R}}\frac{dc_4/\langle 123\rangle^3}{(c_1-i\epsilon_1)(c_2-i\epsilon_2)(c_3-i\epsilon_3)(c_4-i\epsilon_4)} \quad (3.155)$$

where c_1,c_2, and c_3 depend on c_4 through the three equations $\bar{Y}=Z(c)$.

In the large c_4 limit, all three dependent variables scale like $O(c_4)$, so the integrand scales like $O(c_4^{-4})$ which has no pole at infinity. We can now integrate over c_4 by applying Cauchy's theorem. The key is to first work out the location of the four poles relative to the real line.

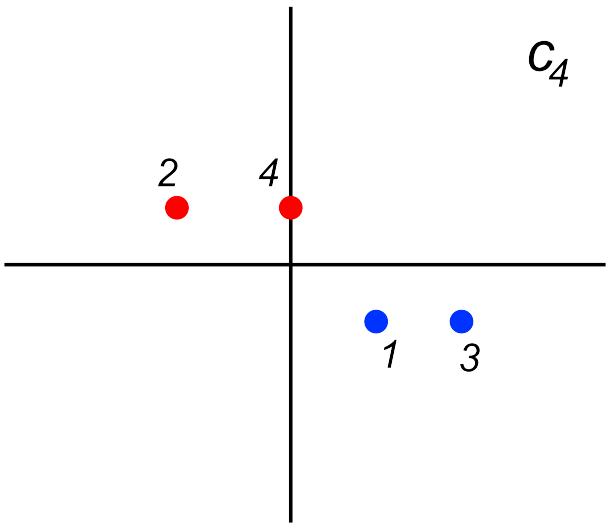

Figure 3.4: The locations of the four poles for the quadrilateral $i\epsilon$ contour, with c_1, c_2 and c_3 dependent on c_4 through $\bar{Y} = c \cdot Z$. A pole is colored red if a counterclockwise contour picks up the residue with a plus sign (e.g. $+\text{Res}(2), +\text{Res}(4)$), while a pole is colored blue if a counterclockwise contour picks up the residue with a minus sign (e.g. $-\text{Res}(1), -\text{Res}(3)$). Of course, the signs are reversed if the contour is clockwise.

We begin with the constraints

$$\bar{Y} = c_1 Z_1 + c_2 Z_2 + c_3 Z_3 + c_4 Z_4 \tag{3.156}$$

which can be re-expressed in terms of three scalar equations by contracting with $Z_2 Z_3$, $Z_3 Z_1$, and $Z_1 Z_2$, respectively.

$$c_4 \langle 234 \rangle = \langle \bar{Y} 23 \rangle - c_1 \langle 123 \rangle \tag{3.157}$$

$$c_4 \langle 134 \rangle = -\langle \bar{Y} 31 \rangle + c_2 \langle 123 \rangle \tag{3.158}$$

$$c_4 \langle 124 \rangle = \langle \bar{Y} 12 \rangle - c_3 \langle 123 \rangle \tag{3.159}$$

We have written the equation so that each bracket is positive, provided that Z_i is cyclically convex and Y is inside the polygon. Both positivity conditions are crucial, because they prescribe the location of the poles.

Now, for any index $i = 1, 2, 3, 4$, we let the "pole at i" refer to the pole at $c_i \to i\epsilon_i$. From the constraints, we find that poles 1 and 3 both provide a negative imaginary part to c_4, so they are below the real line, while poles at 2 and 4 are above the real line (see Figure 3.4). Since there is no pole at infinity, the integral can be performed by closing the contour below to pick up poles $1, 3$, or closing the contour above to pick up poles $2, 4$. The former gives us

$$\underline{\Omega}(\mathcal{A}) = \text{Res}(1) + \text{Res}(3) = [2, 3, 4] + [1, 2, 4] \tag{3.160}$$

while the latter gives

$$\underline{\Omega}(\mathcal{A}) = \text{Res}(2) + \text{Res}(4) = [1, 3, 4] + [1, 2, 3] \tag{3.161}$$

Of course, these are two equivalent triangulations of the quadrilateral. We see therefore that the $i\epsilon$ contour beautifully explains the triangulation independence of the canonical rational function as a consequence of Cauchy's theorem.

Example 3.4.7. We now compute the contour for a pentagon, where new subtleties emerge. We begin as before by integrating over c_1, c_2 and c_3 to get rid of the delta functions. We then re-express the delta function constraints as three scalar equations.

$$c_4 \langle 234 \rangle + c_5 \langle 235 \rangle = \langle \bar{Y} 23 \rangle - c_1 \langle 123 \rangle \tag{3.162}$$

$$c_4 \langle 134 \rangle + c_5 \langle 135 \rangle = -\langle \bar{Y} 31 \rangle + c_2 \langle 123 \rangle \tag{3.163}$$

$$c_4 \langle 124 \rangle + c_5 \langle 125 \rangle = \langle \bar{Y} 12 \rangle - c_3 \langle 123 \rangle \tag{3.164}$$

We now integrate over $c_4 \in \mathbb{R}$. The locations of the poles are the same as before (see Figure 3.4), and we are free to choose how we close the contour. For sake of example, let us close the contour above so we pick up poles 2 and 4. We now analyze both poles individually.

The pole at 4 induces $c_4 \to i\epsilon_4$. Our constraints therefore become:

$$c_5 \langle 235 \rangle = \left\langle \bar{Y} 23 \right\rangle - c_1 \langle 123 \rangle - i\epsilon_4 \langle 234 \rangle \tag{3.165}$$

$$c_5 \langle 135 \rangle = -\left\langle \bar{Y} 31 \right\rangle + c_2 \langle 123 \rangle - i\epsilon_4 \langle 134 \rangle \tag{3.166}$$

$$c_5 \langle 125 \rangle = \left\langle \bar{Y} 12 \right\rangle - c_3 \langle 123 \rangle - i\epsilon_4 \langle 124 \rangle \tag{3.167}$$

There are now four poles left for c_5, corresponding to 1,2,3 and 5. The poles at 1 and 3 are clearly below the real line, as evident in the equations above, while the the pole at 5 is obviously above (see Figure 3.5). The pole at 2, however, is more subtle and deserves closer attention. In the limit $c_2 \to i\epsilon_2$, we find from the second equation above that

$$c_5 \langle 135 \rangle = -\left\langle \bar{Y} 31 \right\rangle + iq \tag{3.168}$$

where $q = \epsilon_2 \langle 123 \rangle - \epsilon_4 \langle 134 \rangle$. If $q > 0$, then the pole at 2 is above the real line, and if $q < 0$, then the pole is below. So the relative size of the ϵ_j parameters makes a difference to the computation. However, as we now show, the final result is unaffected by the sign of q. Suppose $q > 0$, then we can close the c_5 contour above and pick up the following poles

$$\text{Res}(45) + \text{Res}(24) = [123] + [135] \tag{3.169}$$

Alternatively, we can close below and pick up

$$\text{Res}(34) + \text{Res}(14) = [125] + [235] \tag{3.170}$$

The two results, of course, are identical since there is no pole at infinity. So the pole at 4 produces the following result regardless of how the c_5 contour is closed, provided

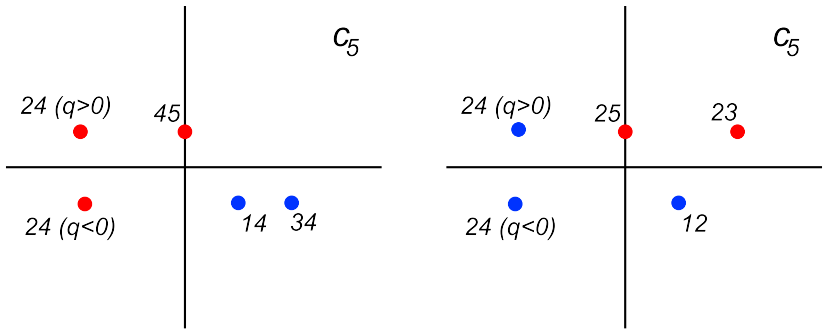

Figure 3.5: The pole locations of c_5 under $c_4 \to i\epsilon_4$ (left) and $c_2 \to i\epsilon_2$ (right). Note that in both graphs the position of the 24 pole relative to the real line differs depending on the sign of q. See the caption under Figure 3.4 for explanations of the pole coloring.

that $q > 0$.

$$c_4 \to i\epsilon_4 \; ; \; q > 0 \quad \sim \; \underline{\Omega}(Z_1, Z_2, Z_3, Z_5) \tag{3.171}$$

If $q < 0$, then Res(24) migrates below the real line, in which case closing the contour above would give

$$\text{Res}(45) = [123] \tag{3.172}$$

and closing below would give

$$\text{Res}(34) + \text{Res}(14) - \text{Res}(24) = [125] + [235] - [135] \tag{3.173}$$

which of course are equivalent. The minus sign in front of Res(24) appears due to the orientation of the contour. In summary,

$$c_4 \to i\epsilon_4 \; ; \; q < 0 \quad \sim \; \underline{\Omega}(Z_1, Z_2, Z_3) \tag{3.174}$$

Now let us move on to the pole of c_4 at 2 which induces $c_2 \to i\epsilon_2$. Again, there are four poles left for c_5, this time corresponding to 1,3,4,5. After re-arranging the

constraints using Schouten identities, we find

$$\begin{aligned} c_5 \langle 123\rangle \langle 345\rangle &= \left\langle \bar{Y}34\right\rangle \langle 123\rangle - \langle 123\rangle \left(c_1 \langle 134\rangle + i\epsilon \langle 234\rangle\right) && (3.175)\\ c_4 \langle 145\rangle \langle 123\rangle &= -\left\langle \bar{Y}41\right\rangle \langle 123\rangle + \langle 123\rangle \left(i\epsilon_2 \langle 124\rangle + c_3 \langle 134\rangle\right) && (3.176)\\ c_5 \langle 135\rangle &= \left\langle \bar{Y}13\right\rangle + i\epsilon_2 \langle 123\rangle - c_4 \langle 134\rangle && (3.177) \end{aligned}$$

Evidently, the poles at 3 and 5 are above the real line, while the pole at 1 is below (see Figure 3.5). The pole at 4, however, is above if $q > 0$ and below if $q < 0$.

For $q > 0$, closing the c_5 contour above gives

$$\text{Res}(23) - \text{Res}(24) + \text{Res}(25) = [145] - [135] + [134] \tag{3.178}$$

while closing below gives

$$\text{Res}(12) = [345] \tag{3.179}$$

which are equivalent, so

$$c_2 \to i\epsilon_2 \ ; \ q > 0 \ \sim \ \underline{\Omega}(Z_3, Z_4, Z_5) \tag{3.180}$$

For $q < 0$, closing the contour above gives

$$\text{Res}(23) + \text{Res}(25) = [145] + [134] \tag{3.181}$$

while closing below gives

$$\text{Res}(12) + \text{Res}(24) = [345] + [135] \tag{3.182}$$

which are again equivalent, so

$$c_2 \to i\epsilon_2 \ ; \ q > 0 \quad \sim \ \underline{\Omega}(Z_1, Z_3, Z_4, Z_5) \tag{3.183}$$

We now sum over the $c_4 \to i\epsilon_4$ and $c_2 \to i\epsilon_2$ contributions. For $q > 0$, we get

$$\underline{\Omega}(\mathcal{A}) = \underline{\Omega}(Z_1, Z_2, Z_3, Z_5) + \underline{\Omega}(Z_3, Z_4, Z_5) \tag{3.184}$$

and for $q < 0$, we get

$$\underline{\Omega}(\mathcal{A}) = \underline{\Omega}(Z_1, Z_2, Z_3) + \underline{\Omega}(Z_1, Z_3, Z_4, Z_5) \tag{3.185}$$

Both results are of course correct. Again, we see triangulation independence as a result of Cauchy's theorem, but with additional subtleties involving the sign of q. Furthermore, we could have closed the c_4 contour below instead and achieved a different set of triangulations.

We now argue for all $m > 0$ and all $n \geq m+1$ that the $i\epsilon$ contour integral (3.149) is equivalent to the dual volume formula (3.118). Let S denote the right hand side of (3.149). We begin by writing the delta function in terms of its Fourier transform with dual variable $W \in \mathbb{R}^{m+1}$.

$$\delta^{m+1}\left(\bar{Y} - \sum_{j=1}^{n} c_j Z_j\right) = \frac{1}{(2\pi)^{m+1}} \int d^{m+1}W \ e^{i\left(-W\cdot\bar{Y} + \sum_{j=1}^{n} c_j W\cdot Z_j\right)} \tag{3.186}$$

Then we integrate over each c_j using the following identity:

$$\int_{\mathbb{R}} \frac{dc_j}{c_j - i\epsilon_j} e^{ic_j W\cdot Z_j} = (2\pi i)\ \theta(W \cdot Z_j) \tag{3.187}$$

where $\theta(x)$ is the Heaviside step function. It follows that

$$S = \frac{i^{m+1}}{m!} \int d^{m+1}W e^{-iW\cdot\bar{Y}} \prod_{j=1}^{n} \theta(W \cdot Z_j) \tag{3.188}$$

We also change variables to radial coordinates $\rho := |W|$ and $\hat{W} := W/|W|$ with $|W|$ denoting the Euclidean norm of W. We have $W = \rho\hat{W}$ so that the measure now becomes $d^{m+1}W = \rho^m d\rho \left\langle \hat{W} d^m \hat{W} \right\rangle / m!$, where $\left\langle \hat{W} d^m \hat{W} \right\rangle$ is the pull back of $\langle W d^m W \rangle$ to the sphere $\hat{W} \in S^m$.

Now recall the Fourier transform identity:

$$\frac{1}{m!} \int_{\mathbb{R}} dx\ x^m \theta(x) e^{-ixy} = \frac{(-i)^{m+1}}{(y - i\epsilon')^{m+1}} \tag{3.189}$$

for some small $\epsilon' > 0$ which we take to zero in the end. The integral over $\rho > 0$ therefore becomes:

$$\frac{1}{m!} \int_0^\infty d\rho\ \rho^m e^{-i\rho\hat{W}\cdot\bar{Y}} = \frac{(-i)^{m+1}}{(\hat{W}\cdot\bar{Y} - i\epsilon')^{m+1}} = \frac{(-i)^{m+1}}{(\hat{W}\cdot Y)^{m+1}} \tag{3.190}$$

where we set $\epsilon' \to 0$ on the right.

It follows that

$$\begin{aligned} S &= \frac{1}{m!} \int_{\hat{W}\in S^m} \left\langle \hat{W} d^m \hat{W} \right\rangle \frac{1}{(\hat{W}\cdot\bar{Y})^{m+1}} \prod_{j=1}^{n} \theta(\hat{W}\cdot Z_j) && (3.191) \\ &= \frac{1}{m!} \int_{\mathcal{A}^*} \langle W d^m W \rangle \frac{1}{(W\cdot\bar{Y})^{m+1}} && (3.192) \end{aligned}$$

which is the volume formula (3.118) for $\underline{\Omega}(\mathcal{A})$ in the limit $\bar{Y} \to Y$. In the last step, we used that fact that the inequalities $W \cdot Z_j > 0$ imposed by the step functions carve out the interior of the dual polytope $\mathcal{A}^* \subset \mathbb{P}^m$. Furthermore, on the last line we removed the "gauge" choice $\hat{W} \in S^m$, since the resulting integral is gauge invariant under $GL(1)$ action.

We stress that it is absolutely crucial for $\bar{Y}$ to be on the polytope's interior. Otherwise, the denominator factor $W \cdot \bar{Y}$ can vanish and cause divergent behavior. From the contour point of view, as shown in examples above, the position of $\bar{Y}$ affects the location of poles relative to the contour.

3.4.4 Projective space contours part II

We now consider an alternative contour integral that is in essence identical to the previous, but represented in a very different way. The result is the following

$$\underline{\Omega}(\mathcal{A})(Y) = \frac{1}{(2\pi)^{n-m-1}m!}\int \frac{d^nB}{\prod_{j=1}^n(C_j^0 - iB_j)}\delta^{m+1}\left(\sum_{j=1}^n B_jZ_j\right) \quad (3.193)$$

$$= \frac{1}{(2\pi)^{n-m-1}m!}\int_{B\in K} \frac{d^{n-m-1}B}{\prod_{j=1}^n(C_j^0 - iB_j)} \quad (3.194)$$

for any point $C^0 = (C_1^0, C_2^0, \ldots, C_n^0) \in \mathbb{R}^n$ such that $Y = \sum_{j=1}^n C_j^0 Z_j$ and $C_j^0 > 0$. In the second equation, $K \subset \mathbb{R}^n$ denotes the $(n-m-1)$ dimensional kernel of the map $Z : \mathbb{R}^n \to \mathbb{R}^{m+1}$. The measure on K is defined as

$$d^{n-m-1}B := \int d^nB\ \delta^{m+1}\left(\sum_{j=1}^n B_jZ_j\right) = \frac{dB_{k_1}\cdots dB_{k_{n-m-1}}}{\langle j_0 \cdots j_m\rangle} \quad (3.195)$$

for any partition $\{j_0, \ldots, j_m\} \cup \{k_1, \ldots, k_{n-m-1}\}$ of the index set $\{1, \ldots, n\}$. On the right, it is understood that $B \cdot Z = 0$.

We now argue that (3.193) is equivalent to (3.149). An immediate consequence is that this contour integral is independent of the choice of C^0.

We begin with the $i\epsilon$ contour (3.149), fix a choice c^0 satisfying $\bar{Y} = c^0 \cdot Z$, and change integration variables $c_j \to b_j = c_j^0 - c_j$.

$$\underline{\Omega}(\mathcal{A})(Y) = \frac{1}{(2\pi i)^{n-m-1}m!}\int \frac{d^nb}{\prod_{j=1}^n(c_j^0 - b_j - i\epsilon_j)}\delta^{m+1}\left(\sum_{j=1}^n b_jZ_j\right) \quad (3.196)$$

For each b_j, there is a pole at $b_j = c_j^0 - i\epsilon_j$ which lives in the fourth quadrant on the complex plane of b_j. Since we are currently integrating over the real line, it is possible to do a clockwise Wick rotation $b_j \to B_j = -ib_j$ to integrate over the imaginary line (i.e. $B_j \in \mathbb{R}$) without picking up any of the poles. It follows that

$$\underline{\Omega}(\mathcal{A})(Y) = \frac{1}{(2\pi)^{n-m-1}m!}\int \frac{d^n B}{\prod_{j=1}^n (c_j^0 - iB_j - i\epsilon_j)}\delta^{m+1}\left(\sum_{j=1}^n B_j Z_j\right) \tag{3.197}$$

We can now set $\epsilon_j \to 0$ as it no longer affects the contour of integration. In this limit, we recover $c_i^0 \to C_i^0$ and $\bar{Y} \to Y$, giving $Y = C^0 \cdot Z$ and hence the desired result. The formula (3.193) was first established as Theorem 5.5 in [44].

Let us work out one example.

Example 3.4.8. Let $\mathcal{A} \subset \mathbb{P}^2$ have vertices $\{(1,0,0),(0,1,0),(0,0,1),(1,1,-1)\}$, as in Example 3.4.4. The kernel is $K = \{(x,x,-x,-x) : x \in \mathbb{R}\} \subset \mathbb{R}^4$. For $Y = (Y^0, Y^1, Y^2)$ we pick $C^0 = (Y^0 - a, Y^1 - a, Y^2 + a, a)$ for some $a \in \mathbb{R}$, with the assumption that all entries are positive. Thus

$$\underline{\Omega}(\mathcal{A})(Y) = \frac{1}{(2\pi)2!}\int_{-\infty}^{\infty} \frac{dx}{(Y^0 - a - ix)(Y^1 - a - ix)(Y^2 + a + ix)(a + ix)} \tag{3.198}$$

$$= \frac{1}{2!}\left(\frac{1}{Y^0 Y^1 Y^2} - \frac{1}{(Y^0 + Y^2)(Y^1 + Y^2)Y^2}\right) \tag{3.199}$$

where we have chosen to close the contour by picking the poles $x = ia$ and $x = i(Y^2 + a)$ with positive imaginary part. This is independent of a, as expected, and agrees with (3.143).

It is interesting to contrast these contour representations with the Newton polytope pushforward formula discussed in Section 3.3.2. For the former, the combinatorial structure of the convex polytope is automatically "discovered" by the contour integration without prior knowledge. For the latter, the combinatorial structure must

be reflected in the choice of the Newton polytope, which may not be possible for polytopes whose combinatorial structure cannot be realized with integral coordinates (e.g. non-rational polytopes [45]).

Chapter 4

The associahedron

We introduce the associahedron, an important polytope discovered by mathematicians in the 1960's [19, 20, 21], from the point of view of positive geometries. We show that an infinite family of associahedra appears naturally in the kinematic space of tree level particle scattering with color ordered particles. Furthermore, we present the striking fact that the canonical form of any of this family of associahedra is the tree level color ordered amplitude of cubic ϕ^3 theory, also known as bi-adjoint scalar theory [13]. Furthermore, we "rediscover" the Feynman diagram expansion as one of many triangulations of the polytope. In this sense, we say that the kinematic associahedron is the amplituhedron of the bi-adjoint theory. While for simplicity we focus our attention on this particular scalar theory in the present section, many of our results generalize to gluons and pions as discussed in Section 6.

We begin by introducing planar scattering forms in Section 4.1, which are differential forms on kinematic space that encode all information about tree level amplitudes. In Section 4.2, we present a precise construction of the associahedron in kinematic space. In Section 4.3, we argue that well-known properties of the amplitudes like factorization and various "soft" limits can be understood as geometric properties. In Section 4.4, we discuss methods for computing the canonical form, and provide

a geometric interpretation of the Feynman diagram expansion. Finally, Section 4.5 provides a discussion on the vertex coordinates of the polytope.

4.1 The planar scattering form on kinematic space

We introduce the *planar scattering form*, which is a *differential form* on the space of kinematic variables that encodes all information about on-shell tree-level scattering amplitudes of the bi-adjoint scalar. We emphasize the importance of constructing amplitudes as forms, as this is the first step to understanding amplitudes from the positive geometry point of view.

4.1.1 Kinematic space

We begin by defining the kinematic space $\mathcal{K}_n$ for n massless momenta p_i for $i = 1, \ldots, n$ as the space spanned by linearly independent Mandelstam variables in space-time dimension $D \geq n-1$:

$$s_{ij} := (p_i + p_j)^2 = 2p_i \cdot p_j \tag{4.1}$$

For $D < n-1$ there are further constraints on Mandelstam variables—Gram determinant conditions—so the number of independent variables is lower. Due to the massless on-shell conditions and momentum conservation, we have n linearly independent constraints

$$\sum_{j=1;\, j\neq i}^{n} s_{ij} = 0 \quad \text{for } i = 1, 2, \ldots, n \tag{4.2}$$

The dimensionality of kinematic space is therefore

$$\dim \mathcal{K}_n = \binom{n}{2} - n = \frac{n(n-3)}{2} \tag{4.3}$$

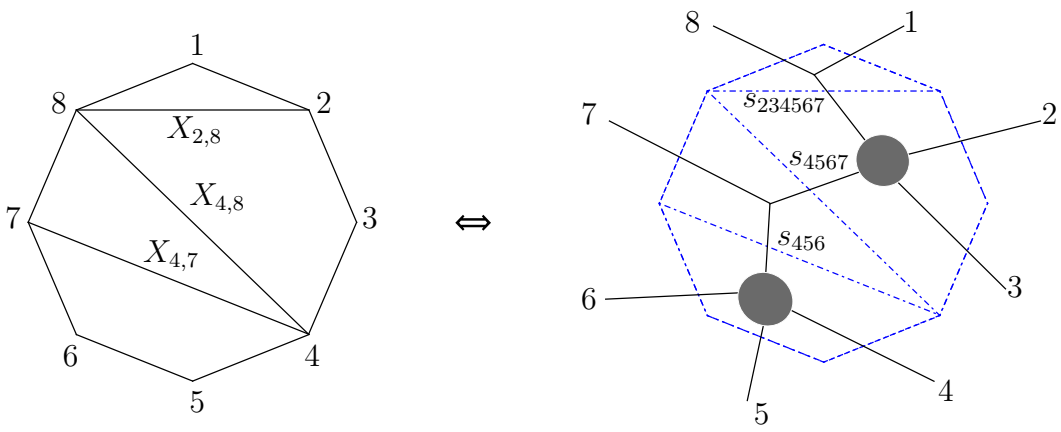

Figure 4.1: Correspondence between a 3-diagonal partial triangulation and a triple cut. Note that the vertices are numbered on the left while the edges/particles are numbered on the right.

More generally, for any set of particle labels $I \subset \{1, \ldots, n\}$, we define the Mandelstam variable

$$s_I := \left(\sum_{i \in I} p_i\right)^2 = \sum_{i,j \in I;\, i<j} s_{ij} \tag{4.4}$$

It follows from momentum conservation that $s_I = s_{\bar{I}}$, where $\bar{I}$ is the complement of I. For mutually disjoint index sets $I_1, \ldots, I_d$, we define $s_{I_1 \cdots I_d} := s_{I_1 \cup \cdots \cup I_d}$. We also define, for any pair of index sets I, J:

$$s_{I|J} := 2\left(\sum_{i \in I} p_i\right) \cdot \left(\sum_{j \in J} p_j\right) = \sum_{i \in I, j \in J} s_{ij} \tag{4.5}$$

4.1.2 Planar kinematic variables

We now focus on kinematic variables that are particularly useful for cyclically ordered particles. For the *standard ordering* $(1, 2, \ldots, n)$, we define *planar variables* with manifest cyclic symmetry:

$$X_{i,j} := s_{i,i+1,\ldots,j-1} \tag{4.6}$$

for any pair of indices $1 \leq i < j \leq n$. Note that $X_{i,i+1}$ and $X_{1,n}$ vanish. Given a convex n-gon with cyclically ordered vertices, the variable $X_{i,j}$ can be visualized as the diagonal between vertices i and j, as in Figure 4.1 (left).

The Mandelstam variables in particular can be expanded in terms of these variables, by the easily verified identity:

$$s_{ij} = X_{i,j+1} + X_{i+1,j} - X_{i,j} - X_{i+1,j+1} \tag{4.7}$$

It follows that the non-vanishing planar variables form a spanning set of kinematic space. However, they also form a basis, since there are exactly $\dim \mathcal{K}_n = n(n-3)/2$ of them. It is rather curious that the number of planar variables is precisely the dimension of kinematic space. Examples of the basis include $\{s := X_{1,3}, t := X_{2,4}\}$ for n=4 particles and $\{s_{12} = X_{1,3}, s_{23} = X_{2,4}, s_{34} = X_{3,5},\ s_{123} = X_{1,4}, s_{234} = X_{2,5}\}$ for n=5.

More generally, for an ordering $\alpha := (\alpha(1), \ldots, \alpha(n))$ of the external particles, we define *α-planar variables*

$$X_{\alpha(i),\alpha(j)} := s_{\alpha(i),\alpha(i+1),\ldots,\alpha(j-1)} \tag{4.8}$$

for any pair $i < j$ modulo n. As before, $X_{\alpha(i),\alpha(i+1)}$ and $X_{\alpha(1),\alpha(n)}$ vanish, and the non-vanishing variables form a basis of kinematic space. Also, each variable can be visualized as a diagonal of a convex n-gon whose vertices are cyclically ordered by α.

4.1.3 The planar scattering form

We now move on to our main task of defining the planar scattering form. Let g denote a (tree) cubic graph with propagators X_{i_a,j_a} for $a = 1, \ldots, n-3$. For each ordering of these propagators, we assign a value $\text{sign}(g) \in \{\pm 1\}$ to the graph with the property that swapping two propagators flips the sign. Then, we assign to the graph a $d\log$

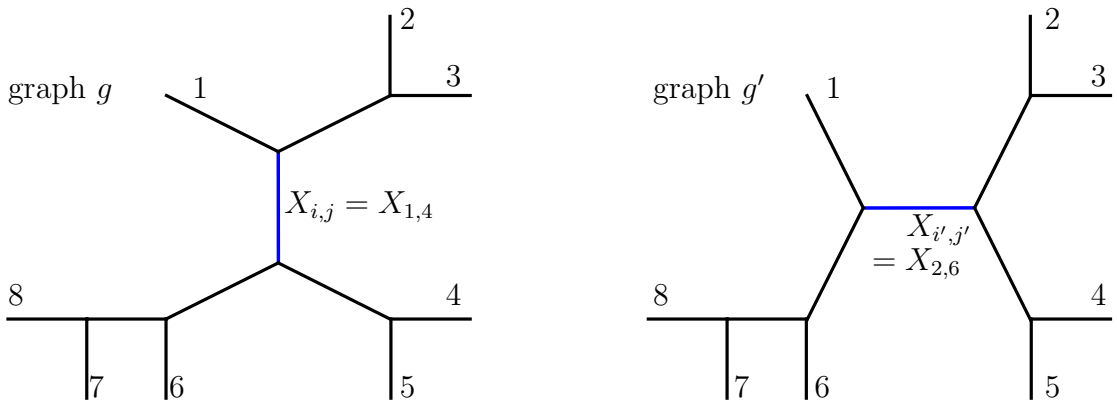

Figure 4.2: Two planar graphs related by a mutation given by an exchange of channel $X_{i,j} \to X_{i',j'}$ in a four point subgraph

form:

$$\text{sign}(g) \bigwedge_{a=1}^{n-3} d\log X_{i_a,j_a} \tag{4.9}$$

where the sign(g) is evaluated on the ordering in which the propagators appear in the wedge product. There are of course two sign choices for each graph. Finally, we introduce the planar scattering form of rank $(n-3)$:

$$\Omega_n^{(n-3)} := \sum_{\text{planar } g} \text{sign}(g) \bigwedge_{a=1}^{n-3} d\log X_{i_a,j_a} \tag{4.10}$$

where we sum over a $d\log$ form for every planar cubic graph g. Note that a particle ordering is implicitly assumed by the construction, so we also denote the form as $\Omega^{(n-3)}[1,\ldots,n]$ when we wish to emphasize the ordering. For n=3, we define $\Omega_{n=3}^{(0)} := \pm 1$.

Since there are two sign choices for each graph, this amounts to many different scattering forms. However, there is a natural choice (unique up to overall sign) obtained by making the following requirement:

The planar scattering form is *projective*.

In other words, we require the form to be invariant under *local* GL(1) transformations $X_{i,j} \to \Lambda(X) X_{i,j}$ for any index pair (i,j), or equivalently $s_I \to \Lambda(s) s_I$ for any index set I. This fixes the scattering form up to an overall sign which we ignore.

Projectivity is equivalent to the natural statement that the form only depends on *ratios* of Mandelstam variables, as we can explicitly see in some simple examples for n=4, 5:

$$\Omega^{(1)}(1,2,3,4) = d\log s - d\log t = \frac{ds}{s} - \frac{dt}{t} = d\log\left(\frac{s}{t}\right) = d\log\left(\frac{X_{1,3}}{X_{2,4}}\right) \tag{4.11}$$

$$\begin{aligned}\Omega^{(2)}(1,2,3,4,5) = \;& d\log X_{1,4} \wedge d\log X_{1,3} + d\log X_{1,3} \wedge d\log X_{3,5} + d\log X_{3,5} \wedge d\log X_{2,5} \\ & + d\log X_{2,5} \wedge d\log X_{2,4} + d\log X_{2,4} \wedge d\log X_{1,4} \\ = \;& d\log\frac{X_{1,3}}{X_{2,4}} \wedge d\log\frac{X_{1,3}}{X_{1,4}} + d\log\frac{X_{1,3}}{X_{2,5}} \wedge d\log\frac{X_{3,5}}{X_{2,4}}\end{aligned} \tag{4.12}$$

where we have written on the last expression for each example the form in terms of ratios of X's only. For n=6, the form is given by summing over 14 planar graphs which can be expressed as ratios in the following way:

$$\begin{aligned}\Omega^{(3)}_{n=6} = \;& d\log\frac{X_{2,4}}{X_{1,3}} \wedge d\log\frac{X_{1,4}}{X_{4,6}} \wedge d\log\frac{X_{1,5}}{X_{4,6}} + d\log\frac{X_{2,6}}{X_{1,3}} \wedge d\log\frac{X_{3,6}}{X_{1,3}} \wedge d\log\frac{X_{4,6}}{X_{3,5}} \\ & - d\log\frac{X_{2,6}}{X_{1,5}} \wedge d\log\frac{X_{2,5}}{X_{3,5}} \wedge d\log\frac{X_{2,4}}{X_{3,5}} - d\log\frac{X_{2,4}}{X_{1,3}} \wedge d\log\frac{X_{4,6}}{X_{3,5}} \wedge d\log\frac{X_{2,6}}{X_{1,5}}\,.\end{aligned}$$

We emphasize that projectivity is a rather remarkable property of the scattering form which is not true for each Feynman diagram separately. Indeed, no proper subset of Feynman diagrams provides a projective form—only the sum over all the diagrams (satisfying the sign flip rule) is projective. This foreshadows something we will see much more explicitly later on in connection to the positive geometry of the associahedron: the Feynman diagram expansion provides just one type of

triangulation of the geometry, which introduces a spurious "pole at infinity" that cancels only in the sum over all terms. But other triangulations that are manifestly projective term-by-term are also possible, and often lead to even shorter expressions.

Projectivity can also be described equivalently by a simple *sign-flip rule*. We say that two planar graphs g, g' are related by a *mutation* if one can be obtained from the other by an exchange of channel in a four-point sub-graph (See Figure 4.2). Let $X_{i,j}, X_{i',j'}$ denote the mutated propagators, respectively, and let X_{i_b,j_b} for $b = 1, \ldots, n{-}4$ denote the shared propagators. Under a local GL(1) transformation, the Λ-dependence of the scattering form becomes:

$$(\text{sign}(g) + \text{sign}(g'))\, d\log\Lambda \wedge \left(\bigwedge_{b=1}^{n-4} d\log X_{i_b,j_b}\right) + \cdots \tag{4.13}$$

where we have only written the terms involving the $d\log$ of all shared propagators of g and g'. Here $\text{sign}(g')$ is evaluated on the same propagator ordering as $\text{sign}(g)$ but with $X_{i,j}$ replaced by $X_{i',j'}$. The form is projective if the Λ-dependence disappears, i.e. when we have

$$\text{sign}(g) = -\text{sign}(g') \tag{4.14}$$

for each mutation.

The sign flip rule has several immediate consequences. For instance, it ensures that the form is cyclically invariant up to a sign:

$$i \to i{+}1 \qquad \Rightarrow \qquad \Omega_n^{(n-3)} \to (-1)^{n-3}\, \Omega_n^{(n-3)} \tag{4.15}$$

since it takes $(n{-}3)$ mutations (mod 2) to achieve the cyclic shift. The sign flip rule also ensures that the form factorizes correctly. Indeed, it suffices to consider the

channel $X_{1,m} \to 0$ for any $m = 3, \ldots, n-1$ for which

$$\Omega^{(n-3)}(1,2,\ldots,n) \xrightarrow{X_{1,m}\to 0} \Omega^{(m-3)}(1,2,\ldots,m-1,I) \wedge \frac{dX_{1,m}}{X_{1,m}} \wedge \Omega^{(n-m-1)}(I^-,m,\ldots,n)\,, \tag{4.16}$$

where $p_I = -\sum_{i=1}^{m-1} p_i$ is the on-shell internal particle. General channels can be obtained via cyclic shift.

Finally, for a general ordering α of the external particles, we define the scattering form $\Omega^{(n-3)}[\alpha]$ by making index replacements $i \to \alpha(i)$ on $\Omega_n^{(n-3)}$, which is equivalent to replacing (4.10) with a sum over α-planar graphs. Recall that a cubic graph is called *α-planar* if it is planar when external legs are ordered by α; alternatively, we say that the graph is *compatible* with the ordering. Projectivity holds regardless of the ordering.

4.2 The kinematic associahedron

We introduce the *associahedron* polytope [21, 19, 20] and discuss its connection to the bi-adjoint scalar theory. We begin by reviewing the combinatorial structure of the associahedron before providing a novel construction of the associahedron in kinematic space. We then argue that the tree level amplitude is the canonical form of the associahedron, thus establishing the associahedron as the "amplituhedron" of the (tree) bi-adjoint theory.

4.2.1 The associahedron from planar cubic diagrams

There are many beautiful, combinatorial ways of constructing associahedra; an excellent survey of the subject, together with comprehensive references to the literature, is given by [34]. In this section, we discuss one of the most fundamental descriptions

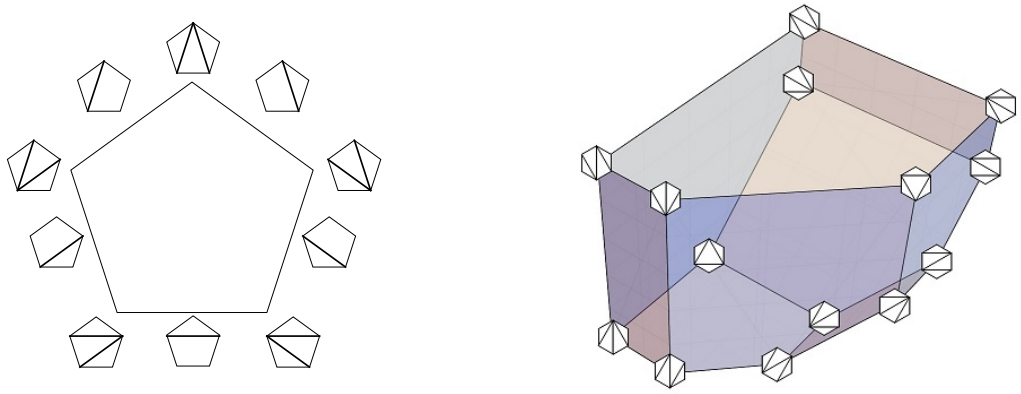

Figure 4.3: Combinatorial structure of the n=5 associahedron (left) and the n=6 associahedron (right). For simplicity, only vertices are labeled for the latter.

of the associahedron which is also most closely related to scattering amplitudes. We begin by clarifying some terminology regarding polytopes.

A *boundary* of a polytope refers to a boundary of any codimension. A k-boundary is a boundary of dimension k. A *facet* is a codimension 1 boundary. Given a convex n-gon, a *diagonal* is a straight line between any two non-adjacent vertices. A *partial triangulation* is a collection of mutually non-crossing diagonals. A *full triangulation* or simply a *triangulation* is a partial triangulation with maximal number of diagonals, namely $(n-3)$.

For any $n\geq 3$, consider a convex polytope of dimension $(n-3)$ with the following properties:

1. For every $d = 0, 1, \ldots, n-3$, there exists a one-to-one correspondence between the codimension d boundaries and the d-diagonal partial triangulations of a convex n-gon.

2. A codimension d boundary F_1 and a codimension $d+k$ boundary F_2 are adjacent if and only if the partial triangulation of F_2 can be obtained by addition of k diagonals to the partial triangulation of F_1.

In particular, the triangulation with no diagonals corresponds to the polytope's interior, and:

The vertices correspond to the full triangulations. (4.17)

A classic result in combinatorics says that the number of full triangulations, and hence the number of vertices of our polytope, is the Catalan number C_{n-2} [46]. Any polytope $\mathcal{A}_n$ satisfying these properties is an *associahedron*. See Figure 4.3 for examples.

We make a few observations that will guide us to finding the connection to amplitudes. Let us order the edges of the n-gon cyclically with $1, \ldots, n$, and recall that:

d-diagonal partial triangulations of the n-gon are in one-to-one correspondence with d-cuts on n-particle planar cubic diagrams. (See Figure 4.1) (4.18)

The edges of the n-gon correspond to external particles, while the diagonals correspond to cuts.

Furthermore, the associahedron *factorizes combinatorially*. That is, consider a facet F corresponding to some diagonal that subdivides the n-gon into a m-gon and a $(n-m+2)$-gon (See Figure 4.11). The two lower polygons provide the combinatorial properties for two lower associahedra $\mathcal{A}_m$ and $\mathcal{A}_{n-m+2}$, respectively, and the facet is combinatorially identical to their direct product:

$$F \cong \mathcal{A}_m \times \mathcal{A}_{n-m+2} \tag{4.19}$$

We show in Section 4.3.1 that this implies the factorization properties of amplitudes.

Finally, we observe that the associahedron is a *simple* polytope, meaning that each vertex is adjacent to precisely $\dim \mathcal{A}_n = (n-3)$ facets. Indeed, given any asso-

ciahedron vertex and its corresponding triangulation, the adjacent facets correspond to the $(n-3)$ diagonals.

4.2.2 The kinematic associahedron

We now show that there is an associahedron naturally living in the kinematic space for n particles. The construction depends on an ordering for the particles which we take to be the standard ordering for simplicity.

We first define a region Δ_n in kinematic space by imposing the inequalities

$$X_{i,j} \geq 0 \quad \text{for all } 1 \leq i < j \leq n \tag{4.20}$$

Recall that $X_{i,i+1}$ and X_{1n} are trivially zero and therefore do not provide conditions. Since the number of non-vanishing planar variables is exactly the dimension of kinematic space, it follows that Δ_n is a simplex with a facet at infinity. This leads to an obvious problem. The associahedron $\mathcal{A}_n$ should have dimension $(n-3)$, which for $n > 3$ is lower than the kinematic space dimension. We resolve this by restricting to a $(n-3)$-subspace $H_n \subset \mathcal{K}_n$ defined by a set of constants:

$$\begin{aligned} &\text{Let } c_{ij} := X_{i,j} + X_{i+1,j+1} - X_{i,j+1} - X_{i+1,j} \text{ be a } \textit{positive constant} \\ &\qquad\qquad \text{for every pair of } \textit{non-adjacent} \text{ indices } 1 \leq i < j \leq n-1 \end{aligned} \tag{4.21}$$

Note that we have deliberately omitted n from the index range. Also, (4.7) implies the following simple identity:

$$c_{ij} = -s_{ij} \tag{4.22}$$

The condition (4.21) is therefore equivalent to requiring s_{ij} to be a *negative constant* for the same index range. Counting the number of constraints, we find the desired

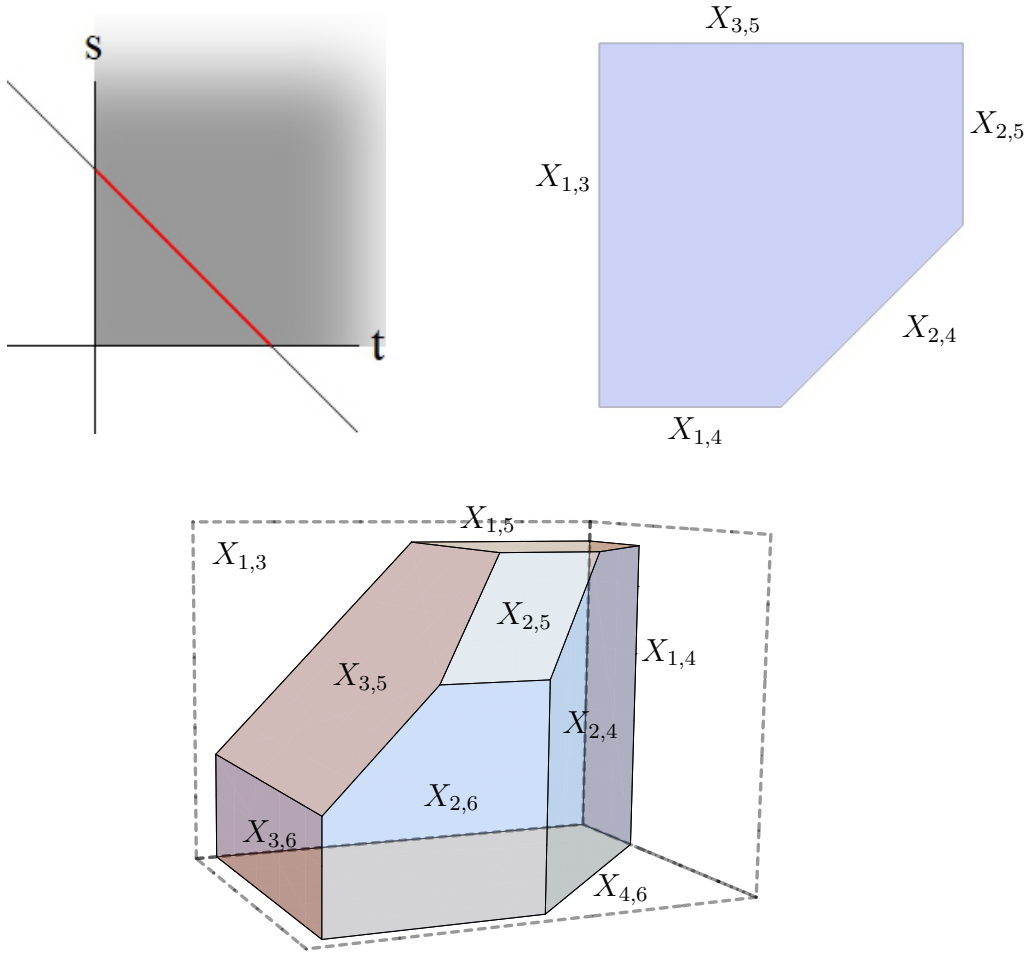

Figure 4.4: Kinematic associahedra for n=4 (top left), n=5 (top right) and n=6 (bottom).

dimension:

$$\dim H_n = \dim \mathcal{K}_n - \frac{(n-2)(n-3)}{2} = n-3 \tag{4.23}$$

Finally, we let $\mathcal{A}_n := H_n \cap \Delta_n$ be a polytope. We claim that $\mathcal{A}_n$ *is an associahedron of dimension* $(n-3)$. See Figure 4.4 for examples. Recall from Section 4.2.1 that the associahedron factorizes combinatorially, meaning that each facet is combinatorially the direct product of two lower associahedra as in (4.19). In Section 4.3.1, we show that the same property holds for the kinematic polytope $\mathcal{A}_n$, thereby implying our claim.

Here we highlight the key observation needed for showing factorization and hence the associahedron structure. Note that the boundaries are enforced by the positivity conditions $X_{i,j} \geq 0$, so that we can reach any codimension 1 boundary by setting some particular $X_{i,j} \to 0$. But then, to reach a lower dimensional boundary, we cannot set $X_{k,l} \to 0$ for any diagonal (k,l) that *crosses* (i,j) (See Figure 4.5). Indeed, if we begin with the basic identity (4.21) with (i,j) replaced by (a,b) and sum a,b over the range $i \leq a < j$ and $k \leq b < l$, the sums telescope and we find

$$X_{j,k} + X_{i,l} = X_{i,k} + X_{j,l} - \sum_{\substack{i \leq a < j \\ k \leq b < l}} c_{ab} \tag{4.24}$$

for any $1 \leq i < j < k < l \leq n$. Now consider a situation like Figure 4.6 (top) where the diagonals $X_{i,k} = 0$ and $X_{j,l} = 0$ cross, then

$$X_{j,k} + X_{i,l} = - \sum_{\substack{i \leq a < j \\ k \leq b < l}} c_{ab} \tag{4.25}$$

which is a contradiction since the left side is *nonnegative* while the right side is *strictly negative*. Geometrically, this means that every boundary of $\mathcal{A}_n$ is labeled by a set of non-crossing diagonals (i.e. a partial triangulation), as expected for the associahedron.

Let us do some quick examples. For n=4, the kinematic space with variables (s,t,u) satisfies the constraint $s + t + u = 0$ and is 2-dimensional. However, the kinematic associahedron is given by the line segment $0 < s < -u$ where $u < 0$ is a constant, as shown in Figure 4.4 (top left). For n=5, the kinematic space is 5-dimensional, but the subspace $H_{n=5}$ is 2-dimensional defined by three constants c_{13}, c_{14}, c_{24}. If we parameterize the subspace in the basis $(X_{1,3}, X_{1,4})$, then the associ-

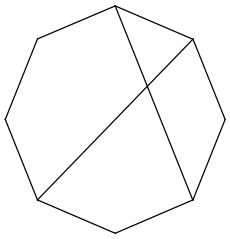

Not allowed!

Figure 4.5: Planar variables $X_{i,j}$ corresponding to crossing diagonals cannot be simultaneously set to zero.

ahedron $\mathcal{A}_{n=5}$ is a pentagon with edges given by:

$$X_{1,3} \geq 0 \tag{4.26}$$

$$X_{3,5} = -X_{1,4} + c_{14} + c_{24} \geq 0 \tag{4.27}$$

$$X_{2,5} = -X_{1,3} + c_{13} + c_{14} \geq 0 \tag{4.28}$$

$$X_{2,4} = X_{1,4} - X_{1,3} + c_{13} \geq 0 \tag{4.29}$$

$$X_{1,4} \geq 0 \tag{4.30}$$

where the edges are given in clockwise order (See Figure 4.4 (top right)). The n=6 example is given in Figure 4.4 (bottom).

The associahedron $\mathcal{A}_n$ in kinematic space is only one step away from scattering amplitudes, as we now show.

4.2.3 Bi-adjoint cubic scalar amplitudes

We now show the connection between the kinematic associahedron $\mathcal{A}_n$ and scattering amplitudes in bi-adjoint scalar theory. The discussion here applies to tree amplitudes with a pair of standard ordering, which we denote by m_n. We generalize to arbitrary ordering pairs $m[\alpha|\beta]$ in Section 4.2.4.

We make two claims in this section:

1. The pullback of the cyclic scattering form $\Omega_n^{(n-3)}$ to the subspace H_n is the canonical form of the associahedron $\mathcal{A}_n$.

2. The canonical form of the associahedron $\mathcal{A}_n$ determines the tree amplitude of the bi-adjoint theory with identical ordering.

Recall that the associahedron is a simple polytope, and the canonical form of a simple polytope (See (3.126)) is a sum over its vertices. For each vertex Z, let $X_{i_a,j_a} = 0$ denote its adjacent facets for $a = 1, \ldots, n-3$. Furthermore, for each ordering of the facets, let $\text{sign}(Z) \in \{\pm 1\}$ denote its orientation relative to the inherited orientation. The canonical form is therefore

$$\Omega(\mathcal{A}_n) = \sum_{\text{vertex } Z} \text{sign}(Z) \bigwedge_{a=1}^{n-3} d \log X_{i_a,j_a} \tag{4.31}$$

where $\text{sign}(Z)$ is evaluated on the ordering of the facets in the wedge product. Since the form is defined on the subspace H_n, it may be helpful to express the $X_{i,j}$ variables in terms of a basis of $(n-3)$ variables like (4.68).

We argue that (4.31) is equivalently the pullback of the scattering form (4.10) to the subspace H_n. Since there is a one-to-one correspondence between vertices Z and planar cubic graphs g, it suffices to show that the pullback of the g term is the Z term. This is true by inspection since g and its corresponding Z have the same propagators X_{i_a,j_a}. The only subtlety is that the $\text{sign}(Z)$ appearing in (4.31) is defined geometrically, while the $\text{sign}(g)$ appearing in (4.10) is defined by local GL(1) invariance. We now argue equivalence of the two by showing that $\text{sign}(Z)$ satisfies the sign flip rule.

Suppose Z, Z' are vertices whose triangulations are related by a mutation. While mutations are defined as relations between planar cubic graphs (See Figure 4.2), they can equivalently be interpreted from the triangulation point of view. Indeed, two triangulations are related by a mutation if one can be obtained from the other by ex-

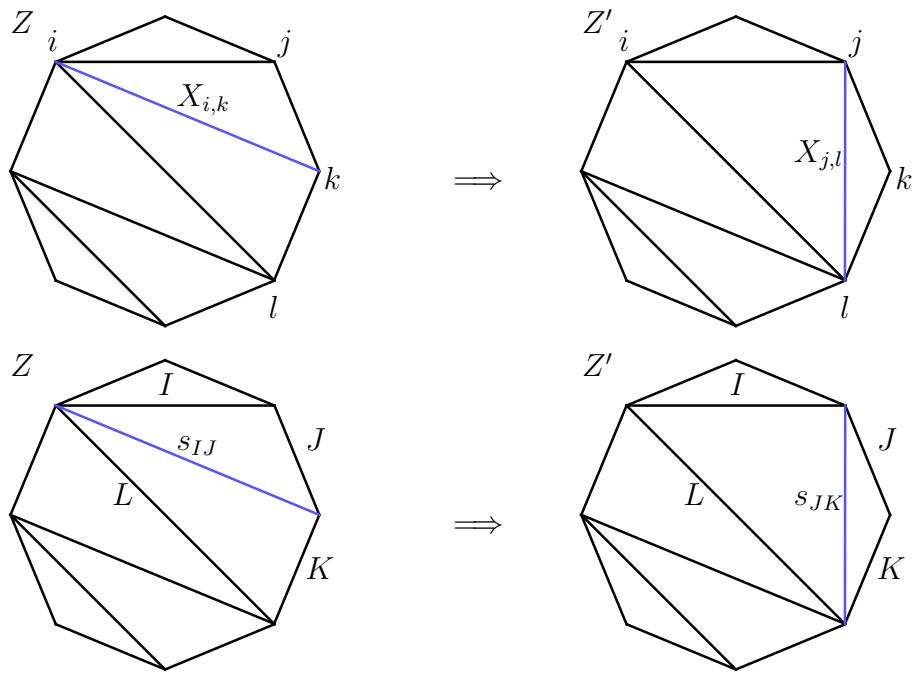

Figure 4.6: Two triangulations related by a mutation $X_{i,k} \to X_{j,l}$ (top) or equivalently $s_{IJ} \to s_{JK}$ (bottom).

changing exactly one diagonal. For example, the two triangulations of a quadrilateral are related by mutation. For a generic triangulation of the n-gon, every mutation can be obtained by identifying a quadrilateral in the triangulation and exchanging its diagonal. In Figure 4.6 (top), we show an example where a mutation is applied to the quadrilateral (i, j, k, l) with the diagonal (i, k) in Z exchanged for the diagonal (j, l) in Z'. Note that we have implicitly assumed $1 \leq i < j < k < l \leq n$. Furthermore, taking the exterior derivative of the kinematic identity (4.24) gives us

$$dX_{j,k} + dX_{i,l} = dX_{i,k} + dX_{j,l}\,. \tag{4.32}$$

Note that the two propagators on the left appear in both diagrams, while the two propagators on the right are related by mutation. It follows that

$$\bigwedge_{a=1}^{n-3} dX_{i_a,j_a} = -\bigwedge_{a=1}^{n-3} dX_{i'_a,j'_a} \tag{4.33}$$

The crucial part is the minus sign, which implies the sign flip rule:

$$\text{sign}(Z) = -\text{sign}(Z') \tag{4.34}$$

We can therefore identify $\text{sign}(Z) = \text{sign}(g)$. Furthermore, an important consequence of (4.33) is that the following quantity is independent of g on the pullback:

$$d^{n-3}X := \text{sign}(g) \bigwedge_{a=1}^{n-3} dX_{i_a,j_a} \tag{4.35}$$

Substituting into (4.31) gives

$$\Omega(\mathcal{A}_n) = \left(\sum_{\text{planar } g} \frac{1}{\prod_{a=1}^{n-3} X_{i_a,j_a}} \right) d^{n-3}X = m_n d^{n-3}X \tag{4.36}$$

which gives the expected amplitude m_n, thus completing the argument for our second claim. For convenience we sometimes denote the item in parentheses as $\underline{\Omega}(\mathcal{A}_n)$, called the *canonical rational function*. Thus,

$$\underline{\Omega}(\mathcal{A}_n) = m_n \tag{4.37}$$

Let us do a quick and informative example for n=4. We use the usual Mandelstam variables $(s,t,u) := (X_{1,3}, X_{2,4}, -X_{1,3} - X_{2,4} = -c_{13})$. Here u is a negative constant, and the associahedron is simply the line segment $0 \leq s \leq -u$ in Figure 4.4 (top left), whose canonical form is

$$\Omega(\mathcal{A}_{n=4}) = \left(\frac{1}{s} - \frac{1}{s+u} \right) ds = \left(\frac{1}{s} + \frac{1}{t} \right) ds \tag{4.38}$$

which of course is also the desired amplitude up to the ds factor. Now consider pulling back the planar scattering form (4.11). Since u is a constant on $H_{n=4}$ and

$s+t+u=0$, hence $ds=-dt$ on the pullback. It follows that

$$\Omega^{(1)}_{n=4}|_{H_{n=4}} = \left(\frac{1}{s}+\frac{1}{t}\right) ds \tag{4.39}$$

which is equal to (4.38). We also demonstrate an example for $n=5$ where the associahedron is a pentagon as shown in Figure 4.4 (top right). We argue that the pullback of (4.12) determines the 5-point amplitude by showing that the numerators have the expected sign on the pullback, namely $dX_{1,4}dX_{1,3} = dX_{1,3}dX_{3,5} = dX_{3,5}dX_{2,5} = dX_{2,5}dX_{2,4} = dX_{2,4}dX_{1,4}$. For instance, the identity $X_{3,5} = -X_{1,4} + c_{14} + c_{24}$ implies $\partial(X_{1,4}, X_{1,3})/\partial(X_{1,3}, X_{3,5}) = 1$, leading to the first equality. We leave the rest as an exercise for the reader. It follows that the pullback determines the corresponding amplitude.

$$\Omega^{(2)}_{n=5}|_{H_{n=5}} = \left(\frac{1}{X_{1,3}X_{1,4}} + \frac{1}{X_{3,5}X_{1,3}} + \frac{1}{X_{1,4}X_{2,4}} + \frac{1}{X_{2,5}X_{3,5}} + \frac{1}{X_{2,4}X_{2,5}}\right) d^2X \tag{4.40}$$

Of course, this is also the canonical form of the pentagon.

4.2.4 All ordering pairs of bi-adjoint cubic amplitudes

We now generalize our results to every ordering pair of the bi-adjoint theory. Given an ordering pair α, β, the amplitude is given by the sum of all cubic diagrams *compatible* with both orderings, with an overall sign from the trace decomposition [13] that we postpone to Section 6.4 and more specifically (6.48). Here we ignore the overall sign and simply define $m[\alpha|\beta]$ to be the sum over the cubic graphs.

We first review a simple diagrammatic procedure [13] for obtaining all the graphs appearing in $m[\alpha|\beta]$ as illustrated in Figure 4.7:

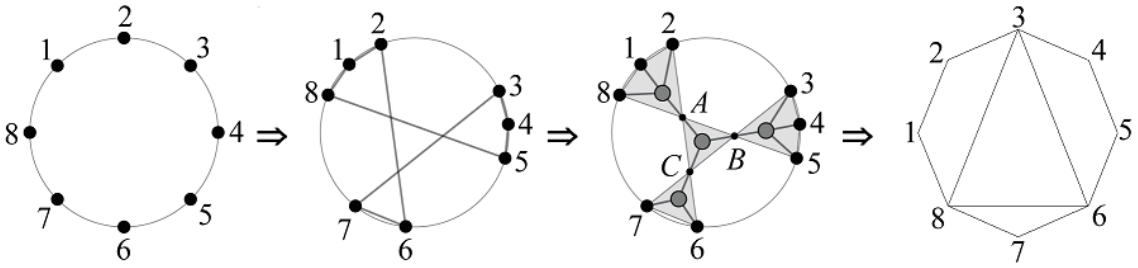

Figure 4.7: Step-by-step procedure for obtaining the mutual cuts (3rd picture) and the mutual partial triangulation (4th) for $(\alpha, \beta) = (12345678|81267354)$. The first three pictures are found in [13].

1. Draw n points on the boundary of a disk ordered cyclically by α.

2. Draw a closed path of line segments connecting the points in order β. These line segments enclose a set of polygons, forming a polygon decomposition.

3. The internal vertices of the decomposition correspond to cuts on cubic graphs called *mutual cuts*.

4. The cuts correspond to diagonals of the α-ordered n-gon, forming a *mutual partial triangulation*.

The cubic graphs compatible with both orderings are precisely those that admit all the mutual cuts. Equivalently, they correspond to all triangulations of the α-ordered n-gon containing the mutual partial triangulation. Conversely, given a graph of mutual cuts or equivalently a mutual partial triangulation, we can reverse engineer the ordering β up to dihedral transformation as follows:

1. Color each vertex of the graph white or black like Figure 4.8 so that no two adjacent vertices have the same color.

2. Draw a closed path that winds around white vertices clockwise and black vertices counterclockwise.

3. The path gives the ordering β up to cyclic shift. Changing the coloring corresponds to a reflection.

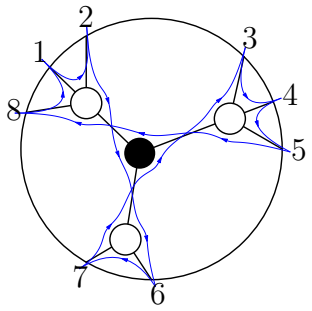

Figure 4.8: This mutual cut diagram gives rise to $(\alpha, \beta) = (12345678, 81267354)$ by the described rules.

The path gives the β up to cyclic shift. Swapping the colors reverses the particle ordering. It follows that β can be obtained up to dihedral transformations.

We are now ready to construct the kinematic polytope for an arbitrary ordering pair. We break the symmetry between the two orderings by using planar variables $X_{\alpha(i),\alpha(j)}$ discussed at the end of Section 4.1.2. In analogy with (4.20), we define a simplex $\Delta[\alpha]$ in kinematic space by requiring that:

$$X_{\alpha(i),\alpha(j)} \geq 0 \text{ for all } 1 \leq i < j \leq n. \tag{4.41}$$

Similar to before, $X_{\alpha(i),\alpha(i+1)}$ and $X_{\alpha(1),\alpha(n)}$ vanish and therefore do not provide conditions. We can visualize the variable $X_{\alpha(i),\alpha(j)}$ as the diagonal $(\alpha(i), \alpha(j))$ of a regular n-gon whose vertices are labeled by α. Furthermore, we construct a $(n-3)$-subspace $H[\alpha|\beta]$ of kinematic space by making the following requirements:

1. For each diagonal $(\alpha(i), \alpha(j))$ that crosses at least one diagonal in the mutual partial triangulation, we require $b_{\alpha(i),\alpha(j)} := X_{\alpha(i),\alpha(j)} > 0$ to be a positive constant.

2. The mutual triangulation (assuming d diagonals) subdivides the n-gon into $(d+1)$ sub-polygons, and we impose the non-adjacent constant conditions (4.21) to each sub-polygon.

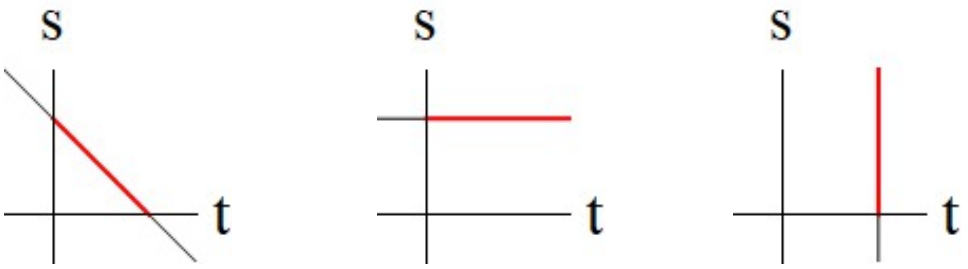

(a) (1234)
$u < 0$ const
$d\log(s/t)$

(b) (1324)
$s > 0$ const
$d\log t$

(c) (2134)
$t > 0$ const
$d\log s$

Figure 4.9: Three orderings for the n=4 kinematic polytopes. We assume the same $\alpha = (1234)$ but different β (displayed above). Furthermore, we present the constant and canonical form for each geometry.

For the last step, it is necessary to omit an edge from each sub-polygon when imposing the non-adjacent constants. By convention, we omit edges corresponding to the diagonals of the mutual triangulation as well as edge n of the n-gon so that no two sub-polygons omit the same element. A moment's thought reveals that there is only one way to do this. Finally, we define the kinematic polytope $\mathcal{A}[\alpha|\beta] := H[\alpha|\beta] \cap \Delta[\alpha]$. In particular, for the standard ordering $\alpha = \beta = (1, \ldots, n)$, we recover $(\Delta[\alpha], H[\alpha|\beta], \mathcal{A}[\alpha|\beta]) = (\Delta_n, H_n, \mathcal{A}_n)$.

Let us get some intuition for the shape of the kinematic polytope. Clearly $\mathcal{A}[\alpha|\alpha]$ is just the associahedron with boundaries relabeled by α. For general α, β, we can think of the mutual partial triangulation (with d diagonals) as a partial triangulation corresponding to some codimension d boundary of the associahedron $\mathcal{A}[\alpha|\alpha]$. Now imagine "zooming in" on the boundary by pushing all non-adjacent boundaries to infinity. The non-adjacent boundaries precisely correspond to partial triangulations of the α-ordered n-gon that cross at least one diagonal of the mutual partial triangulation. This provides the correct intuition for the "shape" of the kinematic polytope $\mathcal{A}[\alpha|\beta]$. Said in another way, the polytope $\mathcal{A}[\alpha|\beta]$ is again an associahedron but with incompatible boundaries pushed to infinity.

For n=4, the three distinct kinematic polytopes are shown in Figure 4.9. For n=5, consider the case $(\alpha, \beta) = (12345, 13245)$. The mutual partial triangulation consists of the regular pentagon with the single diagonal $(2, 4)$ (See Figure 4.10 (left)) with two compatible cubic graphs corresponding to the channels $(X_{2,4}, X_{2,5})$ and $(X_{2,4}, X_{1,4})$. The constants are given by

$$b_{1,3} := X_{1,3} > 0 \tag{4.42}$$

$$b_{3,5} := X_{3,5} > 0 \tag{4.43}$$

$$c_{14} := X_{1,4} + X_{2,5} - X_{2,4} > 0 \tag{4.44}$$

and the inequalities are given by

$$X_{2,4} \geq 0 \tag{4.45}$$

$$X_{2,5} \geq 0 \tag{4.46}$$

$$X_{1,4} \geq 0 \tag{4.47}$$

Finally we plot this region in the basis $(X_{2,4}, X_{2,5})$ as shown in Figure 4.10 where the first two inequalities simply give the positive quadrant while the last inequality gives the diagonal boundary $X_{1,4} = c_{14} - X_{2,5} + X_{2,4} \geq 0$.

Having constructed the kinematic polytope $\mathcal{A}[\alpha|\beta]$, we now discuss its connection to bi-adjoint tree amplitude $m[\alpha|\beta]$ (omitting the overall sign). We make the following two claims in analogy to the two claims made near the beginning of Section 4.2.3:

1. The pullback of the cyclic scattering form $\Omega^{(n-3)}[\alpha]$ to the subspace $H[\alpha|\beta]$ is the canonical form of the kinematic polytope $\mathcal{A}[\alpha|\beta]$. That is,

$$\Omega^{(n-3)}[\alpha]|_{H[\alpha|\beta]} = \Omega(\mathcal{A}[\alpha|\beta]) \tag{4.48}$$

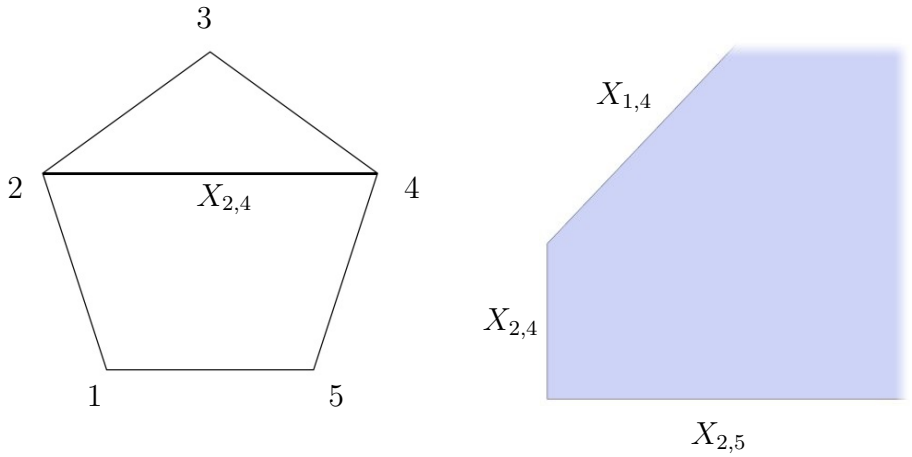

Figure 4.10: The mutual partial triangulation for $(\alpha, \beta) = (12345, 13245)$ (left) and its kinematic polytope (right). The faded area corresponds to the boundary at infinity. The two vertices correspond to the two cubic graphs compatible with both orderings.

2. The canonical form of the kinematic polytope $\mathcal{A}[\alpha|\beta]$ determines the amplitude $m[\alpha|\beta]$. That is,

$$\underline{\Omega}(\mathcal{A}[\alpha|\beta]) = m[\alpha|\beta] \tag{4.49}$$

The derivation is not substantially different than what we have seen before, so we simply highlight a few subtleties. For the first claim, recall that the scattering form is a sum over all α-planar graphs:

$$\Omega^{(n-3)}[\alpha] = \sum_{\alpha\text{-planar } g} \text{sign}(g) \bigwedge_{a=1}^{n-3} d \log X_{\alpha(i_a),\alpha(j_a)} \tag{4.50}$$

We claim that on the pullback to the subspace $H[\alpha|\beta]$, the numerator is identical and non-zero for every (α, β)-planar graph g and zero otherwise:

$$\text{sign}(g) \bigwedge_{a=1}^{n-3} dX_{\alpha(i_a),\alpha(j_a)} = \begin{cases} d^{n-3}X & \text{if } g \text{ is } \beta\text{-planar} \\ 0 & \text{otherwise} \end{cases} \tag{4.51}$$

The pullback therefore sums all the β-planar diagrams and destroys all other diagrams, thus giving the desired amplitude $m[\alpha|\beta]$:

$$\Omega^{(n-3)}[\alpha]|_{H[\alpha|\beta]} = \left(\sum_{(\alpha,\beta)\text{-planar } g} \frac{1}{\prod_{a=1}^{n-3} X_{\alpha(i_a),\alpha(j_a)}} \right) d^{n-3}X = m[\alpha|\beta] d^{n-3}X \quad (4.52)$$

As before, it can be shown that this is also the canonical form of the kinematic polytope $\mathcal{A}[\alpha|\beta]$. The canonical forms for the n=4 examples are given in Figure 4.9. The canonical form for the n=5 example in Figure 4.10 is

$$\begin{aligned} \Omega(\mathcal{A}[12345|13245]) &= d\log X_{2,5} d\log X_{2,4} + d\log X_{2,4} d\log X_{1,4} \\ &= \left(\frac{1}{X_{2,5}X_{2,4}} + \frac{1}{X_{2,4}X_{1,4}} \right) d^2X \end{aligned} \quad (4.53)$$

where we used the fact that $dX_{2,5}dX_{2,4} = dX_{2,4}dX_{1,4}$ on the pullback, which follows from the identity $X_{1,4} = c_{14} - X_{2,5} + X_{2,4}$.

4.2.5 The associahedron as the amplituhedron for bi-adjoint cubic theory

Let us summarize the story so far for the bi-adjoint ϕ^3 theory. We have an obvious kinematic space $\mathcal{K}_n$ parametrized by the $X_{i,j}$ which is $n(n-3)/2$-dimensional. We also have a scattering form $\Omega_n^{(n-3)}$ of rank $(n-3)$ defined on this space, which for $n > 3$ is of lower than top rank. This scattering form is fully determined by its association with a positive geometry living in the kinematic space defined in the following way. First, there is a top-dimensional "positive region" in the kinematic space given by $X_{i,j} \geq 0$ whose boundaries are associated with all the poles of the planar graphs. Next, there is a family of $(n-3)$-dimensional linear subspaces defined by $X_{i,j} + X_{i+1,j+1} - X_{i,j+1} - X_{i+1,j} = c_{ij}$. With appropriate positivity constraints on the constants $c_{ij} > 0$, this subspace intersects the "positive region" in a positive

geometry—the kinematic associahedron $\mathcal{A}_n$. Furthermore, the scattering form $\Omega_n^{(n-3)}$ on the full kinematic space is fully determined by the property of pulling back to the canonical form of the associahedron on this family of subspaces. Hence, the physics of on-shell tree-level bi-adjoint ϕ^3 amplitudes are completely determined by the positive geometry not in any auxiliary space but directly in kinematic space.

Furthermore, there is a striking similarity between this description of bi-adjoint ϕ^3 scattering amplitudes and the description of planar $\mathcal{N} = 4$ super Yang-Mills (SYM) with the amplituhedron as the positive geometry [22]. Indeed the general structure is identical. There is once again a kinematic space, which for planar $\mathcal{N} = 4$ SYM is given by the momentum twistor variables $Z_i \in \mathbb{P}^3(\mathbb{R})$ for $i = 1, \ldots, n$, and a differential form $\Omega_n^{(4k)}$ of rank $4 \times k$ (for N^{k}MHV) on kinematic space that is fully determined by its association with a positive geometry. We again begin with a "positive region" in the kinematic space which enforces positivity of all the poles of planar graphs via $\langle Z_i Z_{i+1} Z_j Z_{j+1} \rangle \geq 0$; however, also required is a set of topological "winding number" conditions enforced by a particular "binary code" of sign-flip patterns for the momentum twistor data. This is a top-dimensional subspace of the full kinematic space. There is also a canonical $4 \times k$ dimensional subspace of the kinematic space, corresponding to an affine translation of a given set of external data Z_* in the direction of a fixed k-plane Δ in n dimensions; this subspace is thus specified by a $(4+k) \times n$ matrix $\mathcal{Z} := (Z_*, \Delta)^T$. Provided the condition that all ordered $(4+k) \times (4+k)$ minors of $\mathcal{Z}$ are positive, this subspace intersects the "positive region" in a positive geometry—the (tree) amplituhedron. The form $\Omega_n^{(4k)}$ on the full space is fully determined by the property of pulling back to the canonical form of the amplituhedron found on this family of subspaces. Once again this connection between scattering forms and positive geometry is seen directly in ordinary momentum twistor space, without any reference to the auxiliary Grassmannian spaces where amplituhedra were originally defined to live.

The nature of the relationship between "kinematic space", "positive region", "positive family of subspaces" and "scattering form" is literally identical in the two stories. We say therefore that "the associahedron is the amplituhedron for bi-adjoint ϕ^3 theory".

Of course there are some clear differences as well. Most notably, the scattering form $\Omega_n^{(4k)}$ is directly the super-amplitude with the differentials dZ_i^I interpreted as Grassmann variables η_i^I, whereas for the bi-adjoint ϕ^3 theory we have forms on the space of Mandelstam variables with no supersymmetric interpretation. While the planar $\mathcal{N} = 4$ scattering forms are unifying different helicities into a single natural object, what are the forms in Mandelstam space doing? As we have already seen in the bi-adjoint example, and with more to come in later sections, these forms are instead *geometrizing color factors*, as established in Section 6.

4.3 Factorization and "soft" limit

We now derive two important properties of amplitudes by exploiting geometric properties of the associahedron:

1. The amplitude factorizes on physical poles.

2. The amplitude vanishes in a "soft" limit.

We emphasize that both properties follow from geometric arguments. While amplitude factorization is familiar, here it emerges from the "geometric factorization" of the associahedron; and the vanishing in the "soft" limit is a property of the amplitude that is made more manifest by the geometry than Feynman diagrams.

4.3.1 Factorization

Recall from Section 4.2.1 that the associahedron factorizes combinatorially, i.e. each facet is combinatorially identical to a product of two lower associahedra (See (4.19)). We now demonstrate this explicitly for the kinematic polytope $\mathcal{A}_n$, thus giving a simple derivation of the fact that $\mathcal{A}_n$ is indeed an associahedron. While (4.19) is a purely combinatorial statement, we go further in this section and find explicit geometric constructions for the two lower associahedra. We therefore say that $\mathcal{A}_n$ *factorizes geometrically*. Furthermore, we argue that *geometric factorization* of $\mathcal{A}_n$ directly implies *amplitude factorization*, so that locality and unitarity of the amplitude are *emergent properties* of the geometry.

We rewrite the kinematic associahedron $\mathcal{A}_n$ as $\mathcal{A}(1, 2, \ldots, \bar{n})$ to emphasize the particle labels and their ordering; we put a bar over index n to emphasize that the subspace H_n is defined with non-adjacent indices omitting n (See (4.21)). We make the following observations:

1. *Geometric factorization*: The facet $X_{i,j} = 0$ is equivalent to a product polytope

$$\mathcal{A}_n|_{X_{i,j}=0} \cong \mathcal{A}_L \times \mathcal{A}_R \tag{4.54}$$

where

$$\begin{aligned} \mathcal{A}_L &:= \mathcal{A}(i, i{+}1, \ldots, j{-}1, \bar{I}) \\ \mathcal{A}_R &:= \mathcal{A}(1, \ldots, i{-}1, I, j, j{+}1, \ldots, \bar{n}) \end{aligned} \tag{4.55}$$

and I denotes the intermediate particle. The cut can be visualized as the diagonal (i, j) on the convex n-gon (See Figure 4.11).

2. *Amplitude factorization*: The residue of the canonical form along the facet $X_{i,j} = 0$ factors:

$$\text{Res}_{X_{i,j}=0}\Omega(\mathcal{A}_n) = \Omega(\mathcal{A}_L) \wedge \Omega(\mathcal{A}_R) \tag{4.56}$$

This implies factorization of the amplitude.

We first construct the "left associahedron" $\mathcal{A}_L$ and the "right associahedron" $\mathcal{A}_R$ by (4.55) as *independent* associahedra living in *independent* kinematic spaces. The indices appearing in the construction are nothing more than well-chosen labels at this point. To emphasize this, we use independent planar variables for $\mathcal{A}_L$ and $\mathcal{A}_R$:

$$\mathcal{A}_L \quad : \quad L_{a,b} \text{ for } i \leq a < b < j \tag{4.57}$$

$$\mathcal{A}_R \quad : \quad R_{a,b} \text{ for } 1 \leq a < b < n \text{ except } i \leq a < b < j \tag{4.58}$$

The index ranges can be visualized as Figure 4.11 where the "left" planar variables $L_{a,b}$ correspond to diagonals of the "left" subpolygon, and likewise for the "right". Furthermore, the two associahedra come with positive non-adjacent constants l_{ab}, r_{ab}, respectively. For l_{ab} the indices consist of all non-adjacent pairs a, b in the range $i \leq a < b < j$. For r_{ab} they consist of all non-adjacent pairs a, b in the range $(1, \ldots, i{-}1, I, j, j{+}1, \ldots, n{-}1)$.

We now argue that there exists a one-to-one correspondence:

$$\mathcal{A}_L \times \mathcal{A}_R \cong \mathcal{A}_n|_{X_{i,j}=0} \tag{4.59}$$

We begin by picking a kinematic basis for $\mathcal{A}_L$ consisting of $L_{a,b}$ variables corresponding to some triangulation of the left subpolygon in Figure 4.11, and similarly for the $R_{a,b}$ variables. The two triangulations combine to form a partial triangulation of the n-gon with the diagonal (i, j) omitted. Each diagonal corresponds to a planar variable,

thus providing a basis for the subspace $H_n|_{X_{i,j}=0}$. Furthermore, we assume that the non-adjacent constants match so that $c_{ab} = l_{ab}$ for all l_{ab}. As for r_{ab}, we assume that $c_{ab} = r_{ab}$ for all r_{ab} where $a, b \neq I$. Furthermore, $r_{aI} = \sum_{k \in I} c_{ak}$ for all r_{aI}.

We then write down the most obvious map $\mathcal{A}_L \times \mathcal{A}_R \to H_n|_{X_{i,j}=0}$ given by:

$$X_{a,b} = L_{a,b} \text{ for all left basis variables } L_{a,b} \tag{4.60}$$

$$X_{a,b} = R_{a,b} \text{ for all right basis variables } R_{a,b} \tag{4.61}$$

Since the $X_{a,b}$ variables in the image form a basis for $\mathcal{A}_n|_{X_{i,j}=0}$, this completely defines the map. We observe that $X_{a,b} = L_{a,b}$ holds not just for left basis variables, but for all left variables $L_{a,b}$. The idea is to rewrite $L_{a,b}$ in terms of basis variables and non-adjacent constants. Since the same formula holds for $X_{a,b}$, and the constants match by assumption, therefore the desired result must follow. Similarly, $X_{a,b} = R_{a,b}$ holds for all right variables $R_{a,b}$.

Now we argue that the image of the embedding lies in the facet $\mathcal{A}_n|_{X_{i,j}=0}$, which requires showing that all planar propagators $X_{a,b}$ are positive under the embedding except for $X_{i,j} = 0$. This is trivially true for propagators whose diagonals do not cross (i, j), since either $X_{a,b} = L_{a,b}$ or $X_{a,b} = R_{a,b}$. Now consider a crossing diagonal (k, l) satisfying $1 \leq i < k < j < l \leq n$. Applying (4.24) with indices j, k swapped and setting $X_{i,j} = 0$ gives

$$X_{k,l} = X_{k,j} + X_{i,l} + \sum_{\substack{i \leq a < k \\ j \leq b < l}} c_{ab} \tag{4.62}$$

Since $X_{k,j}$ is a diagonal of the left subpolygon and $X_{i,l}$ is a diagonal of the right, they are both positive. It follows that the right hand side is term-by-term positive, hence our crossing term $X_{k,l}$ must also be positive, as claimed. We emphasize that $X_{k,l}$ is actually strictly positive, implying that it cannot be cut. This is important because

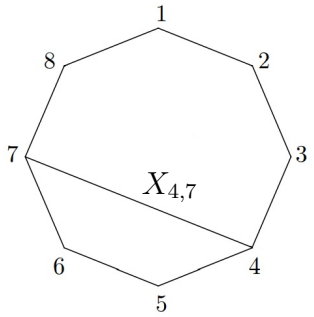

Figure 4.11: The diagonal $(4, 7)$ subdivides the 8-gon into a 4-gon (on the "left") and a 6-gon (on the "right"), suggesting that the facet $X_{4,7} = 0$ of the associahedron $\mathcal{A}_{n=8}$ is combinatorially identical to $\mathcal{A}_{n=4} \times \mathcal{A}_{n=6}$.

cutting crossing propagators simultaneously would violate the planar graph structure of the associahedron. Finally, it is easy to see that this is a one-to-one map, thus completing our argument for the first assertion (4.54).

As an example, consider the n=6 kinematic associahedron shown in Figure 4.4 (bottom). Let us consider the facet $X_{2,5} = 0$ which by geometric factorization is a product of 4-point associahedra (i.e. a product of line segments) and must therefore be a quadrilateral. This agrees with Figure 4.4 (bottom) by inspection. The same is true for the facets $X_{1,4} = 0$ and $X_{3,6} = 0$. In contrast, the facet $X_{3,5} = 0$ is given by the product of a point with a pentagon, and is therefore also a pentagon. The same holds for the remaining 5 facets.

The second assertion (4.56) follows immediately from the first:

$$\text{Res}_{X_{i,j}=0}\Omega(\mathcal{A}_n) = \Omega(\mathcal{A}_n|_{X_{i,j}=0}) = \Omega(\mathcal{A}_L \times \mathcal{A}_R) = \Omega(\mathcal{A}_L) \wedge \Omega(\mathcal{A}_R) \tag{4.63}$$

where the first equality follows from the residue property ((P2) of Section 2.1), the second from the first assertion (4.54) and the third from the product property (2.1). This provides a geometric explanation for the factorization of the amplitude first discussed in (4.16).

4.3.2 "Soft" limit

The associahedron geometry suggests a natural "soft limit" where the polytope is "squashed" to a lower dimensional one, whereby the amplitude obviously vanishes.

Consider the associahedron $\mathcal{A}_n$ which lives in the subspace H_n defined by non-adjacent constants c_{ij}. Let us consider the "soft" limit where the non-adjacent constants $c_{1i} \to 0$ go to zero for $i = 3, \ldots, n-1$. It follows from kinematic constraints that

$$X_{1,3} + X_{2,n} = s_{12} + s_{1n} = -\sum_{i=3}^{n-1} s_{1i} = \sum_{i=3}^{n-1} c_{1i} \to 0 \tag{4.64}$$

But since both terms on the left are nonnegative $X_{1,3}, X_{2,n} \geq 0$ inside the associahedron, the limit "squashes" the geometry to a lower dimension where $X_{1,3} = X_{2,n} = 0$. The canonical form must therefore vanish everywhere on H_n, implying that the amplitude is identically zero. Note that if we restrict kinematic variables to the interior of the associahedron, then $p_1 \cdot p_i \to 0$ for every i, yielding the true soft limit $p_1 \to 0$. A similar argument can be given to show that the canonical form vanishes in the "soft" limit where $c_{i,n-1} \to 0$ for every $i = 1, \ldots, n-3$. And by cyclic symmetry, the amplitude must vanish under every "soft" limit given by $s_{ij} \to 0$ for some fixed index i and every index $j \neq i-1, i+1$.

Furthermore, given any triangulation of the associahedron $\mathcal{A}_n$ of the kind discussed in Section 4.4.4, every piece of the triangulation is squashed by the "soft" limit. It follows that the canonical form of each piece must vanish individually.

The fact that the amplitude m_n vanishes in this limit is rather non-trivial from a physical point of view. While the geometric argument we provided is straightforward, there does not appear to be any obvious physical reason for it. It is another feature of the amplitude made obvious by the associahedron geometry.

As an example, the n=5 amplitude (4.40) vanishes in the limit $c_{13}, c_{14} \to 0$, which can be seen by substituting the equivalent limits $X_{1,3} \to X_{1,4} - X_{2,4}$ and $X_{2,5} \to X_{2,4} - X_{1,4}$ directly into the amplitude (4.40).

4.4 Triangulations and recursion relations

Since the scattering forms pull back to the canonical form on our associahedra, it is natural to expect that concrete expressions for the scattering amplitudes correspond to natural triangulations of the associahedron. This connection between triangulations of a positive geometry and various physical representations of amplitudes has been vigorously explored in the context of the positive Grassmannian/amplituhedron, with various triangulations of spaces and their duals corresponding to BCFW and "local" forms for scattering amplitudes. In the present case of study for bi-adjoint ϕ^3 theories, we encounter a lovely surprise: one of the canonical triangulations of the associahedron literally reproduced the Feynman diagram expansion! Ironically this representation also introduces spurious poles (at infinity) that only cancel in the full sum over all diagrams; also, other properties of the amplitude, such as the vanishing in the "soft" limit discussed in Section 4.3.2, are also not manifest term-by-term in this triangulation. We also explore a number of other natural triangulations of the geometry that make manifest the features hidden by the Feynman diagram triangulation. Quite surprisingly, some triangulations lead to even more compact expressions for these familiar and already very simple amplitudes! Finally, we introduce a novel recursion relation for amplitudes based on the factorization properties discussed in Section 4.3.1.

4.4.1 The dual associahedron and its volume as the bi-adjoint amplitude

Recall that every convex polytope $\mathcal{A}$ has a *dual polytope* $\mathcal{A}^*$ whose volume determines the canonical rational function of $\mathcal{A}$.

$$\underline{\Omega}(\mathcal{A}) = \text{Vol}(\mathcal{A}^*) \tag{4.65}$$

Applying (4.65) to our discussion implies that the canonical form of the associahedron $\mathcal{A}_n$ is determined by the volume of the *dual associahedron* $\mathcal{A}_n^*$:

$$\underline{\Omega}(\mathcal{A}_n) = \text{Vol}(\mathcal{A}_n^*) \tag{4.66}$$

But in the same way, the canonical rational function is determined by the amplitude m_n via (4.37), thus suggesting that the amplitude is the volume of the dual:

$$m_n = \text{Vol}(\mathcal{A}_n^*) \tag{4.67}$$

This leads to yet another geometric interpretation of the bi-adjoint amplitude. For the remainder of this section, we describe the construction of the dual associahedron in more detail, and provide the example for n=5.

We embed the subspace H_n in projective space $\mathbb{P}^{n-3}(\mathbb{R})$, and we choose a basis of Mandelstam variables $X_{i'_1,j'_1}, \ldots, X_{i'_{n-3},j'_{n-3}}$ to denote coordinates on the subspace:

$$Y = (1, X_{i'_1,j'_1}, \ldots, X_{i'_{n-3},j'_{n-3}}) \in \mathbb{P}^{n-3}(\mathbb{R}) \tag{4.68}$$

Here we have introduced a zeroth component "1" since the coordinates are embedded projectively. Any other basis can be obtained via a $GL(n-2)$ transformation. Furthermore, we denote the facets of the associahedron in projective coordinates.

Recall that every facet of $\mathcal{A}_n$ is of the form $X_{i,j} = 0$. We rewrite this in the form $W_{i,j} \cdot Y = 0$ for some dual vector $W_{i,j}$. For example, consider $n = 5$ in the basis $Y = (1, X_{1,3}, X_{1,4})$. Then

$$Y \cdot W_{2,5} = X_{2,5} = c_{13} + c_{14} - X_{1,3} = (c_{13} + c_{14}, -1, 0) \cdot Y \tag{4.69}$$

which implies that $W_{2,5} = (c_{13} + c_{14}, -1, 0)$. More generally, the components of any $W_{i,j}$ can be read off from the expansion of $X_{i,j}$ in terms of basis variables $X_{i'_a,j'_a}$ and non-adjacent constants. Here we present all the dual vectors for the $n = 5$ pentagon in Figure 4.4 (top right):

$$\begin{aligned} W_{1,3} &= (0, 1, 0) \\ W_{3,5} &= (c_{14} + c_{24}, 0, -1) \\ W_{2,5} &= (c_{13} + c_{14}, -1, 0) \\ W_{2,4} &= (c_{13}, -1, 1) \\ W_{1,4} &= (0, 0, 1) \end{aligned} \tag{4.70}$$

Once the coordinates for the dual vectors $W_{i,j}$ are computed, they can be thought of as *vertices* of the dual associahedron $\mathcal{A}_n^*$ in the dual projective space. For n=5, the dual associahedron is a pentagon whose vertices are (4.70) (See Figure 4.12).

4.4.2 Feynman diagrams as a triangulation of the dual associahedron volume

We now compute the volume of $\mathcal{A}^*$ by triangulation in the manner described in Example 3.4.2. Let Z denote a *facet* of the dual $\mathcal{A}_n^*$. Then Z is adjacent to some vertices $W_{i_1,j_1}, \ldots, W_{i_{n-3},j_{n-3}}$ corresponding to propagators $X_{i_1,j_1}, \ldots, X_{i_{n-3},j_{n-3}}$, respectively. By taking the convex hull of the facet Z with W_*, and taking the union over all facets,

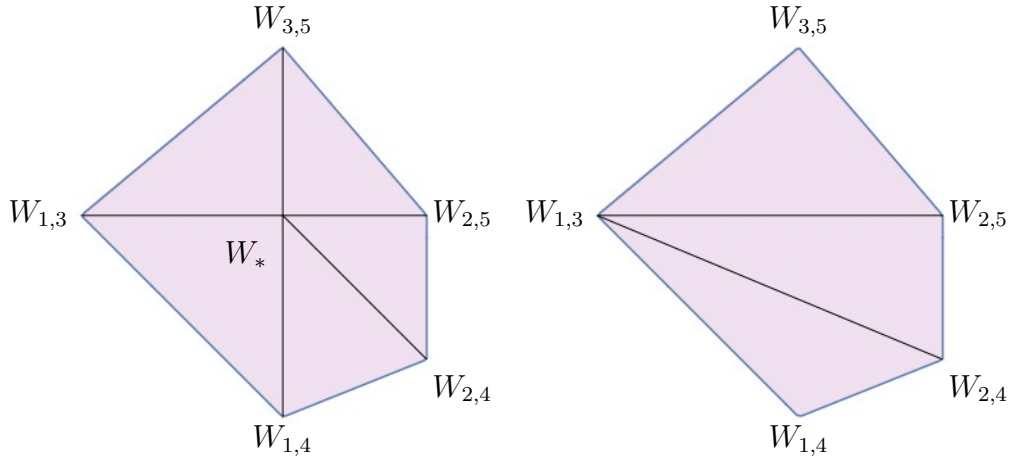

Figure 4.12: Two triangulations of the dual associahedron $\mathcal{A}^*_{n=5}$

we get a triangulation of the dual associahedron whose volume is the sum over the volume of each simplex. Recalling the formula for the volume of a simplex (3.125), we find

$$\begin{aligned} \mathrm{Vol}(\mathcal{A}^*_n) &= \sum_{\text{vertex } Z} \mathrm{Vol}(W_*, W_{i_1,j_1}, \ldots, W_{i_{n-3},j_{n-3}}) \\ &= \sum_{\text{vertex } Z} \frac{\mathrm{sign}(Z)\left\langle W_* W_{i_1,j_1} \cdots W_{i_{n-3},j_{n-3}}\right\rangle}{(Y\cdot W_*)\prod_{a=1}^{n-3}(Y\cdot W_{i_a,j_a})} \end{aligned} \tag{4.71}$$

where $\mathrm{sign}(Z)$ is the orientation of the adjacent vertices $W_{i_1,j_1}, \ldots, W_{i_{n-3},j_{n-3}}$ (in that order) relative to the inherited orientation. Note that the antisymmetry of $\mathrm{sign}(Z)$ is compensated by the antisymmetry of the determinant $\langle \cdots \rangle$ in the numerator, and the sum is independent of the choice of reference point W_*. Furthermore, the $\mathrm{sign}(Z)$ here is equivalent to the $\mathrm{sign}(Z)$ appearing in (4.31) where Z denotes the corresponding *vertex* of $\mathcal{A}_n$.

We now argue that for an appropriate choice of reference point W_*, the Feynman diagram expansion (4.36) is term-by-term equivalent to the expression (4.71), where each Z is associated with its corresponding planar cubic graph g. With the benefit of hindsight, we set the reference point to $W_* = (1, 0 \ldots, 0)$, which is particularly convenient because the numerators in (4.71) are now equivalent for all Z. Indeed,

since $X_{i_a,j_a} = Y \cdot W_{i_a,j_a}$, we have

$$\left\langle W_* W_{i_1,i_1} \cdots W_{i_{n-3},j_{n-3}} \right\rangle = \frac{\partial(X_{i_1,j_1}, \ldots, X_{i_{n-3},j_{n-3}})}{\partial(X_{i'_1,j'_1}, \ldots, X_{i'_{n-3},j'_{n-3}})} = \text{sign}(Z)/\text{sign}(Z') \tag{4.72}$$

where the primed variables form the basis we chose back in (4.68), and the second equality follows from (4.33). This shows that all the numerators in (4.71) are equivalent to sign(Z'), which we set to one. Finally, substituting $(Y \cdot W_*) = 1$ and $(Y \cdot W_{i_a,j_a}) = X_{i_a,j_a}$ into (4.71) and replacing Z by g gives

$$\text{Vol}(\mathcal{A}_n^*) = \sum_{\text{planar } g} \frac{1}{\prod_{a=1}^{n-3} X_{i_a,j_a}} \tag{4.73}$$

which is precisely the Feynman diagram expansion (4.36) for the amplitude. It follows that the amplitude is the volume of the dual associahedron

$$\text{Vol}(\mathcal{A}_n^*) = \underline{\Omega}(\mathcal{A}_n) = m_n \tag{4.74}$$

of which the Feynman diagram expansion is a particular triangulation.

We point out that the Feynman diagram expansion introduces a spurious vertex W_*, which term-by-term gives rise to a pole at infinity that cancels in the sum. From the point of view of the original associahedron, this corresponds to a "signed" triangulation of $\mathcal{A}_n$ with overlapping simplices, whereby every simplex consists of all the facets that meet at a vertex together with the boundary at infinity. The presence of bad poles at infinity in individual Feynman diagrams that only cancel in the sum over all diagrams bears striking resemblance to the behavior of Feynman diagrams under BCFW shifts in gauge theories and gravity. There too, individual Feynman diagrams have poles at infinity, even though the final amplitude does not, and this surprising vanishing at infinity is critically related to the magical properties of amplitudes in these theories. Indeed, the absence of poles at infinity in Yang-Mills theory finds a

deeper explanation in terms of the symmetry of dual conformal invariance. It is thus particularly amusing to see an analog of this hidden symmetry even for something as innocent-seeming as bi-adjoint ϕ^3 theory! Furthermore, the scattering form in the full kinematic space is projectively invariant, a symmetry invisible in individual diagrams. And the pullback of the forms to the associahedron subspaces are *also* projectively invariant, with no pole at infinity. In Yang-Mills theories, we have discovered representations (such as those based on BCFW recursion relations) that make the dual conformal symmetry manifest term-by-term, and these were much later seen to be associated with triangulations of the amplituhedron. Similarly, we now turn to other natural triangulations of the associahedron which do not introduce new vertices and thus have no spurious poles at infinity, thus making manifest term-by-term the analogous feature of bi-adjoint ϕ^3 amplitudes that is hidden in Feynman diagrams.

4.4.3 More triangulations of the dual associahedron

Returning to (4.71), a different choice of W_* would have led to alternative triangulations, and hence novel formulas for the amplitude. For instance, for n=5, we can take the limit $W_* \to W_{13}$. This kills two volume terms and gives a three-term triangulation as shown in Figure 4.12 (right):

$$m_{n=5} = \frac{X_{1,3} + X_{2,5}}{X_{1,3}X_{3,5}X_{2,5}} + \frac{X_{1,3} + X_{2,5}}{X_{1,3}X_{2,5}X_{2,4}} + \frac{X_{1,3} - X_{1,4} + X_{2,4}}{X_{1,3}X_{2,4}X_{1,4}} \tag{4.75}$$

Note that we have re-written the non-adjacent constants c_{ij} in terms of planar variables via (4.21). The sum of these three volumes gives the volume of the dual associahedron, and hence the amplitude. Furthermore, since no spurious vertices are introduced, the result makes manifest term-by-term the absence of poles at infinity. This contrasts the Feynman diagram expansion where spurious poles appear term-

by-term. Finally, this method of setting W_* to one of the vertices can be repeated for arbitrary n, and in general produces fewer terms than with Feynman diagrams.

4.4.4 Direct triangulations of the kinematic associahedron

Recall that canonical forms are triangulation independent. We now exploit this property to compute the canonical form of the associahedron, thus establishing another method for computing amplitudes.

We wish to compute the n=5 amplitude for which the associahedron is a pentagon. We choose the basis $Y = (1, X_{13}, X_{14})$, and triangulate the associahedron as the union of three triangles ABC, ACD and ADE (See Figure 4.13). It follows that

$$\Omega(\mathcal{A}_{n=5}) = \Omega(ABC) + \Omega(ACD) + \Omega(ADE) \tag{4.76}$$

Note that the triangles must be oriented in the same way as the associahedron (clockwise in this case). Getting the wrong orientation would cause a sign error. The boundaries of the triangles are given by $W \cdot Y = 0$ for:

$$\begin{aligned} W_{AB} = (0,1,0) \quad W_{BC} = (c_{14}+c_{24},0,-1) \\ W_{CD} = (c_{13}+c_{14},-1,0) \quad W_{DE} = (c_{13},-1,1) \quad W_{AE} = (0,0,1) \\ W_{AC} = (0,-c_{14}-c_{24},c_{13}+c_{14}) \quad W_{AD} = (0,-c_{14},c_{13}+c_{14}) \end{aligned} \tag{4.77}$$

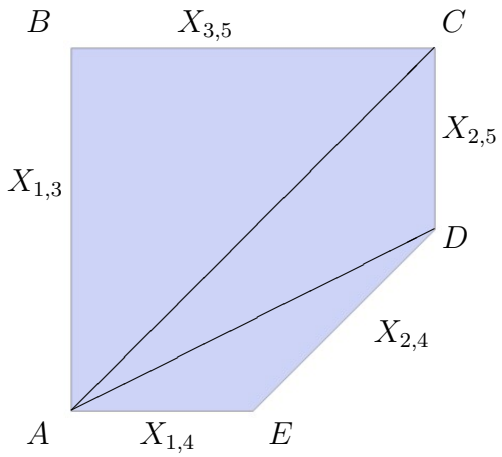

Figure 4.13: A triangulation of the associahedron $\mathcal{A}_{n=5}$

Recalling the canonical form for a simplex (2.17), we get

$$\begin{aligned}
\Omega(ABC) &= \frac{(X_{1,3}+X_{2,5})(X_{1,4}+X_{3,5})d^2X}{X_{1,3}X_{3,5}(X_{1,4}X_{2,5}-X_{1,3}X_{3,5})} \\
\Omega(ACD) &= \frac{(X_{1,3}+X_{2,5})^2(X_{2,4}-X_{2,5}+X_{3,5})d^2X}{X_{2,5}(-X_{1,4}X_{2,5}-X_{1,3}X_{2,4}+X_{1,3}X_{2,5})(X_{1,4}X_{2,5}-X_{1,3}X_{3,5})} \\
\Omega(ADE) &= \frac{(X_{1,3}-X_{1,4}+X_{2,4})(-X_{2,4}+X_{1,4}+X_{2,5})d^2X}{X_{1,4}X_{2,4}(-X_{1,4}X_{2,5}-X_{1,3}X_{2,4}+X_{1,3}X_{2,5})}
\end{aligned}$$

$$\Omega(\mathcal{A}_{n=5}) = \Omega(ABC)+\Omega(ACD)+\Omega(ADE)$$

where again we have rewritten the non-adjacent constants c_{ij} in terms of planar variables via (4.21). The sum of these three quantities determines the amplitude. This expansion is fundamentally different in character from the Feynman diagram expansion due to the appearance of (non-linear) spurious poles that occur in the presence of spurious boundaries AC and AD.

This approach can be extended to all n provided that a triangulation is known. Two important properties of the bi-adjoint amplitude, which are obscured by individual Feynman diagrams, become manifest in this triangulation. First, unlike that for each Feynman diagram, the form for each piece of the triangulation is projective,

which means it only depends on the ratio of X variables. Moreover, geometrically it is obvious that the vanishing "soft" limit also works term-by-term, which is certainly not the case for each Feynman diagram.

4.5 Vertex coordinates of the kinematic associahedron

We now provide a recursive algorithm for deriving the vertices of the associahedron $\mathcal{A}_n$. Consider a vertex Z_0 corresponding to a triangulation of the n-gon. Our goal is to work out all planar components $X_{i,j}$ of Z_0 in terms of the non-adjacent constants c_{kl}. Our strategy is to compute the components one planar basis (i.e. a basis of planar variables given by the diagonals of any triangulation) at a time by starting with the basis where all components vanish, and applying a sequence of mutations. Since every planar basis can be reached by such a sequence, this establishes a recursive procedure for computing all planar components. It suffices then to discuss how the components are related by mutation. Consider a mutation $Z \to Z'$ like the one shown in Figure 4.6 (top) where $X_{i,k}$ mutates to $X_{j,l}$. From (4.24) we find

$$X_{j,l} = X_{j,k} + X_{i,l} - X_{i,k} + \sum_{\substack{i \le a < j \\ k \le b < l}} c_{ab} \tag{4.78}$$

which computes $X_{j,l}$ from the basis of Z, thus completing the algorithm.

Here we present the vertex coordinates for the kinematic associahedron $\mathcal{A}_{n=5}$ from Figure 4.4 (top right) in the basis $Y = (1, X_{13}, X_{14})$:

$$Z_A = (1, 0, 0) \tag{4.79}$$

$$Z_B = (1, 0, c_{14} + c_{24}) \tag{4.80}$$

$$Z_C = (1, c_{13} + c_{14}, c_{14} + c_{24}) \tag{4.81}$$

$$Z_D = (1, c_{13} + c_{14}, c_{14}) \tag{4.82}$$

$$Z_E = (1, c_{13}, 0) \tag{4.83}$$

$$\tag{4.84}$$

Chapter 5

The worldsheet

We have seen that scattering amplitudes can be thought of as differential forms on the space of kinematic variables that pullback to the canonical forms of associahedra in kinematic space. This is a deeply satisfying connection. After all, the associahedron is perhaps the most fundamental and primitive object whose boundary structure embodies "factorization" as a combinatorial and geometric property.

Furthermore, string theorists have long known of the fundamental role of the associahedron for the open string. After all, the boundary structure of the open string moduli space—the moduli space of n ordered points on the boundary of a disk—also famously "factorizes" in the same way. In fact, it is well-known that the Deligne-Mumford compactification [23, 24] of this space has precisely the same boundary structure as the associahedron. The implications of this "worldsheet associahedron" for aspects of stringy physics have also been explored in e.g. [47, 48].

Moreover, from general considerations of positive geometries we know that there should also be a "worldsheet canonical form" associated with this worldsheet associahedron, which turns out to be the famous "worldsheet Parke-Taylor form" [49] (for related discussions see e.g. [48, 50]), an object whose importance has been highlighted

in Nair's observation [51] and Witten's twistor string [5], and especially in the story of scattering equations and the CHY formulas for scattering amplitudes [11, 12, 10, 13].

But how is the worldsheet associahedron related to the kinematic associahedron? This simple question has a striking answer: The scattering equations act as a *diffeomorphism* from the worldsheet associahedron to the kinematic associahedron! From general grounds, it follows that the kinematic scattering form is the pushforward of the worldsheet Parke-Taylor form under the scattering equation map. This gives a beautiful meaning to the scattering equations, and a quick geometric derivation of the bi-adjoint CHY formulas. We now explain these ideas in more detail.

5.1 Associahedron from the open string moduli space

Recall that the moduli space of genus zero $\mathcal{M}_{0,n}$ is the space of configurations of n distinct punctures on the Riemann sphere $\mathbb{CP}^1$ modulo $\mathrm{SL}(2,\mathbb{C})$. The real part $\mathcal{M}_{0,n}(\mathbb{R})$ is the *open-string moduli space* consisting of all distinct points σ_i ($i = 1,\ldots,n$) on the real line (and infinity) modulo $\mathrm{SL}(2,\mathbb{R})$. While there are $n!$ ways of ordering the σ_i variables, any pair of orderings related by dihedral transformation are $\mathrm{SL}(2,\mathbb{R})$ equivalent. It follows that the real part is tiled by $(n-1)!/2$ distinct regions given by inequivalent orderings of the σ_i variables [24]. The region given by the standard ordering is called the *positive part* of the open string moduli space or more simply the *positive moduli space*

$$\mathcal{M}^+_{0,n} := \{\sigma_1 < \sigma_2 < \cdots < \sigma_n\}/\mathrm{SL}(2,\mathbb{R}) \tag{5.1}$$

where the $\mathrm{SL}(2,\mathbb{R})$ redundancy can be "gauge fixed" in the standard way by setting fixing three variables $(\sigma_1,\sigma_{n-1},\sigma_n) = (0,1,\infty)$ in which case $\mathcal{M}^+_{0,n} = \{0 < \sigma_2 < \cdots <$

$\sigma_{n-2} < 1\}$. Sometimes we also denote the space by $\mathcal{M}^+_{0,n}(1,2,\ldots,n)$ to emphasize the ordering. Furthermore, recall that $\mathcal{M}^+_{0,n}$ can also be constructed as the (strictly) positive Grassmannian $\mathrm{G}_{>0}(2,n)$ modded out by the torus action $\mathbb{R}^n_{>0}$. More precisely, we consider the set of all $2\times n$ matrices $(C_1,\ldots,C_n)$ with positive Plücker coordinates $(ab) := \det(C_a, C_b) > 0$ for $1 \le a < b \le n$, modded out by GL(2) action and column rescaling.

In analogy to what we did for the kinematic polytope, we make two claims for the positive moduli space:

1. The (compactified) positive moduli space is an associahedron which we call the *worldsheet associahedron*.

2. The canonical form of the worldsheet associahedron is the Parke-Taylor form,

$$\omega_n^{\mathrm{WS}} := \frac{1}{\mathrm{vol}\ [\mathrm{SL}(2)]} \prod_{a=1}^{n} \frac{d\sigma_a}{\sigma_a - \sigma_{a+1}} = \frac{1}{\mathrm{vol}\ [\mathrm{SL}(2)\times\mathrm{GL}(1)^n]} \prod_{a=1}^{n} \frac{d^2 C_a}{(a\,a{+}1)} \quad (5.2)$$

   where in the last expression we rewrote the form in Plücker coordinates.

More precisely, the process of compactification provides the positive moduli space $\mathcal{M}^+_{0,n}$ with boundaries of all codimensions, and here we present a natural compactification called the *u-space compactification* that produces the boundary structure of the associahedron. Of course, the associahedron structure of the positive moduli space is well-known [23, 24], but the discussion we present here is instructive for later sections.

The compactification is very subtle in σ_i variables because our naive gauge choice fails to make all boundaries manifest. Nonetheless, all the boundaries can be visualized via a "blowup" procedure. Consider the case n=5 where only three of the five boundaries are manifest in the standard gauge as shown in Figure 5.1. The two "hidden" boundaries can be recovered by introducing a blowup at the vertices $(\sigma_2,\sigma_3) = (0,0)$ and $(1,1)$ as shown in Figure 5.1. A similar procedure applies for all

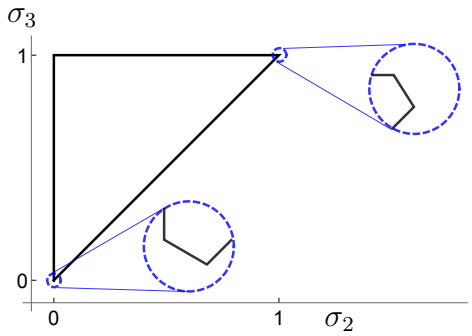

Figure 5.1: A blowup of the n=5 worldsheet associahedron showing all boundaries.

n. We will come back to this picture when we discuss the canonical form, but now we provide an explicit compactification that makes manifest all the boundaries.

We introduce the variables $u_{i,j}$ for $1 \leq i < j-1 < n$ which are constrained to the region $0 \leq u_{i,j} \leq 1$. The $u_{i,j}$ is analogous to the planar kinematic variable $X_{i,j}$ introduced in (4.6), and can therefore be visualized as the diagonal (i,j) of a convex n-gon with cyclically ordered labels like Figure 4.1 (left). There are of course $n(n-3)/2$ of these variables. Furthermore, we impose the *non-crossing identity*

$$u_{i,j} = 1 - \prod_{(k,l)\in(i,j)^c} u_{k,l} \tag{5.3}$$

for each diagonal (i,j), where $(i,j)^c$ denotes the set of all diagonals that cross (i,j). Only $(n-2)(n-3)/2$ of these $n(n-3)/2$ constraints are independent, so the space is of dimension $(n-3)$. See [52] for a generalization of these identities.

Let us consider some examples. For n=4 we have two variables with one constraint

$$u_{1,3} = 1 - u_{2,4} \tag{5.4}$$

For n=5 we have five variables satisfying the constraint

$$u_{1,3} = 1 - u_{2,4}\, u_{2,5}\,, \tag{5.5}$$

and four others related by cyclic shift; but only three constraints are independent, thus giving a 2-dimensional surface shown in Figure 5.2. For n=6, there are two types of constraints corresponding to two types of diagonals of the hexagon. Here we present the constraints for the diagonals $(1,3)$ and $(1,4)$, and the rest are related via cyclic shift.

$$u_{1,3} = 1 - u_{2,4}\ u_{2,5}\ u_{2,6} \qquad u_{1,4} = 1 - u_{2,5}\ u_{2,6}\ u_{3,5}\ u_{3,6}\,, \tag{5.6}$$

This gives $6 + 3 = 9$ constraints, but only six are independent.

The u-space provides an explicit compactification of the positive moduli space. To see this, we begin by constructing a map from the positive moduli space $\mathcal{M}_{0,n}^{+}$ to the interior of u-space via the following cross ratio formula:

$$u_{i,j} = \frac{(\sigma_i - \sigma_{j-1})(\sigma_{i-1} - \sigma_j)}{(\sigma_i - \sigma_j)(\sigma_{i-1} - \sigma_{j-1})} = \frac{(i\ j{-}1)(i{-}1\ j)}{(i\ j)(i{-}1\ j{-}1)} \tag{5.7}$$

which has already been studied extensively in the original dual resonance model (*c.f.* [53] and more recently in [54]). The map provides a diffeomorphism between the positive moduli space and the u-space interior. Taking the closure in u-space thereby provides the required compactification. Henceforth we denote u-space by $\overline{\mathcal{M}}_{0,n}^{+}$.

We now argue that the compactification $\overline{\mathcal{M}}_{0,n}^{+}$ is an associahedron. We begin by showing that there are exactly $n(n{-}3)/2$ codimension 1 boundaries given individually by $u_{i,j} = 0$ for every diagonal (i,j). We then show that every codimension 1 boundary "factors" like (4.19), from which the desired conclusion follows.

Clearly the boundaries of the space are given by $u_{i,j} = 0$ or 1. However, if $u_{i,j} = 1$ then by the non-crossing identity (5.3) we must have $u_{k,l} = 0$ for at least one diagonal $(k,l) \in (i,j)^c$. It therefore suffices to only consider $u_{i,j} = 0$. We claim that every boundary $u_{i,j} = 0$ "factors" geometrically into a product of lower-dimensional

worldsheets:

$$\partial_{(i,j)}\overline{\mathcal{M}}^{+}_{0,n} \cong \overline{\mathcal{M}}^{+}_{0,n_L} \times \overline{\mathcal{M}}^{+}_{0,n_R} \tag{5.8}$$

where

$$\overline{\mathcal{M}}^{+}_{0,n_L} := \overline{\mathcal{M}}^{+}_{0,n_L}(i,\ldots,j{-}1,I) \tag{5.9}$$

$$\overline{\mathcal{M}}^{+}_{0,n_R} := \overline{\mathcal{M}}^{+}_{0,n_R}(1,\ldots,i{-}1,I,j,\ldots,n) \tag{5.10}$$

with I denoting an auxiliary label and $(n_L, n_R) = (j{-}i{+}1, n{+}i{-}j{+}1)$. Similar to the geometric factorization of the kinematic polytope discussed in Section 4.3.1, we visualize the geometric factorization of the compactification as the diagonal (i,j) that subdivides the convex n-gon into a "left" subpolygon and a "right" subpolygon as shown in Figure 4.11. Furthermore, note that (5.8) immediately implies that the boundary is of dimension $(n-4)$ and hence codimension 1. From the σ-space point of view, the limit $u_{i,j} = 0$ corresponds to the usual degeneration where the σ_a for all $a = i,\ldots,j{-}1$ pinch together on the left subpolygon, and similarly the σ_a for all $a = j,\ldots,n,1,\ldots,i{-}1$ pinch together on the right subpolygon.

To derive (5.8), let L, R denote the set of diagonals of the left and right subpolygons, respectively. Then in the limit $u_{i,j} = 0$, we get $u_{k,l} = 1$ for every diagonal (k,l) that crosses (i,j). It follows that the constraints (5.3) split into two independent sets of constraints, one for each subpolygon:

$$\text{Left:} \qquad \left\{ u_{k,l} = 1 - \prod_{(p,q)\in(k,l)^c\cap L} u_{p,q} \;\middle|\; (k,l) \in L \right\} \tag{5.11}$$

$$\text{Right:} \qquad \left\{ u_{k,l} = 1 - \prod_{(p,q)\in(k,l)^c\cap R} u_{p,q} \;\middle|\; (k,l) \in R \right\} \tag{5.12}$$

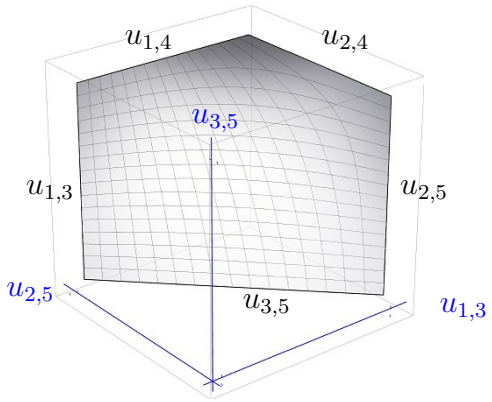

Figure 5.2: The worldsheet associahedron for n=5 presented in a coordinate chart where all boundaries are manifest. We caution the reader that some coordinate charts do not make manifest all the boundaries.

These provide precisely the constraints for the left and right factors $\overline{\mathcal{M}}^+_{0,n_L}$ and $\overline{\mathcal{M}}^+_{0,n_R}$, thereby implying (5.8). We conclude therefore that the compactified space $\overline{\mathcal{M}}^+_{0,n}$ is an associahedron. As an example, the n=5 worldsheet associahedron is shown in Figure 5.2.

We now compute the canonical form. Since the worldsheet associahedron has the same boundary structure as the kinematic associahedron, therefore its canonical form should take on a similar form as (4.31). Indeed, let us work in the standard gauge $(\sigma_1, \sigma_{n-1}, \sigma_n) = (0, 1, \infty)$ where the moduli space interior is the simplex $0 < \sigma_2 < \sigma_3 < \cdots < \sigma_{n-2} < 1$. We now blow up the boundaries of the simplex to form an associahedron polytope, in the manner discussed earlier. We assume that our blowup is small of order ϵ, with boundaries given by $B_{i,j}(\epsilon; \sigma) \geq 0$ corresponding to the diagonals (i, j) of the n-gon. The exact expression for $B_{i,j}$ is not unique; however, since the boundary (i, j) corresponds to the limit where $\sigma_i, \sigma_{i+1}, \ldots, \sigma_{j-1}$ pinch, it is thereby necessary that $\lim_{\epsilon \to 0} B_{i,j}(\epsilon, \sigma) = \sigma_{i,j-1}$. Now, we compute the canonical form by substituting $X_{i,j} \to B_{i,j}$ into (4.31), then removing the blowup by taking

the limit $\epsilon \to 0$:

$$\Omega\left(\overline{\mathcal{M}}_{0,n}^{+}\right) = \lim_{\epsilon\to 0} \sum_{\text{planar } g} \text{sign}(g) \bigwedge_{a=1}^{n-3} d\log B_{i_a,j_a}(\epsilon;\sigma) \tag{5.13}$$

$$= \sum_{\text{planar } g} \text{sign}(g) \bigwedge_{a=1}^{n-3} d\log \sigma_{i_a,j_a-1} \tag{5.14}$$

where we sum over all planar cubic graphs g, and for every g the (i_a, j_a) for $a = 1, \ldots, n-3$ are the diagonals of the corresponding triangulation. The $\text{sign}(g)$ is defined by the sign flip rule (4.14) as before. We caution the reader that the naive substitution $X_{i,j} \to u_{i,j}$ is incorrect; since the $u_{i,j}$ variables are constrained by non-linear equations (i.e. the non-crossing identities (5.3)), hence there is no known dual polytope with boundaries $u_{i,j} \geq 0$ whose volume takes the form (4.31).

Furthermore, since the $\epsilon \to 0$ limit reduces to a simplex, the canonical form must also reduce to the form for that simplex, which we recognize as the Parke-Taylor form (5.2) given below. The particular way in which the simplex is blown up does not matter, since they all reduce to the same geometry in this limit.

$$\Omega\left(\overline{\mathcal{M}}_{0,n}^{+}\right) = -\frac{d^{n-3}\sigma}{\sigma_2(\sigma_2-\sigma_3)\cdots(\sigma_{n-2}-1)} \tag{5.15}$$

While (5.13) and (5.15) look very different, their equivalence is guaranteed by the geometric argument provided. In fact, the former can be thought of as a triangulation (with overlapping pieces that "cancel") of the latter.

Finally, we present (5.13) in a SL(2) invariant way:

$$\Omega\left(\overline{\mathcal{M}}_{0,n}^{+}\right) = \sum_{\text{planar } g} \text{sign}(g) \bigwedge_{a=1}^{n-3} d\log\left(\frac{\sigma_{i_a,j_a-1}\ \sigma_{1,n}\ \sigma_{n-1,n}}{\sigma_{1,n-1}\ \sigma_{i_a,n}\ \sigma_{j_a-1,n}}\right) \tag{5.16}$$

5.2 Scattering equations as a diffeomorphism between associahedra

We have now seen two associahedra: the kinematic associahedron $\mathcal{A}_n$ in kinematic space $\mathcal{K}_n$ and the worldsheet associahedron $\overline{\mathcal{M}}^+_{0,n}$ in moduli space $\mathcal{M}_{0,n}$. Furthermore, recall that the scattering equations [11] relate points in moduli space to points in kinematic space. It is therefore natural to expect that the same equations should relate the two associahedra. We begin by reinterpreting the scattering equations as a map from moduli space to kinematic space, giving the *scattering equation map*. We then make the striking observation that the scattering equation map acts as a *diffeomorphim* between the two associahedra.

$$\mathcal{M}_{0,n} \xrightarrow[\text{as a map}]{\text{scattering equations}} \mathcal{K}_n \tag{5.17}$$

$$\overline{\mathcal{M}}^+_{0,n} \xrightarrow[\text{as a diffeomorphism}]{\text{scattering equations}} \mathcal{A}_n \tag{5.18}$$

This has immediate consequences for amplitudes, including a novel derivation of the CHY formula for bi-adjoint scalars and much more. But before jumping ahead, let us establish the map.

Recall that the scattering equations [11] read

$$E_i := \sum_{j=1;j\neq i}^{n} \frac{s_{ij}}{\sigma_{i,j}} = 0 \quad \text{for } i = 1, \ldots, n \tag{5.19}$$

where $\sigma_{i,j} := \sigma_i - \sigma_j$, and only $(n-3)$ equations are independent due to SL(2) redundancy. It is convenient to first send $\sigma_n \to \infty$ so that by adding all $E_1, E_2, ..., E_c$ together we find

$$s_{c,c+1} = -\sum_{\substack{1\leq i\leq c \\ c+1\leq j\leq n-1 \\ (i,j)\neq(c,c+1)}} \sigma_{c,c+1}\frac{s_{ij}}{\sigma_{i,j}}\,. \tag{5.20}$$

for the range $1 \leq c \leq n-2$. Combining variables $s_{c,c+1}$ that have adjacent indices and variables s_{ij} that have non-adjacent indices (i.e. $j-i > 1$) gives us a formula for every planar variable $X_{a,b}$:

$$X_{a,b} = -\sum_{\substack{1\leq i<a\\ a<j<b}} \sigma_{a,j}\,\frac{s_{ij}}{\sigma_{i,j}} - \sum_{\substack{a\leq i<b\\ b\leq j<n}} \sigma_{i,b-1}\,\frac{s_{ij}}{\sigma_{i,j}} - \sum_{\substack{1\leq i<a\\ b\leq j<n}} \sigma_{a,b-1}\,\frac{s_{ij}}{\sigma_{i,j}}\,, \tag{5.21}$$

whereby every index pair i, j on the right hand side is non-adjacent with $i, j \neq n$. This provides a remarkable rewriting of the scattering equations because every Mandelstam variable on the right is a constant $s_{ij} = -c_{ij}$. Substituting the constants and recovering the SL(2) invariance by rewriting the σ variables as cross-ratios of Plücker coordinates gives

$$X_{a,b} = \sum_{\substack{1\leq i<a\\ a<j<b}} \frac{(a\,j)(i\,n)}{(i\,j)(a\,n)}\,c_{ij} + \sum_{\substack{a\leq i<b-1\\ b\leq j<n}} \frac{(j\,n)(i\,b{-}1)}{(i\,j)(b{-}1\,n)}\,c_{ij} + \sum_{\substack{1\leq i<a\\ b\leq j<n}} \frac{(i\,n)(j\,n)(a\,b{-}1)}{(i\,j)(a\,n)(b{-}1\,n)}\,c_{ij} \tag{5.22}$$

Since the right hand side consists only of constants and σ variables, this provides a map $\sigma \to X$ from moduli space to kinematic space (more specifically to the subspace H_n when the σ_i variables are real), thus providing the *scattering equation map* that we are after.

Let us look at the map more closely. First and foremost, every point $X_{a,b}$ on the image is manifestly positive when the σ_i variables are ordered since the constants $c_{ij} > 0$ are positive. It follows that (5.22) maps the worldsheet associahedron $\overline{\mathcal{M}}^{+}_{0,n}$ into the kinematic associahedron $\mathcal{A}_n$.

Moreover, every boundary of the worldsheet associahedron (of any codimension) is mapped to the corresponding boundary of the kinematic associahedron. Indeed, consider a codimension 1 boundary $u_{a,b} \to 0$. In this limit, the variables $\sigma_a, \ldots, \sigma_{b-1}$ all pinch to a point so that $\sigma_{i,j} \to 0$ for all $a \leq i < j < b$. By direct inspection of (5.22) we find that $X_{a,b} \to 0$ in this limit. It follows therefore that every boundary

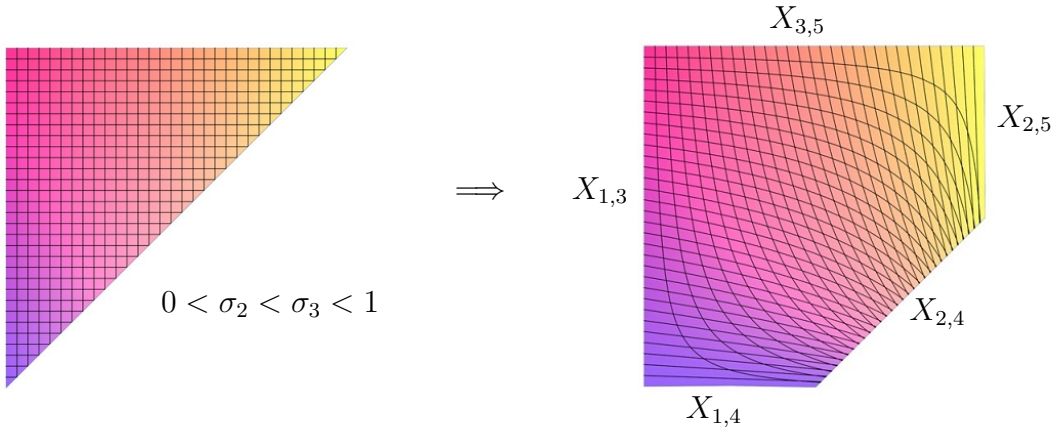

Figure 5.3: Graphical evidence demonstrating that for n=5, the interior of the worldsheet associahedron is mapped diffeomorphically to the interior of the kinematic associahedron by the scattering equation map. Each contour line denotes a locus where one of σ_2, σ_3 is constant.

$u_{a,b} = 0$ of the worldsheet associahedron is mapped to the corresponding boundary $X_{a,b} = 0$ of the kinematic associahedron. An extended statement holds for boundaries of all codimensions. We say therefore that the scattering equation map preserves the associahedron boundary structure. Furthermore, this suggests that every point on the kinematic associahedron is reached by the map.

Finally, we make a numerical observation. For every point on the interior of the kinematic polytope, exactly one of the $(n-3)!$ solutions of the scattering equations lies on the interior of the worldsheet associahedron. In other words, provided that planar propagators $s_{a\cdots b-1} > 0$ are positive and the non-adjacent constants $s_{ij} < 0$ are negative, then there exists exactly one real ordered solution $\sigma_1 < \cdots < \sigma_n$. We have checked this thoroughly up to n=10 for a substantial amount of data. Note that our kinematic inequalities are different from the ones introduced in [55] where all solutions are *real*.

We conjecture therefore that the scattering equation map is a *diffeomorphism* from the worldsheet associahedron to the kinematic associahedron. For n=5, the scattering

equation map is given by

$$X_{1,3} = \frac{\sigma_2}{\sigma_3}(c_{13} + \sigma_3 c_{14}) \tag{5.23}$$

$$X_{1,4} = \frac{1}{1-\sigma_2}((\sigma_3 - \sigma_2)c_{24} + \sigma_3(1-\sigma_2)c_{14}) \tag{5.24}$$

In Figure 5.3, we present graphical evidence showing that these equations provide a diffeomorphism.

Diffeomorphisms play an important role in the theory of positive geometries and canonical forms. Recall from Heuristic 2.3.1 that provided a diffeomorphism $\phi : \mathcal{A} \to \mathcal{B}$ between two positive geometries, the map pushes the canonical form of one to the other:

$$\mathcal{A} \xrightarrow{\text{diffeomorphism } \phi} \mathcal{B} \tag{5.25}$$

$$\Omega(\mathcal{A}) \xrightarrow{\text{pushforward by } \phi} \Omega(\mathcal{B}) \tag{5.26}$$

Applying this to our scenario, we find that the scattering equation map pushes the canonical form of the worldsheet associahedron to that of the kinematic associahedron.

$$\overline{\mathcal{M}}^+_{0,n} \xrightarrow[\text{as diffeomorphism}]{\text{scattering equations}} \mathcal{A}_n \tag{5.27}$$

$$\Omega\left(\overline{\mathcal{M}}^+_{0,n}\right) \xrightarrow[\text{scattering equations}]{\text{pushforward by}} \Omega(\mathcal{A}_n) \tag{5.28}$$

But (5.15) and (4.36) imply

$$\omega_n^{\text{WS}} \xrightarrow[\text{scattering equations}]{\text{pushforward by}} m_n d^{n-3}X \tag{5.29}$$

It follows that the amplitude m_n can be obtained by pushing forward the Parke-Taylor form via the scattering equations. Recalling the definition of the pushforward as a sum over roots, we obtain the amplitude form by taking the Parke-Taylor form,

substituting all roots of the scattering equations and summing over all roots.

$$\sum_{\text{sol. } \sigma} \omega_n^{\text{WS}} = m_n d^{n-3} X \tag{5.30}$$

For a general ordering pair α, β, this generalizes to the following statement

$$\sum_{\text{sol. } \sigma} \omega_n^{\text{WS}}[\alpha] = m[\alpha|\beta] d^{n-3} X \tag{5.31}$$

where $\omega_n^{\text{WS}}[\alpha]$ denotes the Parke-Taylor form for the ordering α, and the scattering equations are reinterpreted as a map $\mathcal{M}_{0,n} \to \mathcal{K}_n$ that restricts to a diffeomorphism $\overline{\mathcal{M}}_{0,n}^{+}[\alpha] \to \mathcal{A}[\alpha|\beta]$, where $\overline{\mathcal{M}}_{0,n}^{+}[\alpha]$ denotes the (compactified) α-ordered part of the open string moduli space.

We caution the reader that the pullback of the right hand side in (5.30) does *not* produce the left hand side. Indeed, pulling back a canonical form does not necessarily produce another canonical form. For instance, pulling back $d\log y$ via $y = x^2$ gives $2d\log x$, which does not even have unit residue.

We observe that (5.31) is reminiscent of the CHY formula for the bi-adjoint scalar. Indeed they are equivalent, as we now show. We begin by rewriting our pushforward in delta function form:

$$m_n = \int \omega_n^{\text{WS}}[\sigma] \left[\prod_{a=1}^{n-3} \delta(X_{i_a,j_a} - \phi_a(\sigma)) \right] \tag{5.32}$$

where the variables X_{i_a,j_a} form a planar basis (corresponding to the diagonals of a triangulation), and $X_{i_a,j_a} = \phi_a(\sigma)$ is the scattering equation map (5.22). It is necessary that the basis variables appear with unit Jacobian in the delta functions, because m_n is obtained from $\Omega(\mathcal{A}_n)$ by stripping away $\prod_{a=1}^{n-3} ds_{I_a}$. In other words, the delta functions must be normalized in the basis in which m_n is obtained from $\Omega(\mathcal{A}_n)$.

Now we claim that (5.32) is equivalent to the corresponding CHY formula:

$$m_{n,\text{CHY}} := \int \omega_n^{\text{WS}}[\sigma] \left[\frac{1}{\prod_{a=1}^{n}(\sigma_a - \sigma_{a+1})} \prod_a{}' \delta \left(\sum_{b \neq a} \frac{s_{ab}}{\sigma_a - \sigma_b} \right) \right] \tag{5.33}$$

Here we have deliberately isolated the Parke-Taylor form and grouped the other Parke-Taylor factor with the delta function. With a little bit of work, it can be shown that the square bracket expressions in (5.33) and (5.32) are equivalent. Thus, the second Parke-Taylor factor acts as a Jacobian factor for pushing forward onto the subspace H_n. More generally, a delta function dressed with an α-ordered Parke-Taylor factor provides the pushforward onto the subspace $H[\alpha]$ defined in (6.44) or equivalently $H[\alpha|\alpha]$ defined in Section 4.2.4. It follows that

$$m_n = m_{n,\text{CHY}} \tag{5.34}$$

We have thus provided a novel derivation of the CHY formula for the bi-adjoint scalar. This derivation is purely geometric, and does not rely on the usual arguments involving factorization.

Finally, we make a brief comment about all ordering pairs. In Section 4.2.4, we obtained the partial amplitude $m[\alpha|\beta]$ from the pullback of the planar scattering form $\Omega^{(n-3)}[\alpha]$ to the subspace $H[\alpha|\beta]$. However, around (6.48) we argue that the same amplitude can also be obtained by pulling back the same form to a different subspace $H[\beta]$. Hence, the amplitude can be expressed as the integral of the α-ordered Parke-Taylor form over the delta function dressed with β-ordered Parke-Taylor factor, which is precisely the CHY formula. It follows that

$$m[\alpha|\beta] = m_{\text{CHY}}[\alpha|\beta] \tag{5.35}$$

for every ordering pair.

Chapter 6

Color and kinematics

We explain a new manifestation of the color-kinematics duality. We begin by considering generalized scattering forms that apply to all colored/flavored amplitudes, including gluons and pions. We find that projectivity of the form leads to many further consequences in this generalized context. In particular, we find that they lead to the well-known kinematic Jacobi relations, as well as the BCJ relations. In addition, we find a general duality between colored/flavored amplitudes and differential forms on kinematic space, which relies on the curious observation that differential forms satisfy a set of "Jacobi relations" analogous to the Jacobi relations satisfied by structure constants.

6.1 The big kinematic space

We begin by constructing the *big kinematic space* $\mathcal{K}_n^*$, which is an extended version of the usual kinematic space. The importance of the big kinematic space will become clear when we introduce generalized scattering forms. Consider a set of abstract variables S_I indexed by all subsets $I \subset \{1, 2, \ldots, n\}$ subject to two conditions,

- $S_I = S_{\bar{I}}$ where $\bar{I}$ is the complement of I

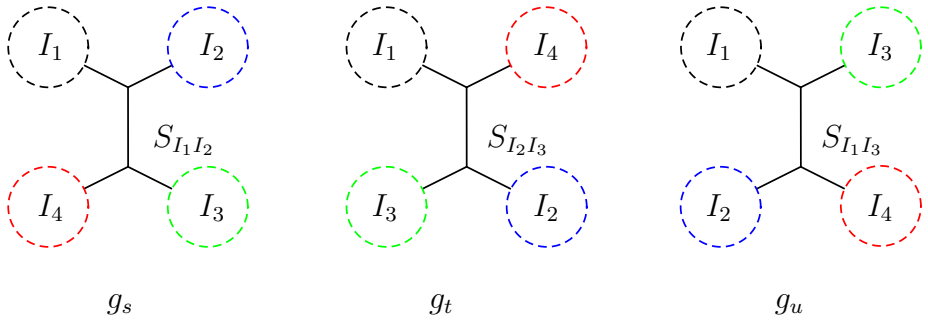

Figure 6.1: A four set partition $I_1 \sqcup I_2 \sqcup I_3 \sqcup I_4$ of the external labels and the three corresponding channels. The three graphs g_s, g_t, g_u are identical except for a 4-point subgraph.

- $S_I = 0$ for $|I| = 0, 1, n-1, n$

For example, $\mathcal{K}^*_{n=4}$ is a 3-dimensional space spanned by the variables

$$\{S_{12} = S_{34}, \quad S_{13} = S_{24}, \quad S_{14} = S_{23}\} \tag{6.1}$$

while $\mathcal{K}^*_{n=5}$ is a 10-dimensional space spanned by S_{ij}'s, and $\mathcal{K}^*_{n=6}$ is a 25-dimensional space spanned by 15 S_{ij}'s and 10 S_{ijk}'s. The dimension for general n is given by

$$\dim \mathcal{K}^*_n = 2^{n-1} - n - 1 \tag{6.2}$$

which for $n > 3$ is higher than the dimension $n(n-3)/2$ of the small kinematic space $\mathcal{K}_n$. Nonetheless, the latter can be recovered by imposing a *7-term identity* which we now describe.

For every partition of n particles into four subsets

$$I_1 \sqcup I_2 \sqcup I_3 \sqcup I_4 = \{1, 2, \cdots, n\} \tag{6.3}$$

we impose the following identity consisting of 7 terms (See Figure 6.1):

$$S_{I_1 I_2} + S_{I_2 I_3} + S_{I_1 I_3} = S_{I_1} + S_{I_2} + S_{I_3} + S_{I_4} \tag{6.4}$$

where $S_{IJ} := S_{I \cup J}$. We can visualize this identity as a triplet of cubic graphs which are identical except for a four point subgraph, with the propagators on the left corresponding to the three channels of the subgraph, and the propagators on the right corresponding to the four legs of the subgraph. See Figure 6.1 for an illustration. Moreover, recall that while (6.4) is usually presented as a derived property of 4-point kinematics, here we take a different point of view whereby the small kinematic space $\mathcal{K}_n$ is constructed by requiring (6.4) as an "axiomatic identity" from which the usual kinematic identities follow:

$$S_I = \sum_{i<j;\, i,j \in I} S_{ij} \quad \text{for all } I; \qquad \sum_{j=1; j \neq i}^{n} S_{ij} = 0 \quad \text{for all } i \tag{6.5}$$

We derive the first identity by induction on $m = |I|$, which is trivial for $m \leq 2$. Now assume that the assertion has been proven for $m < k$, and $|I| = k$ for some index set I. We first isolate two elements $a, b \in I$ and define $K := I \backslash \{a, b\}$. Applying (6.4) to the partition $\bar{I} \sqcup K \sqcup \{a\} \sqcup \{b\}$ gives

$$S_{ab} + S_{aK} + S_{bK} = S_K + S_{\bar{I}} \tag{6.6}$$

where we used $S_a = S_b = 0$. It follows that

$$S_I = S_{\bar{I}} = S_{ab} + S_{aK} + S_{bK} - S_K = \sum_{i<j;\, i,j \in I} S_{ij} \tag{6.7}$$

where for the last equality we applied the induction hypothesis to each of the four terms on the left hand side. This completes the derivation.

For the second identity in (6.5), we apply the first identity to $\bar{I}$ for $I := \{i\}$ which gives

$$\sum_{a<b;\ a,b\neq i} S_{ab} = S_{\bar{I}} = S_I = 0 \tag{6.8}$$

Applying the first identity again to the full index set gives

$$\sum_{a<b} S_{ab} = 0 \tag{6.9}$$

Subtracting (6.8) from (6.9) gives the desired result.

It follows therefore that the 7-term identity reduces the big kinematic space $\mathcal{K}_n^*$ to the small kinematic space $\mathcal{K}_n$, in which case the abstract variables can be identified with Mandelstam variables:

$$S_I = s_I \quad \text{for each } I \tag{6.10}$$

For some purposes, we find it useful to study geometries and differential forms directly in the big kinematic space prior to imposing the 7-term identity.

6.2 Scattering forms and projectivity

We introduce *scattering forms* as a generalization of the planar scattering forms from Section 4.1.3 to *all* cubic graphs. We then explore the implications of *projectivity* in this general framework and discover *Jacobi identities* for kinematic numerators as a direct consequence.

Before defining the scattering forms, we establish the properties of cubic graphs from the point of view of the big space. Recall that a cubic graph g consists of $(n-3)$ Mandelstam variables s_{I_a} corresponding to the propagators of the graph. Then the

corresponding big S_{I_a} variables form a mutually compatible set, whereby any pair of variables S_I and S_J are said to be *compatible* if the index sets are either disjoint $I \cap J = \emptyset$ or one is contained in the other. Furthermore, we define an *ordered cubic graph* as a pair $(g|\alpha)$ consisting of a cubic graph g and an ordering α for the external legs, assuming that g is compatible with α.

For every ordered cubic graph $(g|\alpha)$ with propagators S_{I_a}, we define a $d\log$ form

$$\Omega^{(n-3)}(g|\alpha) := \mathrm{sign}(g|\alpha) \bigwedge_{a=1}^{n-3} d\log S_{I_a} \tag{6.11}$$

where $\mathrm{sign}(g|\alpha_g) \in \{\pm 1\}$ depends not only on the ordered graph but also on the ordering of the propagators so that swapping two propagators changes the sign. The antisymmetry of the sign is of course compensated by the antisymmetry of the wedge product. Furthermore, we impose relations between the sign of different ordered cubic graphs via a *sign flip rule*. Recall that two graphs g, g' with the same ordering α are related by a *mutation* if one can be obtained from the other by an exchange of channel in a 4-point subgraph like Figure 4.2. We assume that planarity in the ordering α is preserved by the mutation, so that only one mutation is possible in every 4-point subgraph of any cubic graph. Furthermore, we say that two orderings α, α' for the same graph g are related by a *vertex flip* if $(g|\alpha')$ can be obtained from $(g|\alpha)$ by exchanging two legs of a vertex (See Figure 6.2). Finally, we define the sign flip rule by requiring a sign change for every mutation and every vertex flip.

$$\text{Mutation:} \qquad \mathrm{sign}(g|\alpha) = -\mathrm{sign}(g'|\alpha) \tag{6.12}$$

$$\text{Vertex flip:} \qquad \mathrm{sign}(g|\alpha) = -\mathrm{sign}(g|\alpha') \tag{6.13}$$

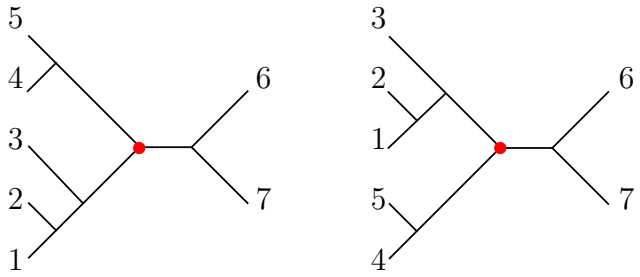

Figure 6.2: A vertex flip at the red vertex

For a generic pair of ordered graphs $(g|\alpha), (g|\beta)$ related by a sequence of sign flips, let $\text{flip}(\alpha, \beta)$ denote the number of flips involved (modulo 2) so that

$$\text{sign}(g|\alpha) = (-1)^{\text{flip}(\alpha,\beta)}\text{sign}(g|\beta) \tag{6.14}$$

If we restrict α to the standard ordering, then the vertex flip is irrelevant and we reduce to the sign flip rule for the planar scattering form (4.14). More generally, we require the sign rule under vertex flip for any quantity $Q(g|\alpha)$ labeled by ordered cubic graphs. It follows that a product like $Q(g|\alpha)Q'(g|\alpha)$ of two such quantities is independent of the ordering and can therefore be written in a condensed form $Q(g)Q'(g)$.

We now define the *scattering form* for n particles as a rank $(n-3)$ form on $\mathcal{K}_n^*$ of the following form

$$\Omega^{(n-3)}[N] = \sum_{\text{cubic } g} N(g|\alpha_g)\Omega^{(n-3)}(g|\alpha_g) \tag{6.15}$$

where we sum over all cubic graphs g, and to every cubic graph we assign an ordering α_g and a kinematic numerator $N(g|\alpha_g)$ which we assume to be independent of big S variables. However, since every term is independent of the ordering α_g, we can

condense our notation as follows:

$$\Omega^{(n-3)}[N] = \sum_{\text{cubic } g} N(g)\Omega^{(n-3)}(g) \tag{6.16}$$

Furthermore, we consider *projective scattering forms*, which are scattering forms that are invariant under *local* GL(1) *transformations* $S_I \to \Lambda(S)S_I$. This imposes constraints on the kinematic numerators which we now explain. Consider a triplet of cubic graphs g_s, g_t, g_u like Figure 6.1. Under the transformation, the Λ-dependence of the scattering form becomes

$$\left(N(g_s|I_1I_2I_3I_4)+N(g_t|I_1I_4I_2I_3)+N(g_u|I_1I_3I_4I_2)\right) d\log\Lambda \wedge \left(\bigwedge_{b=1}^{n-4} d\log S_{J_b}\right) + \cdots \tag{6.17}$$

where the S_{J_b} denote the $(n-4)$ propagators shared by the triplet, and the $\cdots$ denotes similar expressions for all other triplets. Now, since the non-vanishing propagators are independent in the big kinematic space, therefore the Λ-dependence vanishes precisely if the coefficient of every triplet vanishes. This gives us $(2n-5)!!(n-3)/3$ identities (not all independent), one for each triplet, of the following form:

$$N(g_s|I_1I_2I_3I_4)+N(g_t|I_1I_4I_2I_3)+N(g_u|I_1I_3I_4I_2) = 0 \tag{6.18}$$

Note that we have explicitly written out the ordering for each graph which is important for making sure that the three terms add. We refer to (6.18) as a *Jacobi identity* due to its similarity to the Jacobi identity for structure constants of Lie groups. It follows that the scattering form is projective if and only if its numerators satisfy Jacobi identities.

We make a few comments before providing examples. Note that (6.18) is derived without imposing the 7-term identity (6.4). This is crucial, as imposing the identity would reduce us to the small kinematic space $\mathcal{K}_n$ where the set of all propagators no

longer forms a basis (although the set of all *planar* propagators does), in which case we cannot require the coefficient of every triplet in (6.17) to vanish. Furthermore, the GL(1) transformation does not act on the kinematic numerators, which may depend on usual kinematic quantities like $(p_i \cdot p_j)$, $(\epsilon_i \cdot p_j)$ and $(\epsilon_i \cdot \epsilon_j)$ that we assume to be independent of big S variables. Nonetheless, we can define a similar local GL(1) transformation acting directly on the small space via $p_i \to \sqrt{\Lambda(p)}\ p_i$. It is straightforward then to show that GL(1) invariance in the big space directly implies GL(1) *covariance* in the small space, meaning $\Omega[N]^{(n-3)}(s) \to \Lambda^{D/2}\Omega^{(n-3)}[N](s)$ where D is the mass dimension of the numerators.

Let us consider some examples of projective scattering forms. The simplest case is the *α-planar scattering form*

$$\Omega^{(n-3)}_{\phi^3}[\alpha] = \sum_{\alpha\text{-planar } g} \text{sign}(g|\alpha) \bigwedge_{a=1}^{n-3} d\log S_{I_a} \tag{6.19}$$

where we sum over all cubic graphs g compatible with the ordering α. For the standard ordering this reduces to (4.10) in the small kinematic space. In this case, the kinematic numerator $N(g|\alpha)$ vanishes for any graph incompatible with α, and is ± 1 otherwise. More specifically, for every triplet, either none of the three graphs is compatible, or exactly two are. For instance, if the first two of the triplet g_s, g_t, g_u are compatible, then

$$N(g_s|I_1I_2I_3I_4) = \pm 1 \qquad N(g_t|I_1I_4I_2I_3) = \mp 1 \qquad N(g_u|I_1I_3I_4I_2) = 0 \tag{6.20}$$

One way to generalize the planar scattering form without introducing any additional structures such as spin or color is to drop the planarity requirement and consider all projective scattering forms whose numerators are $0, \pm 1$. This provides a large class of scattering forms called $d\log$ scattering forms of which the planar case is only one. Furthermore, as the planar form is closely tied to the geometry of the asso-

ciahedron, many of these other forms are also closely tied to polytopes of their own such as the permutohedron. We provide more details on this topic in the Outlook.

Furthermore, we point out that while planar forms have cyclic symmetry, it is also possible to construct projective forms with *permutation symmetry*. As will be discussed in the next section, such scattering forms can be obtained from *color-dressed amplitudes* that are permutation invariant, via an important connection between differential forms and color. These include scattering forms for theories like Yang-Mills and Non-linear Sigma Model, which we discuss in more detail in Section 6.6.

Last but not least, we state an important property for any projective scattering form. Since planar scattering forms are projective, it follows that every linear combination of them is also projective:

$$\Omega^{(n-3)}[C] = \sum_{\alpha \in S_n/Z_n} C(\alpha)\Omega^{(n-3)}_{\phi^3}[\alpha] \tag{6.21}$$

where the $C(\alpha)$ coefficients are independent of big S variables. Remarkably, the converse is also true, i.e. every projective scattering form is a linear combination of planar scattering forms. A detailed derivation is given in Appendix C of [1], and the upshot is that any projective scattering form can be expanded in terms of a basis of $(n-2)!$ planar forms,

$$\Omega^{(n-3)}[C'] = \sum_{\pi \in S_{n-2}} C'(\pi)\ \Omega^{(n-3)}_{\phi^3}[1, \pi(2), \ldots, \pi(n-1), n]\,. \tag{6.22}$$

6.3 Duality between color and form

We establish the *duality between color factors and differential forms on kinematic space* $\mathcal{K}_n$ by showing that the latter satisfy *Jacobi relations* similar to the usual Jacobi relations for structure constants. This leads naturally to a *duality between color-dressed amplitudes and scattering forms*.

We begin by reviewing the algebra of color. Given an ordered graph we define a color factor $C(g|\alpha)$ by first drawing g as a planar graph whose external legs are ordered clockwise by α (See Figure 6.3 (left)). Then, for each internal and external line we assign an index, and for each vertex v we assign a structure constant $f^{a_v b_v c_v}$, where the indices a_v, b_v, c_v correspond to the three adjacent lines in clockwise order. Finally, we obtain the color factor by multiplying the structure constants and contracting repeated indices (which occur along internal lines). Hence,

$$C(g|\alpha) = \prod_v f^{a_v b_v c_v} \tag{6.23}$$

where index contraction is implicitly assumed. The antisymmetry of the structure constants implies the vertex flip sign rule (6.24) while the usual Jacobi identities for the structure constants imply Jacobi identities for the color factors (6.25) for any triple like Figure 6.1:

$$C(g|\alpha) = (-1)^{\text{flip}(\alpha,\beta)} C(g|\beta) \tag{6.24}$$

$$C(g_s|I_1I_2I_3I_4)+C(g_t|I_1I_4I_2I_3)+C(g_u|I_1I_3I_4I_2) = 0 \tag{6.25}$$

We now argue that a similar set of identities hold for differential forms on the kinematic space $\mathcal{K}_n$. For every ordered graph $(g|\alpha)$ with propagators s_{I_a} for $a = 1, \ldots, n-3$, we define the $(n-3)$-form

$$W(g|\alpha) = \text{sign}(g|\alpha) \bigwedge_{a=1}^{n-3} ds_{I_a} \tag{6.26}$$

We claim that the form satisfies the vertex flip sign rule (6.27) and the Jacobi identity (6.28) in perfect analogy with color factors.

$$W(g|\alpha) = (-1)^{\text{flip}(\alpha|\beta)} W(g|\beta) \tag{6.27}$$

$$W(g_s|I_1I_2I_3I_4)+W(g_t|I_1I_4I_2I_3)+W(g_u|I_1I_3I_4I_2) = 0 \tag{6.28}$$

The former follows from the $\text{sign}(g|\alpha)$ factor in (6.26). The latter follows from applying the 7-term identity (6.4) to the triplet g_s, g_t, g_u from Figure 6.1:

$$ds_{I_1I_2} + ds_{I_2I_3} + ds_{I_1I_3} = ds_{I_1} + ds_{I_2} + ds_{I_3} + ds_{I_4} \tag{6.29}$$

Note that on the left the propagators correspond to the three channels of the triplet, while on the right the propagators correspond to the legs of the 4-point subgraph. Moreover, let s_{J_b} for $b = 1, \ldots, n-4$ denote the propagators shared by the triplet. It follows that

$$(ds_{I_1I_2} + ds_{I_2I_3} + ds_{I_1I_3}) \wedge \bigwedge_{b=1}^{n-4} ds_{J_b} = 0 \tag{6.30}$$

where every term on the right hand side has vanished. In particular, external legs vanish by on-shell condition while internal legs vanish since they already appear in the product $\wedge_{b=1}^{n-4} ds_{J_b}$. The result is precisely the sought after Jacobi relation.

This implies a *duality between color factors and differential forms on kinematic space* $\mathcal{K}_n$:

$$C(g|\alpha) \qquad \leftrightarrow \qquad W(g|\alpha) \tag{6.31}$$

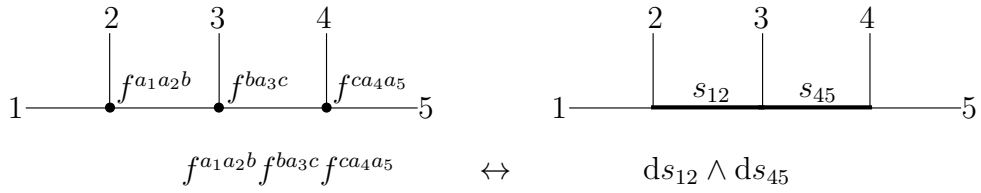

Figure 6.3: An example of the duality between color factors and differential forms

Hence "Color is Kinematics". We emphasize that the 7-term identity is absolutely crucial for this property to hold, thus providing one of the motivations for constructing kinematic space $\mathcal{K}_n$ by the 7-term identity directly.

We provide some examples for low n. For n=4, there are three color factors dual to 1-forms:

$$\begin{aligned} C_s &= f^{a_1a_2b}f^{ba_3a_4} \qquad \leftrightarrow \qquad ds \\ C_t &= f^{a_1a_4b}f^{ba_2a_3} \qquad \leftrightarrow \qquad dt \\ C_u &= f^{a_1a_3b}f^{ba_4a_2} \qquad \leftrightarrow \qquad du \end{aligned}$$

For n=5, color factors are dual to 2-forms. Here we provide one example as illustrated in Figure 6.3.

Furthermore, the duality (6.31) leads naturally to a *duality between color-dressed amplitudes and scattering forms*. Consider a colored-dressed amplitude $\mathbf{M}_n[N]$ with kinematic numerators N:

$$\mathbf{M}_n[N] = \sum_{\text{cubic } g} N(g|\alpha_g)C(g|\alpha_g)\prod_{I\in g}\frac{1}{s_I} \tag{6.32}$$

where we sum over all cubic graphs g, and s_I for $I \in g$ denote the propagators in the graph. We now map this amplitude to a form on kinematic space by applying (6.31) to each color factor individually, giving

$$\Omega^{(n-3)}[N] = \sum_{\text{cubic } g} N(g|\alpha_g)W(g|\alpha_g)\prod_{I\in g}\frac{1}{s_I} \tag{6.33}$$

which we recognize as a scattering form (6.15) with $S_I \to s_I$. Likewise, we can return to the amplitude (6.32) by applying (6.31) backwards. Thus, the duality (6.31) implies the duality (6.34)

$$\mathbf{M}_n[N] \qquad \leftrightarrow \qquad \Omega^{(n-3)}[N] \tag{6.34}$$

We henceforth refer to both dualities as *color-form* duality. Note that for any permutation-invariant color-dressed amplitude, (6.34) gives a scattering form that is nicely permutation invariant. Furthermore, we comment on the role of projectivity. Recall that the numerators $N(g)$ satisfy Jacobi relations provided that the scattering form $\Omega^{(n-3)}[N](s)$ is derived from a projective form in the big kinematic space. The dual amplitude $\mathbf{M}_n[N]$ therefore admits an expansion with $N(g)$ as *BCJ numerators*, first proposed by Bern, Carrasco and Johansson in [14].

For the special case of bi-adjoint scalar with double color group $\mathrm{SU}(N) \times \mathrm{SU}(N)$. The scattering form is obtained by simply choosing $N(g) = C(g)$ for every graph g:

$$\Omega^{(n-3)}_{\phi^3} = \sum_{\text{cubic } g} C(g|\alpha_g)\, \mathrm{sign}(g|\alpha_g) \bigwedge_{a=1}^{n-3} d\log s_{I_a} \tag{6.35}$$

which is both permutation invariant and projective. The corresponding double color-dressed amplitude is given by

$$\mathbf{M}_{\phi^3,n} = \sum_{\text{cubic } g} \frac{C(g)\tilde{C}(g)}{\prod_{I\in g} s_I} \tag{6.36}$$

6.4 Trace decomposition from scattering form

We explore color-form duality further by examining *partial amplitudes* and their interpretation from the differential form point of view. We find that *trace decomposition*

of color-dressed amplitudes are dual to pullbacks of the scattering form to appropriate subspaces of dimension $(n-3)$.

Recall that for the color groups $\mathrm{U}(N)$ and $\mathrm{SU}(N)$, the color factors can be decomposed as traces from which partial amplitudes are obtained. More precisely, we have

$$C(g|\alpha) = \sum_{\beta \in O(g)/Z_n} (-1)^{\mathrm{flip}(\alpha,\beta)} \mathrm{Tr}(\beta(1), \ldots, \beta(n)) \tag{6.37}$$

where $O(g)/Z_n$ denotes all 2^{n-2} orderings compatible with the graph g modulo cyclic transformations. In other words, out of all $(n-1)!$ distinct trace terms, the color factor $C(g|\alpha)$ is expanded precisely in terms of those traces whose ordering is compatible with the graph.

Substituting (6.37) into (6.32) for every graph g gives us the trace decomposition for the amplitude:

$$\mathbf{M}_n[N] = \sum_{\beta \in S_n/Z_n} \mathrm{Tr}(\beta(1), \ldots, \beta(n)) M_n[N;\beta] \tag{6.38}$$

where the *partial amplitude* $M_n[N;\beta]$ is given by a sum over β-planar graphs:

$$M_n[N;\beta] = \sum_{\beta-\text{planar } g} N(g|\beta) \prod_{I \in g} \frac{1}{s_I} \tag{6.39}$$

As an example, for n=4, the color factors decompose as

$$C_s = \mathrm{Tr}(1234) - \mathrm{Tr}(2134) - \mathrm{Tr}(1243) + \mathrm{Tr}(2143) \tag{6.40}$$

$$C_t = \mathrm{Tr}(1423) - \mathrm{Tr}(4123) - \mathrm{Tr}(1432) + \mathrm{Tr}(4132) \tag{6.41}$$

$$C_u = \mathrm{Tr}(1342) - \mathrm{Tr}(3142) - \mathrm{Tr}(1324) + \mathrm{Tr}(3124) \tag{6.42}$$

where both the s and t channels contribute to the ordering $\beta = (1234)$, thus giving

$$M_4[N; 1234] = \frac{N(s|1234)}{s} + \frac{N(t|1234)}{t} \tag{6.43}$$

We now argue that the partial amplitude (6.39) can be obtained by pulling back the scattering form (6.33) to an $(n-3)$-dimensional subspace $H[\beta]$ which we define by imposing $(n-2)(n-3)/2$ independent conditions:

$$H[\beta] := \big\{ s_{\beta(i)\beta(j)} \text{ is constant } \mid 1 \leq i < j-1 \leq n-2 \big\} \tag{6.44}$$

This coincides with the subspace H_n define in (4.21) if β is the standard ordering and the constants $s_{\beta(i)\beta(j)}$ are negative. Now for any graph g compatible with β, we define the pullback

$$dV[\beta] := W(g|\beta)|_{H[\beta]} \tag{6.45}$$

which is independent of the graph as shown around (4.35) for the standard ordering. More generally, for a pair of orderings α, β, we have

$$W(g|\alpha)|_{H[\beta]} = \begin{cases} (-1)^{\text{flips}(\alpha,\beta)} dV[\beta] & \text{if } g \text{ is compatible with } \beta \\ 0 & \text{otherwise} \end{cases} \tag{6.46}$$

where the first line follows immediately from the definition (6.45), while the second line requires a proof for which we provide a sketch. Our strategy is to argue by induction on the number of particles, beginning with n=4 which can be verified directly. For higher n, suppose g is a cubic graph that is compatible with α but not with β, and for simplicity let us assume that β is the standard ordering. We observe that the graph must consist of at least one propagator of the form s_{ij} where $i < j$ and $i, j \neq n$. If i, j are non-adjacent, then $ds_{ij} = 0$ on the pullback, and we are done.

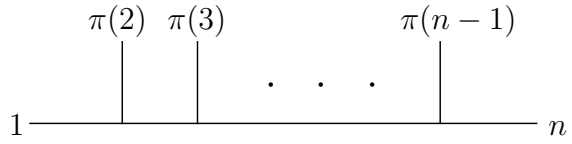

Figure 6.4: Multi-peripheral graph with respect to 1 and n for the ordering $\pi \in S_{n-2}$

Otherwise, the propagator must be $s_{i,i+1}$, giving $W(g) = ds_{i,i+1} \wedge W'(g)$ for some form $W'(g)$. Since factors of $ds_{i,i+1}$ within $W'(g)$ do not contribute, we can therefore think of $W'(g)$ as the form for a reduced graph g' obtained from g by collapsing particles i and i+1 into a single particle. But $W'(g)$ vanishes by induction, thus completing the argument. One subtlety of the last step is that the particle $(i, i+1)$ is generically off-shell with mass-squared given by $s_{i,i+1}$, which appears to violate the induction hypothesis. But since factors of $ds_{i,i+1}$ are effectively zero, the induction still holds. It follows that the pullback of the scattering form $\Omega^{(n-3)}[N]$ to the subspace $H[\beta]$ gives the partial amplitude $M_n[N;\beta]$:

$$\Omega^{(n-3)}[N]|_{H[\beta]} = \left(\sum_{\beta\text{-planar } g} N(g|\beta) \prod_{I \in g} \frac{1}{s_I} \right) dV[\beta] = M_n[N;\beta] dV[\beta] \tag{6.47}$$

Applying this to the planar scattering form $\Omega^{(n-3)}_{\phi^3}[\alpha]$ for the bi-adjoint scalar gives us the double partial amplitude $m[\alpha|\beta]$:

$$\Omega_{\phi^3}[\alpha]|_{H[\beta]} = (-1)^{\text{flip}(\alpha,\beta)} m[\alpha|\beta] dV[\beta] \tag{6.48}$$

This is very different from (4.48) where the same amplitude was obtained by pulling back to a different subspace $H[\alpha|\beta]$. The advantage of the latter is that it provides a geometric interpretation for the amplitude (form) as the canonical form of a positive geometry as in (4.49). The former, however, can be applied to trace decompose any colored tree amplitude.

Finally, we discuss the role of some well-known amplitude relations. Recall the decomposition a la Del Duca, Dixon and Maltoni (DDM) [56] given in (6.49), where g_π

denotes the multi-peripheral graph with respect to 1 and n for the ordering $\pi \in S_{n-2}$ as shown in Figure 6.4.

$$\mathbf{M}_n[N] = \sum_{\pi \in S_{n-2}} C(g_\pi|\pi)\; M_n[N; 1, \pi(2), \ldots, \pi(n-1), n] \tag{6.49}$$

It follows that the color-dressed amplitude can be expanded in terms of only $(n-2)!$ partial amplitudes of the form given in (6.49), which is more efficient than the $(n-1)!$-term expansion of the standard trace decomposition. This also follows from the Kleiss-Kuijf (KK) [57] relations. Furthermore, applying the color-form duality to (6.49) gives an analogous identity for the scattering form

$$\Omega^{(n-3)}[N] = \sum_{\pi \in S_{n-2}} W(g_\pi|\pi)\; M_n[N; 1, \pi(2), \ldots, \pi(n-1), n] \tag{6.50}$$

Note that the expansion is unique both for the color-dressed amplitude and for the form, since the multi-peripheral graphs g_π form a basis. Furthermore, we find that Bern-Carrasco-Johansson (BCJ) relations [14] follow from requiring the scattering form to be projective, as discussed in Section 6.5.

Last but not least, as we have discussed around (6.22), every projective form can be expanded in a basis of $(n-1)!$ planar scattering forms labeled by the orderings $\pi \in S_{n-2}$, and now we can spell out the coefficients. As shown in Appendix C of [1], the coefficient for the π term is nothing but the kinematic numerator $N(g_\pi|\pi)$:

$$\Omega^{(n-3)}[N] = \sum_{\pi \in S_{n-2}} N(g_\pi|\pi)\; \Omega^{(n-3)}_{\phi^3}(1, \pi(2), \cdots, \pi(n-1), n)\,. \tag{6.51}$$

Note that (6.50) and (6.51) are complementary to each other. By the color-form duality, the latter is equivalent to the well-known *dual-basis expansion* [58] of the

color-dressed amplitude:

$$\mathbf{M}_n[N] = \sum_{\pi \in S_{n-2}} N(g_\pi|\pi) M_n^{\phi^3}[1, \pi(2), \ldots, \pi(n-1), n] \tag{6.52}$$

6.5 BCJ relations

We now argue that projectivity of the form implies that the partial amplitudes satisfy kinematic Jacobi relations. A full derivation is given in Appendix C of [1]. Here we simply present an example at $n = 4$, which suffices to demonstrate the structure of the general argument.

We begin by writing down the $n = 4$ scattering form.

$$\begin{aligned}
\Omega^{(1)}[N] &= N_s \frac{ds}{s} + N_t \frac{dt}{t} + N_u \frac{du}{u} && (6.53)\\
&= -\left(-\frac{N_t}{t} + \frac{N_s}{s}\right) dt + \left(\frac{N_u}{u} - \frac{N_s}{s}\right) du && (6.54)\\
&= -M_4[N;1234]dt + M_4[N;1243]du && (6.55)
\end{aligned}$$

where $N_s = N(s|1234)$, $N_t = N(t|1423)$ and $N_u = N(u|1342)$. In the last expression, we simply rewrote the form in terms of partial amplitudes. Under a local GL(1) transformation, the form becomes

$$\Omega^{(1)}[N] \to \Lambda^{D/2}\Omega^{(1)}[N] + \Lambda^{D/2-1}\left(-tM_4[N;1234] + uM_4[N;1243]\right) d\Lambda \tag{6.56}$$

where D is the mass dimension of the numerator factors. The coefficient of $d\Lambda$ vanishes by the requirement of projectivity, from which the BCJ relations follow.

$$tM_4[N;1234] = uM_4[N;1243] \tag{6.57}$$

6.6 Scattering forms for gluons and pions

There are two prime examples of permutation invariant forms on kinematic space: the scattering forms associated with the scattering of gluons in Yang-Mills theory, and of pions in the Non-linear Sigma Model. Let us stress again the central novelty of this claim: there is a differential form on the kinematic space, with coefficients that depend on either momenta and polarization vectors (for Yang-Mills) or Mandelstam variables (for the NLSM), which are fully permutation invariant with no f^{abc} factors anywhere in sight. Nonetheless, the geometrization of color discussed in the previous sections tells us that these forms contain all the information about color-dressed amplitudes.

In fact more is true: the scattering forms for gluons and pions are remarkably rigid objects. For gluons, we find that there is a *unique* differential form with the usual minimal power-counting in momenta that is both gauge invariant and projectively invariant. In particular, the permutation invariance need not be stipulated but is derived. Similarly, the form for pions is the unique form where the requirement of gauge invariance for each leg is replaced with that of the Adler zero in the soft limit. Such "uniqueness theorems" have recently been established in [25], for partial amplitudes from which the uniqueness of the full scattering form follows, provided the crucial extra requirement of projectivity. We also show that these forms have a natural pushforward origin from the worldsheet.

6.6.1 Gauge invariance, Adler zero, and uniqueness of scattering forms for gluons and pions

We establish general conditions under which scattering forms for gluons and (two-derivative-couple, massless) pions are unique. Consider general scattering forms $\Omega^{(n-3)}_{\text{gluon}}$ and $\Omega^{(n-3)}_{\text{pion}}$ for pure gluons and pure pions, respectively. For the gluons, we require the kinematic numerators to consist of contractions in momenta p_i^μ and po-

larizations ϵ_i^μ with each polarization appearing exactly once; moreover we require the expected power counting, which suggests in particular that there can be no more than $(n-2)$ contractions like $(\epsilon_i \cdot p_j)$ in any term; finally, we require gauge invariance (i.e. invariance under the shift $\epsilon_i^\mu \to \epsilon_i^\mu + \alpha p_i^\mu$). For the pions, we require the numerators to be polynomials of Mandelstam variables with the right power counting (i.e. with degree $(n-2)$ in Mandelstams), and the Adler zero condition (*i.e.* vanishing under every soft limit $p_i^\mu \to 0$). Finally, we assume that the forms are projective. We claim that in both cases, the scattering form is unique up to an overall constant.

To derive these two claims, we decompose the scattering forms a la DDM (6.50), and denote the partial amplitudes for the ordering $\pi \in S_{n-2}$ as $M_n^{\text{gluon}}(\pi)$ and $M_n^{\text{pion}}(\pi)$, respectively, which are given by (6.39) with appropriate numerators. Given the linear-independence of the $W(g_\pi|\pi)$ factors, it is clear that each gluon partial amplitude inherits gauge invariance from $\Omega^{(n-3)}_{\text{gluon}}$ while each pion partial amplitude inherits Adler zero from $\Omega^{(n-3)}_{\text{pion}}$. However, the main result of [25] states that any expression satisfying the assumptions of $M_n^{\text{gluon}}(\pi)$ must be the Yang-Mills partial amplitude $M_n^{\text{YM}}(\pi)$ up to a constant, and similarly any expression satisfying the assumptions of $M_n^{\text{pion}}(\pi)$ must be the Non-linear Sigma Model partial amplitude $M_n^{\text{NLSM}}(\pi)$. Hence, there exist constants α_π, α'_π for every π so that

$$M_n^{\text{gluon}}(\pi) = \alpha_\pi M_n^{\text{YM}}(\pi) \qquad\qquad M_n^{\text{pion}}(\pi) = \alpha'_\pi M_n^{\text{NLSM}}(\pi) \tag{6.58}$$

Finally, recall that the partial amplitudes satisfy BCJ relations due to projectivity of the form. It follows that the constants $\alpha := \alpha_\pi$ are identical for all π and likewise for $\alpha' := \alpha'_\pi$ so that the scattering forms are unique up to a constant:

$$\Omega^{(n-3)}_{\text{gluon}} = \alpha\ \Omega^{(n-3)}_{\text{YM}} \qquad\qquad \Omega^{(n-3)}_{\text{pion}} = \alpha'\ \Omega^{(n-3)}_{\text{NLSM}} \tag{6.59}$$

Note that projectivity plays a crucial role without which we could have put arbitrary constants on the right hand side of (6.50), thus leading to a $(n-2)!$-parameter family of solutions. Furthermore, permutation symmetry, unitarity and factorization all emerge as natural consequences of gauge invariance/Adler's zero and projectivity (and some technical constraints on the numerators), even though none was assumed.

For all n, these forms can be obtained from the color-dressed amplitude by directly applying the relation (6.31), thus establishing their existence. Here we give explicit examples for n=4. The NLSM form reads:

$$\Omega^{(1)}_{\rm NLSM} = s\,t\,d\log\left(\frac{s}{t}\right) = t\,d\,s - s\,d\,t \tag{6.60}$$

which also equals $(u\,dt - t\,du) = (s\,du - u\,ds)$ and is thus permutation invariant up to a sign. We can express the YM form as a combination of two ϕ^3 forms:

$$\Omega^{(1)}_{\rm YM} = N_s\,d\log\left(\frac{s}{t}\right) + N_u\,d\log\left(\frac{u}{t}\right) \tag{6.61}$$

where N_s, N_u are BCJ numerators for the s and u channels (see e.g. [59]).

6.6.2 Scattering forms from the worldsheet

We now discuss the worldsheet origin of projective scattering forms with YM and NLSM as the primary examples. First we show that every projective scattering form $\Omega^{(n-3)}[N]$ on $\mathcal{K}_n$ can be obtained as the pushforward of an equivalence class of forms $\omega_n[N]$ on the moduli space $\mathcal{M}_{0,n}$. In particular, the planar scattering form $\Omega^{(n-3)}_{\phi^3}[\alpha]$ is obtained by pushing forward the Parke-Taylor form $\omega^{\rm WS}_n[\alpha]$.

Recall that given any form $\omega_n(\sigma)$ on moduli space, its pushforward is given by substituting and summing over all solutions of the scattering equations

$$\omega(\sigma) \quad \to \quad \sum_{\text{sol. } \sigma} \omega_n(\sigma) \tag{6.62}$$

Note that two forms ω_n and ω'_n are pushed to the same forward if and only if they are equivalent on the support of the scattering equations. We therefore "equate" moduli space forms $\omega_n(\sigma), \omega'_n(\sigma)$ that are equivalent on the support of the scattering equations for which

$$\omega_n(\sigma) \simeq \omega'_n(\sigma) \quad \Longrightarrow \quad \sum_{\text{sol. } \sigma} \omega_n(\sigma) = \sum_{\text{sol. } \sigma} \omega'_n(\sigma) \tag{6.63}$$

We now wish to classify all forms on moduli space that pushforward to projective scattering forms. As discussed in Appendix C of [1], every projective form can be expanded in a basis of $(n-2)!$ planar scattering forms with coefficients given by kinematic numerators for multi-peripheral graphs:

$$\Omega^{(n-3}[N] = \sum_{\pi \in S_{n-2}} N(g_\pi|\pi) \Omega^{(n-3)}_{\phi^3}[1, \pi(2), \ldots, \pi(n-1), n] \tag{6.64}$$

which can obviously be obtained by pushing forward the following form on moduli space:

$$\omega_n[N] = \sum_{\pi \in S_{n-2}} N(g_\pi|\pi) \omega^{\text{WS}}_{\phi^3}(\pi) \tag{6.65}$$

In this way, we can construct a worldsheet form that gives *any* projective form as a linear combination of Parke-Taylor forms with different orderings.

Two important worldsheet forms are the YM and NLSM forms, which are determined by the corresponding CHY half-integrand. More precisely, we claim that

$$\Omega_{\rm YM}^{(n-3)} = \sum_{\text{sol. } \sigma} d\mu_n \ \mathrm{Pf}'\Psi_n \qquad \Omega_{\rm NLSM}^{(n-3)} = \sum_{\text{sol. } \sigma} d\mu_n \ \det' A_n \tag{6.66}$$

where $d\mu_n := d^n\sigma/\text{vol}\ [\mathrm{SL}(2)]$ and $\mathrm{Pf}'\Psi_n$ and $\det' A_n$ are the reduced Pfaffian and determinant (both permutation invariant), respectively, as defined in [12].

$$\mathrm{Pf}'\Psi_n := (-1)^{i+j}\frac{\mathrm{Pf}|\Psi_n|^{i,j}_{i,j}}{\sigma_{i,j}} \quad \det' A_n := \frac{\det|A_n|^{i,j}_{i,j}}{\sigma^2_{i,j}} \quad \text{for any } 1 \le i < j \le n \tag{6.67}$$

Here $\Psi_n(\sigma, \epsilon, p)$ is the $2n \times 2n$ matrix built from polarizations and momenta

$$\Psi_n := \begin{pmatrix} A & -C^T \\ C & B \end{pmatrix} \tag{6.68}$$

where $A_{a,b}, B_{a,b}, C_{a,b}$ are $n \times n$ block matrices given by:

$$\begin{aligned} A_{a,b} &:= \begin{cases} \frac{p_a \cdot p_b}{\sigma_{a,b}} & a \neq b \\ 0 & a = b \end{cases} \qquad B_{a,b} := \begin{cases} \frac{\epsilon_a \cdot \epsilon_b}{\sigma_{a,b}} & a \neq b \\ 0 & a = b \end{cases} \\ C_{a,b} &:= \begin{cases} \frac{\epsilon_a \cdot p_b}{\sigma_{a,b}} & a \neq b \\ -\sum_{c \neq a} C_{a,c} & a = b \end{cases} \end{aligned} \tag{6.69}$$

An important property of these worldsheet forms is that, on the support of scattering equations, $\mathrm{Pf}'\Psi_n$ is manifestly gauge invariant [12] and $\det' A_n$ has the Adler zero [60]:

$$\mathrm{Pf}'\Psi_n(\epsilon_i^\mu \to \epsilon_i^\mu + \alpha p_i^\mu) = \mathrm{Pf}'\Psi_n(\epsilon_i^\mu) \qquad \lim_{p_i^\mu \to 0} \det{}' A_n = 0 \tag{6.70}$$

The uniqueness of the YM and NLSM forms under the conditions discussed above implies that there is a unique equivalence class of worldsheet forms for each theory,

which by (6.70) must be given by $\mathrm{Pf}'\Psi_n$ and $\det' A_n$, respectively. Finally, it is well known that both $\mathrm{Pf}'\Psi_n$ and $\det' A_n$ can be expanded in terms of Parke-Taylor forms with coefficients given by BCJ numerators [13], which reaffirms the result already found in (6.65). For example, the n=4 forms are

$$\begin{aligned} \det{}' A_4 d\mu_4 = \frac{s^2 d\mu_4}{\sigma_{12}^2 \sigma_{34}^2} \quad &\to \quad s\,t\,\left(\omega_{\phi^3}^{\mathrm{WS}}(1234) + \omega_{\phi^3}^{\mathrm{WS}}(1324)\right) = s\,t\,\omega_{\phi^3}^{\mathrm{WS}}(1423) \\ \mathrm{Pf}'\Psi_4 d\mu_4 \quad &\to \quad N_s\;\omega_{\phi^3}^{\mathrm{WS}}(1234) - N_u\;\omega_{\phi^3}^{\mathrm{WS}}(1324) \end{aligned}$$

Chapter 7

The amplituhedron

The amplithedron was first introduced in [17] as an independent, geometric formulation of planar on-shell scattering amplitudes of $\mathcal{N} = 4$ super Yang-Mills. In Section 7.1, we construct the amplituhedron as a positive geometry purely from a mathematical point of view, and postpone discussion of its relation to physics to Section 8. In Section 7.2, we give examples of the amplituhedron in the simplest cases. Throughout subsequent sections, we develop various methods for computing canonical forms of the amplituhedron, including contour integration on Grassmannians, Wilson loop integrals, pushforwards, and volume integrals over dual geometries.

7.1 Properties of the amplituhedron

The amplituhedron is a special case of a more general construction called the Grassmann polytope [33]. Here we give an independent discussion.

Consider a $n \times (k+m)$ matrix Z. We assume that all ordered maximal minors of Z are positive. In other words, we assume that the ordered rows of Z form the vertices of a cyclic polytope. Moreover, we think of Z as a linear map $Z : \mathbb{R}^n \to \mathbb{R}^{k+m}$, which further induces a map that takes every linear subspace in $\mathbb{R}^n$ to a linear subspace of the same dimension in $\mathbb{R}^{k+m}$. We define the *tree amplituhedron* $\mathcal{A}(k, n, m)$ as the

image of the Grassmannian $G_{\geq 0}(k,n)$ under Z,

$$\mathcal{A}(k,n,m) := Z(G_{\geq 0}(k,n)) \tag{7.1}$$

In particular, the tree amplituhedron for $k=1$ is a cyclic polytope in $\mathbb{P}^m(\mathbb{R})$. Furthermore, we define the *L-loop amplituhedron* as the image of the loop Grassmannian $G(k,n;l^L)$ under Z,

$$\mathcal{A}(k,n,m;l^L) := Z(G_{\geq 0}(k,n;l^L)) \tag{7.2}$$

We also refer to this space more simply as the *amplituhedron* whenever the loop level L is understood. In particular, the 0-loop amplituhedron is the tree amplituhedron.

We conjecture that the amplituhedron is a positive geometry. Proving this is a subtle and outstanding problem; in particular, the existence of the canonical form has not been established rigorously. Nonetheless, existence is well motivated by physics, since the form directly determines scattering amplitudes as discussed in Section 8. A more detailed description of the subtleties involved is provided in Section 6.6 of [2].

7.2 The tree amplituhedron for $m = 1, 2$

By now there is a very solid understanding of the tree amplituhedron with $m = 1, 2$ for any k and n, which we now discuss. Here we simply describe without proof some simple triangulations of these amplituhedra, and give their associated canonical forms. We let $\mathcal{A} := \mathcal{A}(k,n,m)$ whenever k, n, m are understood. The results presented here are also provided in [22]. For $m = 1$, see also [61].

In the $m = 1$ amplituhedron, Y_s^I is a k-plane in $(k{+}1)$ dimensions with $s = 1, \ldots, k$ indexing a basis for the plane and $I = 0, \ldots, k$ indexing the vector components in $(k{+}1)$ dimensions. We will triangulate by images of $k-$dimensional cells of $G_{>0}(k,n)$;

in other words for each cell we will look at the image $Y_s^I = \sum_{i=1}^n C_{si}(\alpha_1, \ldots, \alpha_k) Z_i^I$, where $\alpha_1, \ldots, \alpha_k$ are positive $\Delta-$like co-ordinates for that cell. For every collection of k integers $\{i_1, \ldots, i_k\}$ with $1 \leq i_1 < i_2 < \cdots < i_k \leq n-1$, there is a cell where

$$C_{sa}^{\{i_1,\ldots,i_k\}} = \left\{ \begin{array}{cc} 1 & a = i_s \\ \alpha_s & a = i_s + 1 \\ 0 & \text{otherwise} \end{array} \right\} \tag{7.3}$$

with the positive variables $\alpha_s \geq 0$. In other words in this cell we have $Y_s^I = Z_{i_s}^I + \alpha_s Z_{i_s+1}^I$.

Geometrically, in this cell the k-plane Y intersects the cyclic polytope of external data in the k 1-dimensional edges $(Z_{i_1}, Z_{i_1+1}), \ldots, (Z_{i_k} Z_{i_k+1})$. The claim that these cells triangulate the $m = 1$ amplituhedron is then equivalent to the statement that this amplituhedron is the set of all k-planes which intersect the cyclic polytope in precisely k of its 1-dimensional *consecutive* edges (i.e. an edge between two consecutive vertices).

The motivation for this triangulation is given (together with associated new characterizations of the amplituhedron itself) in [22]. For now we can at least show that these cells are non-overlapping in Y space, by noting that in this cell, the following sequence of minors

$$\{\langle Y1\rangle, \langle Y2\rangle, \cdots, \langle Yn\rangle\} \tag{7.4}$$

have precisely k sign flips, with the flips occurring at the locations $(i_s, i_s + 1)$ for $s = 1, \ldots, k$. Since the sign patterns are different in different cells, we can see that the cells are non-overlapping; the fact that they triangulate the amplituhedron is more interesting and will be explained at greater length in [22].

The k-form associated with this cell is

$$\Omega^{\{i_1,\ldots,i_k\}} = Z_* \left(\prod_{s=1}^{k} d\log \alpha_s \right) = \prod_{s=1}^{k} d\log \left(\frac{\langle Y, i_s{+}1\rangle}{\langle Y i_s\rangle} \right) \tag{7.5}$$

and the full form is

$$\Omega(\mathcal{A}) = \sum_{1\le i_1<\cdots<i_k\le n-1} \Omega^{\{i_1,\ldots,i_k\}} \tag{7.6}$$

It is easy to further simplify this expression since the sums collapse telescopically. For instance for $k = 1$ we have

$$\sum_{1\le i_1\le n-1} d\log \left(\frac{\langle Y, i_1{+}1\rangle}{\langle Y i_1\rangle} \right) = d\log \left(\frac{\langle Y n\rangle}{\langle Y 1\rangle} \right) \tag{7.7}$$

Note the cancellation of spurious poles in the sum leading nicely to the final result. The same telescopic cancellation occurs for general k, and for even k we are left with the final form

$$\Omega(\mathcal{A}) = \frac{\mathrm{d}^{k\times(k+1)}Y}{\text{Vol GL(k)}} \sum_{\substack{2\le j_1-1<j_1<\cdots \\ <j_{k/2}-1<j_{k/2}\le n}} [1, j_1{-}1, j_1, \ldots, j_{k/2}{-}1, j_{k/2}] \tag{7.8}$$

while for odd k we are left with

$$\Omega(\mathcal{A}) = \frac{\mathrm{d}^{k\times(k+1)}Y}{\text{Vol GL}(k)} \sum_{\substack{2\le j_1-1<j_1<\cdots \\ <j_{(k-1)/2}-1<j_{(k-1)/2}\le n-1}} [1, j_1{-}1, j_1, \ldots, j_{(k-1)/2}{-}1, j_{(k-1)/2}, n] \tag{7.9}$$

where the brackets denote

$$[j_0, j_1, \ldots, j_k] := \frac{\langle j_0 \ldots j_k\rangle}{\langle Y j_0\rangle \cdots \langle Y j_k\rangle} \tag{7.10}$$

for any indices $j_0, \ldots, j_k$. The brackets satisfy

$$\prod_{s=1}^{k} d\log\left(\frac{\langle Y j_s\rangle}{\langle Y j_{s-1}\rangle}\right) = \frac{\mathrm{d}^{k\times(k+1)}Y}{\mathrm{Vol}\ \mathrm{GL}(k)}[j_0, j_1, \ldots, j_k] \tag{7.11}$$

Note that each bracket can be interpreted as a simplex volume in $\mathbb{P}^k(\mathbb{R})$ whose vertices are the $Z_{j_0}, \ldots, Z_{j_k}$, with Y the hyperplane at infinity. Note also that the combinatorial structure of the triangulation is identical to triangulation of cyclic polytopes discussed in Section 3.2.1. Indeed, when $\langle Y i\rangle > 0$ for each i, the canonical rational function can be interpreted as the volume of the convex cyclic polytope with vertices Z. However, these conditions do not hold for Y on the interior of the amplituhedron, since Y must pass through the interior of the cyclic polytope as it intersects k 1-dimensional consecutive edges.

Starting with $k = 2$, this is not a *positively convex* geometry (see Section 9 of [2]): the form has zeros (and poles) on the interior of the amplituhedron. We can see this easily for e.g. $k = 2, n = 4$. We have a single term with a pole at $\langle Y 2\rangle \to 0$, so it is indeed a boundary component, but it is trivial to see that $\langle Y 2\rangle$ can take either sign in the amplituhedron, so the form has poles and zeros on the interior.

We now consider the case $m = 2$, and triangulate the amplituhedron with the image of a collection of $2 \times k$ dimensional cells of $G_{>0}(k, n)$. That is, for each cell we look at the image $Y_s^I = \sum_{i=1}^{n} C_{si}(\alpha_1, \beta_1, \ldots, \alpha_k, \beta_k) Z_i^I$. Similar to $m = 1$, the cells are indexed by $\{i_1, \ldots, i_k\}$ with $2 \le i_1 < i_2 < \cdots < i_k \le (n-1)$. Now the C matrices are given by

$$C_{si}^{\{i_1,\ldots,i_k\}} = \left\{ \begin{array}{cc} (-1)^{s-1} & i = 1 \\ \alpha_s & i = i_s \\ \beta_s & i = i_s + 1 \\ 0 & \text{otherwise} \end{array} \right\} \tag{7.12}$$

In other words, in this cell we have $Y_s^I = (-1)^{s-1} Z_1^I + \alpha_s Z_{i_s}^I + \beta_s Z_{i_s+1}^I$. As for $m = 1$, it is easy to see that images of these cells are non-overlapping in Y space for essentially the identical reason; in this cell it is easy to check that the sequence of minors

$$\{\langle Y12\rangle, \langle Y13\rangle, \ldots, \langle Y1n\rangle\} \tag{7.13}$$

again has precisely k sign flips, that occur at the locations (i_s, i_s+1) for $s = 1, \ldots, k$.

The $2k$-form associated with this cell is

$$\begin{aligned}
\Omega^{\{i_1,\cdots,i_k\}} &= Z_* \left(\prod_{s=1}^{k} d\log\alpha_s \; d\log\beta_s \right) \\
&= \prod_{s=1}^{k} d\log\left(\frac{\langle Y1 i_s\rangle}{\langle Y i_s, i_s+1\rangle} \right) d\log\left(\frac{\langle Y1, i_s+1\rangle}{\langle Y i_s, i_s+1\rangle} \right) \\
&= \frac{\mathrm{d}^{k(k+2)} Y}{\mathrm{Vol}\ \mathrm{GL}(k)} [1, i_1, i_1{+}1; \ldots; 1, i_k, i_k{+}1]
\end{aligned} \tag{7.14}$$

where

$$[p_1, q_1, r_1; \ldots; p_k, q_k, r_k] := \frac{\left[\left\langle (Y^{k-1})^{s_1} p_1 q_1 r_1 \right\rangle \cdots \left\langle (Y^{k-1})^{s_k} p_k q_k r_k \right\rangle \epsilon_{s_1 \cdots s_k} \right]^k}{2^k \langle Y p_1 q_1\rangle \langle Y q_1 r_1\rangle \langle Y p_1 r_1\rangle \cdots \langle Y p_k q_k\rangle \langle Y q_k r_k\rangle \langle Y p_k r_k\rangle}$$

for any indices p_s, q_s, r_s with $s = 1, \ldots, k$ and

$$(Y^{k-1})^s := Y_{s_1} \wedge \cdots \wedge Y_{s_{k-1}} \epsilon^{s s_1 \cdots s_{k-1}} \tag{7.15}$$

As usual the full form arises from summing over the form for each piece of the triangulation

$$\Omega(\mathcal{A}) = \sum_{2 \le i_1 < \cdots i_k \le n-1} \Omega^{\{i_1,\cdots,i_k\}} \tag{7.16}$$

In particular, for $k=2$, we have

$$\Omega(\mathcal{A}(2,2,n)) = \langle Y d^2 Y_1\rangle \langle Y d^2 Y_2\rangle \times \sum_{2\le i<j\le n-1} \frac{\det \begin{pmatrix} \langle Y_1, i{-}1, i, i{+}1\rangle & \langle Y_1, j{-}1, j, j{+}1\rangle \\ \langle Y_2, i{-}1, i, i{+}1\rangle & \langle Y_2, j{-}1, j, j{+}1\rangle \end{pmatrix}^2}{2^2 \langle Y1i\rangle \langle Y1, i{+}1\rangle \langle Yi, i{+}1\rangle \langle Y1j\rangle \langle Y1, j{+}1\rangle \langle Yj, j{+}1\rangle} \tag{7.17}$$

This is called the *Kermit representation*, and the summands $[1,i,i{+}1;1,j,j{+}1]$ are called *Kermit terms*. These are important for 1-loop MHV scattering amplitudes whose physical amplituhedron $\mathcal{A}(0,n;L{=}1)$ is isomorphic to the amplituhedron $\mathcal{A}(2,n,2)$.

Returning to general k, of course the form also has spurious poles that cancel between the terms, though unlike the case of $m=1$ it cannot be trivially summed into a simple expression with only physical poles. However there is an entirely different representation of the form, not obviously related to the triangulation of the amplituhedron, which is (almost) free of all spurious poles. This takes the form

$$\Omega(\mathcal{A}) = \frac{\mathrm{d}^{k(k+2)}Y}{\mathrm{Vol}\ \mathrm{GL}(k)} \times \sum_{1\le i_1<\cdots<i_k\le n} \frac{\langle \left(Y^{k-1}\right)^{s_1} i_1{-}1, i_1, i_1{+}1\rangle \cdots \langle \left(Y^{k-1}\right)^{s_k} i_k{-}1, i_k, i_k{+}1\rangle \epsilon_{s_1\cdots s_k} \langle X i_1 \cdots i_k\rangle}{\langle YX\rangle \prod_{s=1}^k \langle Y i_s, i_s{+}1\rangle} \tag{7.18}$$

Note the presence of a reference X^{IJ} in this expression, playing an analogous role to a "triangulation point" in a triangulation of a polygon into triangles $[X,i,i{+}1]$. The final expression is however X-independent. Note also that apart from the $\langle YX\rangle$ pole, all the poles in this expression are physical.

This second "local" representation of the form $\Omega(\mathcal{A})$ allows us to exhibit something that looks miraculous from the trianguation expression: $\Omega(\mathcal{A})$ is positive when Y is inside the amplituhedron, and so the $m=2$ amplituhedron is indeed a positively

convex geometry (see Section 9 of [2])! Indeed, if we choose X judiciously to be e.g. $X^{IJ} = (Z_l Z_{l+1})^{IJ}$ for some l, then trivially all the factors in the denominator are positive. Also, $\langle X Z_{i_1} \cdots Z_{i_k} \rangle > 0$ trivially due to the positivity of the Z data. The positivity of the first factor in the numerator is not obvious; however, it follows immediately from somewhat magical positivity properties of the following "determinants of minors". For instance for $k = 2$ the claim is that as long as the Z data is positive,

$$\det \begin{pmatrix} \langle a, i-1, i, i+1 \rangle & \langle a, j-1, j, j+1 \rangle \\ \langle b, i-1, i, i+1 \rangle & \langle b, j-1, j, j+1 \rangle \end{pmatrix} > 0 \tag{7.19}$$

for any $a < b$ and $i < j$. Similarly for $k = 3$,

$$\det \begin{pmatrix} \langle a, b, i-1, i, i+1 \rangle & \langle a, b, j-1, j, j+1 \rangle & \langle a, b, k-1, k, k+1 \rangle \\ \langle a, c, i-1, i, i+1 \rangle & \langle a, c, j-1, j, j+1 \rangle & \langle a, c, k-1, k, k+1 \rangle \\ \langle b, c, i-1, i, i+1 \rangle & \langle b, c, j-1, j, j+1 \rangle & \langle b, c, k-1, k, k+1 \rangle \end{pmatrix} > 0 \tag{7.20}$$

for any $a < b < c; i < j < k$, with the obvious generalization holding for higher k. These identities hold quite non-trivially as a consequence of the positivity of the Z data.

The existence of this second representation of the canonical form, and especially the way it makes the positivity of the form manifest, is quite striking. The same phenomenon occurs for $k = 1$ and any m—the canonical forms are always positive inside the polytope, even though the determination of the form obtained by triangulating the polytope does not make this manifest. For polytopes, this property is made manifest by the much more satisfying representation of the form as the volume integral over the dual polytope. The fact that the same properties hold for the amplituhedron (at least for even m) suggests that we should think of the "local" expression (7.18) for the form we have seen for $m = 2$ as associated with the "triangulation" of a "dual

amplituhedron". We will have more to say about dual amplituhedra in upcoming work.

7.3 Grassmannian contours

We now discuss a novel method for computing canonical forms at tree level. The idea is to take the $i\epsilon$ contour prescription from Section 3.4.3 for computing the $k = 1$ case, and generalize to $k > 1$. So far this approach has only been partially successful, and here we describe both its successes and its difficulties, and we make a conjecture for what a working prescription may look like.

We conjecture that the canonical rational function of the tree amplituhedron is given by a contour integral of the following form,

$$\underline{\Omega}(\mathcal{A}) = \frac{1}{(2\pi i)^{k(n-m-k)}(m!)^k} \int_\Gamma \frac{d^{k\times n}C}{\prod_{i=1}^n C_{i,i+1,\ldots,i+k-1}} \delta^{k\times(k+m)}\left(Y - C\cdot Z\right) \qquad (7.21)$$

where the delta functions impose the usual $Y = C\cdot Z$ constraint while the measure over C is the usual cyclic Grassmannian measure on $G_{\geq 0}(k,n)$. The integral is performed over some contour Γ which we have yet to define. The ultimate goal of this program is to identify a working contour.

For $n = m+k$, there is no contour and we trivially get the expected result. For $n = m+k+1$, we have naively guessed a contour that appears to work for even m according to numerical computations. The idea is to simply change variables $C \to c$ so that for every Plücker coordinate we have $c_{i_1,\ldots,i_k} = C_{i_1,\ldots,i_k} + i\epsilon_{i_1,\ldots i_k}$ for a small constant $\epsilon_{i_1,\ldots,i_k} > 0$. We will assume that $\sum_{1\leq i_1<\cdots<i_k\leq n} \epsilon_{i_1\ldots i_k} Z_{i_1}\wedge\ldots\wedge Z_{i_k} = \epsilon Y$ for some $\epsilon > 0$ and define $\bar{Y} := (1+i\epsilon)Y$ (We are re-scaling Plücker coordinates here, not components of the matrix representation.) so we can re-express $Y = C\cdot Z$ as $\bar{Y} = c\cdot Z$ as we did for the polytope. Again, we assume that $\bar{Y}$ is real and Y is

slightly complex. We then integrate over the real part of c.

$$\underline{\Omega}(\mathcal{A})(Y) = \frac{1}{(2\pi i)^k (m!)^k} \int_\Gamma \frac{d^{k\times(m+k+1)}c}{\prod_{i=1}^{m+k+1} [c_{i,i+1,\ldots,i+k-1} - i\epsilon_{i,i+1,\ldots,i+k-1}]} \times \delta^{k\times(k+m)}\left(\bar{Y} - c\cdot Z\right) \tag{7.22}$$

After integrating over the delta function constraints, there are effectively only k integrals left to do. Conveniently, the poles appearing in the cyclic measure are linear in each integration variable, and can therefore be integrated by applying Cauchy's theorem.

One obvious attempt for generalizing beyond $n > m+k+1$ is to impose the exact same $i\epsilon$ deformation. However, after having integrated over the delta functions, the cyclic minors are at least of quadratic order in the integration variables, thus making the integral very challenging to perform (and possibly ill-defined in the small ϵ limit). It is therefore still a challenge to extend the contour integral picture to the amplituhedron.

Despite the difficulty of extending the $i\epsilon$ contour, our optimism stems from the well-known observation that the canonical rational function of the physical amplituhedron is given by a sum of global residues of the Grassmannian measure constrained on $Y = C\cdot Z$, which was observed in the study of scattering amplitudes. See for instance [36] and references therein. It is therefore reasonable to speculate that a choice of contour would pick up the correct collection of poles whose global residues sum to the expected result, and that different collections of residues that sum to the same result appear as different deformations of the same contour.

We expect these constructions to continue for the L-loop amplituhedron. Namely, we expect that the canonical rational function of the L-loop amplituhedron $\mathcal{A}(k,n,m;l^L)$ to be given by a sum over global residues of the canonical form of the L-loop Grassmannian $G(k,k+m;l^L)$ constrained by $\mathcal{Y} = Z(\mathcal{C})$ for $\mathcal{C}\in G(k,k+m;l^L)$

and $\mathcal{Y} \in \mathcal{A}(k, n, m; l^L)$. A non-trivial example for the 1-loop physical amplituhedron $\mathcal{A}(1, 6; L{=}1)$ is given in [3]. At higher loops, the canonical form of the loop Grassmannian is only known partially.

7.4 Wilson loops and surfaces

Let us now consider yet another approach for computing the canonical form for $k = 0, m = 2$ and $L = 0$. The idea is to extend the dual volume integral for polytopes as described in Section 2.5.3 to a surface integral whose boundary is a Wilson loop.

But let us begin by describing why the problem is challenging, returning to the $k = 1$ polygon example for $m = 2$. Here we have a polygon whose vertices are Z_i^I, and the amplituhedron (a polygon) is just the convex hull of these vertices. Now for any k, the co-dimension one boundaries of the $m = 2$ amplituhedron are $W_i^{IJ} := (Z_i Z_{i+1})^{IJ}$, which are 2-planes in $(2{+}k)$ dimensions. Here the product $Z_i Z_{i+1}$ is a wedge product, so W_i^{IJ} is alternating, and projectively can be thought of as points in $\wedge^2\mathbb{R}^4 \cong \mathbb{R}^6$ or $\mathbb{P}^5$ when projectivized. Loosely speaking, we would like the dual amplituhedron to be the "convex hull of the W_i^{IJ}". But there is a basic difficulty: while we can add vectors (i.e. 1-planes) together to get other vectors, we cannot in general add $k-$planes to get other $k-$planes. In the special case where $k = 1$, the $W_i^{IJ} = \epsilon^{IJK} W_{iK}$ are dual to points W_{iK}, and so can be added. Note of course that the W_{iK} are just vertices of the dual polytope. But for general k, if a natural notion of the "dual" amplituhedron is to exist along these lines we must learn how to deal with adding k-planes together.

We begin by noting that while we cannot add arbitrary 2-planes W_a^{IJ} to get other 2-planes, adding two consecutive W's does yield a 2-plane; to wit:

$$\alpha W_{i-1}^{IJ} + \beta W_i^{IJ} = [Z_i(-\alpha Z_{i-1} + \beta Z_{i+1})]^{IJ} \tag{7.23}$$

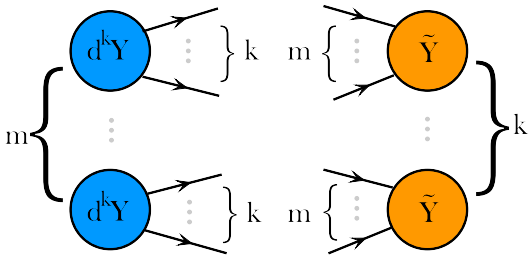

(a) The standard measure on the Grassmannian $G(k, k+m)$ is formed by connecting the arrows on the left with those on the right in the most natural way. Namely, for each blue node, the k outgoing arrows should be connected with each of the k orange nodes.

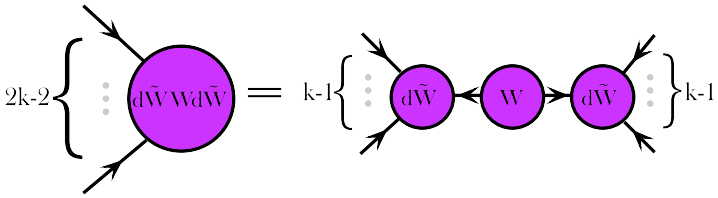

(b) The measure for $(d\tilde{W}Wd\tilde{W})_{I_1 \cdots I_{2k-2}}$. The index contractions are defined graphically. In particular, we note that W^{IJ} should have 2 upstairs indices and hence 2 outgoing arrows, while $d\tilde{W}_{I_1 \ldots I_k}$ should have k incoming arrows.

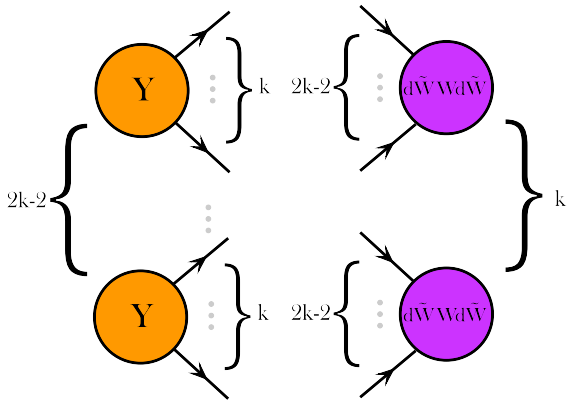

(c) Index contraction for the numerator of $\omega_k(W_1, \ldots, W_k; Y)$. For each orange node, the k outgoing arrows should be connected with each of the k purple nodes.

Figure 7.1: Diagrams representing tensor contractions. Each node denotes a tensor, with each outgoing arrow denoting an upstairs index of the tensor, and each incoming arrow denoting a downstairs index.

For $\alpha, \beta > 0$, this gives us a line from W_{i-1} to W_i within the Grassmannian. Thus there is a natural"polygon" P in $G(2, 2+k)$ with the vertices W_i^{IJ} joined consecutively by line segments as above. Here we have not specified an interior for the polygon, only its edges. In fact, since the embedding space $G(2, 2+k)$ has dimension greater than 2 for $k > 1$, the polygon does not necessarily have a unique interior. We return to this important point shortly.

Since our canonical form has rank $2 \times k$, it is natural to expect the "dual integral" representation to be an integral over a $2 \times k$ dimensional space. Given this canonical one-dimensional boundary in $G(2, 2+k)$, a simple possibility presents itself. Consider *any* 2-dimensional surface whose boundary is the one-dimensional polygon P. Now consider any k of these surfaces Σ_s for $s = 1, \cdots, k$, which may be distinct. Then we would like to consider a k-fold integral over the space $\Sigma := \Sigma_1 \times \cdots \times \Sigma_k$. This gives us a $2 \times k$ dimensional integral as desired but appears to depend on the choice of Σ_s for each s; our only hope is that the forms are closed (in each of the k components independently) and thus the integral depends only on the (canonical) polygon P and not on the particular surface spanning it. As we will see, the structure of this form is essentially fixed by demanding that it is consistently defined on the Grassmannian, and it will indeed turn out to be closed in each component independently.

Let us first recall what fixes the structure of forms on the Grassmannian (see also the discussion in Appendix C of [2]). Consider first the Grassmannian $G(k, k+m)$ associated with a matrix Y_s^I with $s = 1, \ldots, k$ and $I = 1, \cdots, k+m$. We can think of Y in a more GL(k) invariant way as a $k-$fold antisymmetric tensor $Y^{I_1 \cdots I_k} = \epsilon^{s_1 \cdots s_k} Y_{s_1}^{I_1} \cdots Y_{s_k}^{I_k}$. It is also natural to consider the m-plane $\tilde{Y}_{J_1 \cdots J_m} = \epsilon_{I_1 \cdots I_k J_1 \cdots J_m} Y^{I_1 \cdots I_k}$. The Plücker relations satisfied by Y are then contained in the simple statement $Y_s^K Y_{K J_2 \cdots J_m} = 0$.

It will be convenient to introduce a graphical notation for the GL($k+m$) indices here. Each node represents a tensor; and for each tensor, an upstairs index is denoted

by an arrow outgoing from the node and a downstairs index by an incoming one. Then $Y^{I_1\cdots I_k}$ is a node with k outgoing arrows and $\tilde{Y}_{I_1\ldots I_m}$ is a node with m incoming ones, as shown by the orange nodes in Figure 7.1.

Now as discussed in Appendix C of [2], in order for a differential form to be well-defined on the Grassmannian, it must be invariant under *local* $\mathrm{GL}(k)$ transformations, $Y^I_s \to L^t_s(Y)Y^I_t$. We repeat the argument here from a graphical point of view. Since $dY \to L((L^{-1}dL)Y + dY)$ under this transformation, we must have that the measure is unchanged if we replace any single factor of dY^I_s with any Y^I_t. This fixes the standard measure factor $\langle Y d^m Y\rangle$ in projective space up to scale. Generalizing to the Grassmannian, we are looking for a $k \times m$ form. It is natural to consider the $\mathrm{GL}(k)$ invariant k-form $(d^kY)^{I_1\cdots I_k}$, defined as minors of the matrix of dY's, or $(d^kY)^{I_1\cdots I_k} := \epsilon^{s_1\cdots s_k} dY^{I_1}_{s_1}\cdots dY^{I_k}_{s_k}$. For local $\mathrm{GL}(k)$ invariance, every leg of (d^kY) must be contracted with some $\tilde{Y}$, so that the replacement $dY^I_s \to Y^I_t$ vanishes by Plücker. Thus there is a natural $k \times m$ form on the Grassmannian, whose diagram is a complete graph connecting m factors of (d^kY) on one side, and k factors of $\tilde{Y}$ on the other side, as in Figure 7.1a. It is easy to see that in the standard gauge-fixing by $\mathrm{GL}(k)$ where a $k\times k$ block of the matrix representation of $G(k, k+m)$ is set to the identity, this form is simply the wedge product of the remaining variables. Any top-form on $G(k, k+m)$ is expressible as this universal factor multiplied by a $GL(k)$ co-variant function of the Y's with weight $-(k+m)$.

We now use the same ideas to determine the structure of the $2k$-form on Σ. Let us start with the case $k = 2$. We are looking for a 4-form that is the product of two 2-forms, on the space of W_1^{IJ} and W_2^{IJ}. Here the subscripts $1, 2$ index the integration variables, not the vertices W_i; the distinction should be clear form context. By the same logic as above, we will build the form out of the building blocks $(d\tilde{W}Wd\tilde{W})_{IJ}$ (see Figure 7.1b), which are invariant under local GL(2). We then find a form with

appropriate weights under both the W_s and Y rescaling, given by

$$\omega_{k=2}(W_1, W_2; Y) = \frac{\left(d\tilde{W}_1 W_1 d\tilde{W}_1\right)_{IJ} \left(d\tilde{W}_2 W_2 d\tilde{W}_2\right)_{KL} Y^{IK} Y^{JL}}{(\tilde{W}_1 \cdot Y)^3 (\tilde{W}_2 \cdot Y)^3} \tag{7.24}$$

We then claim that the canonical rational function for the $m = 2, k = 2$ amplituhedron can be expressed as

$$\underline{\Omega}(\mathcal{A}(2, 2, n))(Y) = \int_{\Sigma_1 \times \Sigma_2} \omega_{k=2}(W_1, W_2; Y) \tag{7.25}$$

For general k we will have k factors of $(W \cdot Y)^3$ in the denominator, thus to have the correct weight $-(2 + k)$ in minors of Y, we have to have $2k - 2$ factors of Y upstairs. Now the objects $(d\tilde{W}_s W_s d\tilde{W}_i)_{I_1 \cdots I_{2k-2}}$ each have $2k - 2$ incoming arrows (as in Figure 7.1b), while every $Y^{I_1 \cdots I_k}$ has k outgoing arrows. We can thus express $\omega_k(W_1, \cdots, W_k; Y)$ graphically as the complete graph linking the k factors of $(d\tilde{W} W d\tilde{W})$ on one side and the $(2k - 2)$ Y's on the other, as shown in Figure 7.1c. We then claim that

$$\underline{\Omega}(\mathcal{A}(k, 2, n))(Y) = \int_{\Sigma} \omega(W_1, \ldots, W_k; Y) \tag{7.26}$$

These expressions indeed reproduce the correct canonical rational function for the $m = 2$ amplituhedron for all k. Let us illustrate how this works for the case of $k = 2$. A straightforward computation shows that the form $\omega_{k=2}(W_1, W_2; Y)$ is closed in W_1, W_2 independently; indeed it is closed even if the W^{IJ} are not constrained by the Plücker relations, and can be thought of as being general points in $\mathbb{P}^5$. Thus the result of the integral is independent of the surface Σ, provided that $\partial\Sigma_s = P$ for each s. We will thus construct each surface Σ_s by triangulating it like the interior of a polygon. We begin by picking an arbitrary reference point X^{IJ}, and taking the triangle in $\mathbb{P}^5$ with vertices X, W_{i-1}, W_i, which we denote by $[X, W_{i-1}, W_i]$. It follows

that the union $\cup_{i=1}^{n}[X, W_{i-1}, W_i]$ forms a surface with boundary P, so we will take it to be our definition of Σ_s for each s.

Suppose we integrate over the triangle pair $(W_1, W_2) \in [X, W_{i-1}, W_i] \times [X, W_{j-1}, W_j]$. We can parametrize the triangle pair by

$$W_1 = X + \alpha_1 Z_{i-1} Z_i + \beta_1 Z_i Z_{i+1} \tag{7.27}$$

$$W_2 = X + \alpha_2 Z_{j-1} Z_j + \beta_2 Z_j Z_{j+1} \tag{7.28}$$

where $\alpha_{1,2} > 0; \beta_{1,2} > 0$.

The only non-trivial part of the computation is working out the numerator index contraction in (7.24). After a series of index gymnastics, we get for each i, j:

$$\omega_{k=2} = \frac{1}{2} \frac{(\mathcal{N}_1(i,j) + \mathcal{N}_2(i,j)) d^2\alpha d^2\beta}{\left(\langle YX\rangle + \alpha_1 \langle Yi{-}1, i\rangle + \beta_1 \langle Yi, i{+}1\rangle\right)^3 \left(\langle YX\rangle + \alpha_1 \langle Yj{-}j, j\rangle + \beta_1 \langle Yj, j{+}1\rangle\right)^3} \tag{7.29}$$

where

$$\mathcal{N}_1(i,j) := \langle YX\rangle \langle Xij\rangle \langle Y(i{-}1, i, i{+}1) \cap (j{-}1, j, j{+}1)\rangle \tag{7.30}$$

$$\mathcal{N}_2(i,j) := -\langle Y(i{-}1, i, i{+}1) \cap (Xj)\rangle \langle Y(j{-}1, j, j{+}1) \cap (Xi)\rangle \tag{7.31}$$

where $\langle Y(abc) \cap (def)\rangle := \langle Y_1 abc\rangle \langle Y_2 def\rangle - (Y_1 \leftrightarrow Y_2)$ for any vectors a, b, c, d, e, f.

Integrating over $\alpha_{1,2} > 0; \beta_{1,2} > 0$ and summing over all i, j gives us

$$\int_\Sigma \omega_{k=2} = \frac{1}{8} \sum_{i,j=1}^{n} \frac{\mathcal{N}_1(i,j) + \mathcal{N}_2(i,j)}{\langle YX\rangle^2 \langle Yi{-}1, i\rangle \langle Yi, i{+}1\rangle \langle Yj{-}1, j\rangle \langle Yj, j{+}1\rangle} \tag{7.32}$$

This is one of several *local* expressions for the canonical rational function $\underline{\Omega}(\mathcal{A}(2, 2, n))$. That is, there are no spurious singularities, except at $\langle YX\rangle \to 0$. Interestingly, if we keep only one of the numerator terms $\mathcal{N}_1, \mathcal{N}_2$, then the result would still sum to (half)

the correct answer. Perhaps some clever manipulation of the integration measure would make this manifest. If we only keep the first numerator, then we recover the local form given in (7.18).

It is possible, through a clever choice of the surface Σ, to recover the Kermit representation (7.17) of the canonical rational function. While the equivalence between the Kermit representation and the local form appears non-trivial as an algebraic statement, it follows easily from the surface-independence of the integral.

This computation can be extended easily to higher k. Furthermore, since the surfaces $\Sigma_1, \ldots, \Sigma_k$ are independent, it is possible to have picked a different X for each surface, giving a local form with arbitrary reference points $X_1, \ldots, X_k$.

7.5 Pushforwards

We present a pushforward prescription for computing canonical forms of amplituhedra similar to the kind described in Section 3.3 for computing canonical forms of polytopes. In particular, We conjecture that the canonical form can be formulated as a pushforward from the standard simplex.

Conjecture 7.5.1. *Given a morphism $\Phi : \Delta^D \to \mathcal{A}(k, n, m; l^L)$ from positive coordinates to the amplituhedron, the amplituhedron form is given by the pushforward*

$$\Omega(\mathcal{A}(k, n, m; l^L)) = \Phi_* \left(\prod_{a=1}^{D} \frac{dX_a}{X_a} \right) \tag{7.33}$$

where D is the dimension of the amplituhedron.

While this is nothing more than a direct application of our favorite Heuristic 2.3.1, we emphasize that it is in general very challenging to construct diffeomorphisms between the simplex and amplituhedra. In this section, we let $\mathcal{A} := \mathcal{A}(k, n, m; l^L)$. Before providing explicit examples, we reformulate our conjecture in terms of the

canonical rational function $\underline{\Omega}(\mathcal{A})(\mathcal{Y})$ of the amplituhedron, as defined in Appendix C of [2].

Conjecture 7.5.2. *Given a morphism* $\Phi : \Delta^D \to \mathcal{A}(k, n, m; l^L)$ *from positive coordinates to the amplituhedron, the amplitude is given by:*

$$\underline{\Omega}(\mathcal{A})(\mathcal{Y}) = \int \frac{d^D X}{\prod_{a=1}^{D} X_a} \delta^D(\mathcal{Y}; \Phi(X)) \tag{7.34}$$

for any point $\mathcal{Y} \in \mathcal{A}$*. For computational purposes,* $\mathcal{Y}$ *and* $\Phi(X)$ *are represented as matrices modded out by a left group action, as discussed below* (2.70)*.*

The delta function $\delta^D(\mathcal{Y}, \mathcal{Y}')$ is the unique (up to an overall normalization) delta function on $G(k, k+m; l^L)$ that is invariant under the group action $\mathcal{G}(k; \underline{k})$ (defined below 2.70) on $\mathcal{Y}'$, and scales inversely as the measure (C10) of [2] under the same group action on $\mathcal{Y}$. The inverted scaling ensures that the canonical form is locally invariant under the action.

Example 7.5.3. For $k = 1$ and $m = 4$, the *physical* tree amplituhedron $\mathcal{A}$ is a convex cyclic polytope with vertices $Z_i \in \mathbb{P}^4(\mathbb{R})$. Morphisms $\Phi : (\mathbb{P}^4, \Delta^4) \to (\mathbb{P}^4, \mathcal{A})$ are given by convex cyclic Newton polytopes from (3.53), and the amplitude is given by:

$$\underline{\Omega}(\mathcal{A})(Y) = \int \frac{d^4 X}{X_1 X_2 X_3 X_4} \delta^4(Y; \Phi(X)) \tag{7.35}$$

where $Y \in \mathbb{P}^4$ and the delta function is given in (3.59) with $m = 4$.

We now provide some examples for $k = 2, m = 2, l = 2, L = 0$. While we do not have a complete construction of such morphisms for all n, we did find a few non-trivial examples for small n. We stress that the existence of such morphisms is an absolutely remarkable fact. We also speculate that a complete understanding of morphisms to the tree amplituhedron may provide insight on extending toric varieties

to the Grassmannian, as morphisms to the polytope were given by projective toric varieties.

Let us begin by clarifying the pushforward computation, which for the present case is given by:

$$\underline{\Omega}(\mathcal{A}) = \int \frac{d^4X}{X_1X_2X_3X_4}\delta^4(Y;\Phi(X)) \tag{7.36}$$

where

$$\delta^4(Y;Y') = \frac{1}{4}\int \frac{d^{2\times 2}\rho}{(\det\rho)^2}\delta^{2\times 4}(Y-\rho\cdot Y') \tag{7.37}$$

is the delta function that imposes the constraint $Y = Y'$ for any pair of 2×4 matrices Y, Y', where the tilde indicates that the two sides are only equivalent up to an overall GL(2) transformation. The ρ is a 2×2 matrix that acts as a GL(2) transformation on Y' from the left, and the $d^{2\times 2}\rho/(\det\rho)^2$ measure is GL(2) invariant in ρ both from the left and the right. We see therefore that the delta function has GL(2) weights $(-4,0)$ in (Y,Y'), as expected.

Example 7.5.4. Consider the amplituhedron for $(k,m,n,l,L) = (2,2,4,2,0)$, which is simply

$$\mathcal{A} = \{C\cdot Z \in G(2,4) \mid C \in G_{\geq 0}(2,4)\} \tag{7.38}$$

where Z is a 4×4 matrix with positive determinant. Since Z is non-singular, $\mathcal{A}$ is isomorphic to $G_{\geq 0}(2,4)$. A (degree-one) morphism from $(\mathbb{P}^4,\Delta^4)$ to the amplituhedron is therefore:

$$C(X) = \begin{pmatrix} 1 & X_1 & 0 & -X_4 \\ 0 & X_2 & 1 & X_3 \end{pmatrix} \tag{7.39}$$

$$\Phi(X) = C(X)\cdot Z \tag{7.40}$$

sending the interior $\text{Int}(\Delta^4)$ (where $X_i > 0$ for $i = 1, 2, 3, 4$) to the interior of the amplituhedron. Substituting into (7.36) gives:

$$\underline{\Omega}(\mathcal{A}) = \frac{1}{4} \frac{\langle 1234 \rangle^2}{\langle Y12 \rangle \langle Y23 \rangle \langle Y34 \rangle \langle Y14 \rangle} \tag{7.41}$$

Example 7.5.5. We now move on to the first non-trivial example beyond the polytope. Consider the same case as Example 7.5.4 but now with $n = 5$. The amplituhedron is

$$\mathcal{A} = \{C \cdot Z \in G(2, 4) \mid C \in G_{\geq 0}(2, 5)\} \tag{7.42}$$

with all the maximal ordered minors of Z positive. The interior of this amplituhedron has no obvious diffeomorphisms with the interior $\text{Int}(\Delta^4)$ of the 4-simplex. But we have managed to stumble across a few lucky guesses, such as the following:

$$C(X) = \begin{pmatrix} 1 & X_1 & X_1X_2 & X_2 & 0 \\ 0 & X_1X_3 & X_1X_2(X_3{+}X_3X_4) & X_2(X_3{+}X_3X_4{+}X_4) & 1 \end{pmatrix} \tag{7.43}$$

$$\Phi(X) = C(X) \cdot Z \tag{7.44}$$

for $X_1, X_2, X_3, X_4 > 0$. We have verified numerically that the pushforward given by (7.43) gives the correct 5-point 1-loop integrand. A careful analytic argument can be provided to prove that the restriction $\text{Int}(\Delta^4) \xrightarrow{\sim} \text{Int}(\mathcal{A})$ is indeed a diffeomorphism.

Example 7.5.6. We also provide an example for $n = 6$. The setup is the same as Example 7.5.5, with the $C(X)$ matrix given by

$$C(X) = \begin{pmatrix} X_1^3X_2^2 & X_3{+}X_1^2X_2^2X_3 & X_1^5X_2^2X_3X_4^2 & X_1^3X_3X_4^2 & X_1 & 0 \\ -X_1^4X_2^2 & -X_1X_3 & 0 & X_1^2X_3X_4^2 & 1{+}X_1^2X_4^2 & X_1^5X_2^2X_4^2 \end{pmatrix}$$

The pushforward was verified numerically. We challenge the reader to prove that this map restricts to a diffeomorphism $\text{Int}(\Delta^4) \xrightarrow{\sim} \text{Int}(\mathcal{A})$.

7.6 Dual amplituhedra

Recall from Section 2.5.3 that the canonical rational function of a polytope is precisely the volume of the dual polytope. This leads us to conjecture, for every amplituhedron, the existence of a dual geometry whose volume precisely gives the canonical rational function. The existence of this dual geometry has already been established at tree level for $n = k+m$ and any k, m, and even for some loop level cases, and will be described in future work.

We motivate the existence of the dual by thinking about triangulations. As argued in Section 2.2, a signed triangulation of a positive geometry $\mathcal{A} = \sum_i \mathcal{A}_i$ implies $\Omega(\mathcal{A}) = \sum_i \Omega(\mathcal{A}_i)$. This was argued based on the observation that spurious poles cancel among the triangulating terms, thus leaving only the physical poles. In our discussion of the dual polytope in Section 3.4.1, we argued that the volume formulation of the canonical rational function (under certain assumptions) provides an alternative understanding of triangulation independence. We therefore wish to extend these assumptions to the amplituhedron and conjecture a volume interpretation of the canonical rational function. We restrict our conjecture to even m, since the volume formula implies positive convexity (see Section 9 of [2]), which in most cases does not hold for odd m.

Let $\mathcal{A}$ denote an amplituhedron, and let X denote the irreducible variety in which it is embedded. We conjecture the following:

Conjecture 7.6.1. *1. For each $\mathcal{Y} \in X$ not on a boundary component of $\mathcal{A}$, there exists an irreducible variety $X^*_{\mathcal{Y}}$, called the* dual variety at $\mathcal{Y}$*, with a bijection*

$(X, \mathcal{B}) \xrightarrow{\sim} (X^*_{\mathcal{Y}}, \mathcal{B}^*_{\mathcal{Y}})$ *that maps positive geometries in* X *to positive geometries in* $X^*_{\mathcal{Y}}$. *In particular, there exists a* dual amplituhedron $\mathcal{A}^*_{\mathcal{Y}}$ *for each* $\mathcal{Y}$.

2. *Let* $\mathcal{B}_{1,2}$ *be positive geometries in* X. *Then* $\mathcal{B}_1 \subset \mathcal{B}_2$ *if and only if* $\mathcal{B}^*_{2\mathcal{Y}} \subset \mathcal{B}^*_{1\mathcal{Y}}$.

3. *Given a triangulation of* $\mathcal{B}$ *in* X, *we have*

$$\mathcal{B} = \sum_i \mathcal{B}_i \quad \Rightarrow \quad \mathcal{B}^*_{\mathcal{Y}} = \sum_i \mathcal{B}^*_{i\mathcal{Y}}. \tag{7.45}$$

4. *There exists a* $\mathcal{Y}$*-dependent measure* $d\text{Vol}$ *on* $X^*_{\mathcal{Y}}(\mathbb{R})$ *so that:*

$$\underline{\Omega}(\mathcal{B})(\mathcal{Y}) = \text{Vol}\,(\mathcal{B}^*_{\mathcal{Y}}) := \int_{\mathcal{B}^*_{\mathcal{Y}}} d\text{Vol} \tag{7.46}$$

Following the reasoning outlined around (3.124), we arrive at the desired conclusion:

$$\mathcal{A} = \sum_i \mathcal{A}_i \qquad \Rightarrow \quad \mathcal{A}^*_{\mathcal{Y}} = \sum_i \mathcal{A}^*_{i\mathcal{Y}} \quad \Rightarrow \tag{7.47}$$

$$\text{Vol}\,(\mathcal{A}^*_{\mathcal{Y}}) = \sum_i \text{Vol}\,(\mathcal{A}^*_{i\mathcal{Y}}) \qquad \Rightarrow \quad \underline{\Omega}(\mathcal{A}) = \sum_i \underline{\Omega}(\mathcal{A}_i) \tag{7.48}$$

In words, we say that the triangulation independence of the dual volume explains the triangulation independence of the form. This provides an alternative argument to cancellation of spurious poles.

Chapter 8

Planar $\mathcal{N} = 4$ super Yang-Mills

Following the construction of the amplituhedron in Section 7, we now discuss its precise connection to on-shell scattering amplitudes of planar $\mathcal{N} = 4$ super Yang-Mills. We begin in Section 8.1 by introducing supersymmetric momentum twistors, which are kinematic variables that make manifest the hidden dual super conformal symmetry [8]. In Section 8.2, we show how amplitudes are determined by canonical forms of amplituhedra. Finally, in Section 8.3, we discuss BCFW recursion in momentum twistor space and its geometric interpretation.

8.1 Supersymmetric momentum twistors

Momentum twistors were first introduced in [29], which we now review. Denote the n-point N^{k}MHV L-loop amplitude as $\mathcal{A}^{(L)}_{n,k}$ and let $A^{(L)}_{n,k}$ denote the same amplitude with the MHV tree factor stripped off,

$$\mathcal{A}^{(L)}_{n,k} = \frac{\delta^{2\times(2|4)}(\sum_{i=1}^{n} \lambda_i^{\alpha}(\tilde{\lambda}_i^{\dot{\alpha}}|\eta_i^A))}{\langle 12\rangle \dots \langle n{-}1n\rangle\langle n1\rangle} A^{(L)}_{n,k}\,, \tag{8.1}$$

where $\alpha, \dot{\alpha} = 1, 2$ are SU(2) indices of spinors λ_i and their conjugates $\tilde{\lambda}_i$ encoding the null momenta of n particles, and $A = 1, ..., 4$ is the SU(4) index of Grassmann

variables η_i describing their helicity states. The Wilson loop dual to the n-point amplitude is formulated along a n-sided null polygon in a chiral superspace with coordinates (x, θ); for $i = 1, \ldots, n$, we have

$$x_i^{\alpha\dot{\alpha}} - x_{i-1}^{\alpha\dot{\alpha}} = \lambda_i^\alpha \tilde{\lambda}_i^{\dot{\alpha}}, \qquad \theta_i^{\alpha A} - \theta_{i-1}^{\alpha A} = \lambda_i^\alpha \eta_i^A \,, \tag{8.2}$$

The super momentum twistors are in the fundamental representation of the superconformal group of this dual space; explicitly

$$\mathcal{Z}_i = (Z_i^a | \chi_i^A) = (\lambda_{i\alpha}, \mu_i^{\dot{\alpha}} | \chi_i^A) \equiv (\lambda_{i\alpha}, x_i^{\alpha\dot{\alpha}} \lambda_{i\alpha} | \theta_i^{\alpha A} \lambda_{i\alpha}) \,. \tag{8.3}$$

The momentum twistors are unconstrained and they determine $\tilde{\lambda}, \eta$ via,

$$(\tilde{\lambda}|\eta)_i = \frac{\langle i{-}1\, i\rangle (\mu|\chi)_{i+1} + \langle i{+}1\, i{-}1\rangle (\mu|\chi)_i + \langle i\, i{+}1\rangle (\mu|\chi)_{i-1}}{\langle i{-}1\, i\rangle \langle i\, i{+}1\rangle} \tag{8.4}$$

We further define the contraction of four bosonic twistors $\langle ijkl\rangle \equiv \varepsilon_{abcd} Z_i^a Z_j^b Z_k^c Z_l^d$. The factorization poles $x_{i,j}^2 = 0$ where $x_{i,j} \equiv x_i - x_j$ can be written in these variables as $\langle i{-}1\, i\, j{-}1\, j\rangle = 0$. In addition, we have the basic R-invariant of five super-twistors,

$$[i, j, k, l, m] \equiv \frac{\delta^{0|4}(\langle\langle i\, j\, k\, l\, m\rangle\rangle)}{\langle ijkl\rangle \langle jklm\rangle \langle klmi\rangle \langle lmij\rangle \langle mijk\rangle}, \tag{8.5}$$

where the argument of Grassmann delta function is $\langle\langle i\, j\, k\, l\, m\rangle\rangle^A \equiv \chi_i^A \langle jklm\rangle + \text{cyclic}$.

The central object we will study in this paper is the *integrand* of amplitudes/Wilson loops in momentum twistor space. We will denote the integrand for $A_{n,k}^{(L)}$ as $Y_{n,k}^{(L)}$, which is a form of degree $4L$ in the L loop variables denoted as ℓ's. Formally we have

$$A_{n,k}^{(L)} = \int_{\text{reg}} Y_{n,k}^{(L)}(\mathcal{Z}_1, \ldots, \mathcal{Z}_n; \{\ell_1, \ldots, \ell_L\}) = \int_{\text{reg}} \prod_{m=1}^{L} d^4\ell_m \, I_{n,k}^{(L)}(\mathcal{Z}_1, \ldots, \mathcal{Z}_n; \{\ell_1, \ldots, \ell_L\})$$

where "reg" means regularizations which are needed for the loop integrals, and by writing the integral measure explicitly, the remaining part of $Y^{(L)}_{n,k}$, as a rational function, is denoted as $I^{(L)}_{n,k}$. Note that both Y and I are cyclic in external twistors which are denoted as $1,\ldots,n$; they are also completely symmetrized in loop variables.

The loop variables ℓ's correspond to points in dual space. For computing Wilson loops, they are positions of Lagrangian insertions [62]. Accordingly, they are lines in momentum twistor space, and we will always represent ℓ's by bi-twistors $\ell_m \equiv (A_m B_m) \equiv (AB)_m$ for $m = 1,\ldots,L$. The loop integral measure in momentum twistor space is defined as

$$d^4\ell \equiv \langle AB d^2A\rangle\langle AB d^2B\rangle = \frac{d^4Z_A d^4Z_B}{\text{vol}\, GL(2)} \tag{8.6}$$

where the factors of $\langle AB\rangle$ always drop out because the integrand is dual conformal invariant, so we have neglected writing them in (8.6). The integral over the line (AB) is given by that over a pair of points (twistors) Z_A and Z_B, divided by the GL(2) redundancies labeling their positions on the line [28]. The integrand has, in addition to factorization poles, poles from a propagator involving loop variables going on shell, e.g. the so-called single cut corresponds to poles of the form $\langle A_m B_m\, i{-}1\, i\rangle = 0$ for the loop variable ℓ_m.

8.2 Scattering amplitudes from the amplituhedron

As first conjectured in [17], the $m = 4, l = 2$ amplituhedron forms a completely independent, geometric formulation of all the planar scattering amplitudes in $\mathcal{N} = 4$ super Yang-Mills. More precisely, the n-point N^{k}MHV L-loop amplitude is determined by the canonical form of the amplituhderon $\mathcal{A}(k,n,4;2^L)$, in a manner we now describe. Note that we often denote the the physical amplituhedron as

$\mathcal{A}(k,n;L) = \mathcal{A}(k,n,4;2^L)$ for simplicity, and the physical tree amplituhedron as $\mathcal{A}(k,n) = \mathcal{A}(k,n,4;2^0)$.

Recall that the amplituhedron is defined by a $n \times (k+4)$ matrix Z, whose components we write as Z_i^I for $i = 1,\ldots,n$ and $I = 1,\ldots,k+4$. The index i labels the n external particles. For every i, we identify the first four components of Z_i^I with the components of the bosonic momentum twistor Z_i^a. The last k components, however, are more subtle. We first introduce auxiliary Grassmann variables $\phi_{1,A},\ldots,\phi_{k,A}$ for $A = 1,2,3,4$, and we let

$$Z_i^I = (Z_i^a,\ \phi_{1,A}\chi_i^A,\ \ldots,\ \phi_{k,A}\chi_i^A) \tag{8.7}$$

where the index A is implicitly summed in each of the last k components. The goal of this construction is to make the amplituhedron a purely bosonic object that nevertheless contains all information about superamplitudes. This is a rather novel way of encoding supersymmetry, first introduced in [40]. Next, we compute the canonical form of $\mathcal{A}(k,n;L)$ without introducing any auxiliary Grassmann variables; that is, we simply assume all the components of the Z matrix to be real. We then localize the canonical form to a special point $Y_0 = (0_{4\times k}|I_{k\times k})$ before substituting the auxiliary variables (8.7). The localization ensures that the result is a polynomial in the Grassmann variables. Finally, the auxiliary variables are integrated out, giving the super-amplitude, which has Grassmann degree $4k$.

$$Y_{n,k}^{(L)}(\mathcal{Z},l) \ = \ \int d^4\phi_1 \cdots d^4\phi_k \int \Omega(\mathcal{A}(k,n;L))\delta^{4k}(Y;Y_0) \tag{8.8}$$

8.3 BCFW recursion and positive geometry

In [6], a recursion relation was described for on-shell tree amplitudes in Yang-Mills theory. For planar maximally supersymmetric Yang-Mills, an all-loop extension was

described in [28]. We do not prove the recursion relation here. Instead we give a general description for the idea behind the proof, then present the recursion relation in momentum twistor space. Most importantly for our discussion, we interpret the recursion as a triangulation of the amplituhedron.

The construction and proof of the recursion goes as follows. We begin by introducing an extra parameter z and define the shift $Z_n \to Z_n + zZ_{n-1}$, which gives $\Omega(\mathcal{A}) \to \Omega(\mathcal{A}(z))$. The principle of *locality* suggests that the canonical form can only develop *simple poles* in z (including possibly a simple pole at infinity). It follows that

$$\Omega(\mathcal{A}) = \oint_C \frac{dz}{z} \Omega(\mathcal{A}(z)) \tag{8.9}$$

where the contour C is a small counter-clockwise loop around the origin. Applying Cauchy's theorem by expanding the loop to infinity gives

$$\Omega(\mathcal{A}) = -\sum_i \text{Res}_{z \to z_i} \frac{\Omega(\mathcal{A}(z))}{z} + \Omega(\mathcal{A}(\infty)) \tag{8.10}$$

where z_i denotes all the poles. The residue at infinity is simply the canonical form of the amplituhedron with Z_n removed. The residues at z_i are described as follows.

- There exists a Δ-like positive geometry $\mathcal{C}_i$ in the loop Grassmannian $G(k, n; 2^L)$ of dimension $D = \dim(\mathcal{A})$.
- There exists a subset $\mathcal{A}_i$ of $\mathcal{A}$ also of dimension D, called a *BCFW cell*.
- The map under $Z : \mathcal{C}_i \to \mathcal{A}_i$ is a degree-one morphism. Since $\mathcal{C}_i$ is Δ-like, hence so is $\mathcal{A}_i$.

- Given $\Delta-$like coordinates $(1, \alpha_{i1}, \ldots, \alpha_{iD}) \in \mathbb{P}^D(\mathbb{R})$ on $\mathcal{C}_i$, the residue at z_i is given by the following pushforward.

$$-\text{Res}_{z \to z_i} \frac{\Omega(\mathcal{A}(z))}{z} = Z_* \left(\prod_{j=1}^{D} \frac{d\alpha_{ij}}{\alpha_{ij}} \right) = \Omega(\mathcal{A}_i) \tag{8.11}$$

At $L = 0$, each set $\mathcal{C}_i$ is a positroid cell of the positive Grassmannian and $\mathcal{A}_i$ is the image under Z. For $L > 0$ some generalization of this statement is expected to hold. The precise construction of $\mathcal{C}_i$ is explained in Section 9 from the point of view of momentum twistor diagrams. We point out that while BCFW cells are Δ-like, they are not necessarily simplex-like, since their canonical forms may have zeros.

From (8.11) and the discussion in Section 2.2, it follows that the BCFW cells form a boundary triangulation of the amplituhedron:

$$\Omega(\mathcal{A}) = \sum_i \Omega(\mathcal{A}_i) \tag{8.12}$$

Furthermore, it appears based on extensive numerical checks that the BCFW cells have mutually disjoint interiors. We point out that if our assumptions on BCFW cells hold, then the amplituhedron must be a positive geometry.

Finally, we present the formula for the recursion, which describes the integrand as a sum over three different contributions,

$$Y^{(L)}_{n,k}(1, \ldots, n) = \text{B} + \text{FAC} + \text{FL} \tag{8.13}$$

where for simplicity we have used indices $1, 2, ..., n$ to denote super-twistors $\mathcal{Z}_1, \mathcal{Z}_2, ..., \mathcal{Z}_n$, and we have suppressed loop variables.

Here B represents the boundary contribution from $w \to \infty$, given by removing $\mathcal{Z}_n$.

$$\mathrm{B} = Y^{(L)}_{n-1,k}(1,\ldots,n-1)\,. \tag{8.14}$$

The FAC term represents contributions from factorization poles,

$$\mathrm{FAC} = \frac{1}{L!}\sum_{i=3}^{n-2}\sum_{k',L'}\sum_{\sigma(\ell)}[i{-}1,i,n{-}1,n,1]Y^{(L')}_{i,k'}(1,\ldots,i{-}1,\hat{i})Y^{(L-L')}_{n+2-i,k-1-k'}(\hat{i},i,\ldots,n{-}1,\hat{n}_i)$$

where we sum over all the poles of the form $\langle i{-}1\, i\, \hat{n}\, 1\rangle = 0$, and at each pole the internal leg and the shifted leg are given by $\hat{i} \equiv (i{-}1,i){\cap}(1,n{-}1,n)$, $\hat{n}_i = (n{-}1,n){\cap}(1,i-1,i)$, with $(a,b)\cap(c,d,e) \equiv Z_a\langle b\,c\,d\,e\rangle - Z_b\langle a\,c\,d\,e\rangle$ defined as the intersection of the line (a,b) with the plane (c,d,e). In addition, we sum over $k' = 0,\ldots,k{-}1$, $L' = 0,\ldots,L$, and over distributions of $\ell_1,\ldots,\ell_L$ into the two subsets, with L' and $(L{-}L')$ variables, which explains the overall symmetrization factor $1/L!$.

The FL term represents the forward-limit contributions which come from single cuts,

$$\mathrm{FL} = \frac{1}{L}\sum_{m=1}^{L}\int\frac{d^{3|4}\mathcal{Z}_A d^{3|4}\mathcal{Z}_B}{\mathrm{vol\ GL(2)}}\int_{GL(2)}[A_m,B_m,n{-}1,n,1]Y^{(L-1)}_{n+2,k+1}(1,...,n{-}1,\hat{n}_{\ell_m},A_m,B_m)$$

where we sum over L loop variables $\ell_m = (AB)_m$ (with a symmetrization factor $1/L$), and each term comes from the pole $\langle A_m B_m \hat{n} 1\rangle = 0$, with $\hat{n}_\ell = (n-1,n)\cap(A,B,1)$. The $\int_{GL(2)}$ integral is defined as follows. We first set $Z_A \to Z_A + \alpha Z_B \equiv Z'_A$ and $Z_B \to Z_B + \beta Z_A \equiv Z'_B$ for parameters α,β, which is equivalent to moving the two points Z_A, Z_B without changing the line they span. Then, we take a double residue in α,β such that $\langle A',1,n{-}1,n\rangle, \langle B',1,n{-}1,n\rangle \to 0$, which is equivalent to taking

A', B' to lie on the plane $(1, n{-}1, n)$. Formally, we have

$$\int_{GL(2)} \equiv \int_{\langle A',1,n-1,n\rangle\to 0} d\alpha \int_{\langle B',1,n-1,n\rangle\to 0} d\beta\ (1-\alpha\beta)^2 \tag{8.15}$$

This residue is equivalent to setting $Z'_A, Z'_B \to (A, B) \cap (1, n{-}1, n)$. The $(1-\alpha\beta)^2$ is a determinant factor that makes the poles in α, β simple.

Chapter 9

Momentum twistor diagrams

As argued in Section 8.3, every BCFW term appearing in planar $\mathcal{N} = 4$ super Yang-Mills theory corresponds to a cell of the loop Grassmannian whose image under Z gives a cell of the amplituhedron, called a BCFW cell. In this section, we show that every BCFW cell can be described by an equivalence class of plabic diagrams. In particular, every such diagram encodes a set of Grassmannian coordinates for the cell, which can be read off from the diagram by a simple prescription. As discussed in (8.11), the pushforward of the product of d-log of these coordinates gives the corresponding BCFW term. Furthermore, we show that BCFW recursion can be applied diagrammatically, thus providing a recursive algorithm for constructing the equivalence class of diagrams for any BCFW term. The connection between Grassmannians and plabic graphs goes back to the pioneering work of Postnikov [30], which was subsequently applied to planar $\mathcal{N} = 4$ super Yang-Mills in on-shell momentum space [16], and later in momentum twistor space [4].

9.1 On-shell diagrams in momentum twistor space

We start by presenting fundamental ingredients for on-shell diagrams in momentum twistor space. A generic on-shell diagram consists of trivalent white and black vertices

connected by external and internal edges, all drawn on a disk. Note that we do not assume that the diagrams are planar. In fact, as we will discuss later, non-planarity is a surprising feature that only appears in forward limit terms at loop level, despite the fact that they compute planar loop amplitudes.

- Every diagram consists of n external legs connected to the boundary of a disk. They represent the n color-ordered external states, and are associated with momentum twistors $\mathcal{Z}_1, \mathcal{Z}_2, \ldots, \mathcal{Z}_n$.

- Each internal edge of the diagram is associated with a momentum twistor $\mathcal{Z}$ which is then integrated over with the measure

$$d^{3|4}\mathcal{Z} = \frac{d^{4|4}\mathcal{Z}}{\text{vol}\,\text{GL}(1)} \tag{9.1}$$

- Each white vertex with three (internal or external) twistors $\mathcal{Z}_a, \mathcal{Z}_b, \mathcal{Z}_c$ is represented by an integral over $C \in G(1,3)$ (a 1×3 matrix with GL(1) redundancies),

$$W(a,b,c) \;=\; \tag{9.2}$$

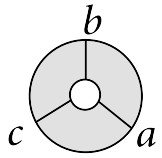

$$= \int \frac{1}{\text{vol}\,\text{GL}(1)} \frac{d^{1\times 3}C}{(a)(b)(c)} \delta^{4|4}(C_a\mathcal{Z}_a + C_b\mathcal{Z}_b + C_c\mathcal{Z}_c) \tag{9.3}$$

where $(i) = C_i$ for $i = a, b, c$. The white vertex thus enforces $\mathcal{Z}_a, \mathcal{Z}_b, \mathcal{Z}_c$ to be on the same projective line.

- Each black vertex with three (internal or external) twistors $\mathcal{Z}_a, \mathcal{Z}_b, \mathcal{Z}_c$ is represented by an integral over $C \in G(2,3)$ (a 2×3 matrix up to GL(2) redundancies,

with minors defined as $(i\,j) \equiv C_{1,i}C_{2,j} - C_{2,i}C_{1,j})$,

$$B(a,b,c) \quad = \tag{9.4}$$

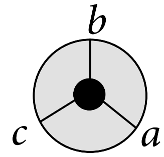

$$= \int \frac{1}{\mathrm{vol\,GL}(2)} \frac{d^{2\times 3}C}{(ab)(bc)(ca)} \prod_{\alpha=1}^{2} \delta^{4|4}(C_{\alpha,a}\mathcal{Z}_a + C_{\alpha,b}\mathcal{Z}_b + C_{\alpha,c}\mathcal{Z}_c) \tag{9.5}$$

The black vertex thus identifies $\mathcal{Z}_a, \mathcal{Z}_b, \mathcal{Z}_c$ projectively. There are degenerate cases: a black vertex with two edges can be deleted from the diagram, with the two edges identified to be one edge (the two twistors are identified); and a black vertex connected to the boundary by one external edge can also be deleted, making the diagram independent of the corresponding external twistor.

9.1.1 The Grassmannian representation of momentum twistor diagrams

We now describe the Grassmannian representation of momentum twistor diagrams in parallel with [16].

We begin by noting that the k-charge here (the Grassmann degree is defined as $4k$) is related to the k-charge in the original space (the MHV degree of the full amplitude) by $k_{\text{here}} = k_{\text{original}} - 2$. The k-charge of a diagram is easy to determine: each trivalent white vertex has $k = 1$ and each trivalent black vertex has $k = 2$; for each internal edge the k is reduced by one, thus the total k-charge is

$$k = n_W + 2n_B - n_I\,, \tag{9.6}$$

where n_W, n_B and n_I are the number of trivalent white vertices, black vertices and internal edges. Another useful relation is

$$n = 3(n_W + n_B) - 2n_I \,. \tag{9.7}$$

Note that for both formulas, we assumed that every vertex is attached to exactly three edges, so lollipops and degenerate cases must be taken into account separately.

The diagram can be evaluated in its Grassmannian representation in the manner described in Section 4 of [16] by a procedure called boundary measurement. To summarize, we perform all integrals over internal twistors, which leaves us with a collection of $4k$ bosonic and $4k$ fermionic delta functions, multiplied by the product of d-log of edge variables,

$$\int \prod_v \frac{1}{\mathrm{vol}\,\mathrm{GL}(1)} \prod_e \frac{d\alpha_e}{\alpha_e} \prod_{I=1}^{k} \delta^{4|4}\big(\sum_{a=1}^{n} C_{I,a}(\alpha)\mathcal{Z}_i\big)\,, \tag{9.8}$$

where v, e runs over all vertices and edges (internal and external), respectively. Here $C \in G(k,n)$ can be computed as follows. We first choose k external edges as "sinks" (i.e. directed inward) labeled by A (or B), and let the remaining $(n-k)$ external edges be "sources" (i.e. directed outward) labeled by a. Furthermore, we impose a direction on each edge so that every white vertex has one sink and two sources, and every black vertex has two sinks and one source. We then set $C_{A,B} = \delta_{A,B}$ to be the identity matrix, and compute $C_{A,a}$ by summing over all directed paths Γ from A to a, with each path evaluated as (minus) the product of edge variables along that path.

$$C_{A,a} = -\sum_{\Gamma \in \{A \to a\}} \prod_{e \in \Gamma} \alpha_e \,. \tag{9.9}$$

Equivalently, one can define the boundary measurements in terms of face variables,

$$C_{A,a} = -\sum_{\Gamma\in\{A\to a\}}\prod_{f\in\hat{\Gamma}}(-f) \tag{9.10}$$

where $\hat{\Gamma}$ is the set of faces enclosed by the counterclockwise completion of Γ, and the value of the graph is given by

$$\int \frac{1}{\mathrm{vol}\,\mathrm{GL}(1)}\prod_f \frac{df}{f}\prod_{I=1}^{k}\delta^{4|4}\big(\sum_{a=1}^{n}C_{I,a}(f)\mathcal{Z}_i\big)\,. \tag{9.11}$$

We note that there is an overall GL(1) redundancy for the face variables since the product of all face variables is unity.

9.1.2 Examples and operations on the diagrams

Given the general prescription, we first study a few simple examples, which are useful for defining some basic operations acting on momentum twistor diagrams.

The so-called "lollipop diagrams" are those with all external edges connected to monovalent black vertices. They evaluate to unity, and are interpreted as the MHV tree amplitude in momentum twistor space. Here we draw a 6 point example.

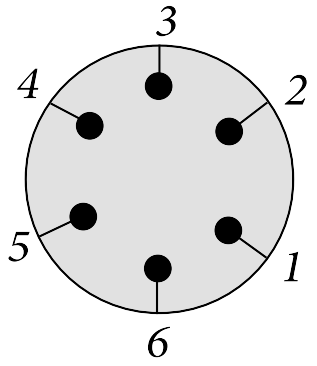

(9.12)

The simplest non-trivial diagram is given by two white vertices connected by an external edge, with $n = 4, k = 1$,

$$\int d^{3|4}\mathcal{Z}_I\, W(a,b,I)W(I,c,d) \tag{9.13}$$

$$= \int \frac{1}{\mathrm{vol}\,\mathrm{GL}(1)} \frac{d\alpha}{\alpha}\frac{d\beta}{\beta}\frac{d\gamma}{\gamma}\frac{d\delta}{\delta}\delta^{4|4}(\alpha\mathcal{Z}_a+\beta\mathcal{Z}_b+\gamma\mathcal{Z}_c+\delta\mathcal{Z}_d) \tag{9.14}$$

$$\equiv W(a,b,c,d) = \int d^{3|4}\mathcal{Z}_I\, W(b,c,I)W(I,d,a)\,. \tag{9.15}$$

where on the second line we have seen that the two collinear constraints together enforce the four twistors $\mathcal{Z}_a, \mathcal{Z}_b, \mathcal{Z}_c, \mathcal{Z}_d$ to be on a projective plane. This is manifestly cyclic, thus we can merge it as a single white vertex with four edges attached to it, which we denote as $W(a,b,c,d)$. We can also expand it along the other channel. These equivalences can be summarized diagrammatically as follows.

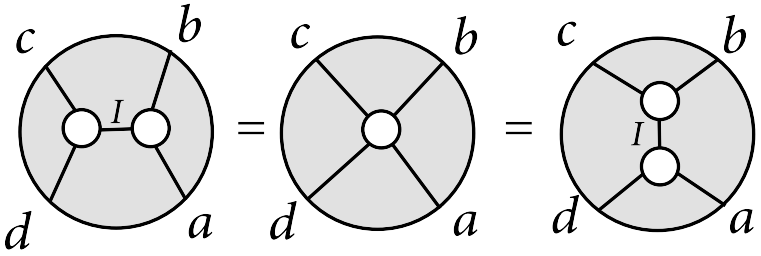

(9.16)

This is nothing but the simplest factorization diagram (i.e. with propagator put on-shell) one can access in momentum twistor space. Note that the two-particle channels of the MHV amplitude is invisible since it is stripped off, thus the simplest factorization would be that of a NMHV ($k = 1$) amplitude, divided by MHV amplitude. Consider the factorization pole $\langle i{-}1\, i\, j{-}1\, j\rangle = 0$, then we can perform the integrals in (9.13) using a reference twistor $\mathcal{Z}_*$ (the result is independent of $*$):

$$W(i{-}1,i,j{-}1,j) \tag{9.17}$$

$$= \delta(\langle i{-}1\, i\, j{-}1\, j\rangle)\frac{\delta^{0|4}(\langle\langle *, i{-}1, i, j{-}1, j\rangle\rangle)}{\langle *\, i{-}1\, i\, j{-}1\rangle\langle *\, i{-}1\, i\, j\rangle\langle *\, j{-}1\, j\, i{-}1\rangle\langle\, *\, j{-}1\, j\, i\rangle} \tag{9.18}$$

which is indeed the residue at the factorization pole $\langle i{-}1\, i\, j{-}1\, j\rangle = 0$ for any NMHV R-invariant with this pole.

Given the factorization diagram that depends on four twistors, we can obtain the full R-invariant, which depends on five twistors, by adding a *BCFW bridge*. The operation involves attaching a bridge with a black vertex and a white vertex to two adjacent external edges. Denoting the original diagram by $Y(1,\ldots,n)$, then adding the bridge $br(n,1)$, with white and black vertex attached to n and 1 respectively, amounts to

$$Y'(1,\ldots,n) = br(n,1)\cdot Y(1,\ldots,n) \equiv \int \frac{dc}{c}\, Y(1,\ldots,\hat{n}) \tag{9.19}$$

where $\hat{\mathcal{Z}}_n = \mathcal{Z}_n + c\,\mathcal{Z}_1$ and c is the edge variable associated with the bridge. Diagrammatically, this gives

$br(n,1)\cdot Y(1,\ldots,n) =$ 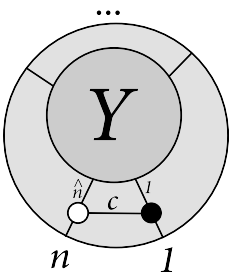

(9.20)

Now consider the four-point diagram $W(a,b,c,d)$ with a black lollipop $B(e)$. By adding a BCFW bridge $br(d,e)$, we obtain

$$br(d,e)\cdot(W(a,b,c,d)\otimes B(e)) = \int \frac{dc}{c}\, W(a,b,c,\hat{d}) = [a,b,c,d,e] \tag{9.21}$$

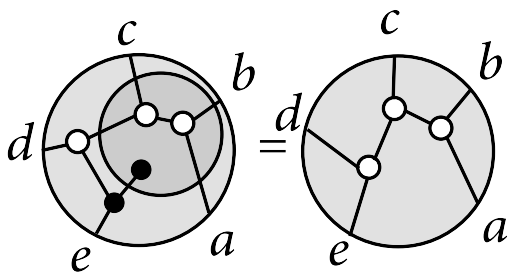

(9.22)

which is the on-shell diagram for an R-invariant that manifests the factorization channel $W(a, b, c, d)$. Furthermore, we can merge and re-expand the white vertices and obtain various different representations of the same R-invariant:

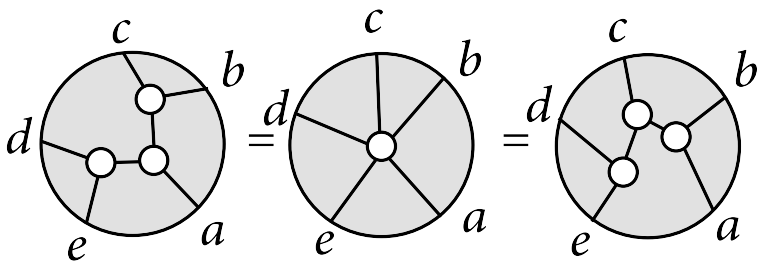

(9.23)

In addition to BCFW bridges, we can have operations that add or remove particles for on-shell diagrams. For a generic diagram with external particles $1, \ldots, n-1$, one can add an additional particle n which produces a diagram with n external particles. This corresponds to the "inverse soft limit", which has two cases, the *k-preserving* and *k-increasing* operations.

The k-preserving operation simply adds a lollipop. The external edge n is attached to a monovalent black vertex, and the evaluation of the diagram is unaffected.

$$Y'(1, \ldots, n) =$$

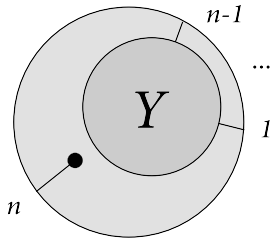

$$= Y(1, \ldots, n-1) \otimes B(n) = Y(1, \ldots, n-1) \tag{9.24}$$

The k-increasing operation is more interesting. It produces an R-invariant factor (thus increase the k-charge by 1) which involves the additional leg n and four

neighboring legs $n{-}2, n{-}1, 1, 2$, and it also involves shifting the two legs $n{-}1, 1$,

$$Y'(1,\ldots,n) \;=\; [n{-}2, n{-}1, n, 1, 2]\, Y(\hat{1},\ldots,\widehat{n{-}1}) \tag{9.25}$$

$$= \tag{9.26}$$

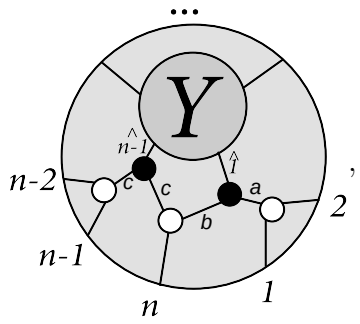

where the shifted variables are $\widehat{n{-}1} = (n{-}2, n{-}1) \cap (n, 1, 2)$ and $\hat{1} = (1, 2) \cap (n{-}2, n{-}1, n)$. As justification for the evaluation of this diagram, we argue that the twistor $\mathcal{Z}_{\hat{1}}$ at the edge labeled $\hat{1}$ indeed evaluates to the twistor $(1, 2) \cap (n{-}2, n{-}1, n)$ as claimed. We first recognize that $\mathcal{Z}_{\hat{1}}, \mathcal{Z}_a, \mathcal{Z}_b$ are projectively identical, since they are connected to a black vertex. Furthermore, $\mathcal{Z}_a$ must lie on the line $(1, 2)$ since $a, 1, 2$ are connected to a white vertex, and $\mathcal{Z}_b$ must lie on the plane $(n{-}1, n{-}2, n)$ since b is connected to $n{-}1, n{-}2, n$ via a sequence of white vertices (the black vertex appearing along this sequence does not affect our argument). The desired result follows. Furthermore, we justify the appearance of the R-invariant. We first observe that, compared to Y, the k-charge of the diagram is higher by 1. Indeed, the diagram introduces 3 new white vertices, 2 new black vertices, and 6 new internal lines, so that $\Delta k = \Delta n_W + 2\Delta n_B - \Delta n_I = 3 + 2 \times 2 - 6 = 1$. Moreover, the only possible R-invariant that could appear is $[n{-}2, n{-}1, n, 1, 2]$. If we look at the shifted variable $\hat{1} = (1, 2) \cap (n{-}2, n{-}1, n)$ that appears in Y, we notice that there are two ways of expanding the shift. Namely,

$$\hat{\mathcal{Z}}_1 \;=\; \mathcal{Z}_1 \langle 2, n{-}2, n{-}1, n\rangle - \mathcal{Z}_2 \langle 1, n{-}2, n{-}1, n\rangle \tag{9.27}$$

$$\hat{\mathcal{Z}}_1 \;=\; \mathcal{Z}_{n-2} \langle 2, 1, n{-}1, n\rangle + \mathcal{Z}_{n-1} \langle 2, n{-}2, 1, n\rangle + \mathcal{Z}_n \langle 2, n{-}2, n{-}1, 1\rangle \tag{9.28}$$

These two expansions must be equivalent. For the bosonic components this is true by the Schouten identity. However, for the fermionic components there is no such identity. The only way for the two expansions to agree is if they are both evaluated on the support of the fermionic delta function

$$\delta^{0|4}(\eta_1 \langle 2, n{-}2, n{-}1, n\rangle + \text{cyclic}) \tag{9.29}$$

This is precisely the delta function provided by the R-invariant that appears in the k-increasing operation, thus justifying our claim. Note that the R-invariant required by the other shift $\widehat{n{-}1}$ is identical, so only one R-invariant is needed.

The opposite operations are those that remove a particle from the diagrams of the form above. Correspondingly they are *k-preserving* and *k-decreasing soft limits*, respectively.

$$\begin{aligned} Y'(1,\ldots,n{-}1) &= Y(1,\ldots,\mathcal{Z}_n \to \mathcal{Z}_{n-1})\,, \\ Y'(1,\ldots,n{-}1) &= \int d^{3|4}\mathcal{Z}_n Y(1,\ldots,n)\,. \end{aligned} \tag{9.30}$$

9.2 Boundary diagrams

We now discuss the diagrammatic representation of BCFW terms from Section 8.3. We begin with the B term, which is the residue at $w \to \infty$. This is nothing but the k-preserving soft limit (9.24) given by a lower point diagram with a lollipop on particle n.

B = 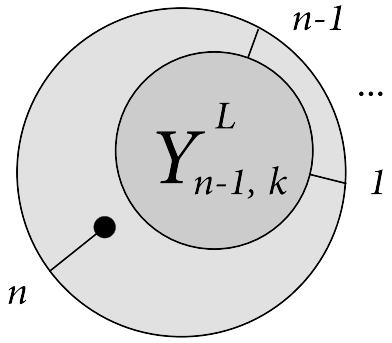

(9.31)

9.3 Factorization diagrams

Now we move to the factorization term corresponding to the pole $\langle j{-}1\, j\, \hat{n}\, 1\rangle = 0$. Recall that we have worked out the simplest cases with $k = 1$ in (9.17), where both left and right part are unity MHV amplitudes. In general, by connecting the left and right amplitudes with $W(j{-}1, j, n, 1)$ we obtain the factorization limit,

$$
\begin{aligned}
& Y_L(\hat{j}, j, \ldots, n)\, W[j{-}1, j, n, 1]\, Y_R(1, \ldots, j{-}1, \hat{j}) \\
= \quad & \frac{\delta(\langle j{-}1\, j\, n\, 1\rangle)\, \delta^{0|4}(\langle\langle *, i{-}1, i, j{-}1, j\rangle\rangle)}{\langle * \, i{-}1\, i\, j{-}1\rangle\langle * \, i{-}1\, i\, j\rangle\langle * \, j{-}1\, j\, i{-}1\rangle\langle \, * \, j{-}1\, j\, i\rangle}\, Y_L(\hat{j}, j, \ldots, n)\, Y_R(1, \ldots, j{-}1, \hat{j})
\end{aligned}
$$

where $\hat{j} = (j{-}1j) \cap (*n1) = (n1) \cap (*j{-}1j)$ is exactly the twistor corresponding to the intersection of the lines $(j{-}1j)$ and $(n1)$, as shown in the diagram of (9.33). The diagram is clearly independent of the reference $*$, and note that at this stage it is symmetric under the exchange of left and right amplitude (including $(j{-}1, j) \leftrightarrow (n, 1)$). The corresponding contribution to the FAC term can be obtained by attaching

the BCFW bridge $br(n,n{-}1)$ to the factorization limit,

$$\begin{aligned} & br(n,n{-}1)\cdot(Y_L(\hat{j},j,\ldots,n)\,W[j{-}1,j,n,1]\,Y_R(1,\ldots,j{-}1,\hat{j})) \\ = \quad & [j{-}1,j,n{-}1,n,1]Y_L(\hat{j},j,\ldots,\hat{n}_j)\,Y_R(1,\ldots,j{-}1,\hat{j}) \end{aligned} \tag{9.32}$$

where we have $\hat{j} = (j{-}1,j)\cap(n{-}1,n,1)$ and $\hat{n}_j = (n{-}1,n)\cap(1,j{-}1,j)$, which are the two intersection points in the diagram. Summing over the relevant poles gives us the full FAC term.

$$\text{FAC} = \sum_{j=3}^{n-2}$$

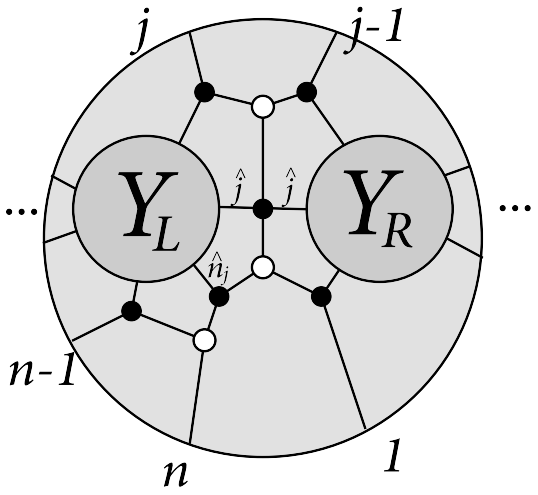

(9.33)

Given that this is our first full-fledged example, we explain it carefully here. Rather than directly computing the diagram, it is more insightful to see why the result is correct, as we did for the k-increasing operation. For instance, we can check that the line $\hat{n}_j$ and the two lines $\hat{j}$ have the correct shifts. Using the rules from before, we find that $\hat{n}_j$ lies on the line $(n{-}1,n)$ and the plane $(1,j{-}1,j)$, which implies that $\hat{n}_j = (j{-}1,j)\cap(1,n{-}1,n)$. Similarly for $\hat{j}$ on $(j{-}1,j)$ and $(n,n{-}1,1)$, thus $\hat{j} = (j{-}1,j)\cap(n{-}1,n,1)$. Furthermore, it is easy to see that the k-charge of the full diagram is given by $k = k_L + k_R + 1$ as required by the FAC term. We denote the sub-diagram with vertices or edges in the diagram not already present in Y_L or Y_R as Δ, then its k-charge is $\Delta k = k - k_L - k_R = \Delta n_W + 2\Delta n_B - \Delta n_I = 3 + 2\times 7 - 16 = 1$. Here recall that the counting only applies to trivalent graphs. Since there is a quartic

vertex at the center of the diagram, we should split that vertex into two cubic vertices, which introduces one new black vertex and one new internal line as shown below.

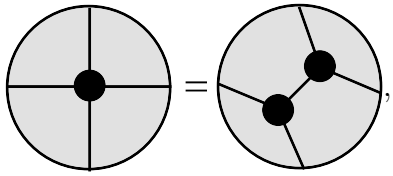

(9.34)

The fact that $\Delta k = 1$ implies that the diagram evaluates to Y_L times Y_R with an extra R-invariant. As before, we claim that the R-invariant that appears in FAC is the only one it could be, because the fermionic components of $\hat{n}_j$ and $\hat{j}$ only make sense on the support of its fermionic delta function. This concludes our justification of the FAC diagram.

9.4 Forward limit diagrams

We now turn to the forward limit term. For the BCFW shift $\hat{\mathcal{Z}}_n = \mathcal{Z}_n + w\mathcal{Z}_{n-1}$, the FL contribution comes from the residue at $\langle AB1\hat{n}\rangle \to 0$ and is given by $Y^{(L-1)}_{n+2,k+1}(1,\ldots,\hat{n},A,B;\{\ell\}/(AB))$. The diagrammatic representation can be expressed as follows,

$$\text{FL} = \int_{GL(2)}$$

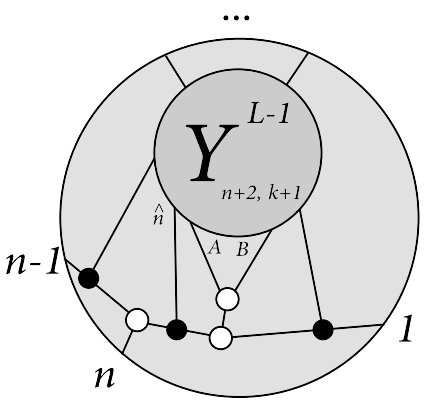

. (9.35)

where the $GL(2)$ integral sign is just there to remind us that there is a $GL(2)$ residue

we must take, which we discuss momentarily. From the diagram it is clear that $\hat{n}$ lies on both the line $(n{-}1, n)$ and the plane $(1, A, B)$, hence $\hat{n} = (n{-}1, n) \cap (1, A, B)$, which gives the required shift. Furthermore, the k-charge of the diagram is given by that of the sub-diagram Y plus $\Delta k = k{-}k_Y = \Delta n_W{+}2\Delta_B{-}\Delta n_I = 3{+}2{\times}3{-}10 = -1$. The minus sign in the degree means that prior to integrating out the fermionic parts of A, B, we should find one R-invariant multiplied by Y. This R-invariant must be $[A, B, 1, n{-}1, n]$ so that the fermionic parts of the shift $\hat{n}$ are well-defined.

One main novelty of the diagrammatic method is that the $GL(2)$ residue can be performed diagrammatically. However, in order to do so, we must first apply BCFW recursion on the sub-diagram $Y^{L-1}_{n+2,k+1}$. In particular, we apply the shift $\mathcal{Z}_B \to \mathcal{Z}_B + w\mathcal{Z}_1$. This gives a boundary term which vanishes, a factorization channel FL-FAC, and a forward limit FL-FL.

For FL-FAC, we have

$$\text{FL-FAC} = \sum_{j=3}^{n-1} \int_{GL(2)} \qquad (9.36)$$

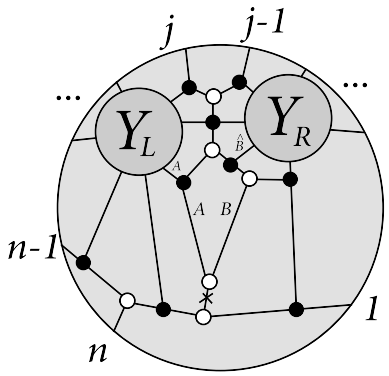

where we sum over all left and right sub-diagrams for which $L_L + L_R = L - 1$, $k_L + k_R = k$, and $n_L + n_R = n + 4$. The boundary case $\mathcal{Z}_j = \hat{\mathcal{Z}}_n$ vanishes after doing the fermionic loop integrals, and so is not included in the summation. Now we can perform the $GL(2)$ integral. Recall that the $GL(2)$ residue takes $\mathcal{Z}_A, \mathcal{Z}_B \to (A, B) \cap (1, n-1, n)$. The point $(A, B) \cap (1, n-1, n)$ can be found on the diagram, and is labeled by a cross. When taking the residue, the line A coming out of the left sub-diagram must be cut and reconnected to the crossed line. Furthermore, a

quick look at the diagram shows that $\hat{\mathcal{Z}}_B = (1, B) \cap (j-1, j, A)$, which also becomes $\hat{\mathcal{Z}}_B \to (A, B) \cap (1, n-1, n)$ when taking the residue. So the $\hat{B}$ line must also be reconnected to the cross. This completes the $GL(2)$ residue. The advantage of using diagrams is that we did not have to do this residue analytically. The final form of the FL-FAC term is thus given by

$$\text{FL-FAC} = \sum_{j=3}^{n-1}$$

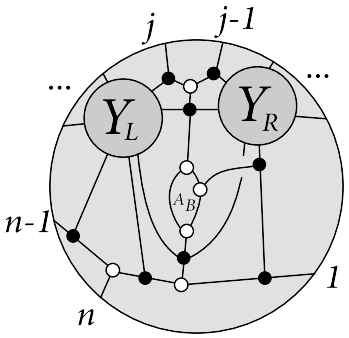

$$= \sum_{j=3}^{n-1}$$

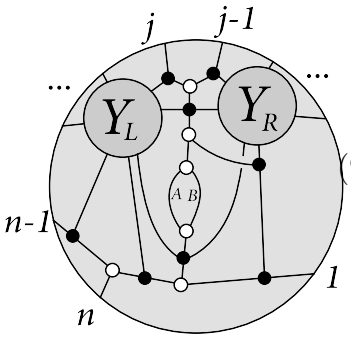

(9.37)

where the second diagram is obtained from the first by merge and expansion of white vertices.

It is important to note that the diagram degenerates for the boundary case with $j = n-1$. In our diagram above, it appears as if the point j appears twice since $n-1$ is identical to j, but this is obviously not the right interpretation. Indeed, we should modify the diagram slightly to account for this case by identifying the external points j and $n-1$. In other words, the line that connects Y_L to the external edge $n-1$ should be merged with the line that connects Y_L to j. We also merge the corresponding two black vertices, and the result is

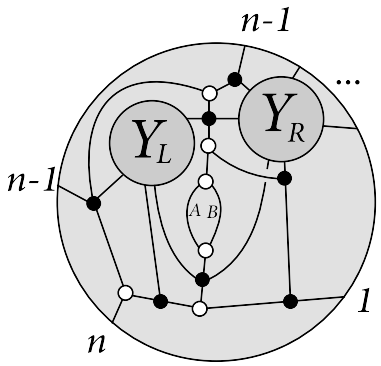

(9.38)

We notice that the process of doing the $GL(2)$ integral introduces one degree of non-planarity in the diagram. Although this may seem peculiar, we can still do boundary measurements in the usual way. Furthermore, we see that the loop variables $\mathcal{Z}_A, \mathcal{Z}_B$ have been isolated in a bubble-like structure. This is convenient for writing down the loop integrand, as we show in a moment. In future work, we show that the non-planarity appearing in the forward limit can always be removed in a systematic way without changing the value of the diagram.

We postpone discussion of Fl-FL to Section 9.7.

9.5 Tree diagrams

We now present computations of tree amplitudes by the diagrammatic recursion relations. Since we are working at tree level, only the boundary and factorization terms are needed. Detailed examples for NMHV and N^{2}MHV are provided.

9.5.1 NMHV tree

We wish to obtain diagrammatically the Yangian invariant $Y_{n,k=1}(\mathcal{Z}_1, .., \mathcal{Z}_n)$ for NMHV trees, where we have suppressed writing the $L = 0$ superscript. Recall that NMHV trees factorize as the product of two MHV trees. By representing MHV amplitudes as a series of lollipops, the factorization term becomes

$$\text{FAC} = \sum_{j=3}^{n-2}$$

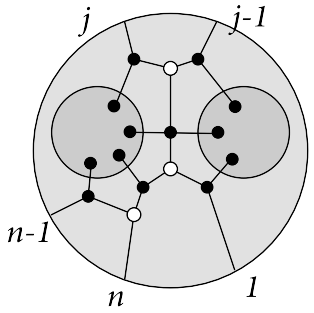

$$= \sum_{j=3}^{n-2}$$

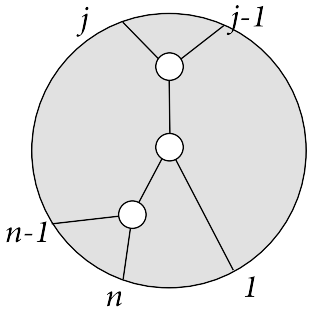

(9.39)

In going from the first diagram to the second, we deleted any lollipops attached to internal lines, and any vertex attached to only two lines. Recall from our earlier discussion that this diagram is just the R-invariant $[1, j{-}1, j, n{-}1, n]$. The BCFW recursion is therefore

$$Y_{n,k=1}(1,...,n) = Y_{n-1,k=1}(1,...,n-1) + \sum_{j=3}^{n-2}[1, j{-}1, j, n{-}1, n] \tag{9.40}$$

As is well known, the following closed form expression for $Y_{n,k=1}$ satisfies the recursion relation.

$$Y_{n,k=1}(1,...,n) = \sum_{i<j}[1, i{-}1, i, j{-}1, j] \ . \tag{9.41}$$

9.5.2 N^{2}MHV trees

We now wish to obtain diagrams for N^{2}MHV trees, which factorize as the product of MHV and NMHV. Consider for example the 6 point case where the B term vanishes. A moment's thought reveals that there is only one FAC diagram that contributes, which contains 5 point NMHV tree on the left and 3-point MHV tree on the right.

FAC = 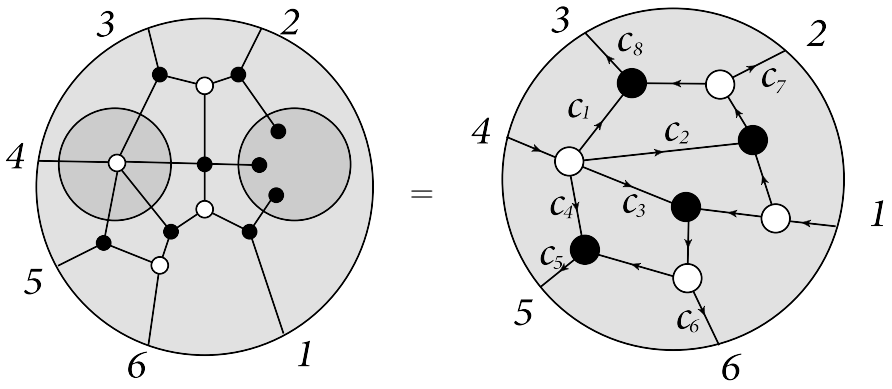

(9.42)

We can then compute this diagram by performing boundary measurements. Since the diagram contains $n_F = 9$ faces, the number of integration variables must be $n_F - 1 = 8$, so we can gauge fix some of the bridge variables until only 8 are left. The

diagram above shows one particular choice of leftover bridge variables. The explicit formula for this diagram is thus given by

$$\begin{aligned} \text{FAC} &= \int \frac{dc_1 \ldots dc_8}{c_1 \ldots c_8} \delta^{4|4}(\mathcal{Z}_1 - c_5\mathcal{Z}_5 - c_6\mathcal{Z}_6 - c_7\mathcal{Z}_2 - c_8\mathcal{Z}_3) \qquad (9.43) \\ &\times \quad \delta^{4|4}(\mathcal{Z}_4 - c_1c_8\mathcal{Z}_3 - c_2(c_7\mathcal{Z}_2 + c_8\mathcal{Z}_3) - c_3(c_5\mathcal{Z}_5 + c_6\mathcal{Z}_6) - c_4c_5\mathcal{Z}_5) \qquad (9.44) \end{aligned}$$

On the support of the first delta function, it is easy to see that

$$\begin{aligned} c_5\mathcal{Z}_5 + c_6\mathcal{Z}_6 &\sim (56) \cap (123) \equiv \mathcal{Z}'_5 \\ c_7\mathcal{Z}_2 + c_8\mathcal{Z}_3 &\sim (23) \cap (156) \equiv \mathcal{Z}'_2 \end{aligned} \qquad (9.45)$$

Substituting these into the second delta function and rescaling the integration variables appropriately gives

$$\begin{aligned} \text{FAC} = \int \frac{dc_1 \ldots dc_8}{c_1 \ldots c_8} &\delta^{4|4}(\mathcal{Z}_1 - c_5\mathcal{Z}_5 - c_6\mathcal{Z}_6 - c_7\mathcal{Z}_2 - c_8\mathcal{Z}_3) \\ &\times\delta^{4|4}(\mathcal{Z}_4 - c_1\mathcal{Z}_3 - c_2\mathcal{Z}'_2 - c_3\mathcal{Z}'_5 - c_4\mathcal{Z}_5)\,. \end{aligned} \qquad (9.46)$$

The integral is now trivial to perform. It just gives us two R-invariants.

$$\begin{aligned} Y_{6,k=2}(\mathcal{Z}_1, ..., \mathcal{Z}_6) &= [3,4,5,2',5'][1,2,3,5,6] \\ &= [3,4,5,(23)\cap(156),(56)\cap(123)][1,2,3,5,6] \end{aligned} \qquad (9.47)$$

As mentioned above, in practice it is usually not productive to work out all the boundary measurements step by step and identify all proper shifts like $\mathcal{Z}'_2$ and $\mathcal{Z}'_5$ on the support of the delta functions; the shifts can be identified more quickly by looking at the diagram and remembering the role of the black and white vertices. From our

general rules and examples, it is straightforward to work out (reduced) momentum twistor diagrams for all tree-level amplitudes/Wilson loops.

9.6 One loop diagrams

We now apply our diagrammatic method to compute one-loop integrands, where the forward limit contribution is needed. One important advantage of our diagrams is that it bypasses the technical difficulties of performing GL(2) integrals in the forward limit, and the result can be read off from the diagram without ever having to the do the integral by hand. We begin by studying MHV integrands. We then move on to general k whereby the Kermit representation [63] is derived diagrammatically.

9.6.1 One loop diagrams for n-point MHV

Consider the one-loop n-point MHV integrand. In this case, only the B and FL-FAC terms contribute, where the latter involves a factorization into two MHV trees. It follows that

$$\text{FL-FAC} = \sum_{j=3}^{n-1}$$

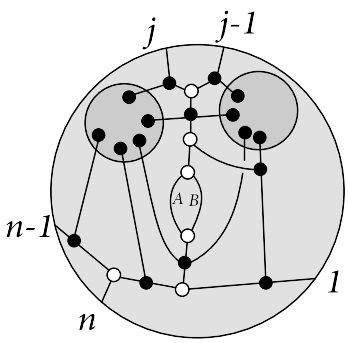

$$= \sum_{j=3}^{n-1}$$

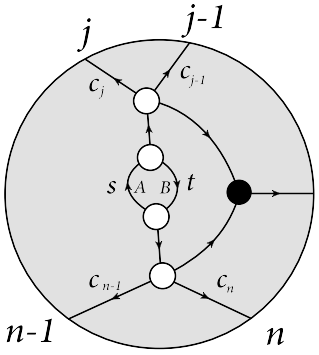

(9.48)

In the boundary case where $j = n-1$, we identify the external lines j and $n-1$ as

follows.

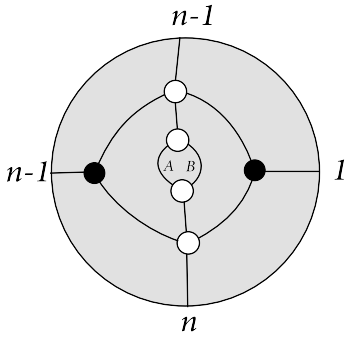

(9.49)

Any one of these diagrams contains $n_F = 7$ faces, and so must involve $n_F - 1 = 6$ integration variables. As a general rule, we will always attach two extra $GL(1)$ gauges for every forward limit we take, so this reduces the diagram to a 4-form. But let us keep all 6 variables for now. There are no delta functions since the k-charge of this diagram is 0 (i.e. there are no arrows going into the diagram). So we have,

$$\frac{ds}{d}\frac{dt}{t}\,\frac{dc_{j-1}}{c_{j-1}}\frac{dc_j}{c_j}\frac{dc_{n-1}}{c_{n-1}}\frac{dc_n}{c_n} \tag{9.50}$$

By following the arrows in the diagram and doing the usual boundary measurements, we can rewrite $c_1, ..., c_4$ in terms of $\mathcal{Z}_A, \mathcal{Z}_B$.

$$\begin{aligned} \mathcal{Z}_A + t\mathcal{Z}_B &= \mathcal{Z}_1 + c_{j-1}\mathcal{Z}_{j-1} + c_j\mathcal{Z}_j \\ \mathcal{Z}_B + s\mathcal{Z}_A &= \mathcal{Z}_1 + c_{n-1}\mathcal{Z}_{n-1} + c_n\mathcal{Z}_n \end{aligned} \tag{9.51}$$

It follows that

$$\text{FL-FAC} = \frac{1}{\text{Vol}[GL(1)]^2}\frac{ds}{s}\frac{dt}{t}\; d^4\ell_{AB}\sum_{j=3}^{n-1} K_{AB}(1, n{-}1, n; 1, j{-}1, j) \tag{9.52}$$

where we have abbreviated $d^4\ell_{AB} = \langle ABd^2A\rangle \langle ABd^2B\rangle$, and we define the Kermit

$$K_{AB}(1, n{-}1, n; 1, j{-}1, j) \tag{9.53}$$

$$\equiv \frac{\langle AB(1, n{-}1, n) \cap (1, j{-}1, j)\rangle^2}{\langle AB1\ n{-}1\rangle \langle AB1\ n\rangle \langle AB\ n{-}1\ n\rangle \langle AB1\ j{-}1\rangle \langle AB1\ j\rangle \langle AB\ j{-}1\ n\rangle} \tag{9.54}$$

We can now gauge fix $s, t \to 1$ to obtain

$$\text{FL-FAC} = d^4\ell_{AB} \sum_{j=3}^{n-1} K_{AB}(1, n{-}1, n; 1, j{-}1, j) \tag{9.55}$$

This last step is universal, so we will often omit writing the $d\log s$ and $d\log t$ factors. Thus the full BCFW recursion for one-loop MHV gives

$$\begin{aligned} Y^{L=1}_{n,k=0}(\mathcal{Z}_1, ..., \mathcal{Z}_n) &= \text{B} + \text{FL-FAC} \\ &= Y^{L=1}_{n-1,k=0}(1, ..., n{-}1) + d^4\ell_{AB} \sum_{j=3}^{n-1} K_{AB}(1, n-1, n; 1, j-1, j) \end{aligned} \tag{9.56}$$

Solving this relation in closed form gives the well-known Kermit form of one-loop MHV,

$$Y^{L=1}_{n,k=0}(\mathcal{Z}_1, ..., \mathcal{Z}_n) = d^4\ell_{AB} \sum_{i<j} K_{AB}(1, i{-}1, i; 1, j{-}1, j) \tag{9.57}$$

It is well known that each Kermit diagram is given by $d\log c_{i-1}\, d\log c_i\, d\log c_{j-1}\, d\log c_j$ which corresponds to a cell of the one-loop MHV amplituhedron, and the Kermit expansion provides a triangulation of the amplituhedron.

9.6.2 One loop Kermit expansion

For one-loop, in addition to B and FAC terms, only the FL-FAC term contributes with both sub-amplitudes as trees. This gives a generalized Kermit expansion,

FL-FAC = 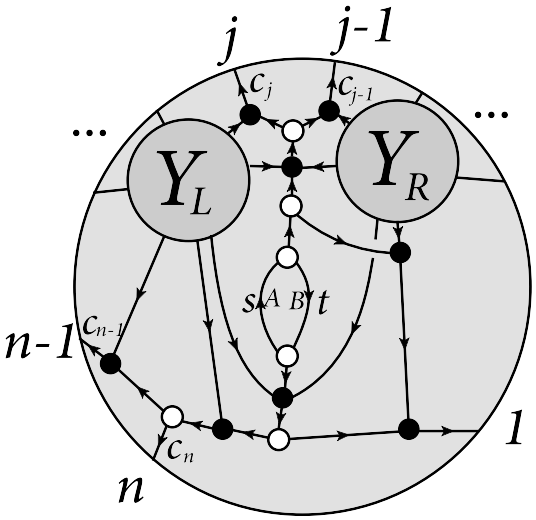

(9.58)

$$= \sum_{j=3}^{n-1} \frac{dc_{j-1}dc_j dc_{n-1}dc_n}{c_{j-1}c_j c_{n-1}c_n} Y^{L_L}_{n_L,k_L}(\hat{\mathcal{Z}}_j, \mathcal{Z}_j, ..., \mathcal{Z}_{n-1}, \hat{\mathcal{Z}}_n, \hat{\mathcal{Z}}_{nAB}) Y^{L_R}_{n_R,k_R}(\mathcal{Z}_1, ..., \mathcal{Z}_{j-1}, \hat{\mathcal{Z}}_j, \hat{\mathcal{Z}}_{nAB}) \tag{9.59}$$

where the loop variables are given by

$$\begin{aligned} \mathcal{Z}_A + t\mathcal{Z}_B &= \mathcal{Z}_1 + c_{j-1}\mathcal{Z}_{j-1} + c_j\mathcal{Z}_j \\ \mathcal{Z}_B + s\mathcal{Z}_A &= \mathcal{Z}_1 + c_{n-1}\mathcal{Z}_{n-1} + c_n\mathcal{Z}_n \end{aligned} \tag{9.60}$$

and $\hat{\mathcal{Z}}_j = (j-1, j) \cap (1, A, B)$, $\hat{\mathcal{Z}}_{nAB} = (A, B) \cap (1, n-1, n)$ and $\hat{\mathcal{Z}}_n = (n-1, n) \cap (1, A, B)$. It follows that the $d\log c$ form just becomes a Kermit, so we get

$$\begin{aligned} \text{FL-FAC} &= d^4\ell_{AB} \sum_{j=3}^{n-1} K_{AB}(1, j-1, j; 1, n-1, n) \\ &\quad \times Y^{L_L}_{n_L,k_L}(\hat{\mathcal{Z}}_j, \mathcal{Z}_j, ..., \mathcal{Z}_{n-1}, \hat{\mathcal{Z}}_n, \hat{\mathcal{Z}}_{nAB}) Y^{L_R}_{n_R,k_R}(\mathcal{Z}_1, ..., \mathcal{Z}_{j-1}, \hat{\mathcal{Z}}_j, \hat{\mathcal{Z}}_{nAB}) \end{aligned}$$

9.6.3 One loop 5 point NMHV

Here we present a compute calculation of the one loop 5-point NMHV integrand $Y^{L=1}_{5,k=1}$, which requires FAC and FL-FAC contributions.

The FAC term involves only one diagram and is given by the factorization with 4-point 1-loop MHV on the left and 3-point MHV tree on the right.

FAC = 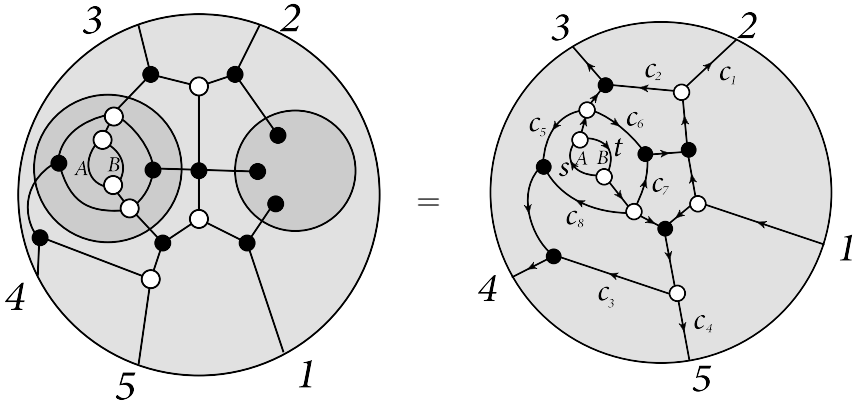

(9.61)

This graph has $n_F = 11$ faces, so it should have $n_F - 1 = 10$ integration variables. But remember that we mod out the s, t using two $GL(1)$ gauges so we really only have 8 integrations. There is only one arrow going into the diagram, which means that the diagram is NMHV, so there should be one delta function $\delta^{4|4}(...)$. Indeed, the diagram is given by

$$\text{FAC} = \int \frac{dc_1 \ ... \ dc_8}{c_1 \ ... \ c_8} \delta^{4|4}(\mathcal{Z}_1 - c_1\mathcal{Z}_2 - c_2 Z_3 - c_3\mathcal{Z}_4 - c_4\mathcal{Z}_5) \tag{9.62}$$

Doing the boundary measurements for the loop variables gives

$$\begin{aligned} \mathcal{Z}_A + t\mathcal{Z}_B &= \mathcal{Z}_3 + c_5\mathcal{Z}_4 + c_6(c_1\mathcal{Z}_2 + c_2\mathcal{Z}_3) \\ \mathcal{Z}_B + s\mathcal{Z}_A &= (c_3\mathcal{Z}_4 + c_4\mathcal{Z}_5) + c_7(c_1\mathcal{Z}_2 + c_2\mathcal{Z}_3) + c_8\mathcal{Z}_4 \end{aligned} \tag{9.63}$$

On the support of the delta function, we see that

$$\begin{aligned} c_1\mathcal{Z}_2 + c_2\mathcal{Z}_3 &\sim (23)\cap(145) \equiv \mathcal{Z}_2' \\ c_3\mathcal{Z}_4 + c_4\mathcal{Z}_5 &\sim (45)\cap(123) \equiv \mathcal{Z}_4' \end{aligned} \tag{9.64}$$

After rescaling some of the integration variables we get

$$\begin{aligned} \mathcal{Z}_A + t\mathcal{Z}_B &= \mathcal{Z}_3 + c_5\mathcal{Z}_4 + c_6\mathcal{Z}_2' \\ \mathcal{Z}_B + s\mathcal{Z}_A &= \mathcal{Z}_4' + c_7\mathcal{Z}_2' + c_8\mathcal{Z}_4 \end{aligned} \tag{9.65}$$

This looks just like the Kermit, so the $c_5, ..., c_8$ part of the form would just give a Kermit. The remaining variables $c_1, ..., c_4$ can be integrated trivially over the delta function to yield the R-invariant $[1, 2, 3, 4, 5]$. The result is

$$\text{FAC} = d^4\ell_{AB} K_{AB}(432'; 44'2')[1, 2, 3, 4, 5] \tag{9.66}$$

which simplifies to

$$\text{FAC} = d^4\ell_{AB} \frac{\delta^{0|4}(\eta_1 \langle 2345\rangle + \eta_2 \langle 3451\rangle + \eta_3 \langle 4512\rangle + \eta_4 \langle 5123\rangle + \eta_5 \langle 1234\rangle)}{\langle 1245\rangle \langle 1235\rangle \langle AB23\rangle \langle AB34\rangle \langle AB45\rangle \langle AB1(45)\cap(123)\rangle} \tag{9.67}$$

Now let us work on the FL-FAC term. There are two diagrams FL-FAC = FL-FAC-1 + FL-FAC-2. The first diagram FL-FAC-1 is the forward limit of a factorization channel with 5-point NMHV tree on the left and 4-point MHV tree on the

right.

FL-FAC-1 = 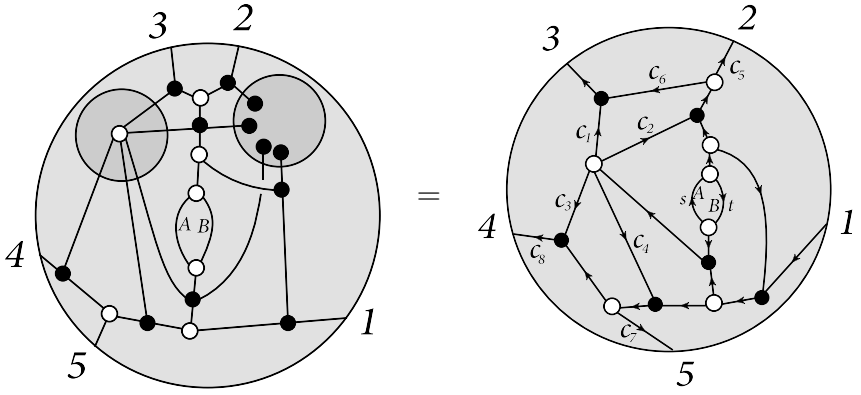

(9.68)

Again, this diagram has $n_F = 11$ faces, so we should find 8 integration variables and one delta function $\delta^{4|4}(...)$. We find

$$\text{FL-FAC-1} = \int \frac{dc_1 \ ... \ dc_8}{c_1 \ ... \ c_8} \delta^{4|4}((\mathcal{Z}_1 - c_7\mathcal{Z}_5 - c_8\mathcal{Z}_4) - \xi) \tag{9.69}$$

The loop variables are given by

$$\begin{aligned} \mathcal{Z}_A + s\mathcal{Z}_B &= c_5\mathcal{Z}_2 + c_6\mathcal{Z}_3 + (c_7\mathcal{Z}_5 + c_8\mathcal{Z}_4 + \xi) \\ \mathcal{Z}_B + t\mathcal{Z}_A &= \xi \end{aligned} \tag{9.70}$$

where

$$\xi = c_1\mathcal{Z}_3 + c_2(c_5\mathcal{Z}_2 + c_6\mathcal{Z}_3) + c_3c_8\mathcal{Z}_4 + c_4(c_7\mathcal{Z}_5 + c_8\mathcal{Z}_4) \tag{9.71}$$

On the support of the delta function, we can rewrite the loop variables as

$$\begin{aligned} \mathcal{Z}_A + s\mathcal{Z}_B &= \mathcal{Z}_1 + c_5\mathcal{Z}_2 + c_6\mathcal{Z}_3 \\ \mathcal{Z}_B + t\mathcal{Z}_A &= \mathcal{Z}_1 - c_7\mathcal{Z}_5 - c_8\mathcal{Z}_4 \end{aligned} \tag{9.72}$$

Using these new loop variable expressions, we find the following shifts

$$\begin{aligned}
\mathcal{Z}_1 - c_7\mathcal{Z}_5 - c_8\mathcal{Z}_4 &\sim (AB)\cap(145) \equiv \mathcal{Z}''_A \\
c_7\mathcal{Z}_5 + c_8\mathcal{Z}_4 &\sim (45)\cap(1AB) \equiv \mathcal{Z}''_4 \\
c_5\mathcal{Z}_2 + c_6\mathcal{Z}_3 &\sim (23)\cap(1AB) \equiv \mathcal{Z}''_2
\end{aligned} \tag{9.73}$$

Substituting these into the delta function and rescaling the integration variables appropriately gives us

$$\text{FL-FAC-1} = \int \frac{dc_1 \ldots dc_8}{c_1 \ldots c_8}\delta^{4|4}(\mathcal{Z}''_A + c_1\mathcal{Z}_3 + c_2\mathcal{Z}''_2 + c_3\mathcal{Z}_4 + c_4\mathcal{Z}''_4) \tag{9.74}$$

Like before, the loop variables take on the Kermit form, so the $c_5, ..., c_8$ part of the form just gives us a Kermit, and the remaining integrals can be integrated over the delta function to give an R-invariant. The result is

$$\begin{aligned}
\text{FL-FAC-1} &= d^4\ell_{AB}K_{AB}(123;145)[3,4,A'',4'',2''] \\
&= d^4\ell_{AB}\frac{\delta^{0|4}(\eta_1\langle 2345\rangle + \eta_2\langle 3451\rangle + \eta_3\langle 4512\rangle + \eta_4\langle 5123\rangle + \eta_5\langle 1234\rangle)}{\langle 2345\rangle\langle AB12\rangle\langle AB23\rangle\langle 1345\rangle\langle AB15\rangle\langle AB4(15)\cap(234)\rangle}
\end{aligned} \tag{9.75}$$

Finally, the last term FL-FAC-2 is given as the forward limit of the factorization with 4-point MHV tree on the left and 5-point NMHV tree on the right. We just give the

result here

FL-FAC-2 = 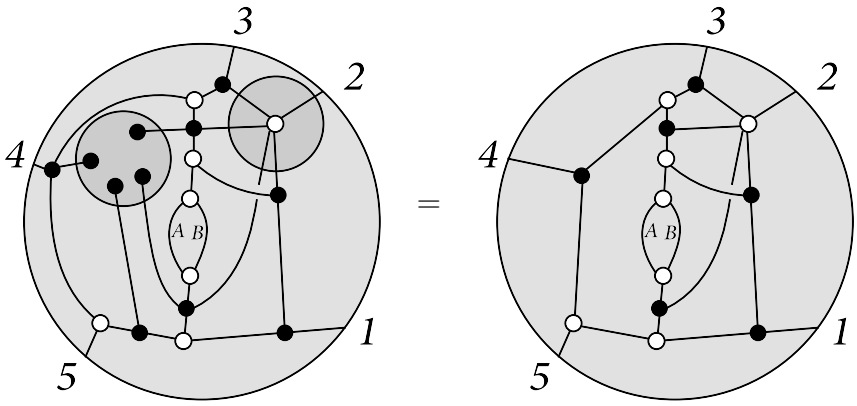

(9.76)

which is equal to

$$\text{FL-FAC-2} = d^4\ell_{AB} K_{AB}(134;145)[1,2,3,(34)\cap(1AB),(AB)\cap(145)] \tag{9.77}$$

$$= \quad d^4\ell_{AB} \frac{\delta^{0|4}(\eta_1\langle 2345\rangle + \eta_2\langle 3451\rangle + \eta_3\langle 4512\rangle + \eta_4\langle 5123\rangle + \eta_5\langle 1234\rangle)\langle AB14\rangle^2}{\langle 1234\rangle\langle AB12\rangle\langle AB34\rangle\langle AB45\rangle\langle AB15\rangle\langle AB1(45)\cap(123)\rangle\langle AB4(51)\cap(234)\rangle}$$

The final result for the 5-point 1-loop NMHV integrand is the sum of all the contributions

$$Y^{L=1}_{5,k=1}(\mathcal{Z}_1,...,\mathcal{Z}_5) = \text{FAC} + \text{FL-FAC-1} + \text{FL-FAC-2}. \tag{9.78}$$

These diagrams also give the three C, D-matrices for three cells of the amplituhedron. It is already non-trivial to see how the three cells provide a triangulation of this one-loop five-point NMHV case.

9.7 Two loop diagrams

At higher loops, the only new feature one would encounter is the iteration of forward limits, and the general structure is very clear: there are L bubbles at L loops. Here

we restrict ourselves to two loops. The B, FAC and FL-FAC contributions are of the same form as before. The new contribution is the FL-FL term, which involves yet another $GL(2)$ residue. Let us call the second loop variable CD. We begin by drawing the diagram corresponding to the two forward limits,

FL-FL (9.79)

$$= \int_{GL(2)}^{AB,CD}$$

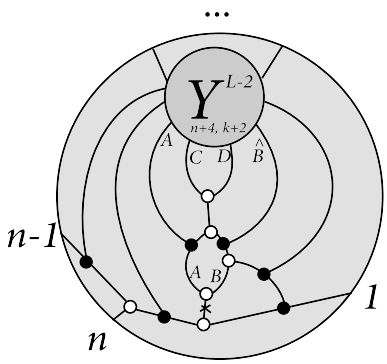

$$= \int_{GL(2)}^{CD}$$

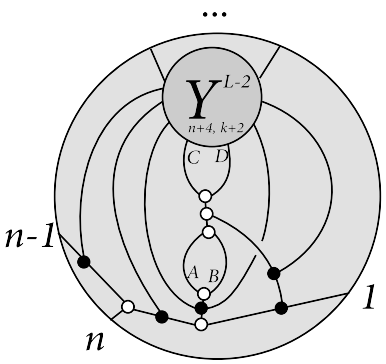

where the second diagram is obtained by doing the $GL(2)$ integral for AB. The procedure here is the same as before. Just reattach the two lines A and $\hat{B}$ coming out of the sub-diagram to the crossed line.

Going one step further, we perform yet another BCFW shift on the sub-diagram. We use the shift $\mathcal{Z}_C \to \mathcal{Z}_C + w\mathcal{Z}_A$, which is convenient because the boundary term vanishes in the forward limit of CD. Hence, the FL-FL-FAC term gives the final contribution at two loops. Diagrammatically, we have the following.

FL-FL-FAC (9.80)

$$= \sum_{j=2}^{n} \int_{GL(2)}^{CD}$$

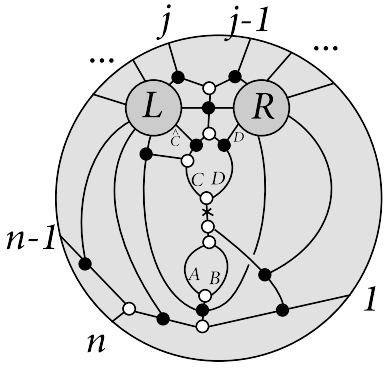

$$= \sum_{j=2}^{n}$$

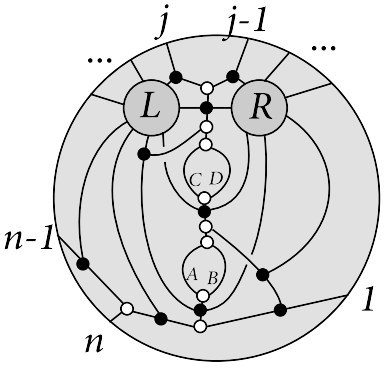

In the second diagram we have done the $GL(2)$ integral for CD by reattaching the two lines $\hat{C}$ and D coming out of the two sub-diagrams to the crossed line. Recalling that the forward limit takes $C, D \to (C, D) \cap (1, A, B)$, we see that the crossed line precisely represents this limit. We note that $k_L{+}k_R = k{+}1$ and $L_L{+}L_R = L{-}2$.

9.7.1 Two loop diagrams for 4 point MHV

We now present a full example: the 4-point 2 loop integrand. The computation is already quite non-trivial and interesting, which shows all the essential features of our diagrammatic formulation of multi-loop integrands. The result is given by the forward limit of the one-loop six-point NMHV integrand, which includes 16 terms. When applying the forward limit to it using (9.80), we find only 8 non-vanishing terms. There are 2 terms for FL-FAC and 6 terms for FL-FL, the expressions for which we list below. For each term we also include the momentum twistor diagram and the corresponding matrix expression as follows.

$$\mathcal{D}^{(2)} \equiv \begin{pmatrix} D_{AB} \\ D_{CD} \end{pmatrix} \tag{9.81}$$

To write the expressions in a more compact form, we introduce shifted twistors.

$$\begin{aligned} \hat{A} &= (A, B) \cap (1, 3, 4), \quad \hat{C}' = (C, D) \cap (1, A, B), \\ \hat{3}' &= (2, 3) \cap (1, A, B), \quad \hat{4}' = (3, 4) \cap (1, A, B), \\ \hat{2} &= (1, 2) \cap (\hat{A}, C, D), \quad \hat{3} = (2, 3) \cap (\hat{A}, C, D), \quad \hat{4} = (3, 4) \cap (\hat{A}, C, D), \end{aligned} \tag{9.82}$$

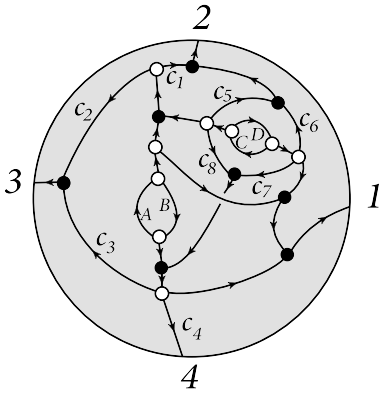

$$\begin{pmatrix} -1 & -c_1 & -c_2 & 0 \\ 1 & 0 & -c_3 & -c_4 \\ c_8 & -c_1-c_5 & -c_2-c_3c_8 & -c_4c_8 \\ 1+c_7 & c_6 & -c_3c_7 & -c_4c_7 \end{pmatrix} \tag{9.83}$$

$$\text{FL-FAC-1} = \frac{\langle 1234\rangle^4\langle AB13\rangle^2}{\langle AB23\rangle\langle AB34\rangle\langle AB14\rangle\langle CD12\rangle\langle CD23\rangle\langle CD\hat{3}'\hat{A}\rangle\langle CD1\hat{A}\rangle} \tag{9.84}$$

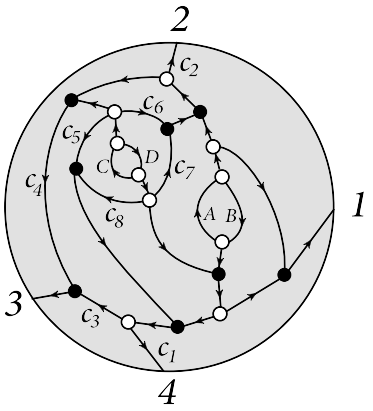

$$\begin{pmatrix} 1 & c_2 & c_4 & 0 \\ -1 & 0 & c_3 & c_1 \\ 0 & c_2c_6 & c_4+c_3c_5+c_4c_6 & c_1c_5 \\ -1 & -c_2c_7 & c_3-c_4c_7+c_3c_8 & c_1+c_1c_8 \end{pmatrix} \tag{9.85}$$

$$\text{FL-FAC-2} = \frac{\langle 1234\rangle^4\langle AB13\rangle^2}{\langle AB12\rangle\langle AB23\rangle\langle AB14\rangle\langle CD23\rangle\langle CD34\rangle\langle CD\hat{4}'1\rangle\langle CD\hat{3}'\mathcal{A}\rangle} \tag{9.86}$$

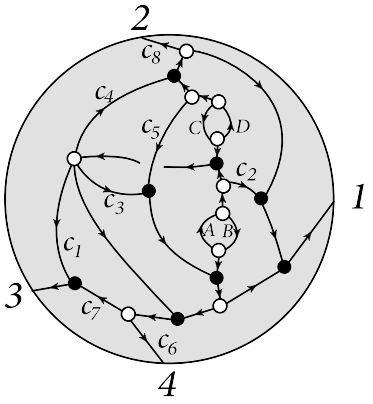

$$\begin{pmatrix} -c_2+c_3-c_4 & -c_4c_8 & -c_1-c_7-c_3c_7 & -c_6-c_3c_6 \\ 1 & 0 & -c_7 & -c_6 \\ c_3-c_4 & -c_4c_8 & -c_1-c_7-c_3c_7 & -c_6-c_3c_6 \\ 1+c_5 & c_8 & -c_5c_7 & -c_5c_6 \end{pmatrix} \tag{9.87}$$

$$\text{FL-FL-1} = \frac{\langle AB(134)\cap(1CD)\rangle^2\langle\mathcal{A}\hat{C}'12\rangle^2\langle 1234\rangle^3\langle AB34\rangle\langle CD\mathcal{A}1\rangle^2}{\langle AB14\rangle\langle ABCD\rangle\langle CD12\rangle\langle CD\mathcal{A}2\rangle\langle\hat{C}'134\rangle\langle\hat{2}\hat{4}'\hat{C}'\mathcal{A}\rangle\langle\hat{2}3\mathcal{A}\hat{C}'\rangle\langle\hat{C}'\hat{2}34\rangle} \tag{9.88}$$

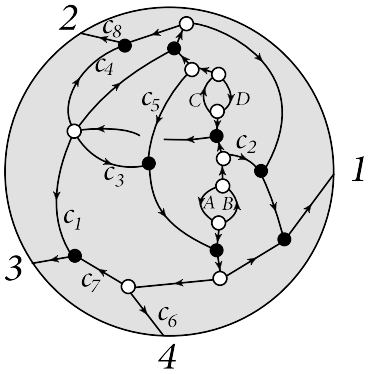

$$\begin{pmatrix} 1 & 0 & -c_7 & -c_6 \\ 1+c_2-c_3 & c_8+c_4c_8 & c_1+c_3c_7 & c_3c_6 \\ 1+c_5 & c_8 & -c_5c_7 & -c_5c_6 \\ 1-c_3 & c_8+c_4c_8 & c_1+c_3c_7 & c_3c_6 \end{pmatrix} \tag{9.89}$$

$$\text{FL-FL-2} = \frac{\langle AB(134)\cap(1CD)\rangle^2\langle\mathcal{A}\hat{C}'12\rangle\langle 1234\rangle^3\langle AB13\rangle^2}{\langle AB14\rangle\langle AB34\rangle\langle ABCD\rangle\langle CD\mathcal{A}1\rangle\langle CD12\rangle\langle\mathcal{A}\hat{C}'23\rangle\langle\mathcal{A}\hat{C}'3\hat{2}\rangle\langle\hat{C}'123\rangle} \tag{9.90}$$

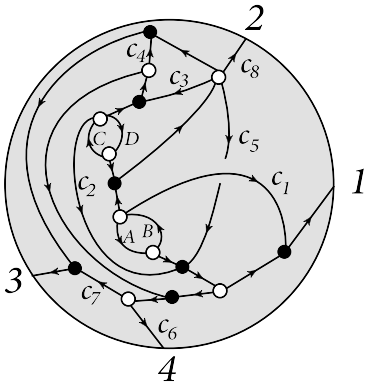

$$\begin{pmatrix} 1 & 0 & -c_7 & -c_6 \\ c_1{+}c_5 & c_8 & 1{+}c_3c_4{+}c_3c_7{-}c_5c_7 & c_3c_6{-}c_5c_6 \\ c_2 & 0 & -c_4{-}c_7{-}c_2c_7 & -c_6{-}c_2c_6 \\ c_5 & c_8 & 1{+}c_3c_4{+}c_3c_7{-}c_5c_7 & c_3c_6{-}c_5c_6 \end{pmatrix} \tag{9.91}$$

$$\text{FL-FL-3} = \frac{\langle AB(134)\cap(1CD)\rangle^2\langle AB34\rangle^3\langle\hat{C}'134\rangle\langle1234\rangle^3}{\langle AB14\rangle\langle ABCD\rangle\langle CD34\rangle\langle CD\hat{4}'\mathcal{A}\rangle\langle\hat{C}'234\rangle\langle\hat{4}\hat{C}'\mathcal{A}2\rangle\langle\hat{C}'\mathcal{A}23\rangle} \tag{9.92}$$

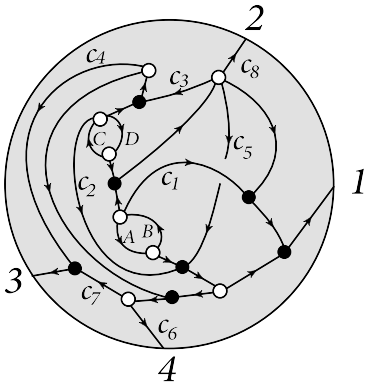

$$\begin{pmatrix} 1 & 0 & -c_7 & -c_6 \\ 1+c_1+c_5 & c_8 & c_3c_4+c_3c_7-c_5c_7 & c_3c_6-c_5c_6 \\ c_2 & 0 & -c_4-c_7-c_2c_7 & -c_6-c_2c_6 \\ 1+c_5 & c_8 & c_3c_4+c_3c_7+c_5c_7 & c_3c_6-c_5c_6 \end{pmatrix} \tag{9.93}$$

$$\text{FL-FL-4} = \frac{\langle AB(134)\cap(1CD)\rangle^2\langle\hat{C}'134\rangle^2\langle\mathcal{A}\hat{4}12\rangle^3}{\langle AB14\rangle\langle ABCD\rangle\langle CD\mathcal{A}3\rangle\langle CD34\rangle\langle\hat{C}'\hat{4}12\rangle\langle\hat{C}'\hat{4}\mathcal{A}1\rangle\langle\hat{C}'\hat{4}\mathcal{A}2\rangle\langle\hat{C}'\mathcal{A}12\rangle\langle CD\hat{4}'1\rangle} \tag{9.94}$$

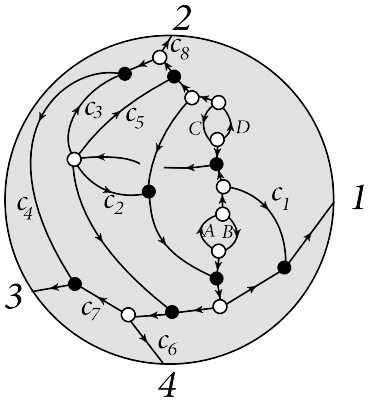

$$\begin{pmatrix} -c_1+c_2 & -c_5c_8 & -c_3c_4-c_4c_5-c_7-c_2c_7 & -c_6-c_2c_6 \\ 1 & 0 & -c_7 & -c_6 \\ c_2 & -c_5c_8 & -c_3c_4-c_4c_5-c_7-c_2c_7 & -c_6-c_2c_6 \\ 1 & c_8 & c_4-c_7 & -c_6 \end{pmatrix} \tag{9.95}$$

$$\text{FL-FL-5} = \frac{\langle AB(134)\cap(1CD)\rangle^2\langle AB34\rangle\langle\hat{C}'\mathcal{A}23\rangle\langle 1234\rangle^3}{\langle AB14\rangle\langle ABCD\rangle\langle CD\mathcal{A}2\rangle\langle CD23\rangle\langle\hat{C}'134\rangle\langle\mathcal{A}\hat{3}\hat{C}'\hat{4}'\rangle\langle\hat{C}'234\rangle} \tag{9.96}$$

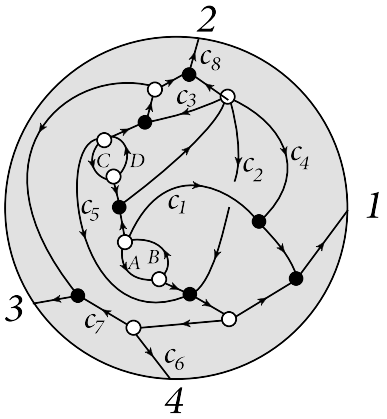

$$\begin{pmatrix} 1 & 0 & -c_7 & -c_6 \\ c_1+c_2+c_4 & c_8+c_3c_8 & c_3-c_2c_7 & -c_2c_6 \\ c_2+c_4 & c_8+c_3c_8 & c_3-c_2c_7 & -c_2c_6 \\ -c_5 & c_8 & 1+c_5c_7 & c_5c_6 \end{pmatrix} \tag{9.97}$$

$$\text{FL-FL-6} = \frac{\langle AB(134)\cap(1CD)\rangle^2\langle\hat{C}'\mathcal{A}23\rangle\langle\mathcal{A}123\rangle^3}{\langle AB13\rangle\langle AB14\rangle\langle AB34\rangle\langle ABCD\rangle\langle CD23\rangle\langle CD3\mathcal{A}\rangle\langle\hat{C}'123\rangle\langle\hat{3}\hat{C}'\mathcal{A}1\rangle\langle\hat{C}'\mathcal{A}12\rangle} \tag{9.98}$$

The two-loop four-point integrand is the sum of the 8 terms, plus the other 8 terms obtained by $(AB \leftrightarrow CD)$. As one can check numerically, given a set of positive data and a random point inside the amplituhedron, it lies in one and only one of the cells with the above $\mathcal{D}$ matrices, except for points on the boundary of cells. The fact that the cells triangulate the amplituhedron is a highly non-trivial statement about geometry, and is in fact very difficult to prove. Nonetheless, BCFW terms appear to provide cells that triangulate the amplituhedron when summed.

We can compare our result to results obtained elsewhere via different methods, such as the following expression from [26].

$$\begin{aligned} Y^{(2)}_{4,0} &= \frac{1}{2}\left[\frac{\langle 1234\rangle^3}{\langle AB12\rangle\langle AB23\rangle\langle AB34\rangle\langle ABCD\rangle\langle CD34\rangle\langle CD14\rangle\langle CD12\rangle}\right. \\ &+ \left.\frac{\langle 1234\rangle^3}{\langle AB23\rangle\langle AB34\rangle\langle AB14\rangle\langle ABCD\rangle\langle CD14\rangle\langle CD12\rangle\langle CD23\rangle}\right] \\ &+ (AB \leftrightarrow CD) \end{aligned} \tag{9.99}$$

We find agreement via numerical checks.

For a discussion on computation of general 2-loop integrands (for any k), which involves a 2-loop extension of the Kermit, see Section 4.3.3 of [4].

Chapter 10

One-loop amplitudes of planar $\mathcal{N} = 4$ super Yang-Mills

We now provide a detailed study of the positive loop Grassmannian $G_{\geq 0}(1, n; 1)$, whose image under Z gives the NMHV one-loop amplituhedron $\mathcal{A}(1, n; 1)$. In particular, we provide a detailed classification of the Grassmannian cells of top dimension. Contrary to tree level, more than one top dimensional cell appears. We describe properties of these top cells in detail, and discuss how they can be obtained from 0-dimensional cells via the method of successive shifts. In Section 10.2, we study the canonical form of top cells called top cell measures. In particular, we argue that every planar one-loop NMHV BCFW integrand can be obtained by taking a sequence of residues on a top cell measure before pushing it forward by Z. This is a generalization of earlier work done at tree level in momentum space [36, 16]. Also, throughout these sections, we generalize to $k > 1$ wherever possible. However, we emphasize that the notion of top cell is still unclear for $k > 1$.

10.1 The one-loop $k = 1$ Grassmannian

The general loop Grassmannian was introduced in Section 2.5.5. Here we specialize to $k = 1$ and $L = 1$, whereby we think of a point $P \in G_{\geq 0}(1, n; 1)$ as a $3 \times n$ matrix whose first two rows form the D matrix and the last row is the C matrix, modded out by the parabolic group $\mathrm{GL}(1; 1)$ (See (2.1) of [3]). Note that in Section 2.5.5, the D matrix is positioned below the C matrix. There is a torus $T_{\geq 0} = \mathrm{GL}_{\geq 0}(1)^n$ that acts on $G_{\geq 0}(1, n; 1)$ by scaling the columns independently by positive scalars.

We describe $X = G_{\geq 0}(1, n; 1)/T_{\geq 0}$ explicitly in terms of spaces of n points in the projective plane $\mathbb{P}^2_{\geq 0} \equiv (\mathbb{R}^2 \times \mathbb{R}_{\geq 0})/\mathbb{R}_+$, which is the space of all vectors of the form $(d_1, d_2, c)^T$ with $c \geq 0$ modded out by overall multiplication by positive scalars. Fix a line at infinity $L_\infty \subset \mathbb{P}^2_{\geq 0}$ which we can take to be the set of all non-zero vectors with $c = 0$, and let $\mathcal{A}^2 = \mathbb{P}^2_{\geq 0} \setminus L_\infty$ denote the affine plane. The space X consists of collections $P \equiv (P_1, P_2, \ldots, P_n)$ of n points where each P_i is either

1. a point $P_i \in \mathcal{A}^2$, or
2. a point $P_i \in L_\infty$, or
3. "zero" (equivalently, a point not on $\mathbb{P}^2_{\geq 0}$).

Case (1) occurs if the third entry of the i-th column of C is non-zero. Then the i-th column of P can be scaled to the column vector $(d_1, d_2, 1)^T$, representing the point $(d_1, d_2)^T \sim (d_1, d_2, 1)^T \in \mathcal{A}^2$.
Case (2) occurs if the third entry of the i-th column of C is zero, but the i-th column of P is non-zero. Then we have the column vector $(d_1, d_2, 0)^T$, representing the point $(d_1, d_2)^T \sim (d_1, d_2, 0)^T \in L_\infty$.
Case (3) occurs if the i-th column of P is the zero vector.

The positivity of the collection $P = (P_1, P_2, \ldots, P_n)$ implies that the column vectors form the ordered vertices of a convex polygon which we also refer to as P,

which may have points at infinity. Furthermore, two matrices P and P' represent the same point in $G_{\geq 0}(1,n;1)$ if they are related by one of the three operations.

1. The $\mathrm{GL}_{\geq 0}(1)$-action on the row C, which rescales the polygon relative to the origin of the affine plane.

2. The $\mathrm{GL}_{\geq 0}(2)$-action on the two rows D, which linearly transforms the polygon on the affine plane while preserving convexity.

3. The T action that adds a multiple of C to one of the rows of D, which translates the polygon.

In other words, X is the space of n-points in $\mathbb{P}^2_{\geq 0}$ in convex position (with a distinguished line at infinity), modulo the action of affine transformations. A simple example of a polygon P is given by the following, where $\theta_s = 2\pi s/6$ for $s = 0, ..., 5$.

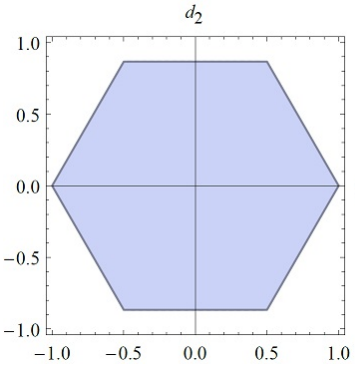

$$P = \begin{pmatrix} \cos\theta_0 & \cos\theta_1 & \cos\theta_2 & \cos\theta_3 & \cos\theta_4 & \cos\theta_5 \\ \sin\theta_0 & \sin\theta_1 & \sin\theta_2 & \sin\theta_3 & \sin\theta_4 & \sin\theta_5 \\ 1 & 1 & 1 & 1 & 1 & 1 \end{pmatrix} \tag{10.1}$$

10.1.1 0-dimensional cells

We now wish to discuss the 0-dimensional cells of $G_{\geq 0}(1,n;1)$. These innocuous parts of the geometry are actually crucial, because they are the seeds from which all other diagrams can be constructed.

We first remind ourselves of the 0-dimensional cells appearing in the tree level Grassmannian $G_{\geq 0}(k,n)$. We pick n external states $a_1, ..., a_k$ and gauge fix the Grassmannian to be identity in the $k \times k$ block corresponding to columns $a_1, ..., a_k$, and

set all other components to zero. For instance, for $G_{\geq 0}(2,5)$ and $(a_1, a_2) = (2,3)$, the 0-dimensional cell is given by the following.

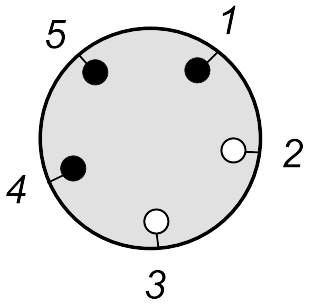

$$C = \begin{pmatrix} 0 & 1 & 0 & 0 & 0 \\ 0 & 0 & 1 & 0 & 0 \end{pmatrix} \tag{10.2}$$

Here we have also included the corresponding momentum twistor diagram. In general, a 0-dimensional cell consists of black and white "lollipops" attached to the external legs of the diagram. The white lollipops are positioned precisely at the indices $a_1, ..., a_k$. The number of white lollipops is therefore the k charge of the diagram. In particular, the MHV tree diagram is just a ring of black lollipops.

We now return to the one-loop $k = 1$ case. The 0-dimensional cells of $G_{\geq 0}(1, n; 1)$ are exactly the torus-invariant points of $G_{\geq 0}(1, n; 1)$. They are determined by picking $a \in \{1, 2, \ldots, n\}$ and another unordered pair $(b, c) \in \{1, 2, \ldots, n\} - \{a\}$. The cell $\Pi_{a;b,c}$ consists of a point $P_a \in \mathcal{A}^2$ and distinct points $P_b, P_c \in L_\infty$. By an affine transformation, we can assume that P_a, P_b, P_c are precisely the standard unit vector basis in $\mathbb{P}^2_{\geq 0}$. For example, if $n = 5$, we have that $\Pi_{1;3,4}$ is represented by the following matrix.

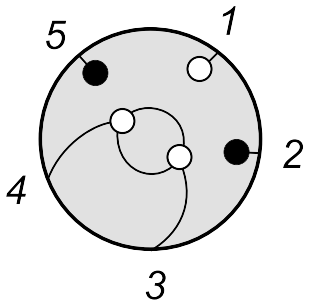

$$P = \begin{pmatrix} 0 & 0 & 1 & 0 & 0 \\ 0 & 0 & 0 & 1 & 0 \\ 1 & 0 & 0 & 0 & 0 \end{pmatrix} \tag{10.3}$$

Again we have included the corresponding diagram. As in the tree level case, we must have one white lollipop at particle a corresponding to the $k = 1$ charge. The novelty at one loop is that we have one "bubble" attached to two external legs. The bubble represents the loop variable while the legs reflect the corresponding $GL(2)$ symmetry. For 0-dimensional cells, these two legs must be connected to the two external particles labeled b, c. At one loop, this is the only type of 0-dimensional cell that can appear. At higher loops, the classification of 0-dimensional cells is still unclear. For instance, we can imagine connecting two bubbles together through their external legs. Whether or not this type of diagram should be classified as a 0-dimensional cell, and what other cells are possible, are still open questions.

10.1.2 Top cells

We now describe the top cells of $G_{\geq 0}(1, n; 1)$; more specifically we describe the corresponding top cells of $X = G_{\geq 0}(1, n; 1)/T_{\geq 0}$.

Suppose that $P = (P_1, \ldots, P_n)$ is a convex n-gon in $\mathcal{A}^2$ with points occuring in cyclic counterclockwise order. Suppose that $a, a+1, b, b+1$ are in cyclic order, where $a + 1$ can equal b, but $a \neq b + 1$. Let us say that the edges $(a, a + 1)$ and $(b, b + 1)$ intersect *positively* if the intersection point $(a, a{+}1) \cap (b, b{+}1) \equiv P_b(a, a{+}1, b{+}1) - P_{b+1}(a, a{+}1, b)$ of the two lines is on the opposite side of the line $(a + 1, b)$ to both a and $b + 1$. If the intersection point X is on the other side of $(a + 1, b)$, then we say that $(a, a + 1)$ and $(b, b + 1)$ intersect negatively. Note that $(a, a + 1)$ and $(b, b + 1)$ intersect positively if and only if $(b, b{+}1)$ and $(a, a{+}1)$ intersect negatively. For short we say that $[a, a + 1; b, b + 1]$ is positive. If $a + 1 = b$, then $[a, a + 1; a + 1, a + 2]$ is always positive. The condition that $[a, a + 1; b, b + 1]$ is positive is equivalent to the algebraic condition

$$[(a, a{+}1) \cap (b, b{+}1)] = [b](a, a{+}1, b{+}1) - [b{+}1](a, a{+}1, b) > 0. \tag{10.4}$$

Here $[a]$ denotes a minor of the row C, and (a, b, c) denotes a minor of the matrix P. For example, suppose $n = 4$ and $a = 1$ and $b = 3$. By an affine transformation, a convex quadrilateral in $\mathcal{A}^2$ can be made to have vertices $(0, 0), (1, 0), (x, y), (0, 1)$, so that the corresponding P matrix is

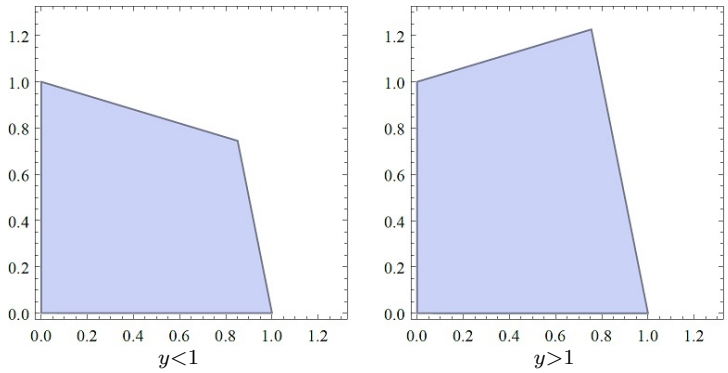

$$P = \begin{pmatrix} 0 & 1 & x & 0 \\ 0 & 0 & y & 1 \\ 1 & 1 & 1 & 1 \end{pmatrix}. \quad (10.5)$$

The convexity of the quadrilateral is equivalent to the conditions $(123) = y > 0$ and $(134) = x > 0$ and $(234) = x + y - 1 > 0$. The condition that (12) and (34) intersect positively is the condition $y < 1$, or equivalently, $[(12) \cap (34)] = [3](124) - [4](123) > 0$.

A top cell can be described in the following way: it is the space of convex n-gons in $\mathcal{A}^2$, considered up to affine transformations, satisfying additional constraints specifying that certain pairs of edges $(a, a+1)$ and $(b, b+1)$ intersect positively. These constraints are only specified for some pairs of edges. Other pairs of edges are allowed to intersect either positively or negatively. There are $\binom{n}{3}$ top cells in total. Given a 3-element subset $S \subset \{1, 2, \ldots, n\}$, we now describe the corresponding top cell Π_S. Let $S = \{a < b < c\} \subset \{1, 2, \ldots, n\}$. Then the intersection constraints for Π_S are that $[a, a+1; b, b+1]$, $[b, b+1; c, c+1]$, and $[c, c+1; a, a+1]$ are positive. Note that $[a, a+1; b, b+1]$ being positive implies that $[a', a'+1; b, b+1]$ is positive for all $a < a' < b$. Thus Π_S is cut out of $G_{\geq 0}(1, n; 1)$ by three quadratic equations of the form (10.4).

Another way to describe $\Pi_{\{a,b,c\}}$ is as follows. Start with the intersection points

$$X_1 = (a, a{+}1) \cap (b, b{+}1), X_2 = (b, b{+}1) \cap (c, c{+}1), X_3 = (c, c{+}1) \cap (a, a{+}1). \quad (10.6)$$

The convex hull of these three points is a big triangle Δ. Then $\Pi_{\{a,b,c\}}$ is the space of n-gons that can be inscribed inside Δ so that the edges $(a, a+1)$, $(b, b+1)$ and $(c, c+1)$ lie on the three edges of Δ, as shown in the following picture.

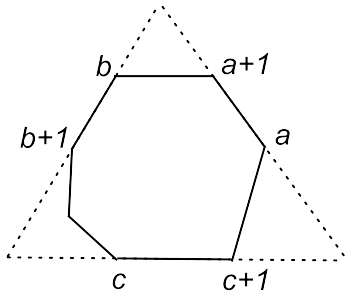

(10.7)

Another way to think about the inscribed n-gon is that it is obtained from Δ by slicing it a number of times. If $a + 1 = b$, then the intersection point $X_1 = (a, a+1) \cap (a+1, a+2)$ is simply $a + 1$, so sometimes Δ shares some of its vertices with the n-gon P.

10.1.3 Shifts

The top cells Π_S can be built up from 0-dimensional cells via shifts of columns of the P matrix. The geometry of the intersection conditions on edges arises naturally in this way.

We consider two kinds of shifts: The shift $(i + 1 \to i)$ acts by adding aP_i to P_{i+1} while $(i \to i + 1)$ acts by adding aP_{i+1} to P_i, where a is positive and will later be interpreted as a bridge variable. These shifts send points in $G_{\geq 0}(1, n; 1)$ to points in $G_{\geq 0}(1, n; 1)$. In terms of point configurations, $(i + 1 \to i)$ moves P_{i+1} to a point on the interval connecting P_i and P_{i+1}, while $(i \to i + 1)$ moves P_i to a point on the

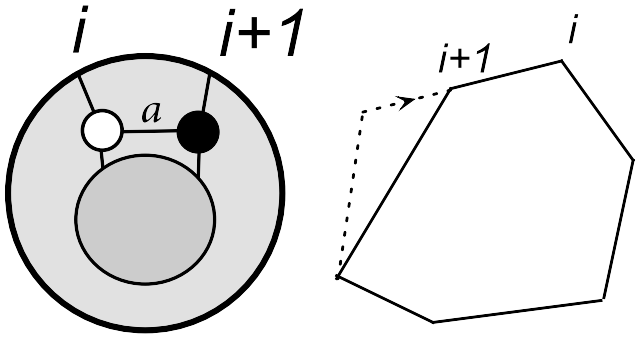

(10.8)

Figure 10.1: The shift $(i+1 \to i)$ where $P_{i+1} \to P_{i+1}+aP_i$

same interval. Note that if $P_{i+1} = 0$ is not on $\mathbb{P}^2$, then $(i+1 \to i)$ just places P_{i+1} at the location of P_i.

As we are showing in Figure 10.1, the shifts have a simple interpretation as a BCFW bridge. For instance, by doing the shift $(i+1 \to i)$ we are simply attaching a new pair of black and white vertices at positions i and $i+1$. The two ways of coloring the vertices reflects the two possible shifts $(i+1 \to i)$ and $(i \to i+1)$, of which we have drawn the former. The variable a appears as a bridge variable on the diagram, which is consistent with the fact that adding a bridge increases the number of faces, and hence the dimension, of the diagram by 1.

Using shifts where a varies over $\mathbb{R}_{>0}$, we can build up higher-dimensional cells from 0-dimensional cells, at least at one loop. We can obtain all top cells of $G_{\geq 0}(1, n; 1)$ in this way, though in general we need to allow non-adjacent shifts, and possibly negative values for a, in which case we use $-a$ so that $a > 0$. The same is probably true to all loops, though it is not clear what all the 0-dimensional cells are in those cases, as discussed earlier.

Any momentum twistor diagram can be decomposed into a sequence of bridges, or shifts. In other words, there exists a sequence of shifts that takes a 0-dimensional cell to the full diagram. In practice, this sequence is obtained by starting with the full diagram and removing one bridge at a time. This is related to the fact that each

permutation in the symmetric group S_n can be written as a composition of transpositions, as explained in the original reference [16]. Of course, the decomposition is not unique, and neither is the 0-dimensional cell.

10.1.4 5 point

We now apply our preceding formalism to the $n = 5$ one-loop NMHV integrand, which is expressed as a sum of three BCFW terms B-1,B-2,B-3. The expressions for these terms are given in Appendix A of [3] as the first 3 of 16 BCFW terms for the $n = 6$ integrand. But since these 3 terms form the boundary contribution to the $n = 6$ case, they can also be interpreted as a complete BCFW expansion of the $n = 5$ integrand. In the discussion that follows, we focus on the term B-1, which corresponds to a Grassmannian cell whose coordinates we construct via shifts starting from a 0-dimensional cell. At each step, we present the coordinates for the P matrix, the momentum twistor diagram, and a picture for the vertices P_i showing their linear relations.

(0) Start with the 0-dimensional cell $\Pi_{1;3,5}$. Thus we have a point $P_1 \in \mathcal{A}^2$, and two points $P_3, P_5 \in L_\infty$.

$$P = \begin{pmatrix} 0 & 0 & 1 & 0 & 0 \\ 0 & 0 & 0 & 0 & 1 \\ 1 & 0 & 0 & 0 & 0 \end{pmatrix} \qquad (10.9)$$

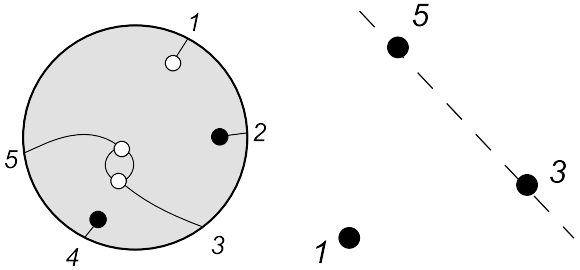

(1) Apply the shift $(2 \to 3)$. This places P_2 at the same location as P_3.

$$P = \begin{pmatrix} 0 & a_1 & 1 & 0 & 0 \\ 0 & 0 & 0 & 0 & 1 \\ 1 & 0 & 0 & 0 & 0 \end{pmatrix}$$

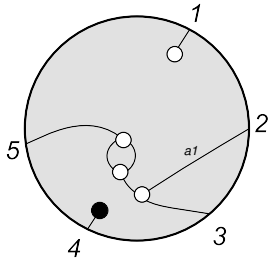

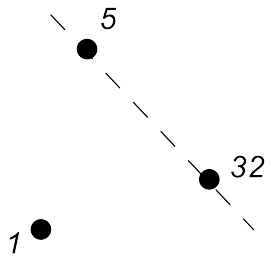

(10.10)

(2) Apply the shift $(4 \to 5)$. This places P_4 at the same location as P_5.

$$P = \begin{pmatrix} 0 & a_1 & 1 & 0 & 0 \\ 0 & 0 & 0 & a_2 & 1 \\ 1 & 0 & 0 & 0 & 0 \end{pmatrix}$$

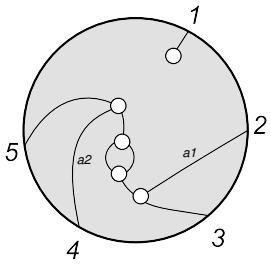

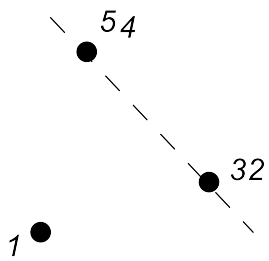

(10.11)

(3) Apply the shift $(2 \to 5)$. This moves P_2 towards P_5. To keep the arrangement convex, this is visualized with P_2 being pushed away from P_5. This is an example of a non-adjacent shift with a negative bridge variable $P_2 \to P_2 - a_2 P_5$. So we have the space of degenerate pentagons $(P_1, P_2, P_3, P_4, P_5)$ in $\mathbb{P}^2$, where P_2, P_3, and $P_4 = P_5$ lie at infinity and P_1 lies in $\mathcal{A}^2$.

$$P = \begin{pmatrix} 0 & a_1 & 1 & 0 & 0 \\ 0 & -a_3 & 0 & a_2 & 1 \\ 1 & 0 & 0 & 0 & 0 \end{pmatrix}$$

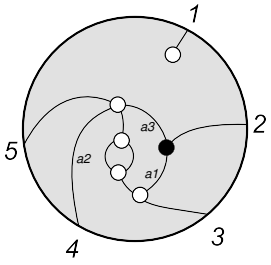

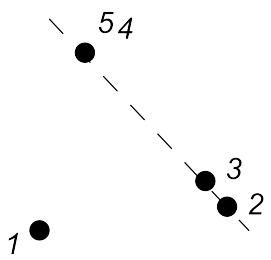

(10.12)

(4) Apply the shift $(5 \to 1)$. Thus P_5 is moved off the line at infinity towards P_1. So we have the space of degenerate pentagons $(P_1, P_2, P_3, P_4, P_5)$ in $\mathbb{P}^2$, where P_2, P_3, and P_4 lie at infinity and P_5 lies on the line joining P_1 and P_4.

$$P = \begin{pmatrix} 0 & a_1 & 1 & 0 & 0 \\ 0 & -a_3 & 0 & a_2 & 1 \\ 1 & 0 & 0 & 0 & a_4 \end{pmatrix} \qquad (10.13)$$

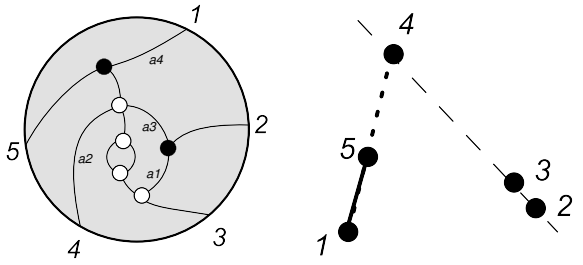

(5) Apply the shift $(4 \to 5)$. Thus P_4 is moved towards P_5. So we have the space of degenerate pentagons $(P_1, P_2, P_3, P_4, P_5)$ in $\mathbb{P}^2$, where P_2 and P_3 lie at infinity and P_5 lies on the line joining P_1 and P_4.

$$P = \begin{pmatrix} 0 & a_1 & 1 & 0 & 0 \\ 0 & -a_3 & 0 & a_2 + a_5 & 1 \\ 1 & 0 & 0 & a_4 a_5 & a_4 \end{pmatrix} \qquad (10.14)$$

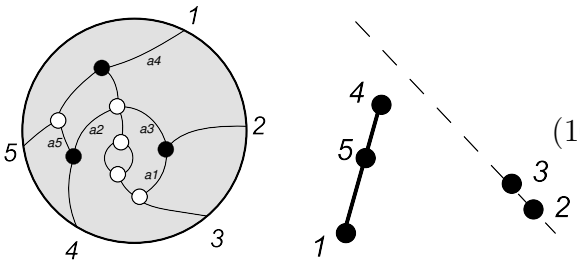

(6) Apply the shift $(4 \to 3)$. Thus P_4 is moved towards P_3. So we now have the space of pentagons $(P_1, P_2, P_3, P_4, P_5)$ in $\mathbb{P}^2$, where P_2 and P_3 lie at infinity.

$$P = \begin{pmatrix} 0 & a_1 & 1 & a_6 & 0 \\ 0 & -a_3 & 0 & a_2 + a_5 & 1 \\ 1 & 0 & 0 & a_4 a_5 & a_4 \end{pmatrix} \qquad (10.15)$$

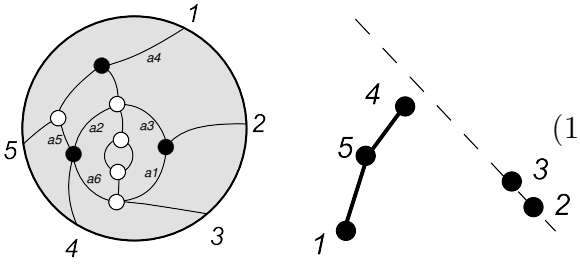

(7) Apply the shift $(2 \to 1)$. Thus P_2 is moved towards P_1. So we now have the space of pentagons $(P_1, P_2, P_3, P_4, P_5)$ in $\mathbb{P}^2$, where P_3 is on the line at infinity. In the diagram below, you should imagine that P_3 is placed infinitely away so that the two dashed lines are parallel, and so that the interior angles at P_4 and P_2 are less than π. In particular, given any point P_* on the half-line $(2, 3)$, the extended lines $(2, 3)$ and

$(4,5)$ intersect on the side of $(4,*)$ containing P_2 and P_5. This observation is crucial for the next step.

$$P = \begin{pmatrix} 0 & a_1 & 1 & a_6 & 0 \\ 0 & -a_3 & 0 & a_2+a_5 & 1 \\ 1 & a_7 & 0 & a_4a_5 & a_4 \end{pmatrix} \qquad (10.16)$$

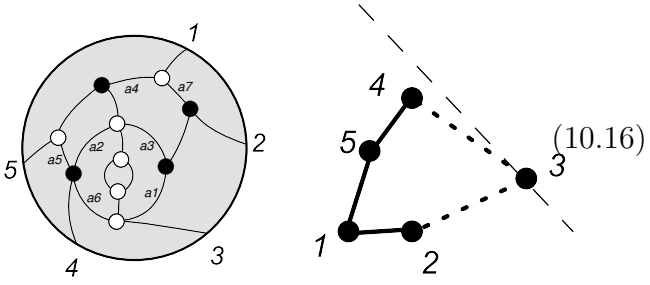

(8) Apply the shift $(3 \to 2)$. This moves P_3 off the line at infinity towards P_2 along $(2,3)$. As noted earlier, the lines $(2,3)$ and $(4,5)$ intersect on the side of $(3,4)$ containing P_2 and P_5. In other words, $[4,5;2,3]$ is positive. So we now have the space of pentagons (P_1,P_2,P_3,P_4,P_5) in $\mathcal{A}^2$, where $(4,5)$ and $(2,3)$ intersect positively. We have thus obtained the top cell Π_S where $S=\{2,3,4\}$. (The conditions that $(2,3)$ intersects $(3,4)$ positively, and $(3,4)$ intersects $(4,5)$ positively are trivially satisfied.)

$$P = \begin{pmatrix} 0 & a_1 & 1+a_1a_8 & a_6 & 0 \\ 0 & -a_3 & -a_3a_8 & a_2+a_5 & 1 \\ 1 & a_7 & a_7a_8 & a_4a_5 & a_4 \end{pmatrix} \qquad (10.17)$$

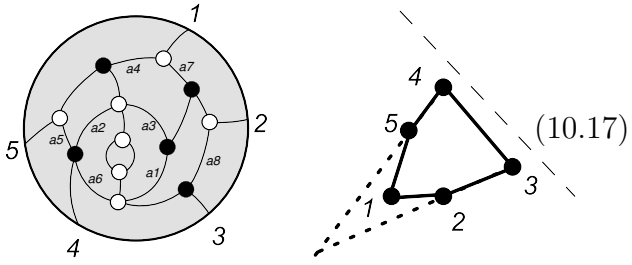

The diagram above is identical to the B-1 diagram in Appendix A of [3] with the black lollipop at particle 6 stripped off, since we are only concerned with the 5 point integrand. However, the matrix P is not the same as the B-1 matrix with the sixth column removed. Nonetheless, they parametrize the same Grassmannian cell, which can be seen by a change of gauge followed by a change of variables. First change the

gauge by acting P on the left by

$$g = \begin{pmatrix} 1 & 0 & 0 \\ 0 & a_4 & 0 \\ 0 & 0 & 1 \end{pmatrix} \in \mathrm{GL}(1;1). \tag{10.18}$$

then perform the monomial coordinate change $a_1 \to c_1 c_6, a_2 \to c_8/c_4, a_3 \to c_1 c_7/c_4, a_4 \to c_4, a_5 \to c_3/c_4, a_6 \to c_5, a_7 \to c_1, a_8 \to c_2/c_1$. Note that this change of variables is a diffeomorphism of $\mathbb{R}^8_{>0}$, which must be the case for any change of gauge between positive variables.

10.1.5 6 point

We repeat the analysis of the previous section for the FL-2 term of the BCFW expansion for the $n = 6$ one-loop NMHV integrand, as provided in Appendix A of [3]. We denote the corresponding top cell as $\Pi_{\text{FL-2}}$.

(0) Start with the 0-dimensional cell $\Pi_{4;1,6}$. Thus we have a point $P_4 \in \mathcal{A}^2$ and distinct points $P_1, P_6 \in L_\infty$. There is a unique such configuration up to affine transformations. The points P_2, P_3, P_5 are not on the projective plane. A representative matrix is

$$P = \begin{pmatrix} 1 & 0 & 0 & 0 & 0 & 0 \\ 0 & 0 & 0 & 0 & 0 & -1 \\ 0 & 0 & 0 & 1 & 0 & 0 \end{pmatrix} \tag{10.19}$$

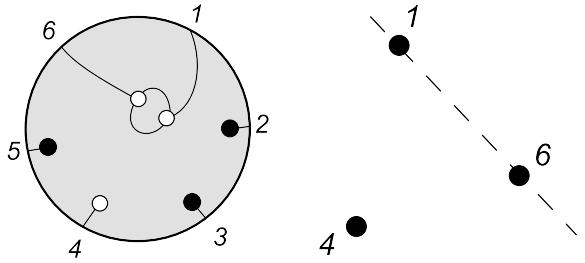

(1) Perform the shift $(2 \to 1)$. This places P_2 on top of P_1. Thus we have the space of degenerate quadrilaterals (P_1, P_2, P_4, P_6) where $P_1 = P_2$ and P_1, P_2, P_6 lie on L_∞.

A representative matrix for this one-dimensional cell is

$$\begin{pmatrix} 1 & a_1 & 0 & 0 & 0 & 0 \\ 0 & 0 & 0 & 0 & 0 & -1 \\ 0 & 0 & 0 & 1 & 0 & 0 \end{pmatrix} \tag{10.20}$$

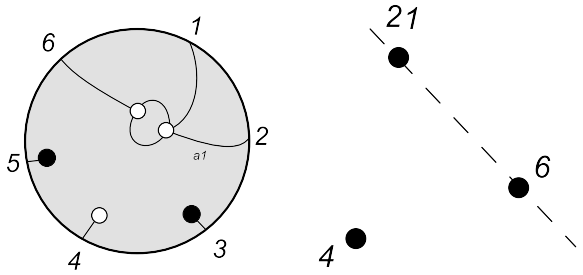

(2) Perform the shift $(6 \to 4)$. This moves P_6 towards P_4 along the line joining P_4 and P_6. Now we have a space of degenerate quadrilaterals (P_1, P_2, P_4, P_6), where two vertices P_4, P_6 lie in $\mathcal{A}^2$, and $P_1 = P_2$ lies on L_∞. A representative matrix for this two-dimensional cell is

$$\begin{pmatrix} 1 & a_1 & 0 & 0 & 0 & 0 \\ 0 & 0 & 0 & 0 & 0 & -1 \\ 0 & 0 & 0 & 1 & 0 & a_2 \end{pmatrix} \tag{10.21}$$

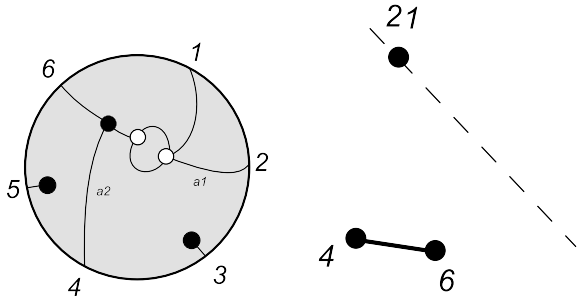

(3) Perform the shift $(2 \to 4)$. This moves P_2 towards P_4 along the line joining P_2 and P_4. So now we have the space of degenerate quadrilaterals (P_1, P_2, P_4, P_6), where P_2 lies on the line segment $(1, 4)$, and P_1 lies on L_∞. A representative matrix for this three-dimensional cell is

$$\begin{pmatrix} 1 & a_1 & 0 & 0 & 0 & 0 \\ 0 & 0 & 0 & 0 & 0 & -1 \\ 0 & a_3 & 0 & 1 & 0 & a_2 \end{pmatrix} \tag{10.22}$$

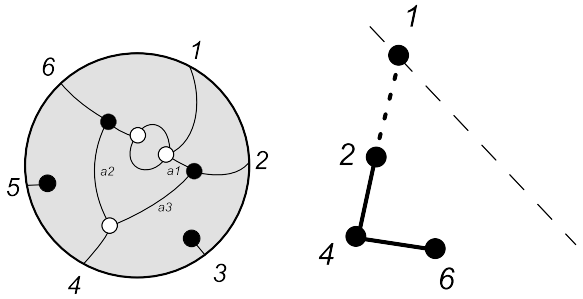

(4) Perform the shift $(5 \to 6)$. This places P_5 at the same location as P_6. Now we have the space of degenerate pentagons $(P_1, P_2, P_4, P_5, P_6)$, where P_2 lies on the line segment $(1, 4)$, and P_1 lies on L_∞, and $P_5 = P_6$. A representative matrix for this four-dimensional cell is

$$\begin{pmatrix} 1 & a_1 & 0 & 0 & 0 & 0 \\ 0 & 0 & 0 & 0 & -a_4 & -1 \\ 0 & a_3 & 0 & 1 & a_4 a_2 & a_2 \end{pmatrix} \qquad (10.23)$$

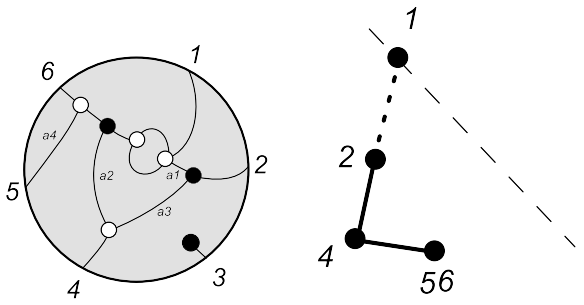

(5) Perform the shift $(1 \to 6)$. This moves P_1 towards P_6 along the line joining P_1 and P_6. So now we have the space of degenerate pentagons $(P_1, P_2, P_4, P_5, P_6)$ where all points lie in $\mathcal{A}^2$, and in addition the edge $(1, 6)$ is parallel to the edge $(2, 4)$, and $P_5 = P_6$. A representative matrix for this five-dimensional cell is

$$\begin{pmatrix} 1 & a_1 & 0 & 0 & 0 & 0 \\ -a_5 & 0 & 0 & 0 & -a_4 & -1 \\ a_5 a_2 & a_3 & 0 & 1 & a_4 a_2 & a_2 \end{pmatrix} \qquad (10.24)$$

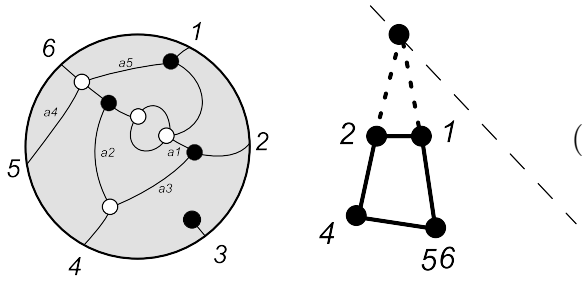

(6) Perform the shift $(5 \to 4)$. This moves P_5 towards P_4 along the line joining P_5 and P_4. So now we have the space of degenerate pentagons $(P_1, P_2, P_4, P_5, P_6)$ where all points lie in $\mathcal{A}^2$, the edge $(1, 6)$ is parallel to the edge $(2, 4)$, and the point P_5 lies

on the edge P_4P_6. A representative matrix for this six-dimensional cell is

$$\begin{pmatrix} 1 & a_1 & 0 & 0 & 0 & 0 \\ -a_5 & 0 & 0 & 0 & -a_4 & -1 \\ a_5a_2 & a_3 & 0 & 1 & a_4a_2+a_6 & a_2 \end{pmatrix}$$

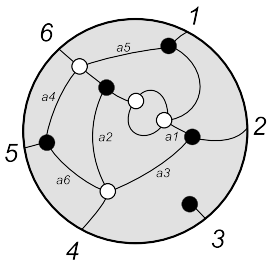

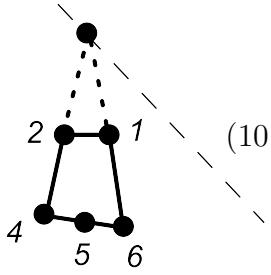

(10.25)

(7) Perform the shift $(3 \to 4)$. This places P_3 at the same location as P_4. So now we have the space of degenerate convex hexagons $(P_1, P_2, P_3, P_4, P_5, P_6)$ where all points lie in $\mathcal{A}^2$, the edge $(1, 6)$ is parallel to the edge $(2, 4)$, the point P_5 lies on the edge P_4P_6, and $P_3 = P_4$. A representative matrix for this seven-dimensional cell is

$$\begin{pmatrix} 1 & a_1 & 0 & 0 & 0 & 0 \\ -a_5 & 0 & 0 & 0 & -a_4 & -1 \\ a_5a_2 & a_3 & a_7 & 1 & a_4a_2+a_6 & a_2 \end{pmatrix}$$

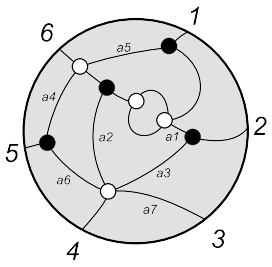

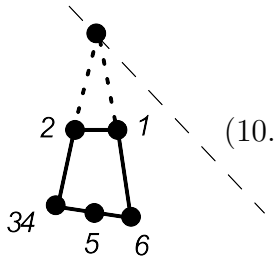

(10.26)

(8) Perform the shift $(3 \to 2)$. This moves P_3 towards P_2 along the line joining P_2 and P_3. So now we have the space of degenerate convex hexagons $(P_1, P_2, P_3, P_4, P_5, P_6)$ where all points lie in $\mathcal{A}^2$, the edge $(1, 6)$ is parallel to the edge $(2, 4)$, the point P_5 lies on the edge $(4, 6)$, and the point P_3 lies on the edge $(2, 4)$. A representative matrix for this eight-dimensional cell is

$$\begin{pmatrix} 1 & a_1 & a_1a_8 & 0 & 0 & 0 \\ -a_5 & 0 & 0 & 0 & -a_4 & -1 \\ a_5a_2 & a_3 & a_7+a_3a_8 & 1 & a_4a_2+a_6 & a_2 \end{pmatrix}$$

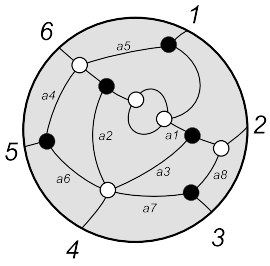

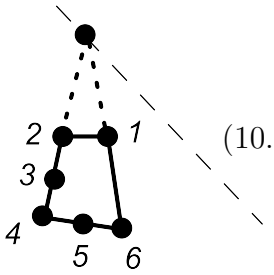

(10.27)

Note that vanishing of the minors (234) and (456) is immediate from the geometric description. The vanishing of $[(16) \cap (24)]$ is equivalent to the statement that the edge $(1,6)$ is parallel to the edge $(2,4)$. Again, in the polygon diagram above, we should imagine that the intersection $(1,6) \cap (2,4)$ is placed infinitely away so that the dashed lines are parallel.

The matrix P parametrizes the same Grassmannian cell as the FL-2 matrix in Appendix A of [3], which can be seen by a change of gauge followed by a change of variables. First act on P from the left by

$$g = \begin{pmatrix} 0 & \frac{1}{a_5} & -\frac{1}{a_2^2 a_5^2} \\ -1 & 0 & \frac{1}{a_2^2 a_5} \\ 0 & 0 & \frac{1}{a_2 a_5} \end{pmatrix} \in \mathrm{GL}(1;1). \tag{10.28}$$

Then perform the monomial coordinate change $a_1 \to c_5, a_2 \to c_8/c_3, a_3 \to c_1 c_5/c_3, a_4 \to c_7/c_8, a_5 \to 1/c_8, a_6 \to c_4 c_7/c_3, a_7 \to c_2 c_6/c_3, a_8 \to c_6/c_5$. As required, this is a diffeomorphism of $\mathbb{R}^8_{>0}$

We can describe the cell $\Pi_{\text{FL-2}} \subset G_{\geq 0}(1,n;1)$ as the space of degenerate convex hexagons $P = (P_1, P_2, P_3, P_4, P_5, P_6)$ where all points lie in $\mathcal{A}^2$, the edge $(1,6)$ is parallel to the edge $(2,4)$, the point P_5 lies on the edge $(4,6)$, and the point P_3 lies on the edge $(2,4)$. We claim that $\Pi_{\text{FL-2}}$ is a codimension-3 boundary of the eleven-dimensional top cell $\Pi_{\{2,4,6\}}$. This top cell is the space of convex hexagons that can be inscribed into a big triangle, so that the edges $(2,3)$, $(4,5)$ and $(6,1)$ lie on the edges of the big triangle, as illustrated below on the left.

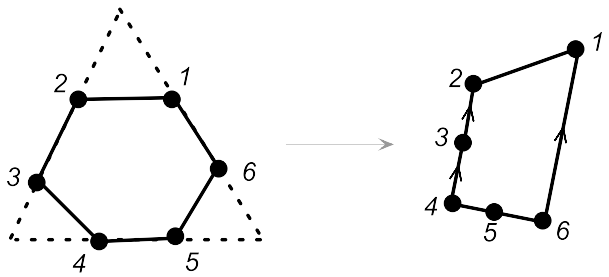

(10.29)

To obtain $\Pi_{\text{FL-2}}$ as a boundary of $\Pi_{\{2,4,6\}}$, first move P_4 away from P_5 until it lies on the line $(2,3)$, then move P_6 away from P_1 until it lies on $(4,5)$. Thus, P_2, P_3, P_4 are now collinear and P_4, P_5, P_6 are now collinear. Finally, move the point P_1 *away* from P_2 until $(1,6)$ is parallel to $(2,3)$. The three steps are equivalent to taking $(234), (456), [(16) \cap (24)]$ to zero. The resulting space of degenerate hexagons, as shown on the upper right diagram where the directed lines are parallel, is the cell $\Pi_{\text{FL-2}}$. We should note that $\Pi_{\{2,4,6\}}$ is not the only top cell from which $\Pi_{\text{FL-2}}$ can be obtained. Another possibility is $\Pi_{\{3,4,6\}}$.

10.2 The one-loop Grassmannian measure

Recall from Section 2.4.6 that the canonical form of the positive Grassmannian $G_{\geq 0}(k,n)$ is the beautiful cyclic measure 2.51. Furthermore, the canonical form for every Grassmannian cell can be obtained by taking a sequence of residues on this measure. We now wish to generalize these ideas to one loop. However, new subtleties arise, since for $k = 1$ there are multiple top cells each with its own canonical form. Also, for $k > 1$, the notion of top cell is still undefined.

We begin with a general discussion of the properties that the measure must satisfy before writing down specific formulas. We mostly focus on the $k = 1$ case where the measure has a beautiful interpretation as the volume of polygon, and generalize to $k > 1$ where possible.

10.2.1 The general setup

We construct a family of integration measures on the one-loop Grassmannian (i.e. the space of P matrices) which we claim generate one-loop BCFW terms. We consider

$$\mathcal{M}_{k,n}(P) = \frac{d^{(k+2)n}P/\text{vol GL}(k;1)}{\prod_{i=1}^{n}(i\ i{+}1\ i{+}2\ \cdots\ i{+}k{+}1)}\ \mathcal{M}'_{k,n}(P) \tag{10.30}$$

which is defined on $G_{\geq 0}(k,n;1)$. The factor $\mathcal{M}'_{k,n}(P)$ is called the geometric factor and $\mathcal{M}_{k,n}(P)$ the measure. We propose that BCFW terms can be generated by taking residues of the following integral

$$\mathcal{Y}_{k,n} = \int \frac{d^{(k+2)n}P}{\prod_{i=1}^{n}(i\ i{+}1\ i{+}2\ \cdots\ i{+}k{+}1)}\ \mathcal{M}'_{k,n}(P)\ \delta^{(k+2)(k+4)}(\mathcal{Y}{-}P.Z) \tag{10.31}$$

where

$$(i_1\ i_2\ \cdots\ i_{k+2}) = \epsilon^{A_1,\ldots,A_{k+2}} P_{A_1 i_1}\cdots P_{A_{k+2} i_{k+2}} \tag{10.32}$$

$$[i_1\ i_2\ \cdots\ i_k] = \epsilon^{a_1,\ldots,a_k} C_{a_1 i_1}\cdots C_{a_k i_k} \tag{10.33}$$

The repeated indices $A_1,\ldots,A_{k+2} = 1,\ldots,k{+}2$ and $a_1,a_2,\ldots,a_k = 1,2,\ldots,k$ are implicitly summed over their respective range. The indices $i_1,i_2,\ldots,i_{k+2} \in \{1,2,\ldots,n\}$ label the columns of the C and P matrices. Thus $(i_1,\ldots,i_{k+2})$ denotes the determinant of the matrix formed by the columns $i_1,\ldots,i_{k+2}$ of the P matrix, while $[i_1,\ldots,i_k]$ denotes the determinant of the matrix formed by the columns $i_1,\ldots,i_k$ of the C matrix. In subsequent parts, we will also make use of the following notation:

$$[i_1\ i_2\ \cdots\ i_s]_{r_1,\ldots,r_t} = \epsilon_{r_1,\ldots,r_t}{}^{a_1,\ldots,a_s} C_{a_1 i_1}\cdots C_{a_s i_s} \tag{10.34}$$

where $s+t=k$. This denotes, up to a sign, the determinant of the matrix formed by columns $i_1,\ldots,i_s$ of the C matrix with rows $r_1,\ldots,r_t$ removed. The indices are raised and lowered with the all plus metric, so we can raise and lower them arbitrarily. For $t=0$, we get back the square bracket defined earlier.

In the definition of our measure, we have not yet used the square bracket. Nonetheless, both brackets are important because they are covariant under $\mathrm{GL}(k;1)$ transformations. The round brackets appearing in the denominator of the measure is the familiar cyclic factor. However, the most important part of the measure is the ge-

ometric factor $\mathcal{M}'_{k,n}(P)$. We provide detailed examples of the geometric factor in the subsequent section. For now we simply describe some constraints it must satisfy. First of all, it must be covariant under $\mathrm{GL}(k;1)$ transformations. Namely, $\mathcal{M}'_{k,n}$ should scale as $\det(G)^k \det(J)^{k+2}$ (See (2.1) of [3]). The exponents are chosen so that a $\mathrm{GL}(k;1)$ transformation on $\mathcal{Y}$ makes the integrand scale as $\det(G)^4 \det(J)^{k+2}$, which is the expected result. Furthermore, covariance implies that $\mathcal{M}'_{k,n}$ should only depend on round brackets and square brackets. The number of integrations we are left with after integrating out the delta functions is $(k+2)(n-k-4)$. We interpret these integrals as contour integrals, or as a sum over multi-variable residues. We show later that the residues of this integral are BCFW terms (or sums of them), provided an appropriate choice of $\mathcal{M}'$.

10.2.2 The measure

The main content of our proposed formula is the geometric factor $\mathcal{M}'_{k,n}(P)$, which we now describe.

For $k = 0$, the full measure is simply the cyclic measure, hence,

$$\mathcal{M}'_{0,n}(P) = 1 \tag{10.35}$$

In the case $n = 4$, there is no contour, and the measure precisely gives the 4-point MHV 1-loop integrand. For higher n, we have a $(2n-8)$-dimensional form, and it is a well known fact that residues of this form give BCFW terms, also known as Kermit terms in [40].

Starting at $k = 1$, the geometric factor $\mathcal{M}'$ is no longer trivial. To guess the form of $\mathcal{M}'$, we begin by analyzing the simplest case $n = 5$. Since there is no contour, we expect the measure to give the exact integrand. Here we skip the details and just

give the result, which is clean and simple.

$$\mathcal{M}'_{1,5} = \sum_{i=1}^{n} \frac{(X_1\ i\ i{+}1)}{[X_1][i][i{+}1]} \tag{10.36}$$

Here $X_1 \in \mathbb{P}^2$ is an arbitrary point. Readers familiar with polytopes in projective space would immediately recognize $\mathcal{M}'$ as the area of the pentagon whose vertices are formed by the columns of the P matrix. We have checked analytically that this measure precisely gives the 5-point 1-loop NMHV integrand.

We now make a curious and surprising observation. It is well known that this integrand consists of three BCFW terms. Naively, we should expect there to exist a measure whose residues give precisely those three terms. This intuition, however, is incorrect. What we have learned from this measure is that the $\overline{\text{MHV}}$ case does not require a contour. In fact, as we will see in a moment, this is true for higher k as well, and is probably true to all loops. But this still does not explain where the three BCFW terms come from. Let us go back to the observation of $\mathcal{M}'_{1,5}$ as the area of a pentagon, which can be written in multiple ways, depending on the choice of triangulation. For instance, we can write

$$\mathcal{M}'_{1,5} = \{3, 4, (23) \cap (45)\} + \{1, 2, (23) \cap (15)\} + \{5, (23) \cap (15), (23) \cap (45)\} \tag{10.37}$$

where $\{a_1, a_2, a_3\}$ denotes the signed area of the triangle whose vertices are the columns a_1, a_2, a_3 of the P matrix, and $(a_1 a_2) \cap (a_3 a_4)$ the intersection of lines $(a_1 a_2)$ and $(a_3 a_4)$. See Appendix A of [3] for precise definitions. (10.37) is simply a triangulation of the measure, which we depict in the following picture.

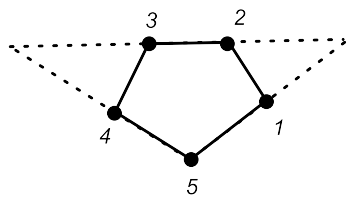

(10.38)

These three terms correspond to the three BCFW terms.

Even before moving on to more complicated cases, there is a great deal of physical insight that can be learned from this measure. Let us write down the full integral explicitly,

$$\int \frac{d^{15}P}{(123)(234)(345)(451)(512)} \sum_{i=1}^{5} \frac{(1\ i\ i{+}1)}{[1][i][i{+}1]} \tag{10.39}$$

where we omitted writing the delta functions, and we have set $X_1 \to 1$. First, we observe that all the poles of the integrand are manifest in the measure. For example, the (123) factor corresponds to the pole $\langle YAB45\rangle$, which is easy to see on the support of the delta functions. In fact, it is generally the case that $(a\ a{+}1\ a{+}2)$ corresponds to the pole $\langle YAB\ a{+}3\ a{+}4\rangle$, where the indices are mod 5 as usual. So all the poles coming from propagators that lie inside the loop are manifest. Of course there are also propagators that do not lie inside the loop. These are manifest in the square brackets. Namely, the square bracket $[a]$ corresponds to the pole $\langle Y\ a{+}1\ a{+}2\ a{+}3\ a{+}4\rangle$. We see that the pole structure of the amplitudes places very severe constraints on the measure. In fact, one may have even guessed the measure purely from this insight.

Furthermore, in the limit where the external data Z is positive and the variables YAB live on the inside of Z, we see that the P matrix, which is uniquely constrained by the delta functions, must be positive in the one-loop Grassmannian sense. Geometrically, positivity of the P matrix means that the polygon is convex. This is a rather neat observation, and is in fact connected to the pole structure of the integrand. For instance, the pole $(a\ a{+}1\ a{+}2) \to 0$ simply corresponds to the vertices $a, a{+}1, a{+}2$ becoming collinear. Moreover, the pole $[a] \to 0$ corresponds to the vertex a going to infinity. Hence, poles involving the loop correspond to a degenerating polygon while poles not involving the loop correspond to a polygon whose area blows up to infinity.

We make one last observation. There are two classes of triangulations of the pentagon discussed so far, which we will refer to as "spurious" and "non-spurious" triangulations respectively. A spurious triangulation consists of triangles formed by edges (possibly extended in either direction if needed) of the pentagon. These triangles lie partially outside the pentagon. The BCFW representation shown above is an example of a spurious triangulation. A non-spurious triangulation consists of triangles formed by vertices of the pentagon. These triangles all lie inside the pentagon and tile the pentagon perfectly. An example of a non-spurious triangulation is (10.39). Non-spurious triangulations are also called "local" triangulations.

For higher n, the canonical form of the positive loop Grassmannian $G_{\geq 0}(1, n; 1)$ is

$$\mathcal{M}'_{1,n}(P) = \sum_{i=1}^{n} \frac{(X_1\ i\ i{+}1)}{[X_1][i][i+1]} \tag{10.40}$$

For $k = 2$, the canonical form of $G_{\geq 0}(2, n; 1)$ is

$$\mathcal{M}'_{2,n}(P) = \sum_{i,j=1}^{n} \frac{\begin{vmatrix} [i{+}1]_1 & [j{+}1]_1 \\ [i{+}1]_2 & [j{+}1]_2 \end{vmatrix} \begin{vmatrix} (X_1\ i\ i{+}1\ i{+}2) & (X_1\ j\ j{+}1\ j{+}2) \\ (X_2\ i\ i{+}1\ i{+}2) & (X_2\ j\ j{+}1\ j{+}2) \end{vmatrix}}{[X_1\ X_2][i\ i{+}1][i{+}1\ i{+}2][j\ j{+}1][j{+}1\ j{+}2]} \tag{10.41}$$

where X_1, X_2 are arbitrary 4-vectors, and the vertical bars denote taking the determinant. We do not yet have a rigorous proof that this is the correct answer, but our answer is supported by the fact that the measure gives the correct 1-loop integrand for the $n = 6$ NNMHV case where there is no contour.

Finally, we present the canonical form of $G_{\geq 0}(k, n; 1)$.

$$\mathcal{M}'_{k,n}(P) = \sum_{i_1,\ldots,i_k=1}^{n} \frac{\det_{st}[i_t{+}1, \ldots, i_t{+}k{-}1]_s\ \det_{st}(X_s\ i_t\ \cdots\ i_t{+}k)}{[X_1, \ldots, X_k] \prod_{p=1}^{k} [i_p\ i_p{+}1\ \cdots\ i_p{+}k{-}1][i_p{+}1\ i_p{+}2\ \cdots\ i_p{+}k]} \tag{10.42}$$

where $\det_{st}$ denotes the determinant of a matrix whose row and column indices are s, t, respectively. The constants $X_1, \ldots, X_k$ are arbitrary $(k+2)$-vectors. We have tested this measure numerically against the integrand in the $\overline{\text{MHV}}$ case up to $k = 4$.

10.2.3 Top cells and BCFW terms

We now address the problem of obtaining BCFW terms as residues of some measure. Naively, one may be tempted to think that BCFW terms are simply residues of a single measure, such as the canonical form of the positive one-loop Grassmannian. However, this is obviously incorrect. Even for $n = 5$, the BCFW terms are given by areas of triangles rather than the full area of the pentagon. In fact, we argue in this section that these triangular pieces are nothing other than the canonical forms of top cells, which we call top cell measures.

For each top cell $\Pi \subset G_{\geq 0}(1, n; 1)$, we let $\mathcal{M}_\Pi$ denote its canonical form. Recall that there exists a triangle Δ whose vertices X_1, X_2, X_3 are given by (10.6), such that the polygon is inscribed inside the triangle. Clearly, we can approach any boundary of Π by going to the limit where one of the vertices of Δ approaches infinity. Thus, it is natural to expect that the measure $\mathcal{M}_\Pi$ should have simple poles at $[X_i] \to 0$ for $i = 1, 2, 3$. It follows that the geometric factor of the top cell measure is given by the area of Δ:

$$\mathcal{M}'_\Pi = \{X_1, X_2, X_3\} \tag{10.43}$$

We prove this in Section 10.2.5.

For $n = 5$, we find that the canonical form of the one-loop Grassmannian is the sum of three top cell measures.

$$\mathcal{M}_{1,5} = \mathcal{M}_{\Pi_{\{2,3,4\}}} + \mathcal{M}_{\Pi_{\{1,2,5\}}} + \mathcal{M}_{\Pi_{\{2,4,5\}}} \tag{10.44}$$

The three measures match term-by-term with the triangle areas in (10.37), and hence also with the BCFW terms. In Section 10.2.4, we show that these three top cells form a triangulation of the one-loop Grassmannian.

We therefore make the conjecture that each BCFW term for $k = 1$ and any n is given as some multi-dimensional residue of a top cell measure. Both the top cell and residue can be identified using a series of simple steps that we now illustrate.

Consider again the FL-2 term for the 6 point NMHV 1-loop integrand. Recall from Section 10.1.5 that the top cell $\Pi_{\text{FL-2}}$ of this term is given by a codimension-3 boundary of $\Pi_{2,4,6}$ by taking $(234), (456), [(16) \cap (24)] \to 0$. It follows that the canonical form $\mathcal{M}_{\text{FL-2}}$ of the FL-2 cell must be obtained from the top cell measure $\mathcal{M}_{\Pi_{\{2,4,6\}}}$ by taking three residues given by the three zero conditions. Hence, the FL-2 term is given by

$$\text{FL-2}_{\text{Y space}} = \int \operatorname*{Res}_{\substack{(234)\to 0 \\ (456)\to 0 \\ [(16)\cap(24)]\to 0}} \frac{d^{18}P}{\prod_{i=1}^{6}(a, a{+}1, a{+}2)}\, \mathcal{M}'_{\Pi_{\{2,4,6\}}} \delta^{15}(\mathcal{Y} - P.Z) \quad (10.45)$$

In practice, the residue can be computed by using the following change of variables.

$$P_3 = \alpha_1 P_2 + \alpha_2 P_4 + z_1 P_1 \quad (10.46)$$

$$P_5 = \alpha_3 P_4 + \alpha_4 P_6 + z_2 P_1 \quad (10.47)$$

$$[(16) \cap (24)] = z_3 \quad (10.48)$$

Then take residues where $z_1, z_2, z_3 \to 0$, which gives the following.

$$\text{FL-2}_{\text{Y space}} = \int \frac{d^4\alpha d^3P_1 d^3P_2 d^3P_4 d^3P_6}{\alpha_1\alpha_2\alpha_3\alpha_4 (124)(246)(612)[4][6]}\, \delta\left([1] - [6]\frac{(124)}{(246)}\right) \delta^{15}(\mathcal{Y} - P.Z) \quad (10.49)$$

The remaining part of the integral is straightforward since there are precisely enough delta functions to localize the integrals.

We should note that the top cell from which the FL-2 cell is obtained is not unique. For each term in Appendix A of [3], we indicate only one possible top cell. In fact, for some BCFW terms, it is possible to obtain the cell for the term as a codimension-3 boundary of the full one-loop positive Grassmannian. In such casees, it is canonical to use the full polygon area as the geometric factor.

10.2.4 Triangulation of the one-loop Grassmannian with top cells

We argue that $G_{\geq 0}(1, n; 1)$ can be triangulated as a union of the top cells Π_S. More precisely, let C_n be a convex n-gon that is different from the n-gon $(P_1, P_2, \ldots, P_n)$. Furthermore, suppose we are given a triangulation $\mathcal{G} = \{S_1, S_2, \ldots, S_{n-2}\}$ of C_n, where each S_i is a triangle of C_n and thus a three-element subset of $\{1, 2, \ldots, n\}$. Then we claim that $\mathcal{T} = \{\Pi_{S_1}, \ldots, \Pi_{S_{n-2}}\}$ is a collection of top cells of $G_{\geq 0}(1, n; 1)$ that triangulate $G_{\geq 0}(1, n; 1)$.

A detailed proof for all n is given in Section 4.4 of [3]. Here we simply demonstrate an example. In particular, for $n = 5$ and $\mathcal{G} = \{125, 234, 245\}$, we claim that the one loop Grassmannian $G_{\geq 0}(1, n; 1)$ is triangulated by the top cells $\mathcal{T} = \{\Pi_{\{1,2,5\}}, \Pi_{\{2,3,4\}}, \Pi_{\{2,4,5\}}\}$. Recall that

- The cell $\Pi_{\{1,2,5\}}$ is given by the condition that $[2, 3; 5, 1]$ is positive.
- The cell $\Pi_{\{2,3,4\}}$ is given by the condition that $[4, 5; 2, 3]$ is positive.
- The cell $\Pi_{\{2,4,5\}}$ is given by the conditions that $[2, 3; 4, 5]$ and $[5, 1; 2, 3]$ are positive.

Given a nondegenerate convex pentagon, $[2, 3; 5, 1]$ is either positive or negative. Similarly, $[4, 5; 2, 3]$ is either positive or negative. It follows that every nondegenerate con-

vex pentagon belongs to exactly one of $\Pi_{\{1,2,5\}}, \Pi_{\{2,3,4\}}, \Pi_{\{2,4,5\}}$, so $\mathcal{T}$ is a triangulation of $G_{\geq 0}(1, n; 1)$, as claimed.

10.2.5 Geometric factor

We prove (10.43) that

$$\mathcal{M}_\Pi = \frac{d^{3n}P/\text{vol GL}(1;1)}{\prod_{i=1}^{n}(i, i+1, i+2)}\{X_1, X_2, X_3\} \tag{10.50}$$

is the canonical form of the top cell Π. In the following, we do not worry about global signs.

The proof is by induction on n, where the base case is $n = 3$. In this case, there is only one top cell $\Pi = \Pi_{\{1,2,3\}}$, and we can gauge fix P to be

$$P = \begin{pmatrix} 1 & 0 & 0 \\ 0 & 1 & 0 \\ \beta\alpha & \alpha & 1 \end{pmatrix} \tag{10.51}$$

where (α, β) are the positive coordinates. Thus the LHS of (10.50) is equal to $(1/\alpha\beta)d\alpha d\beta$. The geometric factor $\{X_1, X_2, X_3\}$ is equal to $1/\alpha^2\beta$ and $d^{(k+2)n}P/\text{vol GL}(1;1) = d\alpha d(\beta\alpha) = \alpha d\alpha d\beta$. Since all the cyclic minors are equal to 1, (10.50) holds in this case.

Now suppose (10.50) holds for some value of n. After cyclically relabelling the $n+1$ vertices, any top cell Π' for $G_{\geq 0}(1, n+1; 1)$ can be obtained from some top cell Π for $G_{\geq 0}(1, n; 1)$ in the following way:

1. Start with the space of n-gons $(P_1, P_2, \ldots, P_n)$ for Π.

2. Perform the shift $(n \to n+1)$, placing P_{n+1} on top of P_n.

3. Perform the shift $(n+1 \to 1)$, moving P_{n+1} towards P_1.

4. Perform the shift $(n \to n-1)$ moving P_n towards P_{n-1}.

Note that each of the shifts (2),(3),(4) increases the dimension of the cell by one (so $\dim \Pi' = \dim \Pi + 3$), and introduces a new positive coordinate denoted α, β, γ respectively. If P is the original matrix for Π with columns $P_1, P_2, \ldots, P_n$, then the new matrix is

$$P' = (P_1, P_2, \ldots, P_{n-1}, P_n + \gamma P_{n-1}, \alpha P_n + \beta P_1).$$

It is not difficult to check that

$$d^{3(n+1)}P'/\text{vol GL}(1;1) = \pm d^{3n}P\alpha(n-1,n,1)d\alpha d\beta d\gamma/\text{vol GL}(1;1)$$

where $(n-1,n,1)$ denotes a minor of P. But we also have

$$\begin{aligned}(n-2,n-1,n)' &= (n-2,n-1,n)\\ (n-1,n,n+1)' &= \beta(n-1,n,1)\\ (n,n+1,1)' &= \alpha\gamma(n-1,n,1)\\ (n+1,1,2)' &= \alpha(n,1,2).\end{aligned}$$

So

$$\frac{d^{3n}P/\text{vol GL}(1;1)}{\prod_{i=1}^{n+1}(i,i+1,i+2)'} = \frac{\alpha}{\alpha^2\beta\gamma}\frac{d^{3n}P/\text{vol GL}(1;1)}{\prod_{i=1}^{n}(i,i+1,i+2)}d\alpha d\beta d\gamma = \frac{1}{\{X_1,X_2,X_3\}}M_{\Pi'}$$

since $\mathcal{M}_{\Pi'} = \mathcal{M}_\Pi \frac{d\alpha d\beta d\gamma}{\alpha\beta\gamma}$. Now as triangles in $\mathbb{P}^2$, the triangle Δ for Π and Δ' for Π' are identical. So $\{X_1,X_2,X_3\} = \{X_1',X_2',X_3'\}$. Thus we have $\frac{1}{\{X_1,X_2,X_3\}}M_{\Pi'} = \frac{1}{\{X_1',X_2',X_3'\}}M_{\Pi'}$, completing the proof of (10.50).

Chapter 11

Conclusion

We have introduced positive geometries and canonical forms as a new mathematical framework for studying scattering amplitudes. In Section 2.1, we described positive geometry as a pair $(X, X_{\geq 0})$ consisting of a complex projective variety X and a non-negative part $X_{\geq 0}$ which generically has boundaries of all codimensions. Associated with every positive geometry is a unique meromorphic top form called its canonical form whose singularities are controlled by the boundaries of the geometry. We then gave a series of examples, including generalized simplices and generalized polytopes. Subsequently, in Section 3, we discussed various techniques for computing canonical forms, including direct construction from poles and zeroes, triangulations, pushforwards, and various integral representations.

In Section 4, we introduced the associahedron as a positive geometry in kinematic space for color-ordered scattering amplitudes, thus providing our first physical example. We showed that there exists an infinite family of associahedra whose canonical form gives the color-ordered tree amplitudes of the bi-adjoint cubic scalar theory. Our formalism provides an independent construction of these amplitudes without reference to any of the traditional machinery of quantum field theory, canonical quantization, or path integrals which rely heavily on the principles of locality and unitarity. On

the contrary, we presented a novel point of view: locality and unitary are *emergent* properties of the positive geometry (see for instance Section 4.3). This is a recurrent theme throughout the remainder of this text. We then discussed the worldsheet as a positive geometry, and showed that its canonical form is the famous Parke-Taylor form. Most importantly, we argued that the worldsheet associahedron is directly related to the kinematic associahedron via a diffeomorphism—the scattering equations. This observation, combined with the machinery of positive geometries, provides a complete and independent explanation for the CHY formula for the bi-adjoint scalar. Finally, in Section 6, we discussed the color-kinematics duality from the point of view of positive geometries, and presented a general duality between colored amplitudes and differential forms on kinematic space called scattering forms. Moreover, we found that various properties of the amplitudes like kinematic Jacobi relations, trace decomposition and BCJ relations can all be understood as geometric properties of the form. In essence, this provides a generalization of our work on the associahedron to a larger class of theories that includes Yang-Mills and Non-linear Sigma Model at tree level.

Beginning in Section 7, we provided a construction of the amplituhedron as a positive geometry, for which the Grassmannian is the fundamental building block. As first discussed in [17], the canonical form of the amplituhdron determines the scattering amplitudes of planar $\mathcal{N} = 4$ super Yang-Mills to all loops, although the language of "canonical forms" was not introduced until [2]. A precise prescription for mapping the canonical form to the scattering amplitude is provided in Section 8.2, which involves a novel procedure for "bosonizing" supersymmetry also discussed for the first time in [17]. Moreover, we demonstrate the striking fact that BCFW recursion is simply a triangulation of the amplituhedron. In Section 9, we provided a diagrammatic procedure for computing any BCFW term, with many examples. In Section 10, we focused on the geometry of the one-loop case.

There are many obvious unanswered questions and open avenues of investigation suggested by our results. For instance: Is there a complete geometrization of scattering forms for YM and the NLSM that brings the polarization vectors into the geometry? This question is of course also relevant to the search for geometries connected to gravity amplitudes. While we do not have any natural scattering forms due to the absence of color, the amplitudes can be obtained using the double-copy construction a la BCJ [14, 15]. More precisely, for a double copy of the form $L \otimes R$ between theories L and R, the amplitude for the product theory can be obtained directly from either $\Omega_L^{(n-3)}$ for the L theory or $\Omega_R^{(n-3)}$ for the R theory by replacing the wedge products $W(g)$ with appropriate kinematic numerators:

$$\mathbf{M}_n^{L\otimes R} = \sum_{\text{cubic } g} \frac{N_L(g)\ N_R(g)}{\prod_{I\in g} s_I} = \Omega_L^{(n-3)}|_{W(g)\to N_R(g)} = \Omega_R^{(n-3)}|_{W(g)\to N_L(g)}\,, \qquad (11.1)$$

For example, we obtain gravity from the product YM $\otimes$ YM, Born-Infeld theory from the product YM $\otimes$ NLSM and the so-called special Galileon theory from NLSM $\otimes$ NLSM [60]. Along this line, it is very tempting to connect our worldsheet picture for the open string to the ambitwistor string [64, 65, 66, 67], and related worldsheet methods using scattering equations [68, 69] which are exclusively for the closed string. Furthermore, could we understand the double-copy construction, and possible geometries for gravity amplitudes in a way similar to the Kawai-Lewellen-Tye relations connecting open- and closed-string amplitudes [70] (See [71, 72] for related ideas)?

Let us end with a few suggestions for immediate avenues of progress which are more continuously connected to the themes introduced in this paper.

General $d\log$ projective forms: permutohedra and beyond Recall that a scattering form (11.2) is called $d\log$ *scattering form* if it is projective and every kinematic numerator is either 0 or ± 1. A classification of all such forms is then

equivalent to solving the Jacobi relations (6.18) provided $N(g|\alpha_g) \in \{0, \pm 1\}$.

$$\Omega^{(n-3)}_{d\log}(S) = \sum_{\text{cubic } g} N(g)\, \Omega^{(n-3)}(g)(S) \tag{11.2}$$

While we do not have a complete classification, we can discuss some general properties. To every $d\log$ scattering form, we assign a connected graph Υ consisting of a vertex for every cubic graph g whose numerator $N(g)$ is non-zero, with a line between any two vertices related by mutation. Furthermore, projectivity is satisfied precisely if every vertex is adjacent to exactly $(n-3)$ lines (*i.e.* the graph is "simple"), and a sign flip occurs between any two vertices related by mutation. In particular, walking along any closed path in the graph Υ should return us back to the same sign. Note that this does not imply that the path must be of even length, since the sign at the initial vertex depends on its propagators which may have been reordered by the sequence of mutations.

The simplest example of of $d\log$ scattering forms is of course the planar scattering form $\Omega^{(n-3)}_{\phi^3}[\alpha]$ whose connected graph Υ is given by the skeleton of the α-ordered associahedron, also known as the Tamari lattice [73]. In fact, for every n, the Tamari lattice provides the smallest number of vertices possible. However, the Tamari lattice is only the beginning of a large class of examples. For n=4, there is only one possible topology for the graph (*i.e.* a line segment). For n=5, we have seen possible topologies are pentagon, hexagon, octagon and nonagon.

For all n, a large class of possible connected graphs are given by the skeleton of the "Cayley polytopes" discussed in [74] whose $d\log$ scattering forms were obtained by pushing forward Cayley functions (expressed as a form on moduli space) via the scattering equations. The Cayley polytopes are polytopes constructed directly in kinematic space, of which the kinematic associahedron is one example. Furthermore,

much of our associahedron discussion generalizes word-for-word to the Cayley polytopes, a summary of which is provided below.

- The Cayley polytope (whose skeleton is the connected graph Υ) is constructed directly in kinematic space $\mathcal{K}_n$ by intersecting a $(n-3)$-dimensional subspace with the positive region defined by setting $s_I \geq 0$ for every propagator appearing in the cubic graphs.

- The pullback of the $d\log$ scattering form to the subspace gives the canonical form of the Cayley polytope.

- The scattering form can be obtained as the pushforward of a form on moduli space $\mathcal{M}_{0,n}$.

Here we present the construction for one example: *permutohedron* $\mathcal{P}_n$ [75], which is the Cayley polytope with largest number of vertices for any n, where each of the $(n-2)!$ vertices corresponding to a multi-peripheral cubic graph with respect to 1 and n as shown in Figure 6.4.

We begin by defining the top-dimensional "positive region" where all possible poles of the multi-peripheral graphs are positive:

$$s_{1a_1\cdots a_m} \qquad \text{for } m = 1,\ldots,n-3 \text{ and } 2 \leq a_1 < \cdots < a_m \leq n-1 \tag{11.3}$$

where every cut corresponds one of the $(2^{n-2}-2)$ facets of the permutohedron. Furthermore, the subspace is given by the following $(n-2)(n-3)/2$ conditions:

$$s_{ij} \qquad \text{is a negative constant for} \quad 2 \leq i < j \leq n-1\,, \tag{11.4}$$

which are the analog of non-adjacent constants for the associahedron case. One can prove that the intersection of the positive region with the subspace gives the permutohedron by showing geometric factorization on all possible boundaries. Note that

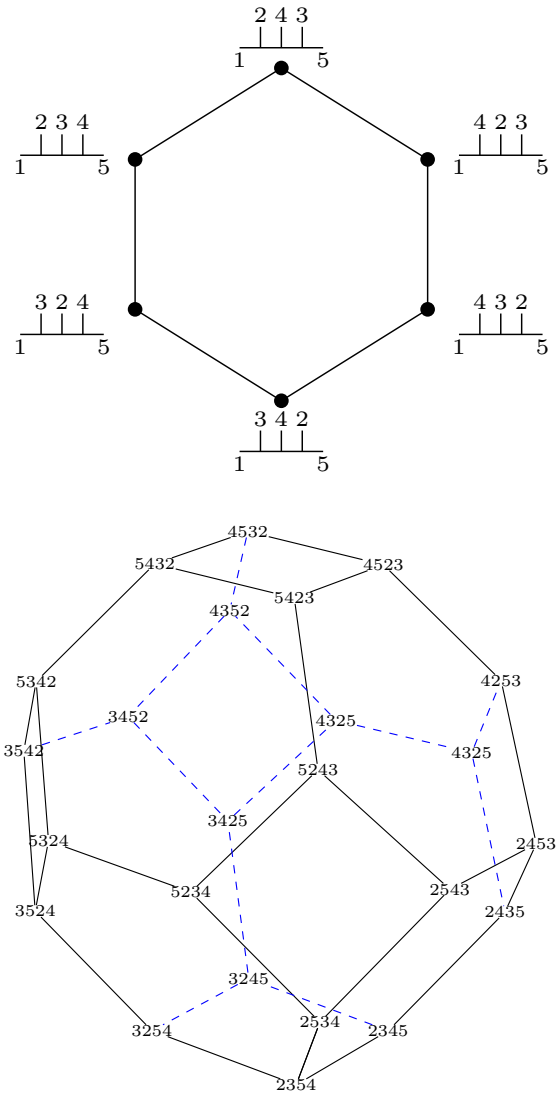

Figure 11.1: Permutohedra for n=5 (left) and n=6 (right)

$\mathcal{P}_{n=4}$ is a line segment; and $\mathcal{P}_{n=5}$ is a hexagon while $\mathcal{P}_{n=6}$ is a truncated octahedron, as shown in Figure (11.1).

Similar to that for associahedron, the (projective) scattering form for $\mathcal{P}_n$ is given by

$$\Omega^{(n-3)}_{\mathcal{P}_n} = \sum_{\pi \in S_{n-2}} \text{sgn}(\pi) \bigwedge_{a=2}^{n-2} d \log s_{1\pi(2)\cdots\pi(a)} \tag{11.5}$$

where $\text{sgn}(\pi)$ is the signum of permutation π. Furthermore, the pullback of the scattering form to the subspace (denoted Q_n) gives the canonical form of the permutohedron:

$$\Omega^{(n-3)}_{\mathcal{P}_n}|_{Q_n} = \left(\sum_{\pi \in S_{n-2}} \frac{1}{\prod_{a=1}^{n-2} s_{1\pi(2)\cdots\pi(a)}} \right) d^{n-3}s \tag{11.6}$$

Finally, the scattering form can be obtained as a pushforward of the following form on moduli space:

$$\omega_{\mathcal{P}_n} := \sum_{\pi \in S_{n-2}} \text{sgn}(\pi) \omega_n^{\text{WS}}(\pi) \tag{11.7}$$

as suggested by (6.65).

The discussion provided above can be generalized to all Cayley polytpes studied in [74]. which belong in the much larger class of *generalized permutohedra* studied by Postnikov [76, 77]. In on-going discussions with Postnikov we have learned that our construction for these polytopes are equivalent to his under a natural change of variables. It is likely that a corresponding $d\log$ scattering form exists for generalized permutohedra. Moreover, for recent studies of worldsheet forms that are relevant to our construction, see [78, 79].

Massive scalar amplitudes, non-logarithmic forms While we have ostensibly focused on amplitudes for massless particles, for the bi-adjoint ϕ^3 theory in particular it is clear that there is no obstruction to dealing with the scattering of massive particles. One interesting point about doing this is the following: we know that we can generate e.g. ϕ^4 couplings from a cubic theory once massive particles are integrated out. Now, suppose we started with a ϕ^4 theory; there are already small subtleties on how to geometrize the scattering form in this case related to the fact that the form simply does not have logarithmic singularities, and have singularities at infinity. The

addiction to "forms with logarithmic singularities" is perhaps the central obstacle to seeing connections to positive geometries. But if we generate the quartic coupling by integrating out massive scalars in a cubic theory, the full theory *does* have logarithmic singularities, and so we can "sneak up" on the hard problem of dealing with non-logarithmic singularities by regulating them as logarithmic ones which are then sent to infinity. Furthermore, the scattering forms for the NLSM have non-trivial residues on all the poles as well as poles at infinity; it would again be fascinating to find a purely geometrical characterization of these residues.

Loops Furthermore, we can immediately start to explore scattering forms and possible positive geometries associated with the loop integrand for e.g. the bi-adjoint scalar theory. We can attempt to mimic the steps needed to "upgrade" the amplitude to a differential form at loop level. An early and obvious source of annoyance is what to do about bubble topologies, since naively including them would give double and higher poles, thus ruining the logarithmic singularities of the form. It is perhaps reasonable to then sum over all diagrams excluding these bubbles. At four points and one loop, this leaves us with a sum over five $d\log$ forms. Can these forms be made to be projective, and is there a positive geometry in the extended kinematic space of loop and Mandelstam variables attached to the loop scattering forms?

Going beyond the bi-adjoint scalar case, one can consider scattering forms for loop integrands in gauge theories and more general theories with color. In particular, it should be straightforward to write down forms for one-loop maximally supersymmetric Yang-Mills amplitudes in general dimensions, since there is no contribution from bubbles. Similarly we expect these forms for loop integrands to have a worldsheet origin that may be related to scattering equations and ambitwistor strings at loop level [65, 80, 81, 82, 83, 84, 85, 86, 87, 88].

Scattering forms, amplituhedron and twistor strings in four dimensions We have now seen *two* notions of scattering forms. In the story of the amplituhedron the forms play the role of combining different helicity amplitudes (as does the super-amplitude) into a single object, while in this paper the differential forms are tied to the geometrization of color. How are these pictures related to each other? There must be a connection, not only for moral reasons, but for more pragmatic and technical ones. We know that the scattering equations and the CHY formula for gluon amplitudes transition smoothly in four-dimensional spacetime to the Roiban-Spradlin-Volovich (RSV) equations and the twistor-string formulas for $\mathcal{N} = 4$ SYM scattering amplitudes [89]. The latter is deeply connected to the geometry of the positive Grassmannian and the amplituhedron, while we have exposed the connection of the former to the worldsheet associahedron. Making progress on these particular questions will undoubtedly need some conceptually new ideas.

On the other hand, first steps have been taken in identifying scattering forms for (tree-level) super-amplitudes in $\mathcal{N} = 4$ SYM and the "amplituhedron" in ordinary, four-dimensional momentum space; these are $(2n-4)$-forms $\Omega_n^{(2n-4)}$ encoding all helicity amplitudes in the space of $\{\lambda_a, \tilde{\lambda}_a \mid a = 1, 2, \cdots, n\}$ subject to momentum conservation, and the $(2n-4)$-dimensional "amplituhedron" lives in a "positive region" in the space with correct "winding numbers" [90, 49]. In close analogy with our associahedron story, there is strong evidence that the four-dimensional scattering equations (RSV) provide a diffeomorphism from $G_{>0}(2, n)$ (the twistor-string worldsheet) to the "amplituhedron" in momentum space; its canonical form, or the pullback of $\Omega_n^{(2n-4)}$ to the subspace where it lives, is then given by the pushforward of the cyclic form of $G_{>0}(2, n)$ [90, 49]. We leave the study of these exciting questions for future investigations.

Extended positive geometries for gluons and pions? It is clear that the gluon and pion scattering forms are fundamental objects, with a canonical purpose in life directly in kinematic space as well as on the worldsheet. What we are still missing is the complete connection of these scattering forms with positive geometries. The obstacle is the most obvious one: while the forms are dictated by god-given properties of gauge-invariance/Adler zero and projective invariance, they are not *canonical forms* which must have not only logarithmic singularities but also unit leading residues. This may be taken as an invitation to e.g. further "geometrize" the polarization vectors—something we have already seen as a critical part of the amplituhedron story in four dimensions—or there may be other ways to more naturally tie the "prefactors" in both YM and the NLSM to the underlying (associahedron) geometry universally associated with the poles of (planar) cubic graphs.

Bibliography

[1] Nima Arkani-Hamed, Yuntao Bai, Song He, and Gongwang Yan. Scattering Forms and the Positive Geometry of Kinematics, Color and the Worldsheet. *JHEP*, 05:096, 2018.

[2] Nima Arkani-Hamed, Yuntao Bai, and Thomas Lam. Positive Geometries and Canonical Forms. *JHEP*, 11:039, 2017.

[3] Yuntao Bai, Song He, and Thomas Lam. The Amplituhedron and the One-loop Grassmannian Measure. *JHEP*, 01:112, 2016.

[4] Yuntao Bai and Song He. The Amplituhedron from Momentum Twistor Diagrams. *JHEP*, 02:065, 2015.

[5] Edward Witten. Perturbative gauge theory as a string theory in twistor space. *Commun. Math. Phys.*, 252:189–258, 2004.

[6] Ruth Britto, Freddy Cachazo, and Bo Feng. New recursion relations for tree amplitudes of gluons. *Nucl. Phys.*, B715:499–522, 2005.

[7] Freddy Cachazo, Peter Svrcek, and Edward Witten. Mhv vertices and tree amplitudes in gauge theory. *Journal of High Energy Physics*, 2004(09):006, 2004.

[8] James M. Drummond, Johannes M. Henn, and Jan Plefka. Yangian symmetry of scattering amplitudes in N=4 super Yang-Mills theory. *JHEP*, 05:046, 2009.

[9] Alexander B Goncharov, Marcus Spradlin, C Vergu, and Anastasia Volovich. Classical polylogarithms for amplitudes and wilson loops. *Physical review letters*, 105(15):151605, 2010.

[10] Freddy Cachazo, Song He, and Ellis Ye Yuan. Scattering in Three Dimensions from Rational Maps. *JHEP*, 10:141, 2013.

[11] Freddy Cachazo, Song He, and Ellis Ye Yuan. Scattering equations and Kawai-Lewellen-Tye orthogonality. *Phys. Rev.*, D90(6):065001, 2014.

[12] Freddy Cachazo, Song He, and Ellis Ye Yuan. Scattering of Massless Particles in Arbitrary Dimensions. *Phys. Rev. Lett.*, 113(17):171601, 2014.

[13] Freddy Cachazo, Song He, and Ellis Ye Yuan. Scattering of Massless Particles: Scalars, Gluons and Gravitons. *JHEP*, 07:033, 2014.

[14] Z. Bern, J. J. M. Carrasco, and Henrik Johansson. New Relations for Gauge-Theory Amplitudes. *Phys. Rev.*, D78:085011, 2008.

[15] Zvi Bern, John Joseph M. Carrasco, and Henrik Johansson. Perturbative Quantum Gravity as a Double Copy of Gauge Theory. *Phys. Rev. Lett.*, 105:061602, 2010.

[16] Nima Arkani-Hamed, Jacob L. Bourjaily, Freddy Cachazo, Alexander B. Goncharov, Alexander Postnikov, and Jaroslav Trnka. *Grassmannian Geometry of Scattering Amplitudes*. Cambridge University Press, 2016.

[17] Nima Arkani-Hamed and Jaroslav Trnka. The Amplituhedron. *JHEP*, 10:030, 2014.

[18] Nima Arkani-Hamed, Andrew Hodges, and Jaroslav Trnka. Positive Amplitudes In The Amplituhedron. *JHEP*, 08:030, 2015.

[19] James Dillon Stasheff. Homotopy Associativity of H-Spaces. I. *Transactions of the American Mathematical Society*, 108(2):275–292, 1963.

[20] James Dillon Stasheff. Homotopy Associativity of H-Spaces. II. *Transactions of the American Mathematical Society*, 108(2):293–312, 1963.

[21] D. Tamari. Monoides préordonnés et chaînes de Malcev. *Bulletin de la Société mathématique de France*, January 1954.

[22] Nima Arkani-Hamed, Hugh Thomas, and Jaroslav Trnka. Unwinding the Amplituhedron in Binary. 2017.

[23] P. Deligne and D. Mumford. The irreducibility of the space of curves of given genus. *Publications Mathématiques de l'Institut des Hautes Études Scientifiques*, 36(1):75–109, Jan 1969.

[24] S. L. Devadoss. Tessellations of Moduli Spaces and the Mosaic Operad. *ArXiv Mathematics e-prints*, July 1998.

[25] Nima Arkani-Hamed, Laurentiu Rodina, and Jaroslav Trnka. Locality and Unitarity from Singularities and Gauge Invariance. 2016.

[26] Nima Arkani-Hamed and Jaroslav Trnka. Into the Amplituhedron. *JHEP*, 12:182, 2014.

[27] Ruth Britto, Freddy Cachazo, Bo Feng, and Edward Witten. Direct proof of tree-level recursion relation in Yang-Mills theory. *Phys. Rev. Lett.*, 94:181602, 2005.

[28] Nima Arkani-Hamed, Jacob L. Bourjaily, Freddy Cachazo, Simon Caron-Huot, and Jaroslav Trnka. The All-Loop Integrand For Scattering Amplitudes in Planar N=4 SYM. *JHEP*, 01:041, 2011.

[29] Andrew Hodges. Eliminating spurious poles from gauge-theoretic amplitudes. *JHEP*, 05:135, 2013.

[30] Alexander Postnikov. Total positivity, Grassmannians, and networks. 2006.

[31] Allen Knutson, Thomas Lam, and David E Speyer. Positroid varieties: juggling and geometry. *Compositio Mathematica*, 149(10):1710–1752, 2013.

[32] Joshua S Scott. Grassmannians and cluster algebras. *Proceedings of the London Mathematical Society*, 92(2):345–380, 2006.

[33] Thomas Lam. Totally nonnegative Grassmannian and Grassmann polytopes. 2015.

[34] Günter M. Ziegler. *Lectures on polytopes (Graduate Texts in Mathematics, Vol. 152)*. Springer-Verlag, 1995.

[35] Phillip Griffiths and Joseph Harris. *Principles of algebraic geometry*. John Wiley & Sons, 2014.

[36] Nima Arkani-Hamed, Freddy Cachazo, Clifford Cheung, and Jared Kaplan. A Duality For The S Matrix. *JHEP*, 03:020, 2010.

[37] Nima Arkani-Hamed, Jacob Bourjaily, Freddy Cachazo, and Jaroslav Trnka. Local Spacetime Physics from the Grassmannian. *JHEP*, 01:108, 2011.

[38] Nima Arkani-Hamed, Jacob Bourjaily, Freddy Cachazo, and Jaroslav Trnka. Unification of Residues and Grassmannian Dualities. *JHEP*, 01:049, 2011.

[39] Paul Filliman. The volume of duals and sections of polytopes. *Mathematika*, 39(1):67–80, 1992.

[40] Nima Arkani-Hamed, Jacob L. Bourjaily, Freddy Cachazo, Andrew Hodges, and Jaroslav Trnka. A Note on Polytopes for Scattering Amplitudes. *JHEP*, 04:081, 2012.

[41] Michael E Peskin. *An introduction to quantum field theory*. CRC Press, 2018.

[42] Michel Brion and Michele Vergne. Arrangement of hyperplanes. i: rational functions and jeffrey-kirwan residue. In *Annales scientifiques de l'Ecole normale supérieure*, volume 32, pages 715–741. Elsevier, 1999.

[43] Livia Ferro, Tomasz Lukowski, Andrea Orta, and Matteo Parisi. Towards the amplituhedron volume. *Journal of High Energy Physics*, 2016(3):14, 2016.

[44] Victor V Batyrev and Yuri Tschinkel. Manin's conjecture for toric varieties. *arXiv preprint alg-geom/9510014*, 1995.

[45] Günter M Ziegler. Nonrational configurations, polytopes, and surfaces. *The Mathematical Intelligencer*, 30(3):36–42, 2008.

[46] Wikipedia: Catalan number. https://en.wikipedia.org/wiki/Catalan_number.

[47] A. J. Hanson and Ji-Ping Sha. A contour integral representation for the dual five-point function and a symmetry of the genus-4 surface in R**6. *J. Phys.*, A39:2509–2537, 2006.

[48] Sebastian Mizera. Combinatorics and Topology of Kawai-Lewellen-Tye Relations. *JHEP*, 08:097, 2017.

[49] Nima Arkani-Hamed. Amplitudes and Correlators as Canonical Forms; Worldsheets as Positive Geometries. http://www.strings2017.org/wp-content/uploads/2017/06/1000_nimastring.pdf.

[50] Leonardo de la Cruz, Alexander Kniss, and Stefan Weinzierl. Properties of scattering forms and their relation to associahedra. 2017.

[51] V. P. Nair. A Current Algebra for Some Gauge Theory Amplitudes. *Phys. Lett.*, B214:215–218, 1988.

[52] Francis C. S. Brown. Multiple zeta values and periods of moduli spaces $\overline{\mathcal{M}}_{0,n}(\mathbb{R})$. *Annales Sci. Ecole Norm. Sup.*, 42:371, 2009.

[53] Ziro Koba and Holger Bech Nielsen. Manifestly crossing invariant parametrization of n meson amplitude. *Nucl. Phys.*, B12:517–536, 1969.

[54] Carlos R. Mafra, Oliver Schlotterer, and Stephan Stieberger. Complete N-Point Superstring Disk Amplitude II. Amplitude and Hypergeometric Function Structure. *Nucl. Phys.*, B873:461–513, 2013.

[55] Freddy Cachazo, Sebastian Mizera, and Guojun Zhang. Scattering Equations: Real Solutions and Particles on a Line. *JHEP*, 03:151, 2017.

[56] Vittorio Del Duca, Lance J. Dixon, and Fabio Maltoni. New color decompositions for gauge amplitudes at tree and loop level. *Nucl. Phys.*, B571:51–70, 2000.

[57] Ronald Kleiss and Hans Kuijf. Multi - Gluon Cross-sections and Five Jet Production at Hadron Colliders. *Nucl. Phys.*, B312:616–644, 1989.

[58] Zvi Bern and Tristan Dennen. A Color Dual Form for Gauge-Theory Amplitudes. *Phys. Rev. Lett.*, 107:081601, 2011.

[59] Carlos R. Mafra, Oliver Schlotterer, and Stephan Stieberger. Explicit BCJ Numerators from Pure Spinors. *JHEP*, 07:092, 2011.

[60] Freddy Cachazo, Song He, and Ellis Ye Yuan. Scattering Equations and Matrices: From Einstein To Yang-Mills, DBI and NLSM. *JHEP*, 07:149, 2015.

[61] Steven N. Karp and Lauren K. Williams. The m=1 amplituhedron and cyclic hyperplane arrangements. 2016.

[62] Simon Caron-Huot. Notes on the scattering amplitude / Wilson loop duality. *JHEP*, 07:058, 2011.

[63] Jacob L. Bourjaily, Simon Caron-Huot, and Jaroslav Trnka. Dual-Conformal Regularization of Infrared Loop Divergences and the Chiral Box Expansion. *JHEP*, 01:001, 2015.

[64] Lionel Mason and David Skinner. Ambitwistor strings and the scattering equations. *JHEP*, 07:048, 2014.

[65] Tim Adamo, Eduardo Casali, and David Skinner. Ambitwistor strings and the scattering equations at one loop. *JHEP*, 04:104, 2014.

[66] Kantaro Ohmori. Worldsheet Geometries of Ambitwistor String. *JHEP*, 06:075, 2015.

[67] Eduardo Casali, Yvonne Geyer, Lionel Mason, Ricardo Monteiro, and Kai A. Roehrig. New Ambitwistor String Theories. *JHEP*, 11:038, 2015.

[68] Eduardo Casali and Piotr Tourkine. On the null origin of the ambitwistor string. *JHEP*, 11:036, 2016.

[69] W. Siegel. Amplitudes for left-handed strings. 2015.

[70] H. Kawai, D. C. Lewellen, and S. H. H. Tye. A Relation Between Tree Amplitudes of Closed and Open Strings. *Nucl. Phys.*, B269:1–23, 1986.

[71] Yu-tin Huang, Warren Siegel, and Ellis Ye Yuan. Factorization of Chiral String Amplitudes. *JHEP*, 09:101, 2016.

[72] Sebastian Mizera. Scattering Amplitudes from Intersection Theory. 2017.

[73] Dov Tamari. The algebra of bracketings and their enumeration. *Nieuw Arch. Wisk*, 3(10):131–146, 1962.

[74] Xiangrui Gao, Song He, and Yong Zhang. Labelled tree graphs, Feynman diagrams and disk integrals. 2017.

[75] Wikipedia: Permutohedron. `https://en.wikipedia.org/wiki/Permutohedron`.

[76] A. Postnikov. Permutohedra, associahedra, and beyond. *ArXiv Mathematics e-prints*, July 2005.

[77] A. Postnikov, V. Reiner, and L. Williams. Faces of Generalized Permutohedra. *ArXiv Mathematics e-prints*, September 2006.

[78] Nick Early. Generalized Permutohedra, Scattering Amplitudes, and a Cubic Three-Fold. 2017.

[79] Freddy Cachazo. Combinatorial Factorization. 2017.

[80] Eduardo Casali and Piotr Tourkine. Infrared behaviour of the one-loop scattering equations and supergravity integrands. *JHEP*, 04:013, 2015.

[81] Yvonne Geyer, Lionel Mason, Ricardo Monteiro, and Piotr Tourkine. Loop Integrands for Scattering Amplitudes from the Riemann Sphere. *Phys. Rev. Lett.*, 115(12):121603, 2015.

[82] Song He and Ellis Ye Yuan. One-loop Scattering Equations and Amplitudes from Forward Limit. *Phys. Rev.*, D92(10):105004, 2015.

[83] Yvonne Geyer, Lionel Mason, Ricardo Monteiro, and Piotr Tourkine. One-loop amplitudes on the Riemann sphere. *JHEP*, 03:114, 2016.

[84] Freddy Cachazo, Song He, and Ellis Ye Yuan. One-Loop Corrections from Higher Dimensional Tree Amplitudes. *JHEP*, 08:008, 2016.

[85] Yvonne Geyer, Lionel Mason, Ricardo Monteiro, and Piotr Tourkine. Two-Loop Scattering Amplitudes from the Riemann Sphere. *Phys. Rev.*, D94(12):125029, 2016.

[86] Song He and Oliver Schlotterer. New Relations for Gauge-Theory and Gravity Amplitudes at Loop Level. *Phys. Rev. Lett.*, 118(16):161601, 2017.

[87] Song He, Oliver Schlotterer, and Yong Zhang. New BCJ representations for one-loop amplitudes in gauge theories and gravity. 2017.

[88] Humberto Gomez, Sebastian Mizera, and Guojun Zhang. CHY Loop Integrands from Holomorphic Forms. *JHEP*, 03:092, 2017.

[89] Radu Roiban, Marcus Spradlin, and Anastasia Volovich. On the tree level S matrix of Yang-Mills theory. *Phys. Rev.*, D70:026009, 2004.

[90] Song He. Scattering amplitudes as differential forms. `http://online.kitp.ucsb.edu/online/scamp_c17/he/`.